AD-A047 851 DAVID W TAYLOR NAVAL SHIP RESEARCH AND DEVELOPMENT CE--ETC F/G 13/10
THE BARBEY REPORT. AN INVESTIGATION INTO CONTROLLABLE PITCH PRO--ETC(U)
AUG 77 C NOONAN, G ANTONIDES, A ZALOUMIS

UNCLASSIFIED DTNSRDC-77-0080

NL

1 OF 4
AD A047851

AD A047851

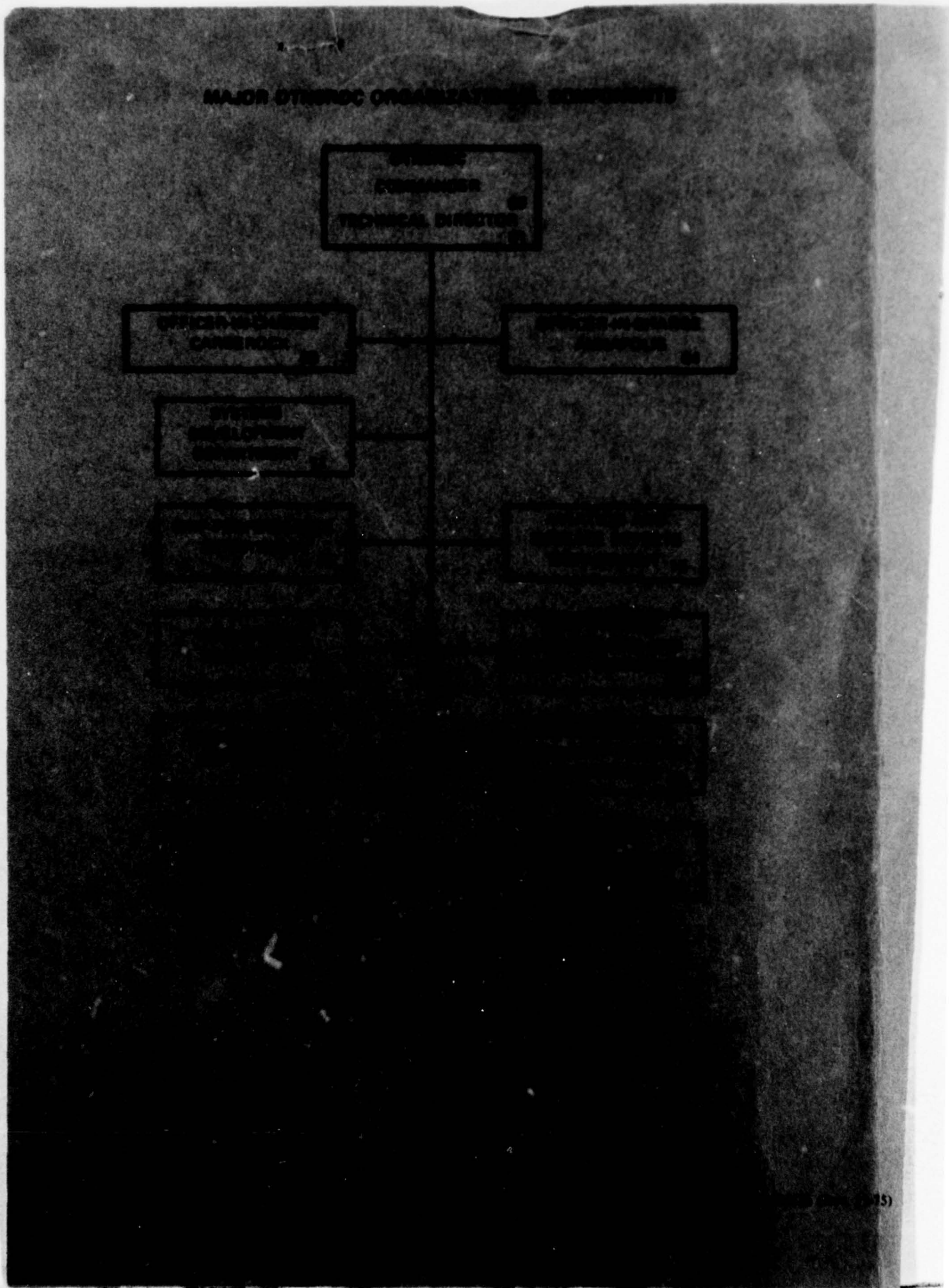

UNCLASSIFIED

SECURITY CLASSIFICATION OF THIS PAGE (When Data Entered)

REPORT DOCUMENTATION PAGE

READ INSTRUCTIONS BEFORE COMPLETING FORM

1. REPORT NUMBER: DTNSRDC-77-0080	2. GOVT ACCESSION NO.
3. RECIPIENT'S CATALOG NUMBER	
4. TITLE (and Subtitle): THE BARBEY REPORT, AN INVESTIGATION INTO CONTROLLABLE PITCH PROPELLER FAILURES FROM THE STANDPOINT OF FULL-SCALE UNDERWAY PROPELLER MEASUREMENTS	5. TYPE OF REPORT & PERIOD COVERED: Final rept., Oct [redacted]75 - June [redacted]976,
	6. PERFORMING ORG. REPORT NUMBER
7. AUTHOR(s): C. Noonan, G. Antonides, A. Zaloumis, B. Corbin and R. Schauer	8. CONTRACT OR GRANT NUMBER(s)
9. PERFORMING ORGANIZATION NAME AND ADDRESS: David W. Taylor Naval Ship Research and Development Center, Bethesda, Maryland 20084	10. PROGRAM ELEMENT, PROJECT, TASK AREA & WORK UNIT NUMBERS: Task Area SSL 24001, Task 19376, Work Unit 1-1962-133-62
11. CONTROLLING OFFICE NAME AND ADDRESS: Naval Sea Systems Command (033), Washington, D.C. 20362	12. REPORT DATE: Aug[redacted]77
	13. NUMBER OF PAGES: 293 p.
14. MONITORING AGENCY NAME & ADDRESS (if different from Controlling Office)	15. SECURITY CLASS. (of this report): UNCLASSIFIED
	15a. DECLASSIFICATION/DOWNGRADING SCHEDULE: None

16. DISTRIBUTION STATEMENT (of this Report)

APPROVED FOR PUBLIC RELEASE: DISTRIBUTION UNLIMITED

17. DISTRIBUTION STATEMENT (of the abstract entered in Block 20, if different from Report)

18. SUPPLEMENTARY NOTES

19. KEY WORDS (Continue on reverse side if necessary and identify by block number)

Propeller Stress, Propeller Bolt Stress, Propeller Crank Disk Stress, Controllable Pitch Propellers, Propeller Forces, Propulsion System Vibration, Static Propeller Loads, Dynamic Propeller Loads, Propeller Pressure Distribution, Bolted Joints, Non-Linear Loading Mechanisms, Propeller Blade Instrumentation

20. ABSTRACT (Continue on reverse side if necessary and identify by block number)

The U.S. Navy has recently made a major commitment to gas turbines as a main propulsion prime mover on a large number of high performance, high horsepower ships. Since this type of engine is unirotational, this also tacitly assumed a commitment to the controllable pitch propeller (CPP) which appeared to be the only practical means of reversing propulsive thrust for maneuvering. ~~Because~~ previous experience with (CPP)'s ~~was~~ → this report reviews the CONTROLLABLE PITCH PROPELLERS

(Continued on reverse side)

DD FORM 1 JAN 73 1473 EDITION OF 1 NOV 65 IS OBSOLETE S/N 0102-LF-014-6601

UNCLASSIFIED

SECURITY CLASSIFICATION OF THIS PAGE (When Data Entered)

387 682

(Block 20 continued)

~~limited~~, two ships of the FF-1052 class were fitted out with CPP's for test and evaluation. One of these ships, the USS BARBEY (FF-1088), experienced difficulties followed by catastrophic failure of the CPP mechanism after a relatively short period of operation.

As part of an extensive investigation into the general CPP design philosophy with particular reference to the failures experienced on BARBEY, the David W. Taylor Naval Ship Research and Development Center (DTNSRDC) instrumented the CPP mechanism on BARBEY and conducted full-scale drydock, dockside, and underway tests. The results showed that the quantitative and qualitative assumptions made in the structural design and propeller blade loads (especially during maneuvers) were not compatible with reality. More explicitly, the propeller blade palm acts as a nonuniform, nonlinear loading mechanism on the blade bolts. It was found that this mechanism causes excessive loads which lead to fatigue damage in the bolts and crank disk. This was most likely the direct cause of the original bolt failures and, together with geometric design and metallurgical deficiencies, contributed significantly to the crank disk failures.

It appears that this is a basic design problem which could be common to all high power CPP's with a bolted palm/crank disk arrangement. Several fixes were evaluated by using a model that incorporated the palm flexural and interfacing characteristics. Results indicated that bolt load redistribution could be affected by altering blade palm geometry. Further investigations with a more rigorous model are recommended together with the development of options such as threaded blade designs.

The report discusses peripheral activity in the area of instrumentation and underwater gage protection related to data acquisition for these trials as well as trials on the USS DOUGLAS (PG-100). In addition, details are given in the unique areas of underway propeller blade pressure measurements and an underwater telemetry system.

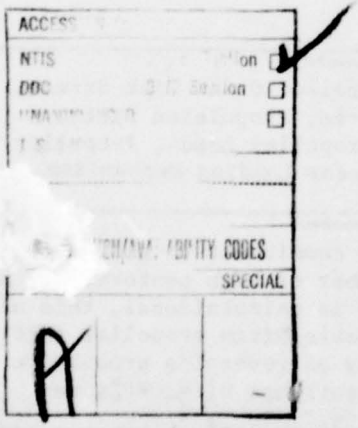

TABLE OF CONTENTS

LIST OF FIGURES

Page

LIST OF TABLES

Page

NOTATION

A	Cross-sectional area
B	Blade
BH	Bolt hole number in crank disk or blade palm
B_c	Compressive bending stress coefficient on a blade section
B_f	Tensile bending stress coefficient on a blade section
b	Blade section width
CCW	Counter clockwise
CD	Crank disk
CPP	Controllable pitch propeller
DAH	Design ahead condition
DAS	Design astern condition
DD	Destroyer
E	Young's modulus
F	Force
FF	Fast frigate
FS	Factor of safety
F_c	Centrifugal force
F_e	Fatigue limit, saltwater
K_B	Bolt stiffness
K_T	Stress concentration factor
K_j	Bolted joint stiffness (includes bolt and plates)
K_p	Bolted plate(s) stiffness
LE	Leading edge of propeller blade
M	Moment
P	Propeller blade pitch angle
PG	Patrol gunboat
Q	Torque
R	Propeller blade radius
RA	Rudder angle

RPM,N	Revolutions per minute of the propeller
RTC	Run, turn, crashback, crashahead maneuver
R_L	Resultant load acting on propeller blade
SA	Single amplitude of an oscillating signal
SHP	Shaft horsepower
S_{avg}	Average tensile stress
S_b	Bending stress
S_{max}	Maximum tensile stress
S_{min}	Minimum tensile stress
S_{ult}	Tensile strength
S_{yp}	Yield point stress
T	Thrust
TDC	Top dead center (12 o'clock)
TE	Trailing edge of propeller blade
T_m	Maximum thickness of propeller blade
YP	Yield point
Z	Section modulus
α	Angle with respect to shaft centerline
β	Bolt head rotation angle
γ	Crank disk rotation angle
ε	Strain
μ	Possion's ratio
θ	Angle with respect to a radial line emanating from the shaft
σ_r	Radial stress
$\sigma_{1,2}$	Principal stress
τ	Shear stress
ω	Circular frequency
$\mathbb{C}_L$	Centerline

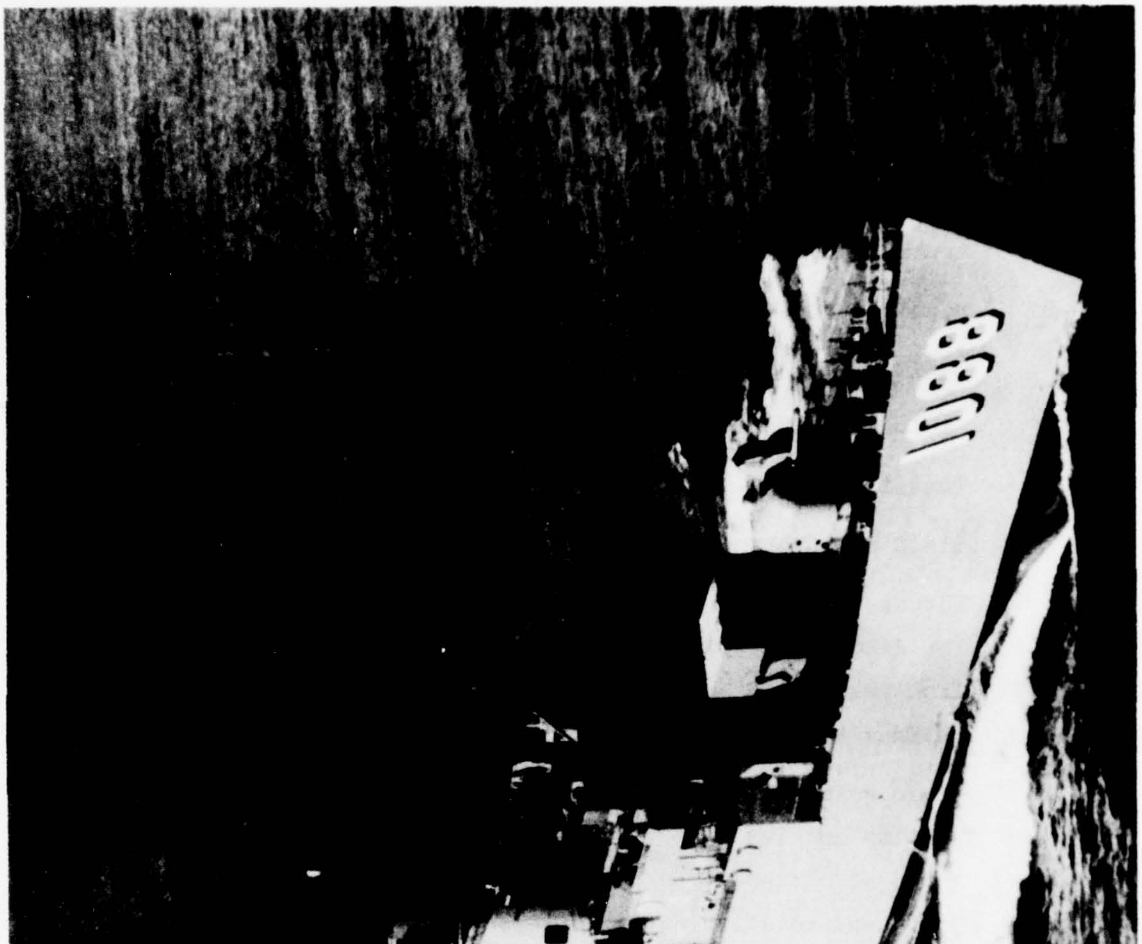

ABSTRACT

The U.S. Navy has recently made a major commitment to gas turbines as a main propulsion prime mover on a large number of high performance, high horsepower ships. Since this type of engine is unirotational, this also tacitly assumed a commitment to the controllable pitch propeller (CPP) which appeared to be the only practical means of reversing propulsive thrust for maneuvering. Because previous experience with CPP's was limited, two ships of the FF-1052 class were fitted out with CPP's for test and evaluation. One of these ships, the USS BARBEY (FF-1088), experienced difficulties followed by catastrophic failure of the CPP mechanism after a relatively short period of operation.

As part of an extensive investigation into the general CPP design philosophy with particular reference to the failures experienced on BARBEY, the David W. Taylor Naval Ship Research and Development Center (DTNSRDC) instrumented the CPP mechanism on BARBEY and conducted full-scale drydock, dockside, and underway tests. The results showed that the quantitative and qualitative assumptions made in the structural design and propeller blade loads (especially during maneuvers) were not compatible with reality. More explicitly, the propeller blade palm acts as a nonuniform, nonlinear loading mechanism on the blade bolts. It was found that this mechanism causes excessive loads which lead to fatigue damage in the bolts and crank disk. This was most likely the direct cause of the original bolt failures and, together with geometric design and metallurgical deficiencies, contributed significantly to the crank disk failures.

It appears that this is a basic design problem which could be common to all high power CPP's with a bolted palm/crank disk arrangement. Several fixes were evaluated by using a model that incorporated the palm flexural and interfacing characteristics. Results indicated that bolt load redistribution could be affected by altering blade palm geometry. Further investigations with a more rigorous model are recommended together with the development of options such as threaded blade designs.

The report discusses peripheral activity in the area of instrumentation and underwater gage protection related to data acquisition for these trials as well as trials on the USS DOUGLAS (PG-100). In addition, details are given in the unique areas of underway propeller blade pressure measurements and an underwater telemetry system.

ADMINISTRATIVE INFORMATION

Work on the USS BARBEY (FF-1088) project was authorized by Naval Ship Sea Command (NAVSEA) message R022107z of October 1974. Work was funded under Task Area SSL 24001, Task 19376, Work Unit 1-1962-133.

Work on the USS DOUGLAS (PG-100) was authorized by Naval Ship Systems Command (NAVSHIPS - now NAVSEA) message P232234z of January 1968. In addition, partial funding was obtained from Subproject SF 35.452.005, Task 01351. Preparation of this report was funded under DTNSRDC Work Unit 1-1962-156-01.

The work contained in the report was performed before formal issuance of the metrication policy of the Center. In the interest of time and economy, conversion to SI units has not been made. Appendix A lists conversion factors to enable readers to compute the SI unit values of measurements if so desired.

INTRODUCTION

Controllable pitch propellers (CPP) are not new to the U.S. Navy; one was installed on the USS MERRIMAC which was originally built in Boston about 1859 as a full rigged ship with auxiliary steam power. As seen in Table 1, past experience could hardly be classed as successful. Despite setbacks, however, it is apparent that the CPP has some benefits to offer. The most obvious is its ability to reverse pitch for maneuvering (stopping and running astern) without the necessity of changing the direction of shaft rotation. This is particularly meaningful for new naval designs that employ high power gas turbines either alone or in combination with other prime movers for ship propulsion.[1] The possibilities for reversing gas turbine ships include controllable pitch propellers, reverse gears, electric drives, and reversing gas turbines. All four methods of reversing have been studied and evaluated over the last 10 to 15 years.

Although the electric drive is feasible, it involves prohibitive weight, space, and efficiency penalties. To date, no satisfactory

---

[1] Boatwright, G.M. and J.H. Strandell, "Controllable Pitch Propellers," Naval Engineers Journal (Aug 1967). A complete listing of references is given on page 269.

TABLE 1 - USN CONTROLLABLE PITCH PROPELLERS

Year	Ship or Class	Numbers Ships/Props.	Propeller Speed shp-rpm	Designer and Builder*	Type System**	Remarks***
1939	YTL-13	1/1	250/400	BLH	EM	Unsuccessful
1941	DAHLGREN	1/2	14000/450	SMS	HS	Poor design—scrapped
1942	SC	182/2	1200/915	GMC	SJS	Numerous failures, scrapped
1942	LCI(L)	1100/2	900/650	GMC	SJS	Numerous failures, scrapped
1947	YTB-500	1/1	1200/180	NAVY	HS	
1947	YTB-501	1/1	1200/180	NAVY	EM	
1947	YTB-502	1/1	1200/180	SMS	HS	
1952	AM-421	92/2	800 1200 1600	NAVY SMS F-B S-M	HS	Working good 24.4% hub
1953	LST 1156	15/2	3000/300	NAVY SMS	HS	
1952	SS525 GUPPY	1/2	3500/–	NAVY	HS	Sea tested—removed for improved design
1957	SS525 GUPPY	1/2	3500/–	SMS	HH2	Redesign of above—shop test successful—not installed
1953	MSL 36 ft	1/1	160/1000	AFC	HS	Removed poor propulsion gas turbine
1954	Study Contract		10000/260	BLH	HHB2	First-two crank balanced design similar to LST-1176
1954	Study Contract		10000/260	SMS	HH2	
1955	Study Contract		20000/100 to 270	BLH	HHB2	Simplified-two crank balanced design similar to 40,000 shp
1955	DE Conv.	1/2	6000/–	RO	HH1	Gas turbine and CPP never installed
1955	IFS-1	1/2	1600/–	NAVY	HS	
1956	PGM-MDAP	5/2	1200/915	GMC	SJS	Troublesome
1956	MHC-43	1/2	550/–	KMW	HH1	
1957	PT812 Conv.	1/2	900/1000	EB	SJH	Transferred to Army inactive
1957	MOS 519	3/2	1350/–	FB	HS	
1958	LST 1176	1/2	6850/300	BLH	HHB2	
1965	PGM 84	6/2	6800/–	L	HH2	Delivered two ships
1961	YTB 752	2/1	1800/180	L	HH1	
1966	LST 1179	20/2	7900/–	KMW	HH1	Building
1974	FF-1061	1/1	35000/240	NAVY BLH	HH1	Troublesome
1974	FF-1088	1/1	35000/240	L	HH1	Failed in service

*Abbreviation Keys – in order of apperance

Designer and Builder

BLH	Baldwin Lima Hamilton Corporation
SMS	S. Morgan Smith Co.
GMC	General Motors Corp.
NAVY	Desinged in BUSHIPS—Buildt Norfolk Naval Shipyard
FB	Farrel Birmingham Co.
SM	Siverson
AFC	A. Feroy Colte Machiner Shop
RO	Rotal Co. of England
KMW	Ka-Me-Wa—Bird Johnson Co. Licensee
EB	Electric Boat Co.
L	Liaaen-Propulsion Systems, Inc. Licensee

**Type of Pitch Actuation System

EM	Electrical—Mechanical
HS	Hydraulic—Servomotor in Shaft
SJS	Mechanical—Screw Jack in Shaft
HHB2	Hydraulic—Servomotor in Hub-Balanced Two Crank
HH2	Hydraulic—Servomotor in Hub-Unbalanced Two Crank
HH1	Hydraulic—Servomotor in Hub Once Crank

***All units delivered are in service unless otherwise indicated

practical large aircraft-type reversing gas turbine has been developed nor does such a device appear to be feasible at the present time. Progress on the reversing gear has been made in some foreign countries, but the present state of the art does not enable the high horsepower of interest in the United States. From the original decision to go to gas turbine power and continuing to the present time, no fully viable alternative to the CPP has been developed for reversing gas turbine ships. Therefore, NAVSEA has proceeded to develop CPP technology which previously had been availalbe in the 1960's only up to 10,000 shp by extending the range to 35,000 - 40,000 hp per shaft.[2]

The first class of mass-produced ships with gas-turbine/CPP installation in the U.S. Navy was the USS ASHVILLE (PG-84)-Class patrol gunboat. Because this class experienced propeller blade failures (blade fracture), full-scale underway propeller blade stress trials were conducted on redesigned* blades of the USS DOUGLAS (PG-100) in January 1971. The preliminary results** indicated that propeller blade stresses were not excessive (Figure 1); the values shown for fatigue limit in saltwater are from Lague.[3] Since no more blade failures were experienced, no further analysis of the data was made. Available data on DOUGLAS are included in Appendix B of this report in order to contribute to the data base of information on this subject.

The newest ships to employ the gas turbine/CPP propeller system as main propulsion are the USS SPRUANCE (DD-963)-Class which are under construction at this writing. That class will have two 40,000-shp CPP systems and represents a considerable increase in horsepower over the ASHVILLE class (6,500 shp). Since the Navy had no full-scale experience with CPP's at the

---

[2]Angelo, J. et al., "U.S. Navy Controllable Pitch Propeller Programs," Paper Presented at Joint Meeting Flagship Section of ASME and Chesapeake Section of ASNE (19 Apr 1977).

[3]Lague, Francis L., "Marine Corrosion Causes and Preventions," A Wiley-Interscience Publication, John Wiley & Sons, New York.

*Redesign essentially included a change of blade material from cast titanium to stainless steel.

**Reported informally in DTNSRDC letter:962:CJN:9870.1 dated 10 Mar 1971.

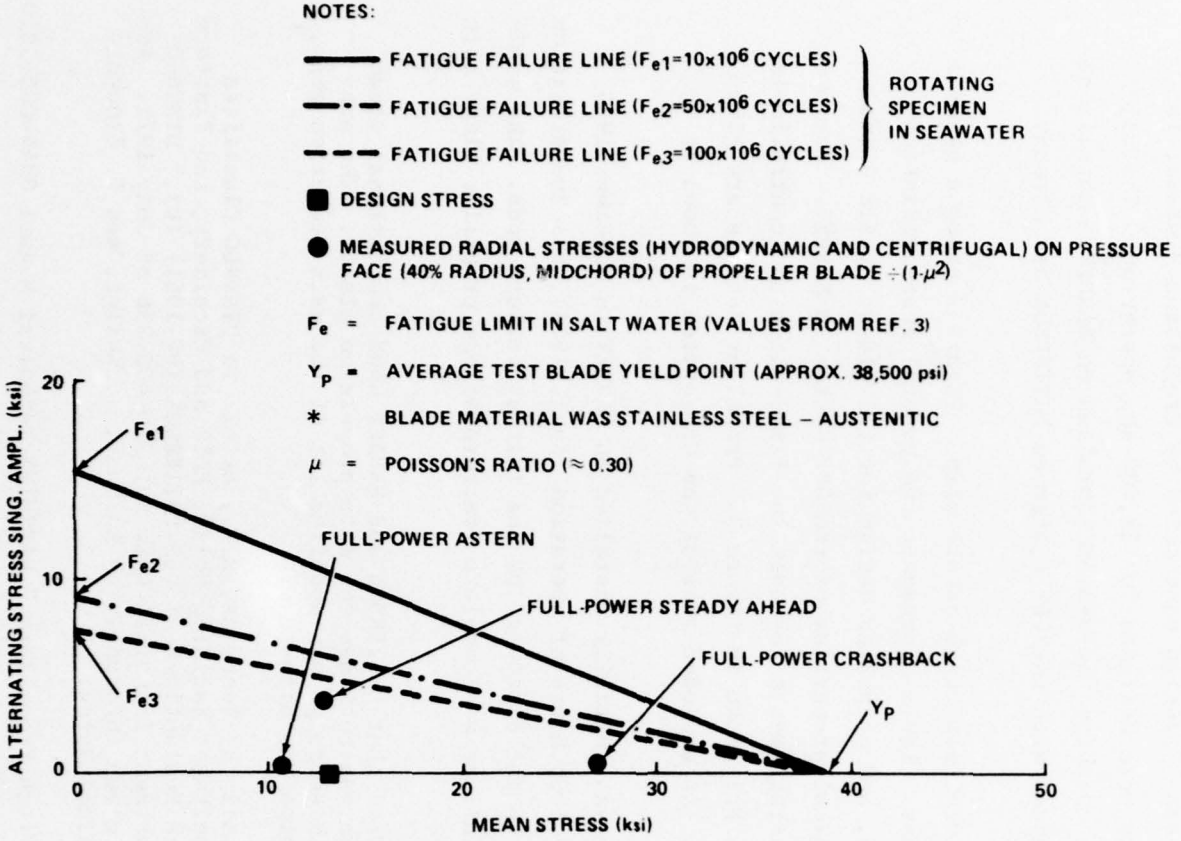

[3]LAQUE, F. L. "MARINE CORROSION CAUSES AND PREVENTION," CHAPTER 9 OF THE CORROSION MONOGRAPH SERIES, WILEY-INTERSCIENCE PUBLICATION, JOHN WILEY & SONS, NEW YORK (1975).

Figure 1 - Working Stress Diagram for Stainless Steel* Propeller Blade on DOUGLAS

higher powering level, two ships in the USS KNOX (FF-1052)-Class were fitted with a CPP for test and evaluation.* One system, jointly developed by the Baldwin-Lima-Hamilton (BLH) Corporation and the U.S. Navy, was installed on the USS PATTERSON (FF-1061). The USS BARBEY (FF-1088) was equipped with a Liaaen[4,5] design contracted by Propulsion Systems, Inc. (PSI). Both systems were designed for 35,000-shp operation. The major body of this report concerns the system installed on BARBEY. Details of operational experiences with the CPP system on PATTERSON are already available.**

BARBEY is a KNOX-Class ocean escort ship. Figure 2 shows a general profile of this class. Table 2 presents the general characteristics of the hull, machinery, and propeller design for the class. Table 3 indicates the metallurgical properties of the CPP system on BARBEY. The propeller and rudder arrangements for both the fixed-pitch and controllable-pitch installations are shown in Figure 3. Propeller details are given in Figures 4 and 5. An exploded view of the CPP system is shown in Figure 6.

The CPP System was initially installed on BARBEY in November 1973. After approximately 1000 hours of operation (April 1974), the investigation of an oil leak led to the discovery of the initial failure mode. The manifestation of this failure was complete fracture of one propeller blade bolt

---

*It should be noted that PATTERSON and BARBEY used conventional steam turbines rather than gas turbines for main propulsion plants. The propulsion system on these ships was modified aft of the main reduction gear, and the astern turbine was blanked off.

**Reported informally by Tompkins, R.W., et al. in DTNSRDC Classified Technical Note "Results of Radiated Noise, Hull and Machinery, and Platform and Sonar Self-Noise Evaluations of USS PATTERSON (DE-1061) (U)," DTNSRDC Ship Acoustics Department Technical Note No. SAD-400-926 of July 1971. Additional data were given informally by R. Hunt, J. Keller, and T. Brockett in Classified Technical Notes.

[4]"Controllable Pitch Propellers," NAVSHIPS Technical Manual 0944-005-5010 (Dec 1961).

[5]"Liaaen Model D-132/5 Controllable Pitch Propeller System for U.S. Navy Destroyer Escort (DE-1088)," Training Text, Long Beach Naval Shipyard (Feb 1972).

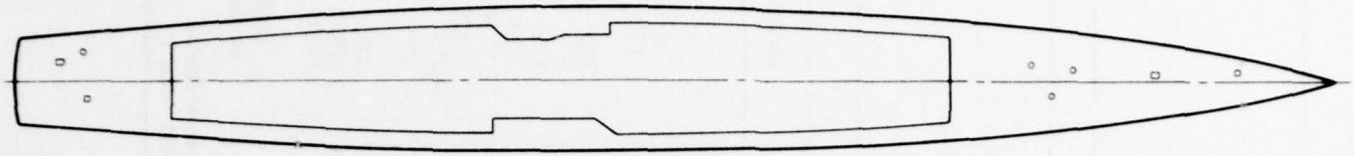

Figure 2b - Main Deck

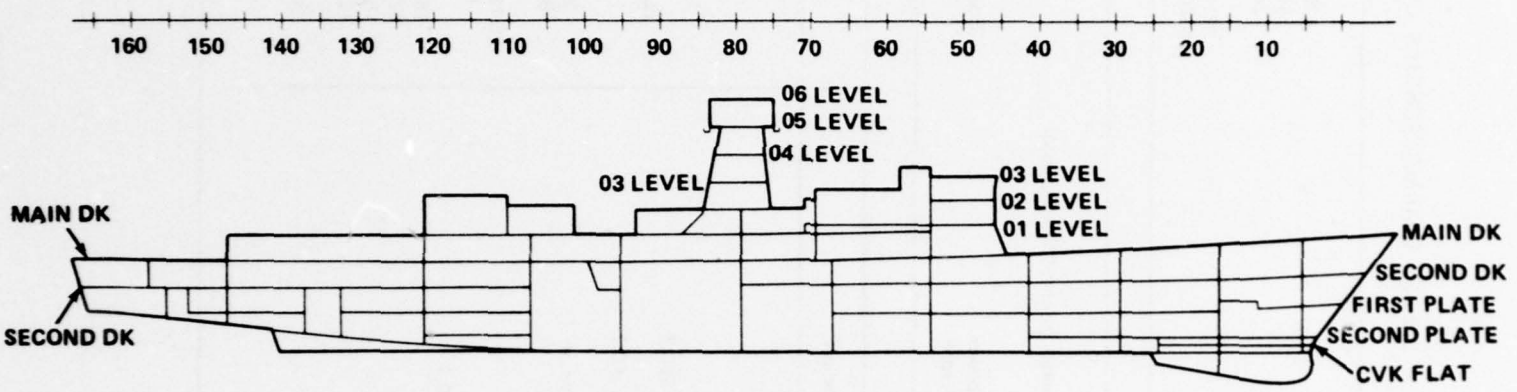

Figure 2a - Inboard Profile

Figure 2 - General Views of BARBEY

TABLE 2 - DESIGN CHARACTERISTICS OF KNOX CLASS

Hull:	
Overall Length, ft	438
Extreme Beam, ft	46.75
Max. Draft, ft	24.75
Displacement (tons)	
STD	3011
Full Load	4100

Machinery:	
Main Engine Type: Geared Turbine (Westinghouse)	
Number of Boilers	2 (1200 psi)
Number of Shafts	1
Maximum Shaft Horsepower	35,000
Maximum Shaft Speed, rpm	240

Propellers:	Fixed Pitch	PSI-CPP
Number of Propellers	1	1
Number of Blades	5	5
Diameter, ft	15	15
Maximum ahead pitch at 0.7 radius, in.	181.47	226
Maximum astern pitch at 0.7 radius, in	N/A	133
Maximum Hub Diameter, in	39.00	52.5
Hub Length, in	86.625	95.50
Hub/Diameter Ratio	0.22	0.29
Weight, incl. Cap, lb	25,125	39,315
Rotation	RH	RH
Design Pitch ahead at 0.7 radius, in	181.47	190
Disk Area, ft^2	176.72	176.72
Developed Area, ft^2	153.10	145.79
Projected area, ft^2	131.27	–
Pitch Ratio at 0.7R	1.008	1.055
WR^2 in Air, in-lb	35.46×10^6	44.35×10^6
Blade Material	Nickel Aluminum Bronze MIL-B-21230 Alloy 1	

TABLE 3 - METALLURGICAL PROPERTIES OF CPP SYSTEM ON BARBEY

Parameter	CPP System Component			
	Blades NI-AL-BZ	Bolts 17-4 PH(H1135)	Crank Disk	
			AISI*	HY-100**
Young's Modulus E, psi x 10^{-6}	18.0	28.5	28.5	29.0
Poisson's Ratio μ	0.33	0.29	0.29	0.30
Yield Strength S_{yp}, ksi	35.0	94.4	113.5	94.0
Tensile Strength S_{ult}, ksi	85.0	136.3	128.0	106.0
Fatigue Strength:				
Air, ksi	N/A	30.0***	64.0†	40.1***
Saltwater, ksi	12.5	15.0***	5.0†	11.6***

*Original (failed) crank disk material was cast steel (AISI4340 forging optional)

**Modified (instrumented) crank disk material

***Rotating cantilever fatigue strengths at 10^8 cycles with notched bars

†Estimated

Note: Stress concentration factor (K_T): Bolt (thread).....3.2
Crank Disk (fillet)....1.3

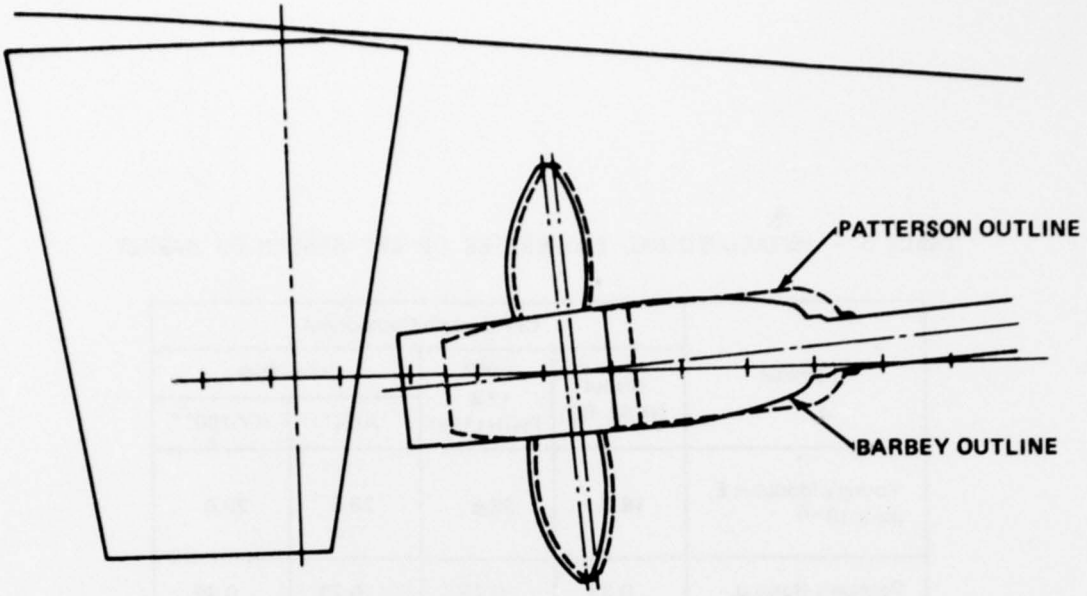

Figure 3b - BARBEY and PATTERSON Hubs

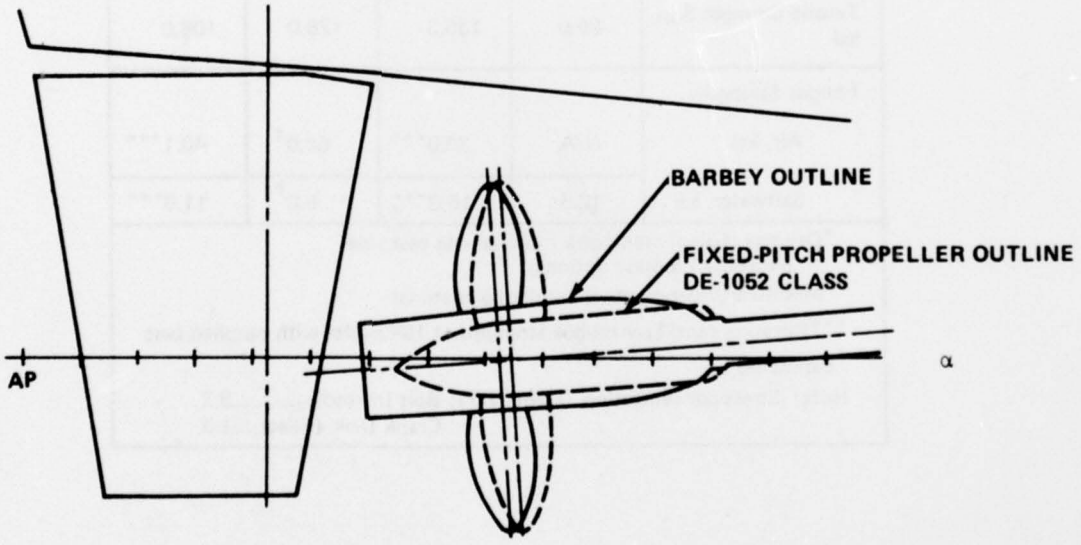

Figure 3a - Fixed Pitch Propelled and BARBEY Hubs

Figure 3 - Propeller and Rudder Arrangements

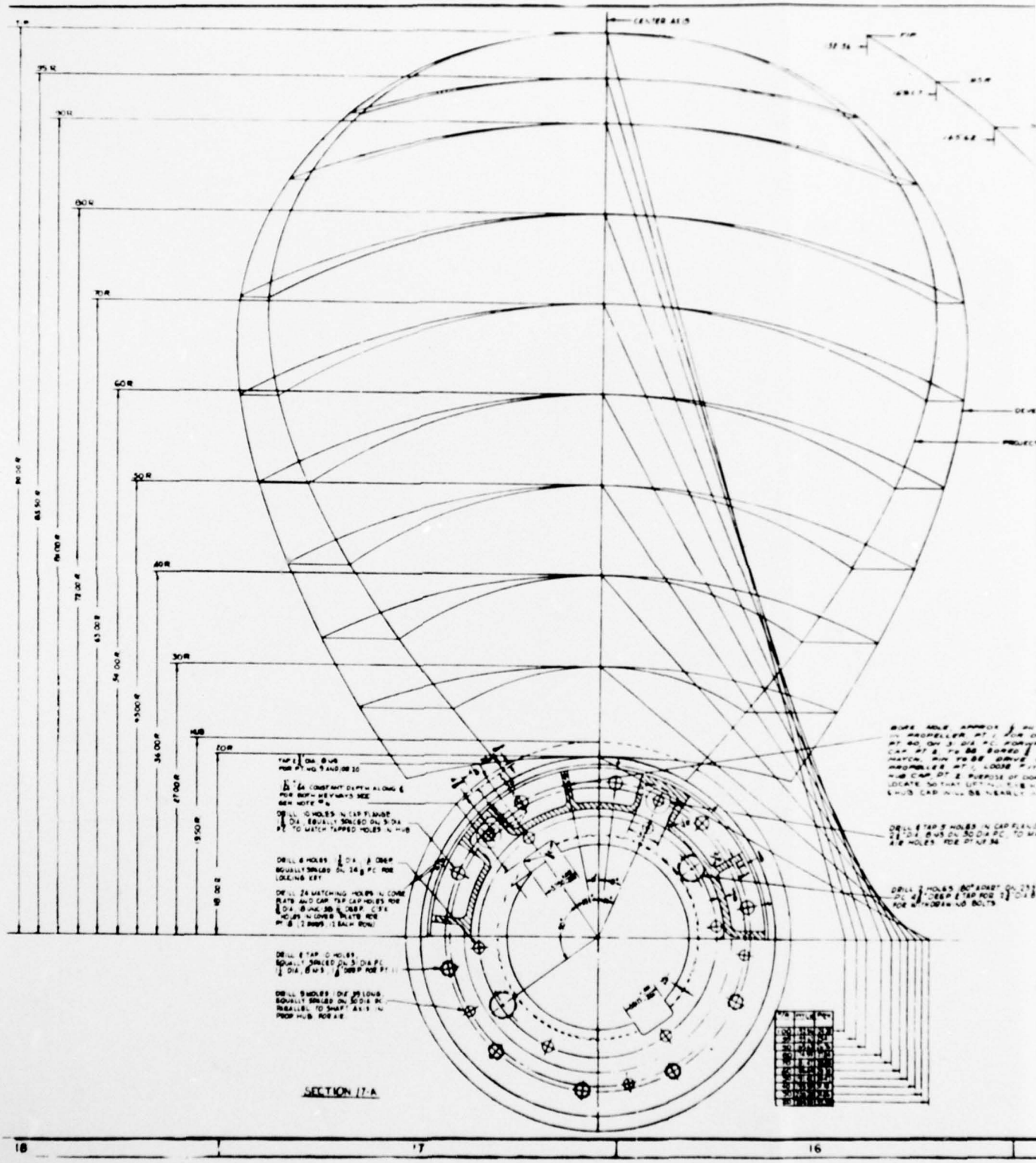
CENTER AXIS
35 R
30 R
60 R
70 R
60 R
50 R
40 R
30 R
HUB
TOP
SECTION 17-A

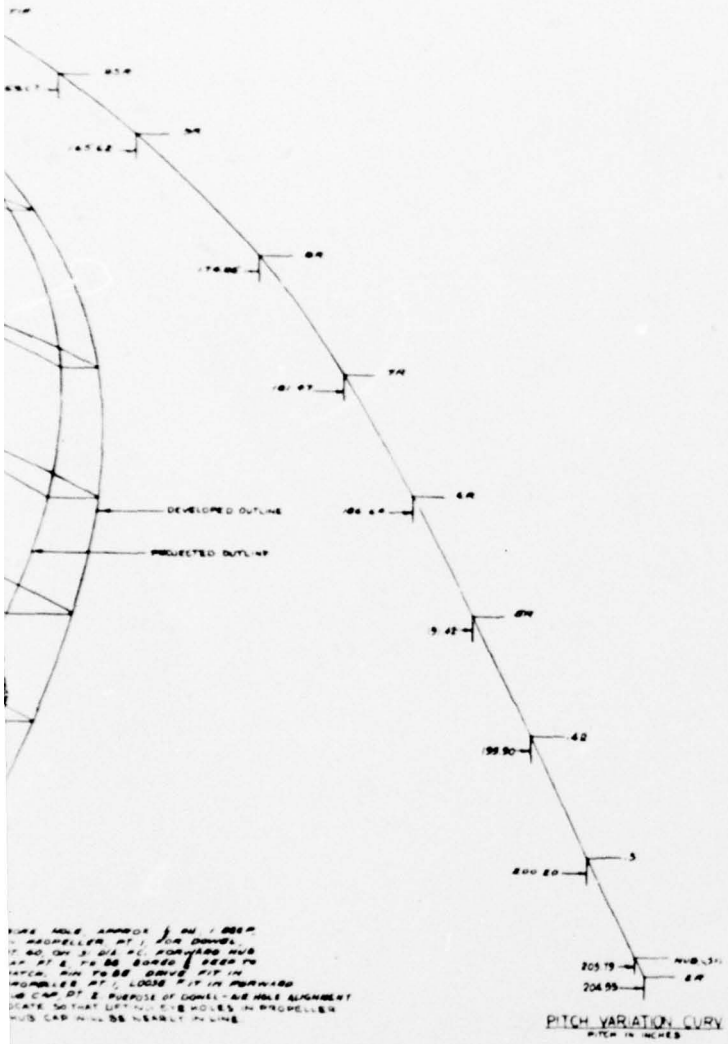

PITCH VARIATION CURV
PITCH IN INCHES

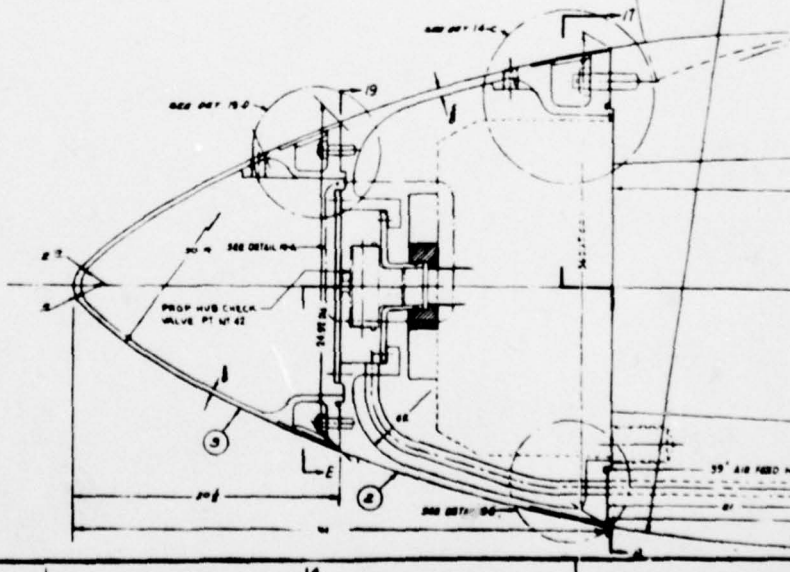

15 14

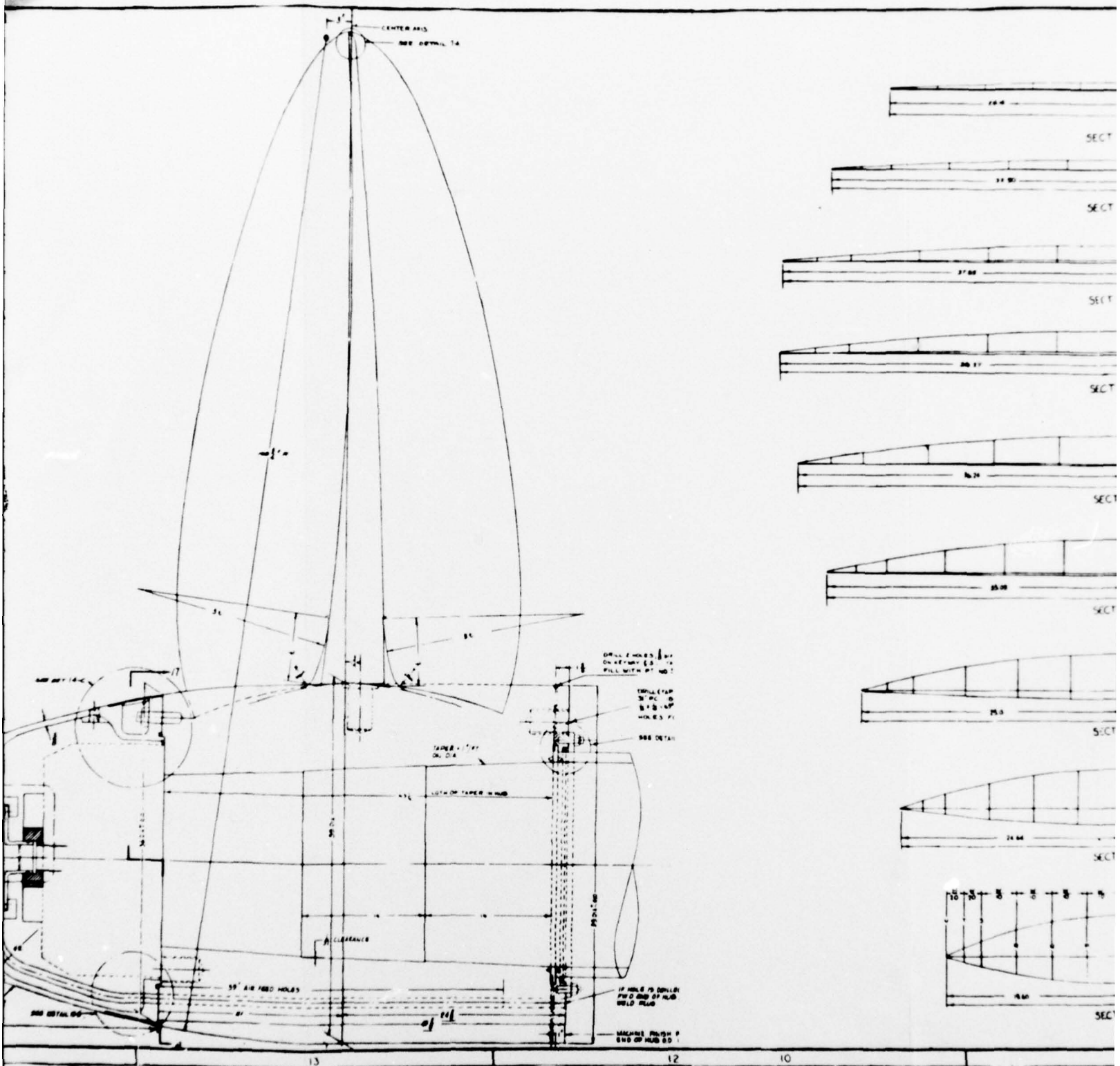

Figure 4 - Details of Fixed P

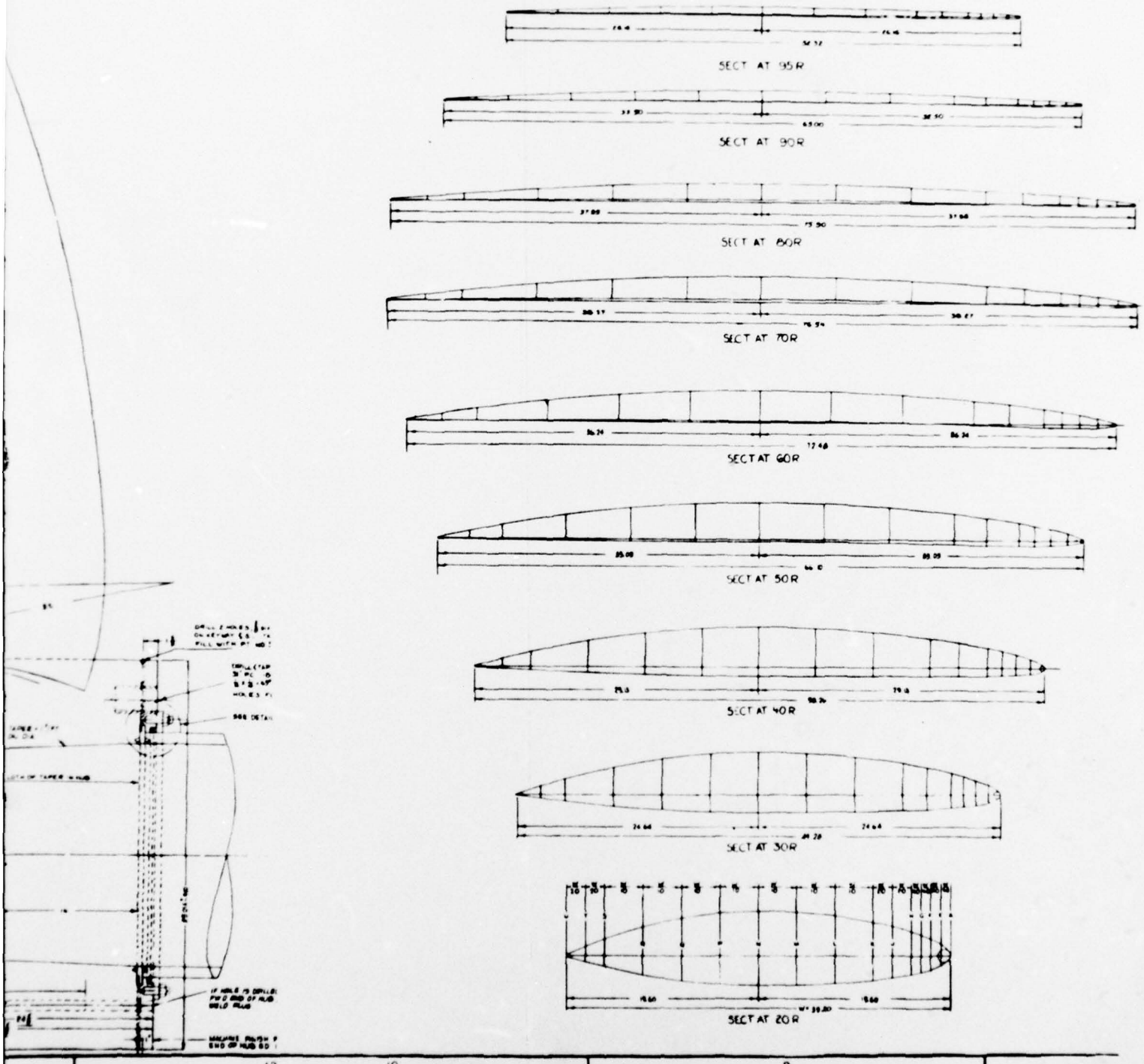

Figure 4 - Details of Fixed Pitch Propeller on BARBEY

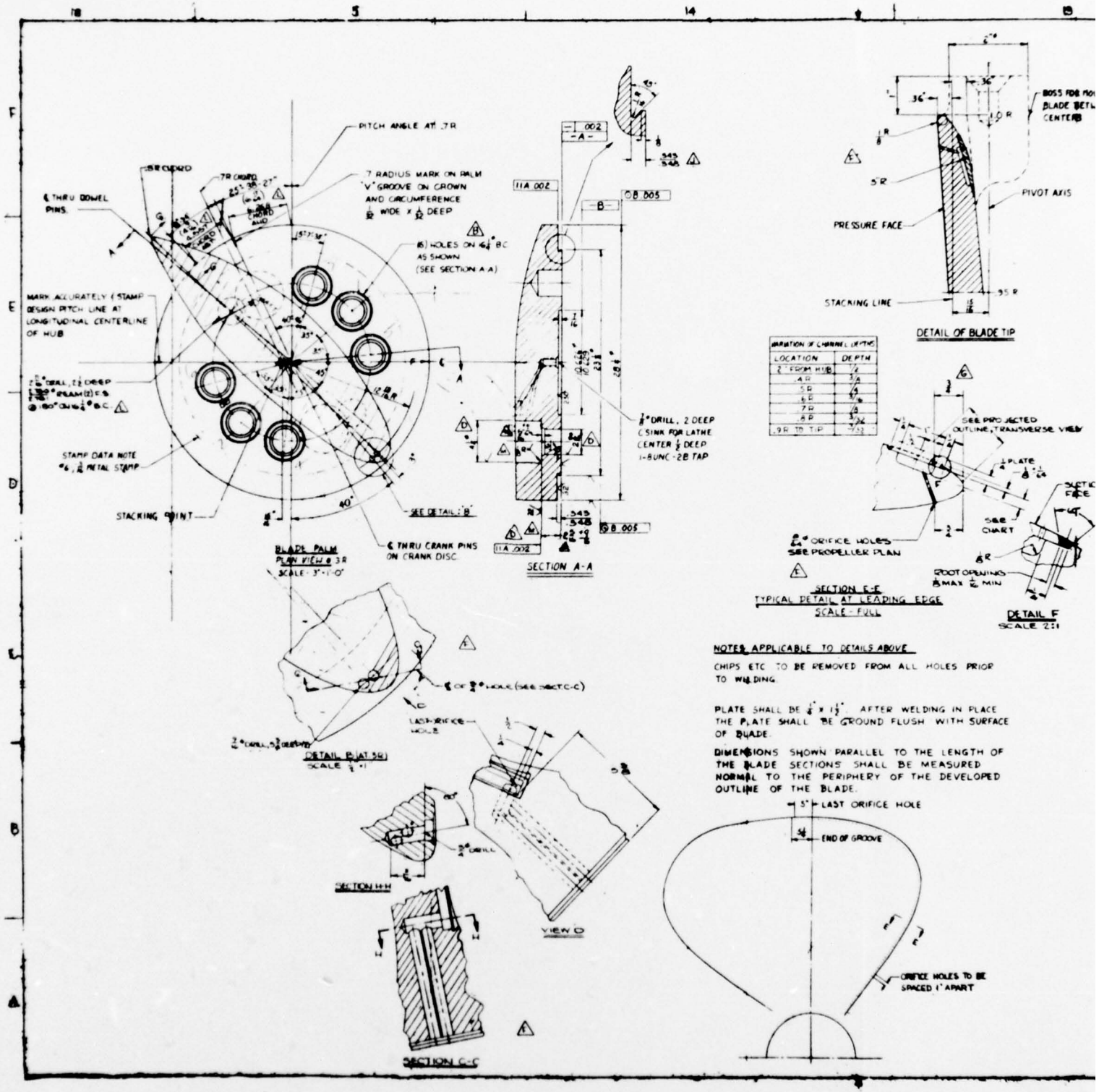

LOCATION	DEPTH
2" FROM HUB	
.4R	
.5R	
.6R	
.7R	
.8R	
.9R TO TIP	

NOTES APPLICABLE TO DETAILS ABOVE

CHIPS ETC TO BE REMOVED FROM ALL HOLES PRIOR TO WELDING.

PLATE SHALL BE X . AFTER WELDING IN PLACE THE PLATE SHALL BE GROUND FLUSH WITH SURFACE OF BLADE.

DIMENSIONS SHOWN PARALLEL TO THE LENGTH OF THE BLADE SECTIONS SHALL BE MEASURED NORMAL TO THE PERIPHERY OF THE DEVELOPED OUTLINE OF THE BLADE.

PRECEDING PAGE BLANK-NOT FILMED

BOSS FOR MOUNTING BLADE BETWEEN CENTERS
PIVOT AXIS
PRESSURE FACE
STACKING LINE
.95 R
DETAIL OF BLADE TIP
SEE PROJECTED OUTLINE, TRANSVERSE VIEW
SECTION FACE
SEE CHART
ORIFICE HOLES SEE PROPELLER PLAN
ROOT OPENING
SECTION E-E
DETAIL F
SCALE 2:1
TO BE REMOVED FROM ALL HOLES PRIOR
SHALL BE GROUND FLUSH WITH SURFACE
LAST ORIFICE HOLE
END OF GROOVE
ORIFICE HOLES TO BE SPACED 1" APART
TIP
.95R
.9R
.8R
.7R
.6R
.5R
.4R
16.50" RADIUS
24.25 RADIUS
90.00 RADIUS
MAX THICKNESS LINE
PROJECTED BL OUTLINE
TRAILING EDGE
HUB
SUGGESTED TEMPLATE
SECTION G-G
TRANSVERSE VIEW
LOOKING FORWARD
SCALE: 3"=1'-0"
P/2π
28.886 AT .3R
29.921 AT .4R
30.558 AT .5R
30.717 AT .6R
30.239 AT .7R
29.157 AT .8R
27.375 AT .9R
26.101 AT .95R
24.669 AT BLADE TIP
16916 - J

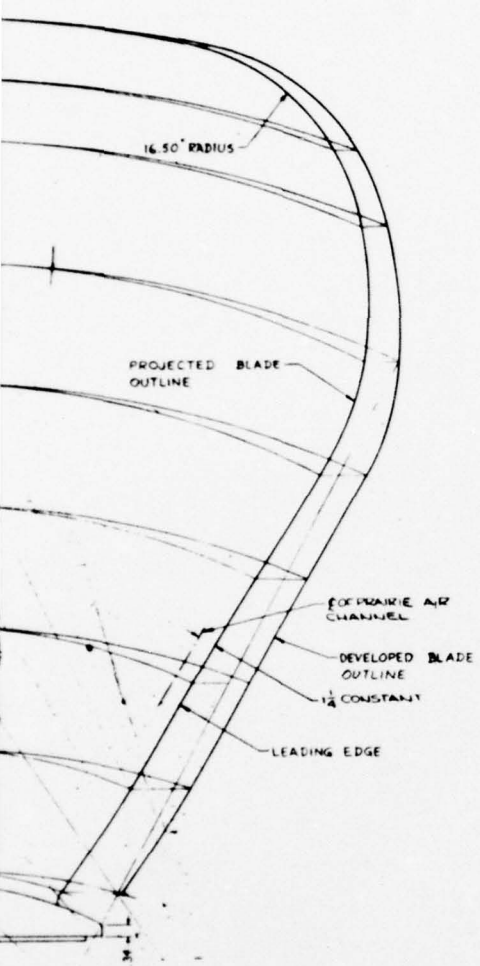

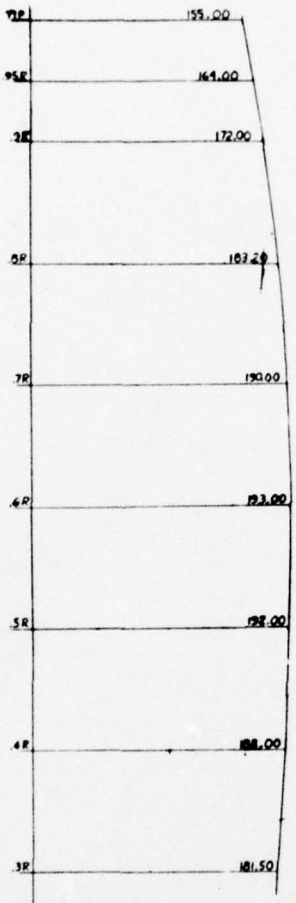

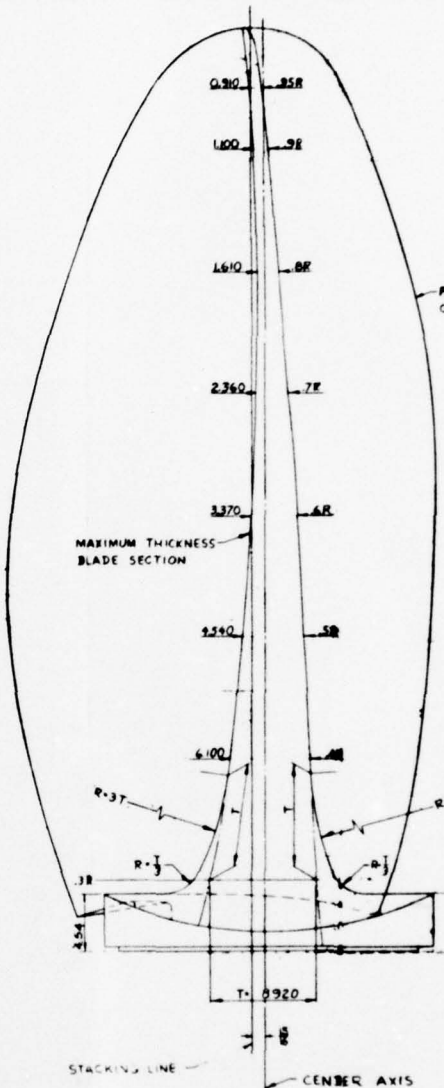

$\frac{P}{2\pi r}$

28.886 AT 3R
29.321 AT 4R
30.358 AT 5R
30.717 AT 6R
30.239 AT 7R
29.157 AT 8R
27.375 AT 9R
26.101 AT .95R
24.669 AT BLADE TIP

PITCH VARIATIONS

SCALE -
VERTICAL - 3"=1'-0"
HORIZONTAL - 1"=10" X .25

LONGITUDINAL VIEW

SCALE - 3"=1'-0"

3

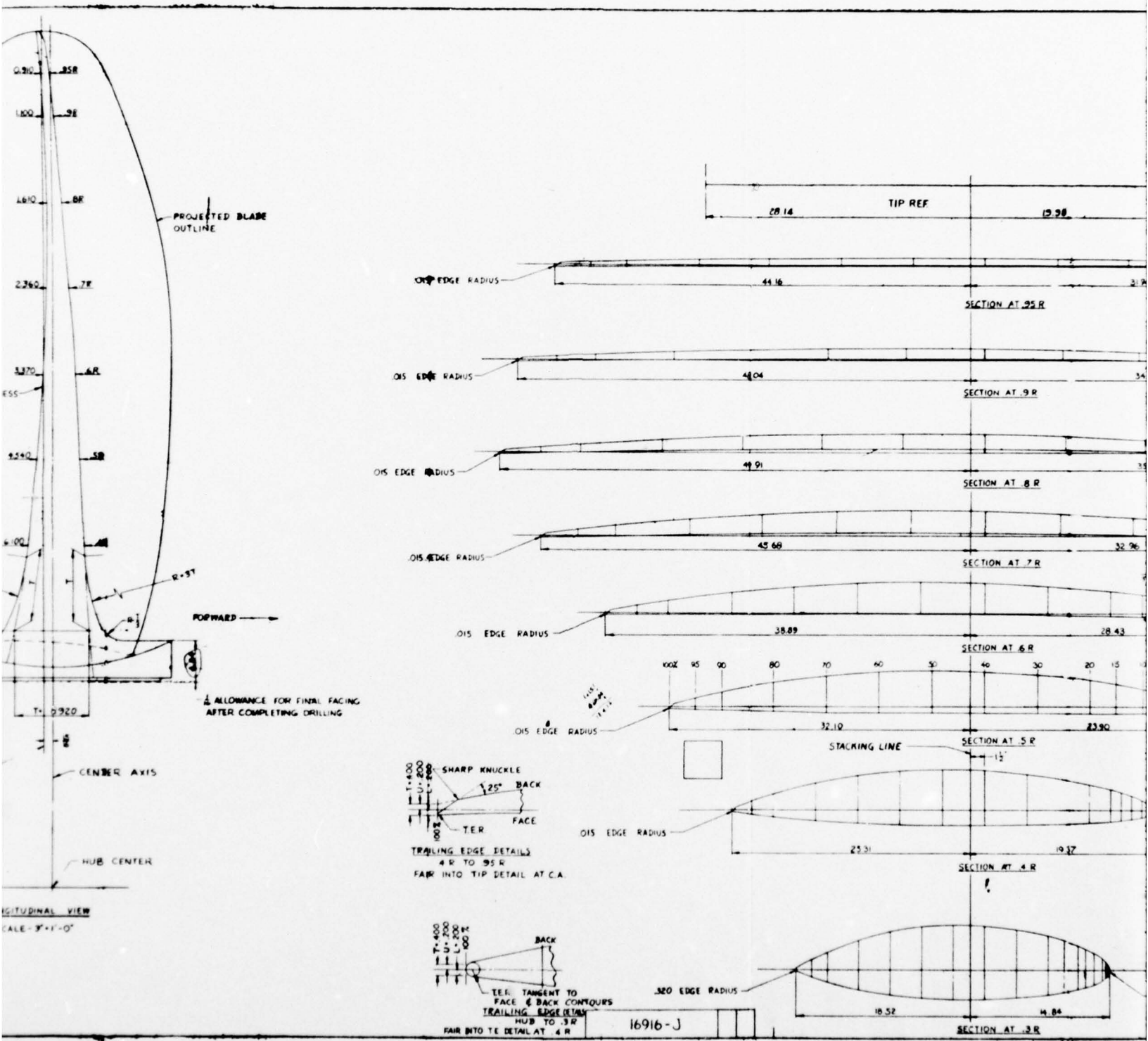

Figure 5 - Details of Controllab

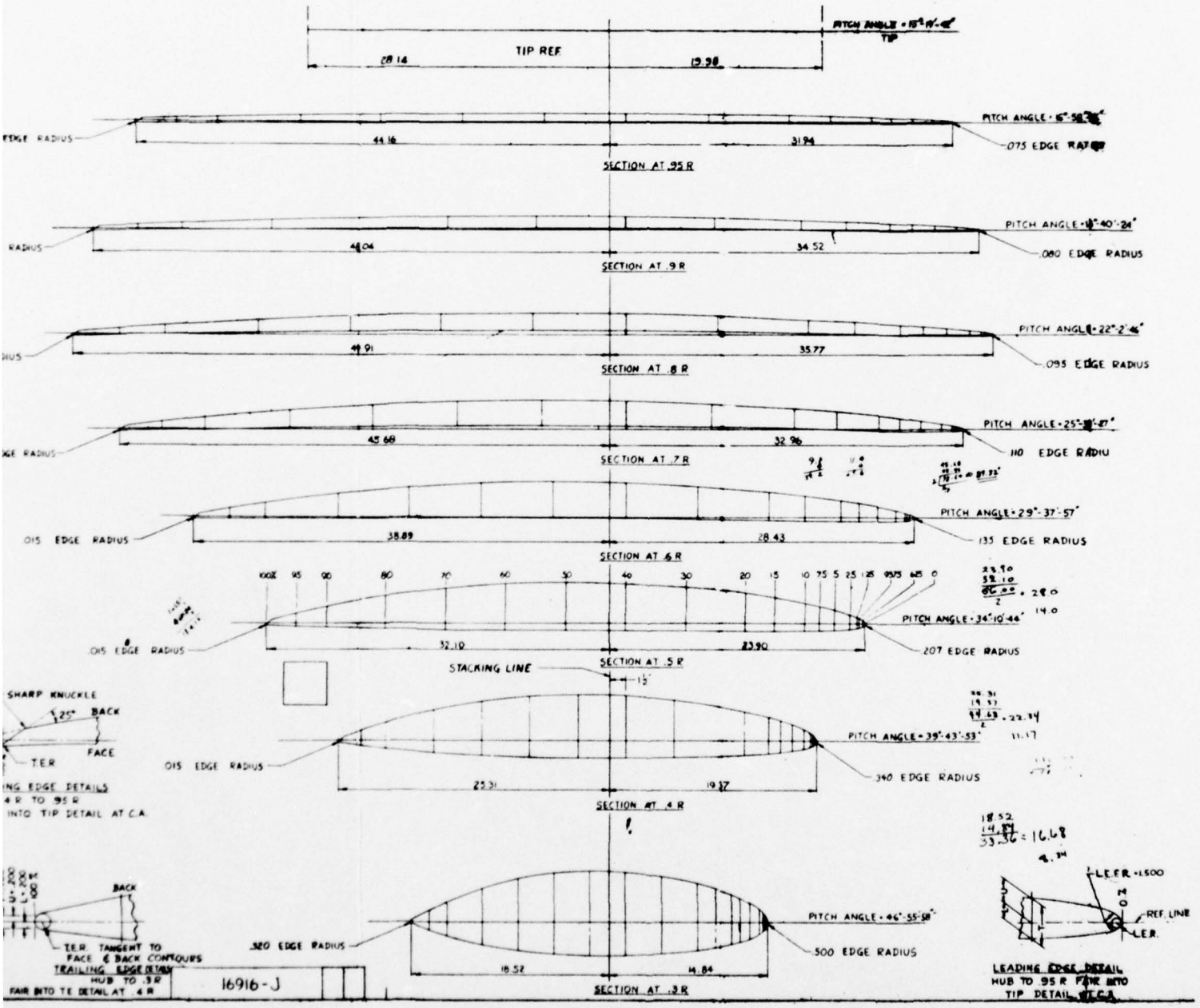

Figure 5 - Details of Controllable-Pitch Propeller on BARBEY

5

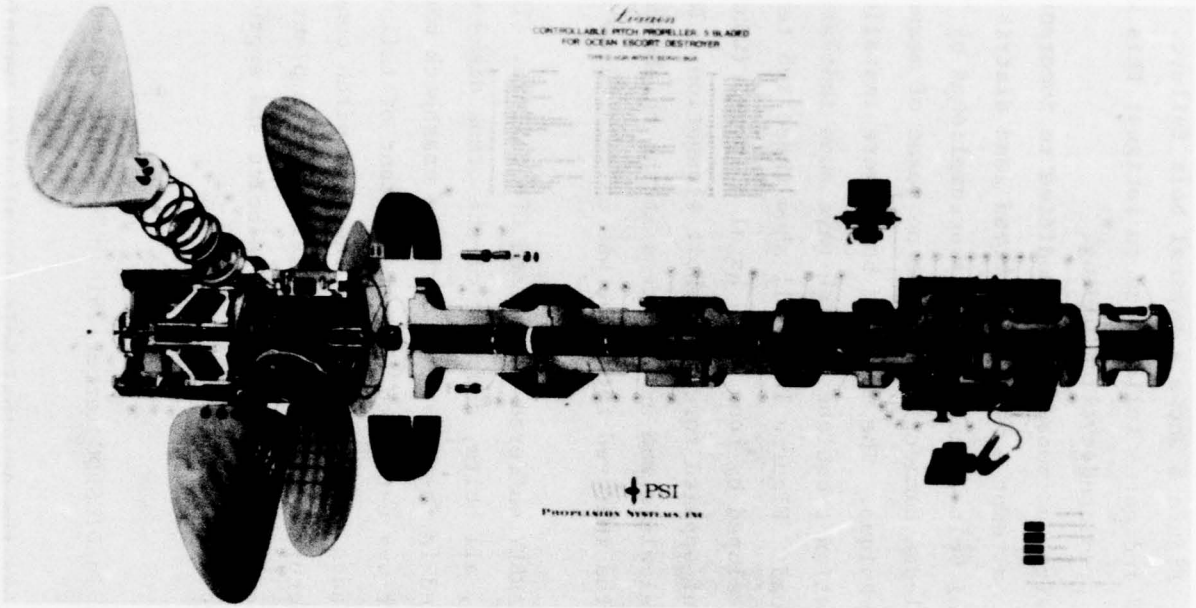

Figure 6 — Exploded View of Controllable-Pitch Propeller System on BARBEY

and cracks in seven other bolts. The fractured bolt and four of the cracked bolts were found in Location 6; see Figure 7 for bolt hole locations. The other three cracked bolts were in Location 2. All bolts failed in the area of the first two threads. Figure 8 shows a typical bolt failure. Surfaces of the bolt that fractured indicated failure due to fatigue; this was attributed to higher than predicted cyclic loading.*

The original bolt design was subsequently modified to incorporate a tapered thread in order to attempt a more even thread load distribution; see Figure 9. The original bolt installation was accomplished by "slugging-up" on the bolts with a sledge hammer. There was no means of measuring bolt preload with this technique. The modified bolts were installed by using an improved installation technique** which gave some indication of the "installed" bolt preload. Figures 10 and 11 show these two techniques. The improved technique developed by Long Beach Naval Shipyard (LBNS) employed the measurement of applied torque and bolt elongation. The two quantities were used to calculate the axial stress at the thread root.*** Bolt preload stress with the improved technique was calculated as approximately 45,000 psi.

On 30 August 1974, BARBEY suffered the second CPP failure. This time all five propeller blades, all bolts, and most of the crank disks were lost when the crank disks failed in fast fracture during a crashback maneuver; see Figures 12 and 13. It was estimated that the instant of failure occurred when the propeller blades were at (or near) the zero pitch condition. When the second failure occurred, the main propulsion system plant had approximately 1000 hr of operation with the modified bolts and approximately 2000 hr of total operation time with the CPP system.

---

*Reported informally in DTNSRDC letter:2814:MGV, 10310, dated 19 June 1974.

**It was recognized that the original bolt installation technique could also have resulted in insufficient bolt preload. That could have contributed significantly to early bolt fatigue failure.

***Reported informally by Long Beach Naval Shipyard (DE-1088) Controllable Pitch Propeller Blade Bolt Installation Data w/304 SST Washers (as installed) as LBNS: CKN Code 260.23 dated 23 November 1974.

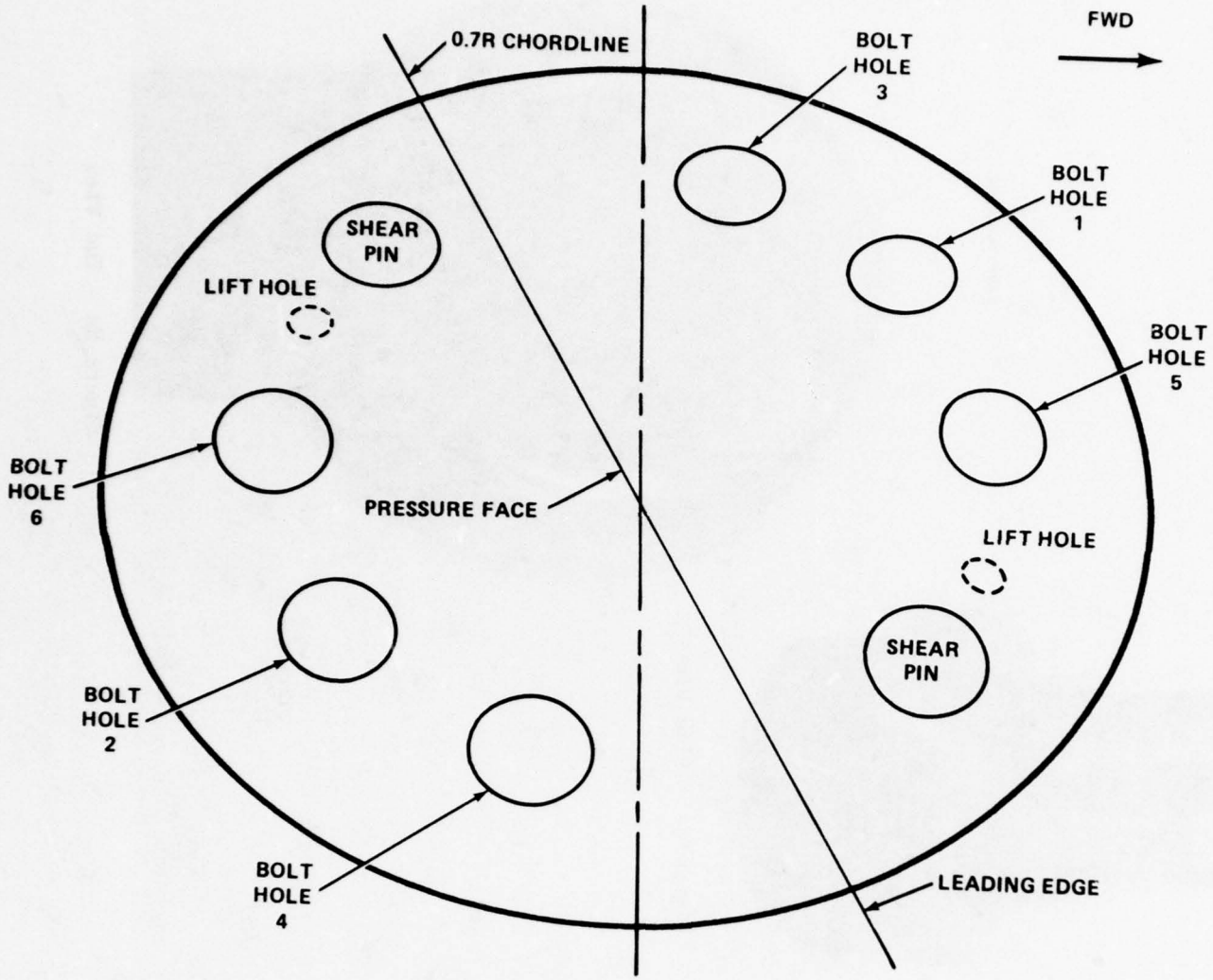

Figure 7 - Layout of Propeller Blade Palm/Crank Disk

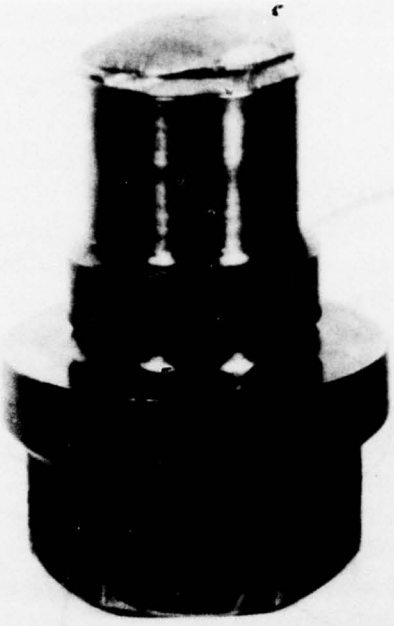

Figure 8b - Side View

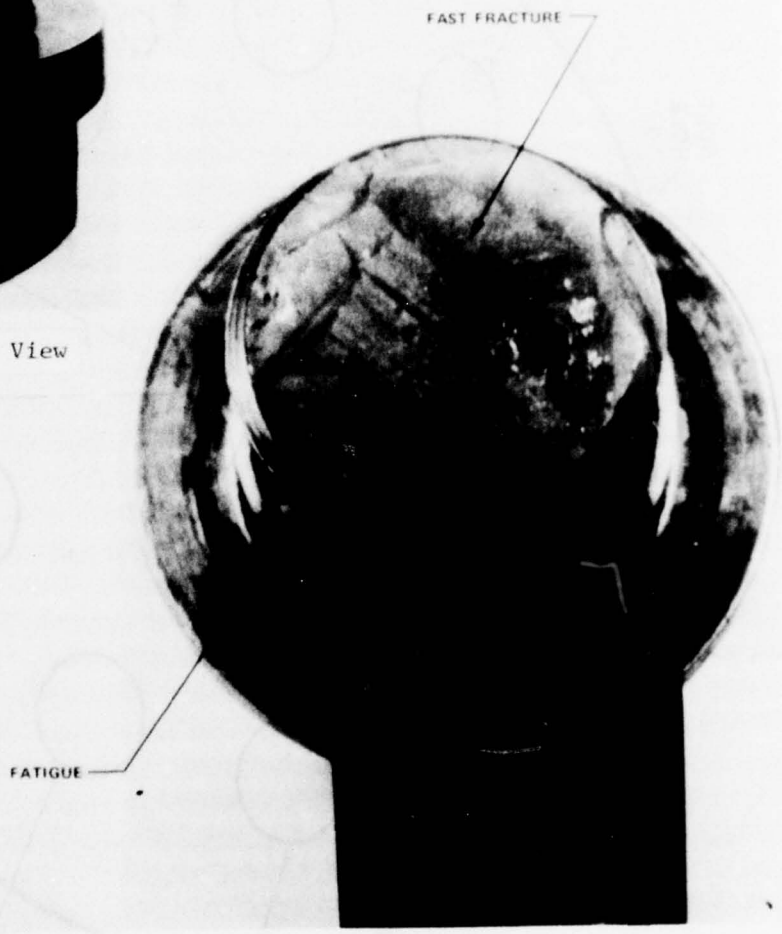

Figure 8a - End View

Figure 8 — Typical Failure of Original Bolt Design for CPP System on BARBEY

Figure 9 - Various Bolt Designs for CPP System on BARBEY

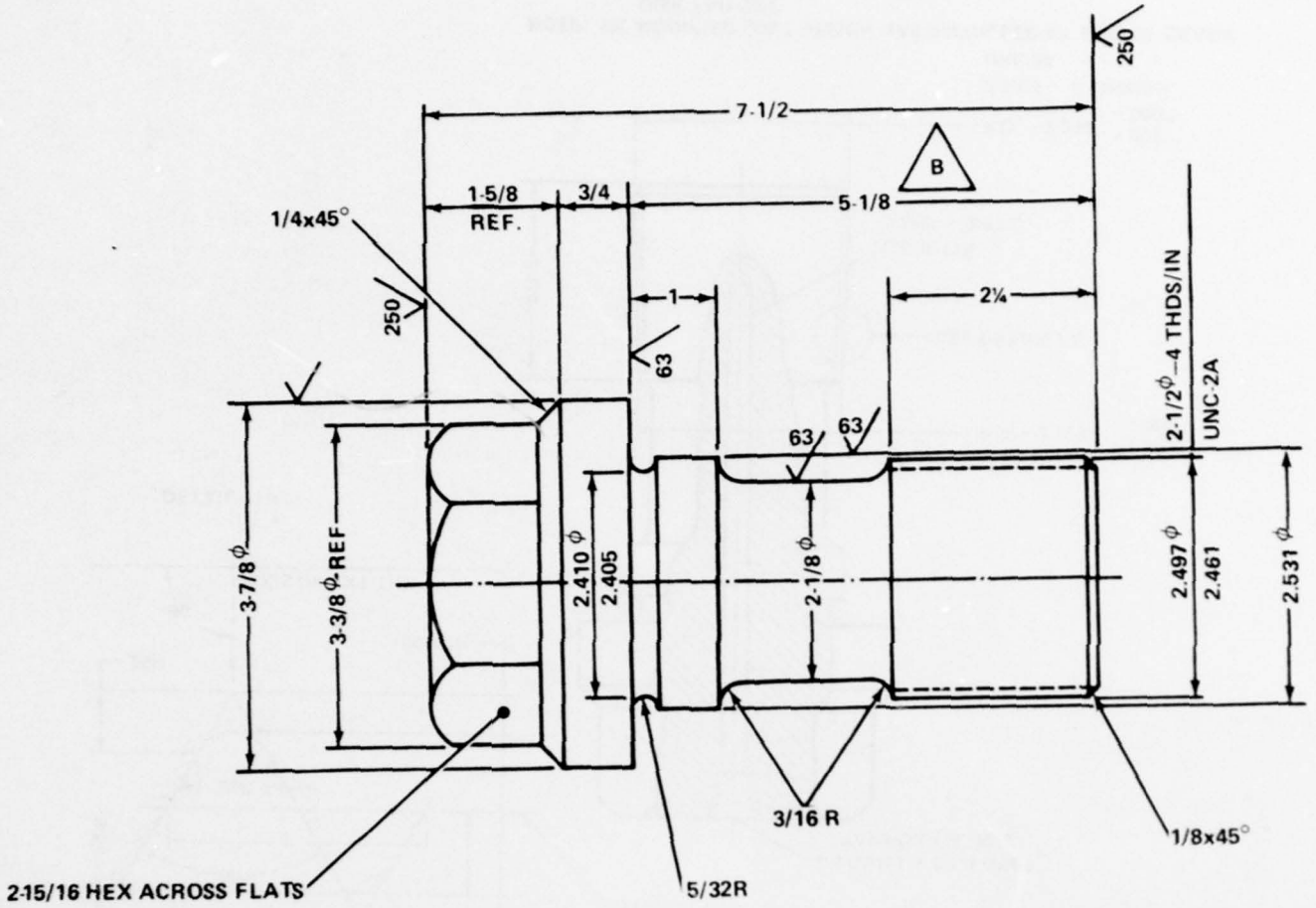

NOTE: (1) BOLTS WHICH FATIGUED IN ORIGINAL FAILURE

Figure 9a - Original Bolt Design(1)

Figure 9 (Continued)

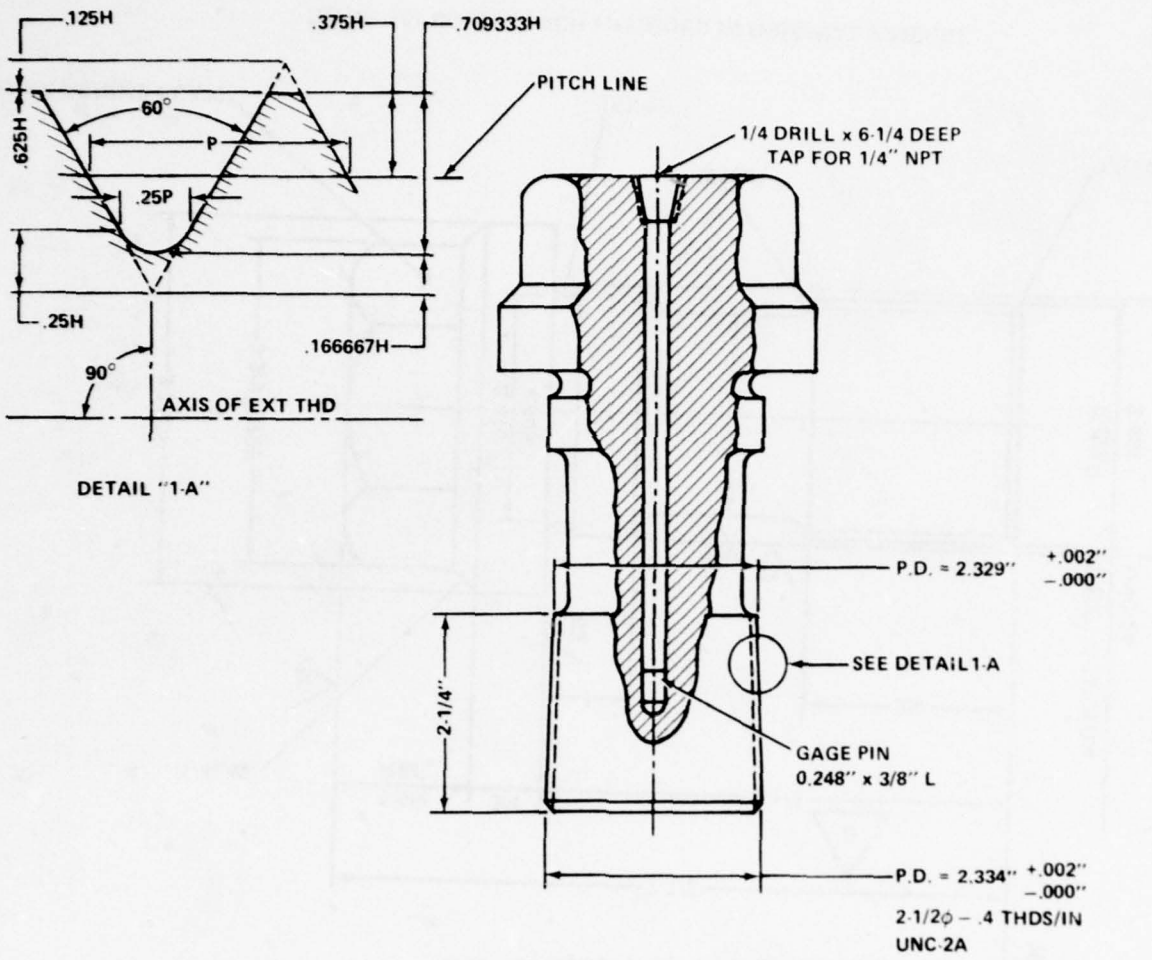

NOTE: (2) MODIFIED BOLT DESIGN WAS INSTALLED AT TIME OF CRANK DISK FAILURE

Figure 9b - Modified Bolt Design[2]

Figure 9 (Continued)

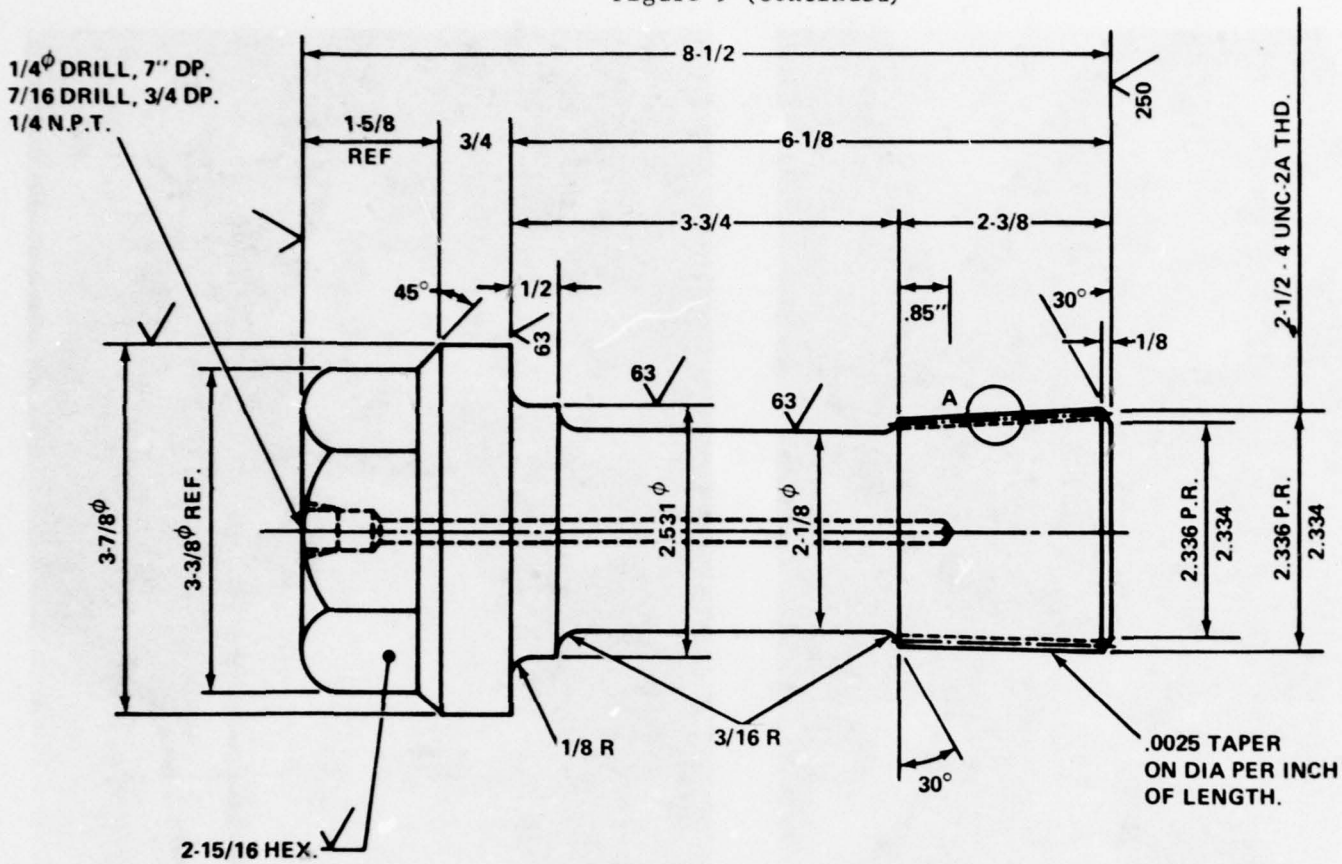

NOTE: (3) FINAL BOLT DESIGN WAS INSTRUMENTED AND INSTALLED FOR CAP SYSTEM TRIALS

Figure 9c - Final Bolt Design[3]

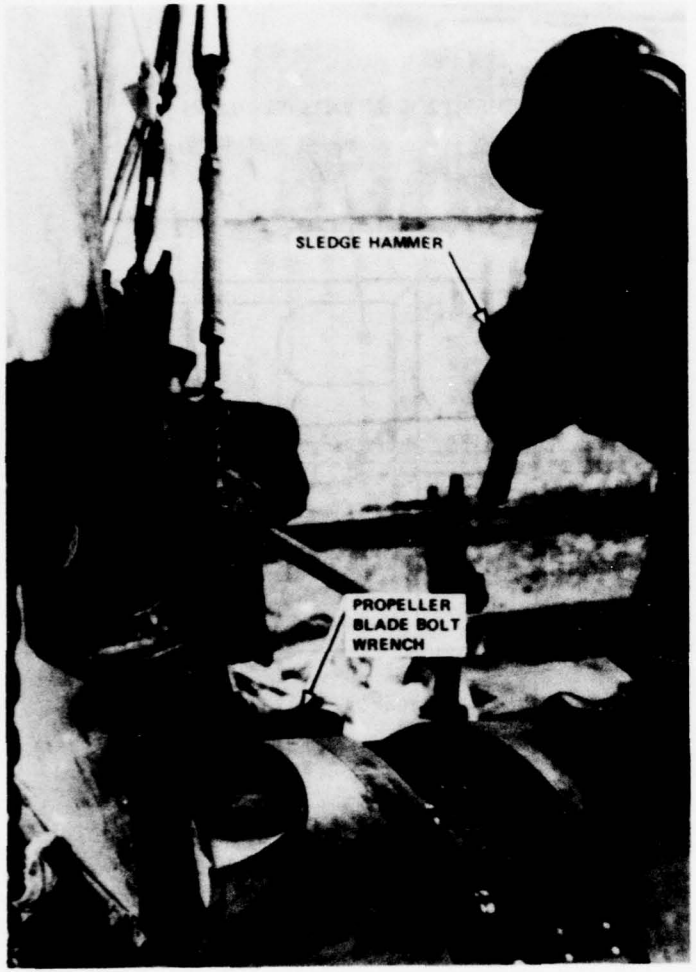

Figure 10 - Original Bolt Installation (Impulse) Technique for BARBEY

Figure 11 - Improved Bolt Installation (Torque/Elongation) Techniques for BARBEY

Figure 12 - Failed Crank Disks on BARBEY

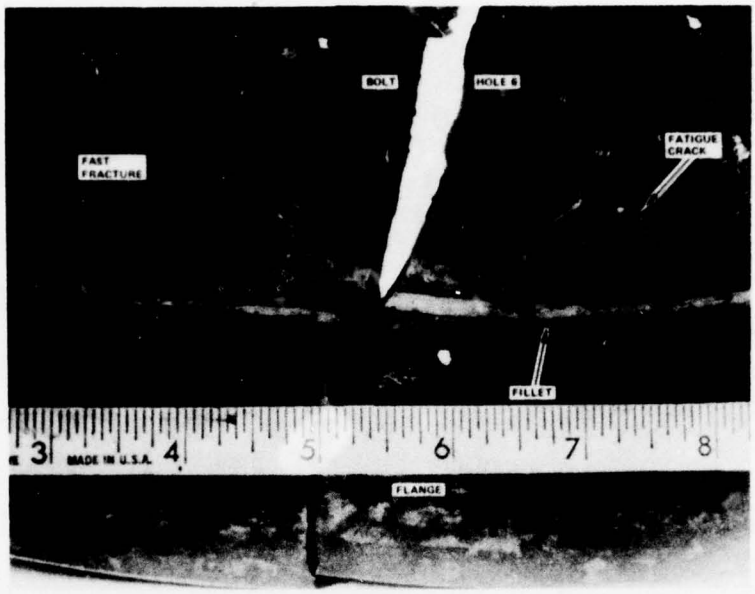

Figure 12a - Fatigue Crack Juxtaposition,
Bolt Hole 6

Figure 12b - Crank Disk 1

Figure 12 (Continued)

Figure 12c - Crank Disk 2

Figure 12d - Crank Disk 3

Figure 12e - Crank Disk 4

Figure 12f - Crank Disk 5

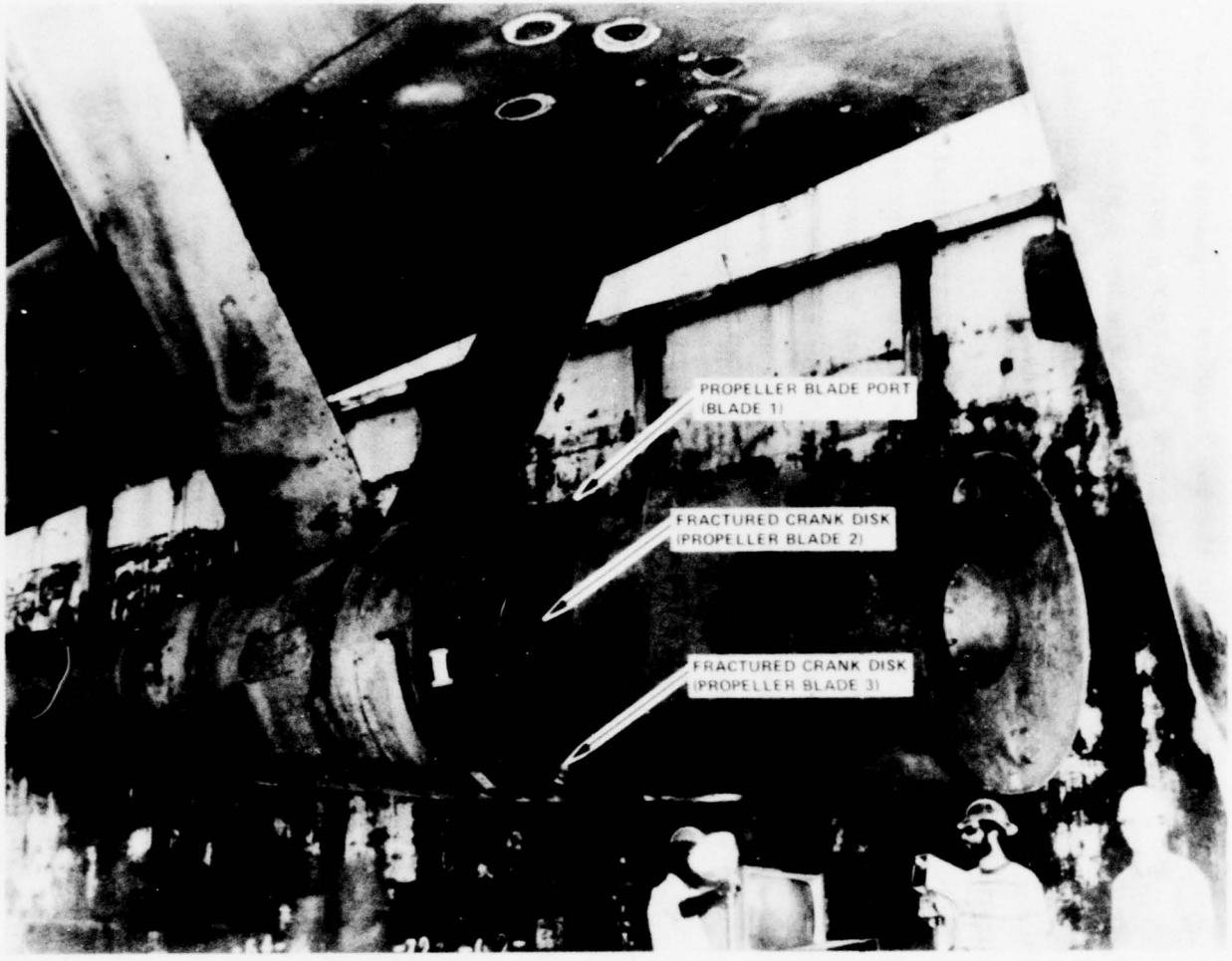

Figure 13 — BARBEY in Drydock after Failure of Crank Disk

Examination of the failed parts after drydocking showed the crank disk material had very low fracture toughness, making the disk susceptible to catastrophic brittle fracture at less than yield strength when accompanied by a critical crack in the structure. Since fatigue cracks were found in Crank Disk 1, it was speculated that the low fracture toughness together with a crack (or inclusion) weakened the crank disk to the point where a fast fracture occurred. As the propeller rotated, the No. 2 blade struck the No. 1 blade and broke. This continued in domino fashion, resulting in the loss of all blades. The disk fracture patterns also tended to support this interpretation of the failure mode.

A review of the BARBEY CPP design indicated that, if basically the same assumptions were made, the failure would not have been predicted by using any of the current design techniques. This was not necessarily a shortcoming of the design procedures since the loads imposed on the structure during maneuvers were not well defined. This design review, however, did suggest changes in the bolt, crank disk, and hub to improve some questionable areas of their design. These are listed in Table 4 and shown in Figure 14.

Following this failure, NAVSEC initiated numerous projects within the Navy organization and with private contractors. The immediate objective was to review current CPP design improvements for the restoration of BARBEY and for latest and future Navy CPP's. The ultimate objective was to develop satisfactory design criteria for all CPP's. The projects can be divided into three investigative areas: (1) material analyses, (2) design analyses including paper studies and laboratory tests, and (3) full-scale measurements of propeller component loads and stresses on BARBEY.

As part of the third phase, DTNSRDC submitted a proposal and was authorized to conduct underway measurements on BARBEY.* The main body of this report is concerned with the work done on BARBEY and its possible applications to:

---

*NAVSEC letter:6148/JJA 9440 Serial 468 dated 19 September 1974, and DTNSRDC letter:9440/7100/1962:AZ dated 2 October 1974.

TABLE 4 - MODIFICATIONS RECOMMENDED FOR BARBEY CPP SYSTEM AFTER CRANK DISK FAILURE

Crank Disk

1. Eliminate radial bearing and increase radial diameter from 19.625 to 20.435 in. This will increase wall thickness at dowel from 5/32 to 23/32 in. thus reducing the stresses in this area.

2. Eliminate inner bearing and increase flange thickness from 2.156 to approximate 2.561 in. plus the amount LBNS machines off hub to give true bearing surface (0.024 to 0.026). This will reduce the bending stresses in the flange.

3. Lengthen the dowel pin hole from a depth of 2-7/16 in. by using a flat bottom drill and a 1/8 in. radius at drill corner. This will lower stress concentration factor at the drill corner and move corner away from the fillet area.

4. Lengthen bolt hole from a depth of 3-1/4 to 4-1/2 in. by a flat bottom drill and a 1/8 in. radius at drill corners. Bottom tap the hole to give maximum thread engagement. This will move the high loads at the ends of the bolt threads away from the fillet.

5. Use a 3/8 in. radius tangent to radial surface and lower thrust surface. This will lower the stress concentration factor at the fillet.

6. Nitride only the crank pin areas. This will avoid making all other area hard and brittle where it is not necessary.

Bolt

1. Increase thread length by 1/8 in. and taper threads 0.0025 in. per 1 in. of length. This will distribute the load more evenly through the threads and insure thread engagement above and below the fillet area, putting the fillet in compression.

2. Grind the thread roots smooth to eliminate stress concentrations in this area.

3. Increase the shank length to 7/8 in. to accommodate the increase in the bolt hole depth of the crank disk.

Hub

1. Bevel the hub in the way of the 3/8 in. to accommodate NSRDC strain gages.

2. Groove hub bearing surfaces every 15 deg. to a depth of .030 and a width of .040 in. This will provide an optimum bearing surface.

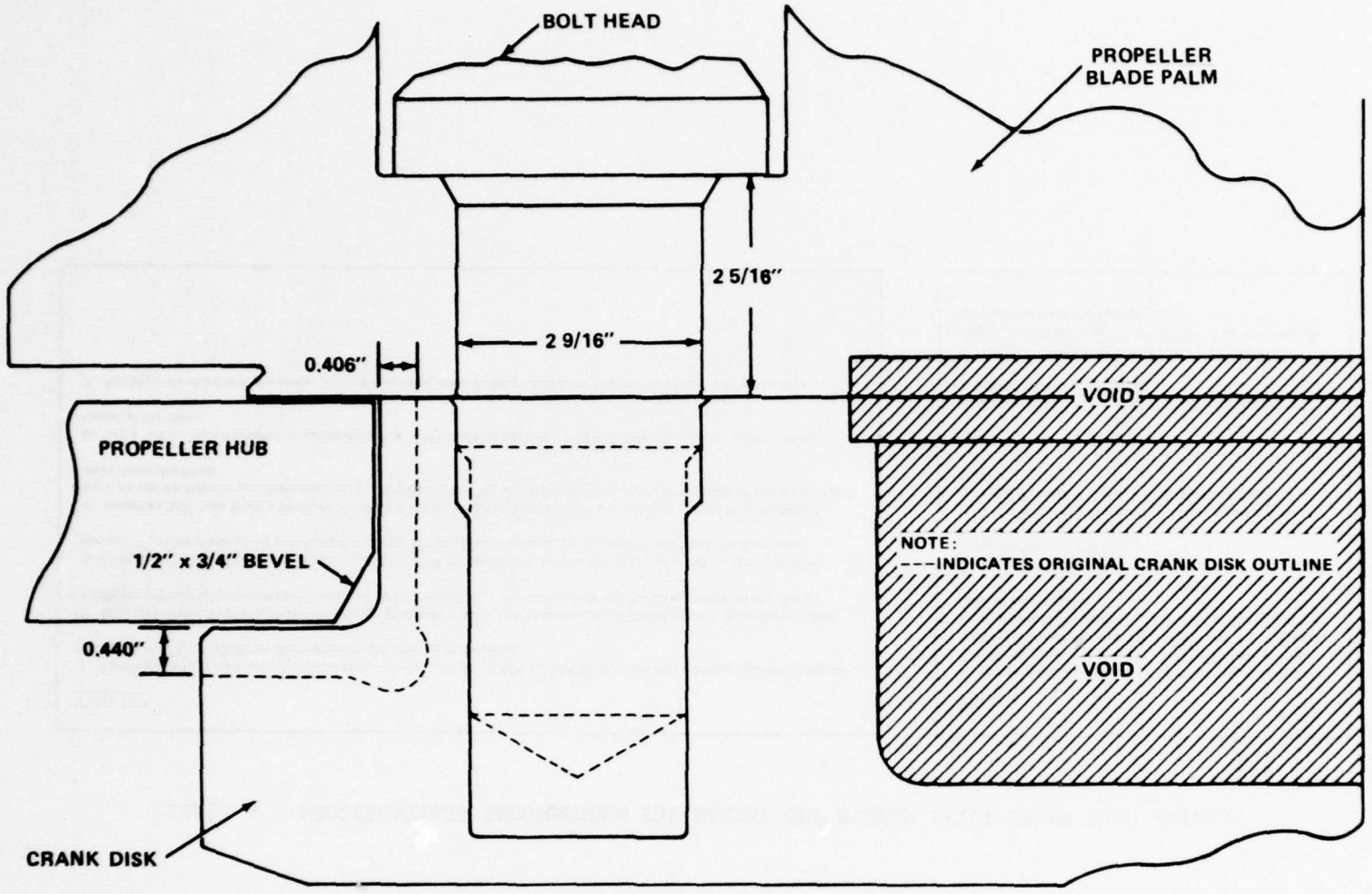

Figure 14 - Crank Disk and Propeller Hub Modifications for BARBEY CPP System

1. The failures experienced by the CPP on BARBEY.
2. The interpretation of propeller blade forces.
3. CPP component stresses as related to design criteria.

These were seen as the immediate (primary) objectives of the BARBEY trials. In addition, this opportunity was utilized to gain necessary background information on propeller blade pressure measurements and signal transmission for the unique instrumentation projected for the SPRUANCE trials.

Preliminary results related to the primary objectives were given orally[6,7] and in informal reports.*,**

APPROACH

In order to achieve the objectives of the BARBEY full-scale trials, an approach was developed to satisfy both the short-term and long-term goals. This approach, which is outlined in Figure 15, basically involved development of suitable instrumentation and a test plan to define th CPP system component stresses as well as provide reasonable indication of the propeller forces. Measurements were to be compared to criteria in order to determine the suitability of the design and this information used to check the validity of the failure analysis of the BARBEY CPP and to develop modifications and/or operational restrictions, if necessary. The information from the BARBEY trial would be documented for use in continuing long-range research and development work in the areas of blade strength, propeller loads, and CPP system design.

---

*Presented informally by C. Noonan and G. Antonides as Enclosure 1 (Preliminary Report on the USS BARBEY (FF-1088) CPP Mechanism Tials) to DTNSRDC letter:1962:CJN, 9870.1 dated 22 April 1975.

**DTNSRDC letter:196:CJN, 9073/Noise,9094/BARBEY dated 29 January 1976.

[6]Presentation 2 to NAVSEA Representatives, DTNSRDC/Carderock (May 1975). "Interim Data on the USS BARBEY (FF-1088) CPP Trials."

[7]Presentation 3 to NAVSEA Representatives, DTNSRDC/Carderock (27 June 1975). "Interim Data on the USS BARBEY (FF-1088) CPP Trials."

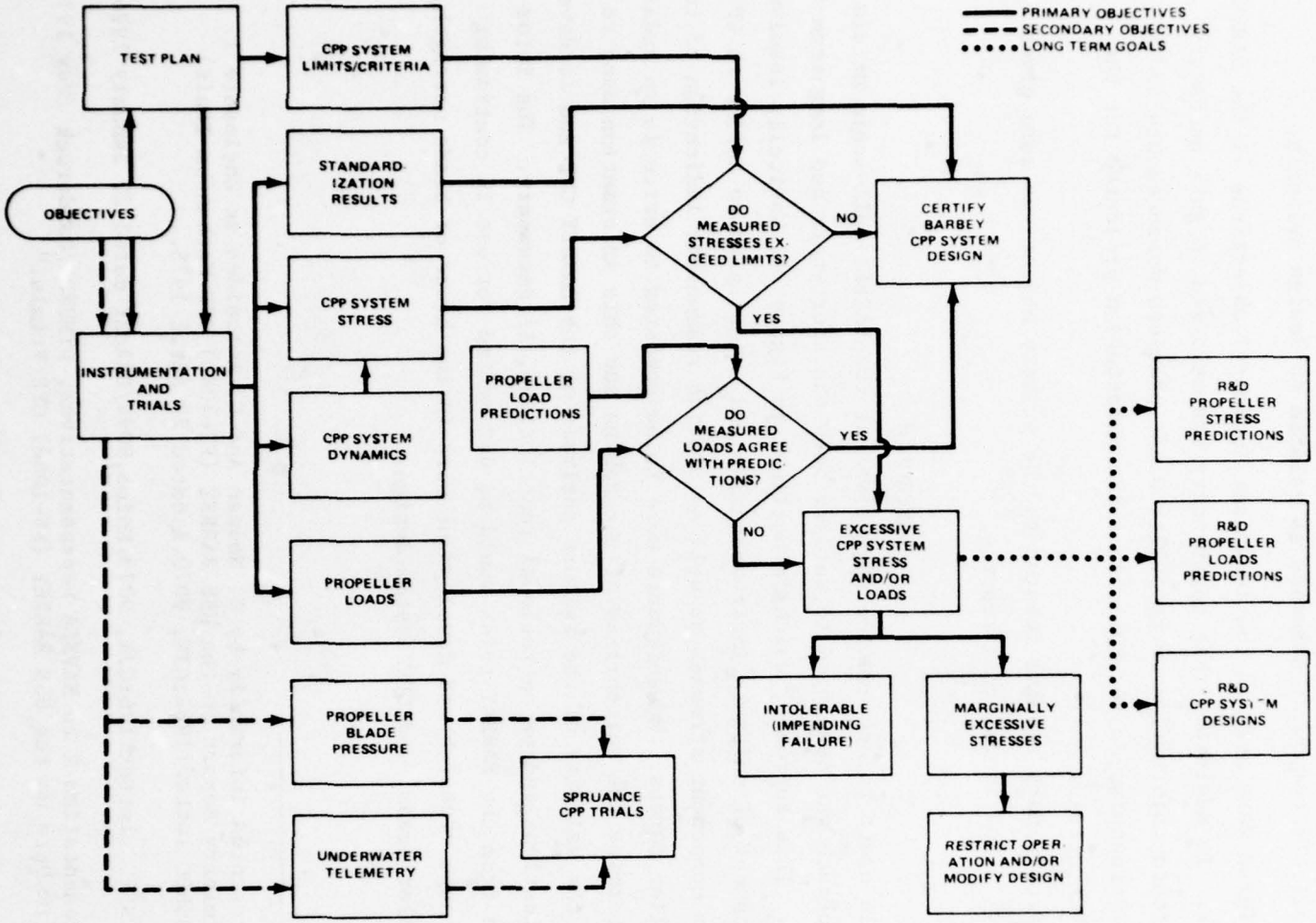

Figure 15 - Implementation Plan for Full-Scale, Underway Propeller Measurements on BARBEY

Parallel with this effort to achieve the primary objectives, instrumentation was developed to obtain necessary information in areas of technology which would be needed for projected CPP trials of SPRUANCE. These were considered secondary and were done on a "not to interfere" basis. The instrumentation and criteria used to obtain primary objectives are described below. Details of secondary instrumentation is given in the section on instrumentation.

MEASUREMENTS OF CPP SYSTEMS COMPONENT STRESSES

Considering the structural complexity and the undefined loading mechansim of the BARBEY CPP system, all CPP system components from the propeller blades to the line shaft should ideally have been instrumented with a large number of strain gages. However, pragmatic considerations involving the instrumentation and the restoration schedule of the ship limited the number of gages which were actually installed. Gage locations were selected mostly on the basis of engineering judgment and modified to reflect laboratory test results.

1. Strain gage rosettes were installed on the face* of Propeller Blade 4 and on both the face and back* of Propeller Blade 5; see Figure 16.

2. Strain gages were installed on the shanks of al[illegible] bolts of Propeller Blade 2; see Figure 17. The gages were arrange[illegible] measure the axial and bending loads which might occur during installation and trials.

3. Strain gages were also installed on the crank disk of Propeller Blades 2 and 4; see Figure 18. Crank disk gages were stacked rosettes, single gages, and strip gages. The strip gages were used to define the distribution of stress in the fillet area; see Figure 19.

4. Gages were placed on the propeller hub to define the state of stress at critical areas; see Figure 20.

---

*Blade face (aft side) is the pressure side of the propeller blade for ahead operation. Blade back (forward side) is the suction side of the propeller blade for ahead operation. For this CPP installation, the propeller shaft had the same propeller shaft rotation (clockwise looking forward) for both ahead and astern operations.

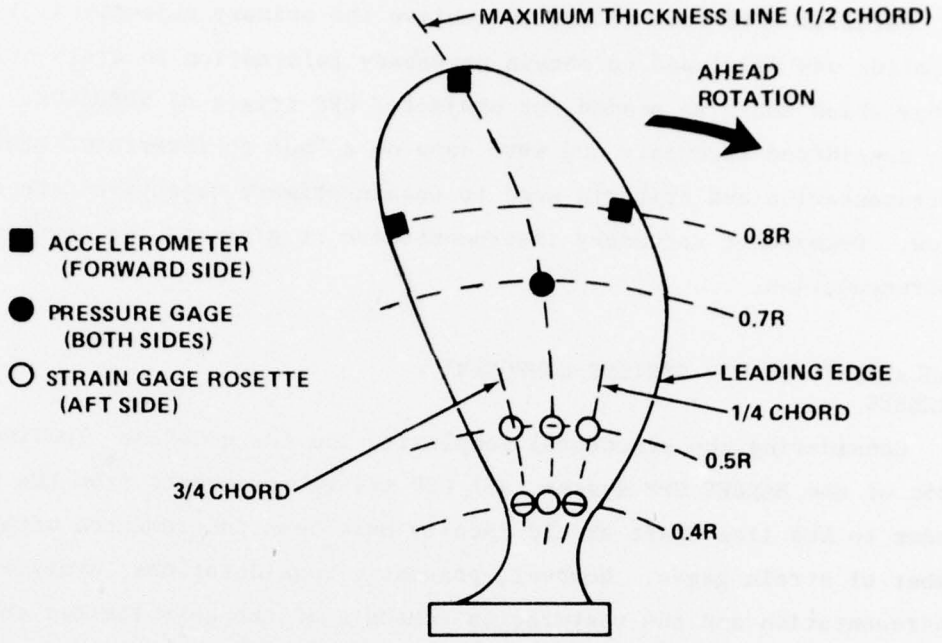

Figure 16a - Propeller Blade 4

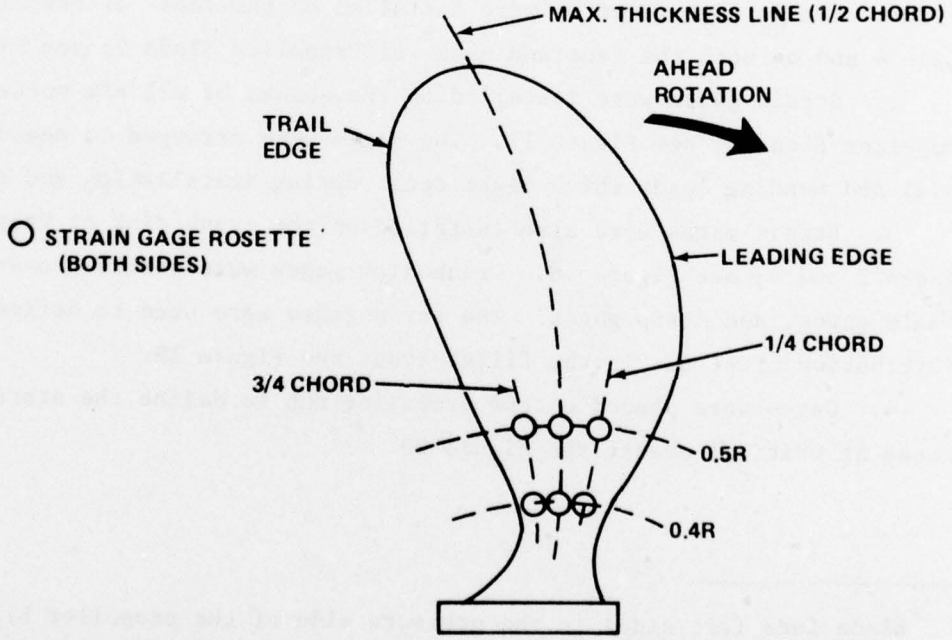

Figure 16b - Propeller Blade 5
Figure 16 - Propeller Blade Gages

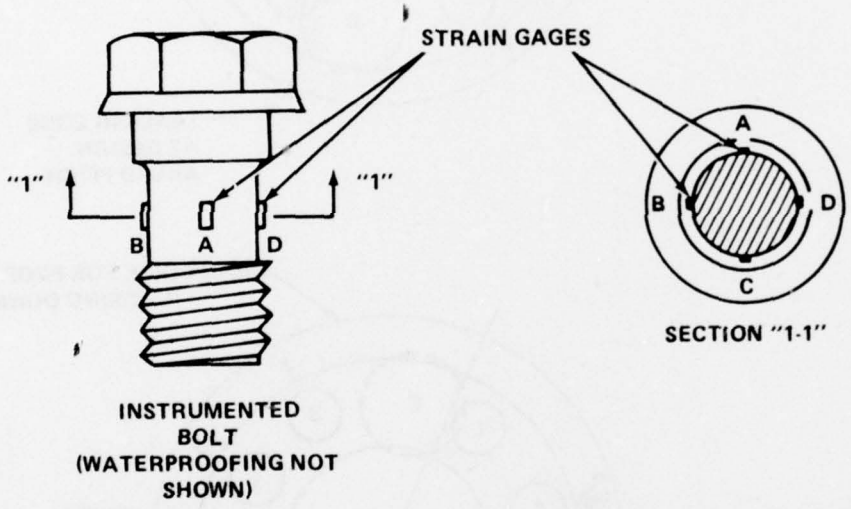

Figure 17 - Propeller Bolt Gages

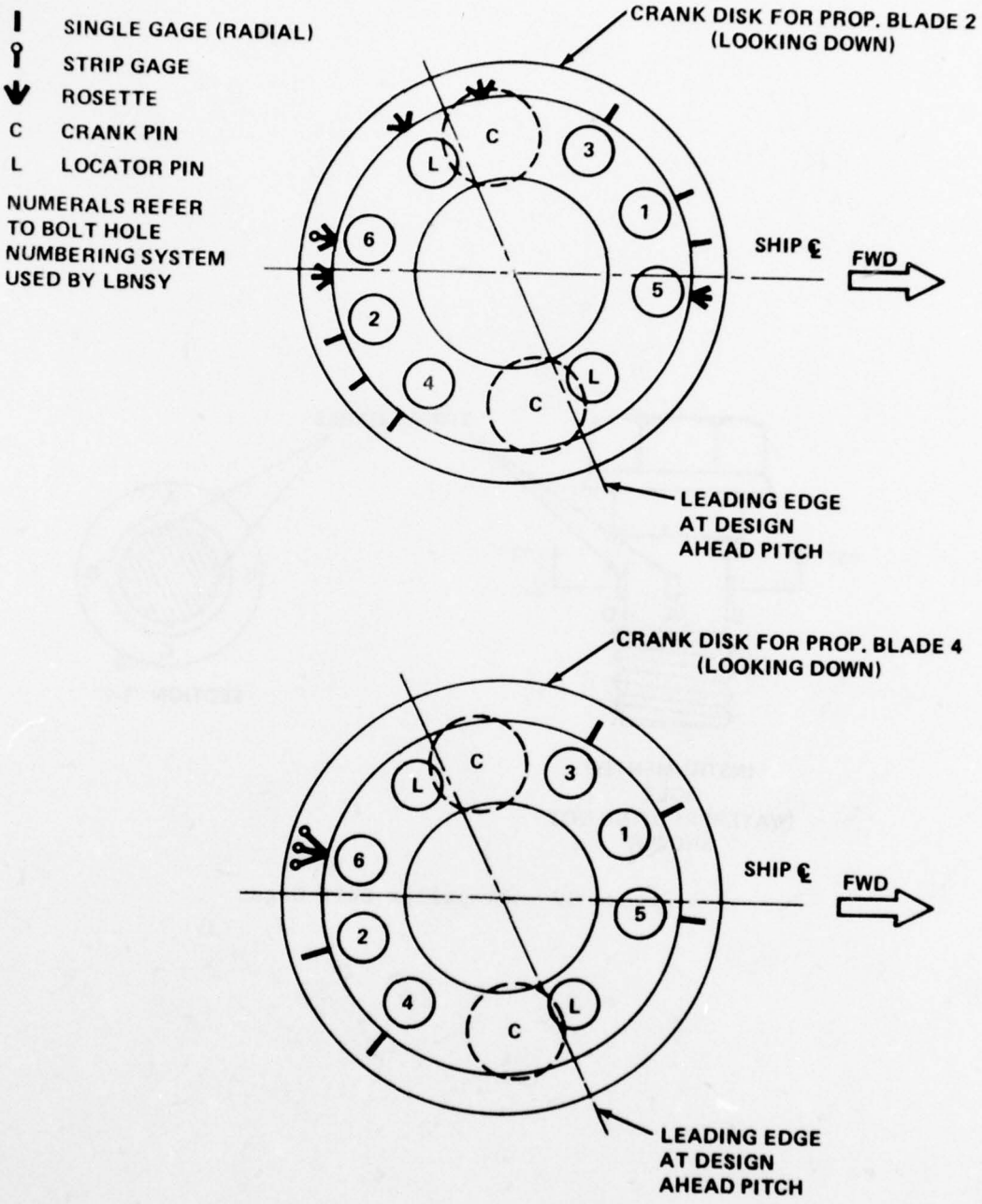

Figure 18 - Crank Disk Gages

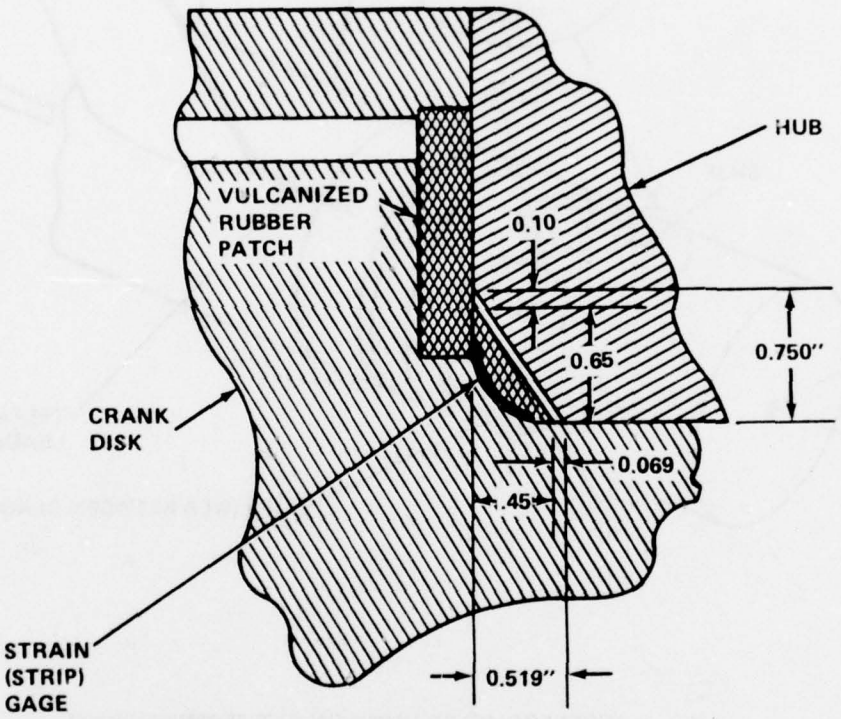

Figure 19 - Details of Modified Crank Disk

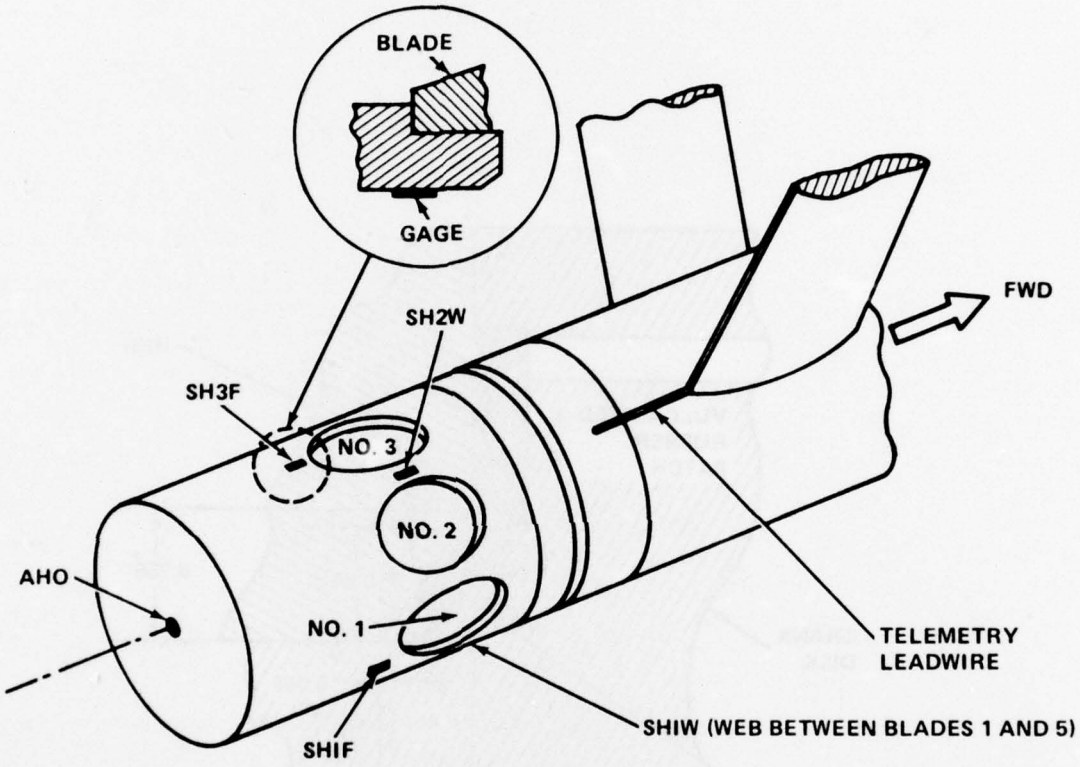

AHO = ACCELEROMETER HUB ℄ (IN AFT TERMINAL BOX)

SH1F, SH3F = HUB STRAIN GAGE ON CRANK DISK BEARING FLANGE

SH1W, SH2W = HUB STRAIN GAGE ON WEB BETWEEN PROPELLER BLADE HOLES

TELEMETRY LEADWIRE WAS IN 1/4" STAINLESS STEEL TUBE FROM STRUT BEARING TO HULL PENETRATION

Figure 20 - Propeller Hub Gages

5. Torque and thrust bridges were placed on the inboard lineshaft to record the mean and alternating valves of shaft torque and thrust; see Figure 21.

DETERMINATION OF PROPELLER FORCES

Proper interpretation of the measured response (stresses) in the CPP system requires a better understanding of the mean and alternating propeller forces which act on the system under all operating conditions. If measured stresses deviate grossly from the design predictions, it could be a result of errors in either the design analysis procedure, the force predictions, or both. Full-scale, underway propeller blade forces (pressure) have never been measured; therefore, a secondary force indication technique had to be used. Its development was based on the fact that the BARBEY propeller blade was essentially wide bladed (i.e., the blade aspect ratio was approximately equal to 1) and knowledge that the blade response for wide-bladed propellers can be considered to be beamlike for steady loading.[8] It was hypothesized that if blade (and/or system) frequencies were sufficiently high to ensure subcritical operation,* then the measured response on the blade could be used to calculate the blade load provided pertinent blade geometric properties were known. Instrumentation of propeller blades, and propeller shafts (strain gage rosettes and accelerometers — Figures 16, 20, and 21) was chosen to validate these assumptions as well as to provide input to propeller force calculations. In order to appreciate the simplicity of this approach to estimating blade forces, it must be realized that minor discrepancies from calculations were not considered. If the strength analysis technique for the CPP was reasonable, then one explanation for gross differences between measured stresses and calculated predictions (other than, or together with, the metallurgical weaknesses

---

[8] McCarthy, J. and J. Brock, "Static Stresses on Wide-Bladed Propellers," NSRDC Report 3182 (Feb 1970).

* Subcritical to the first blade mode ($\omega/\omega_n \approx 0.3$) or sufficiently removed from blade and system criticals so as not to experience any dynamic amplification.

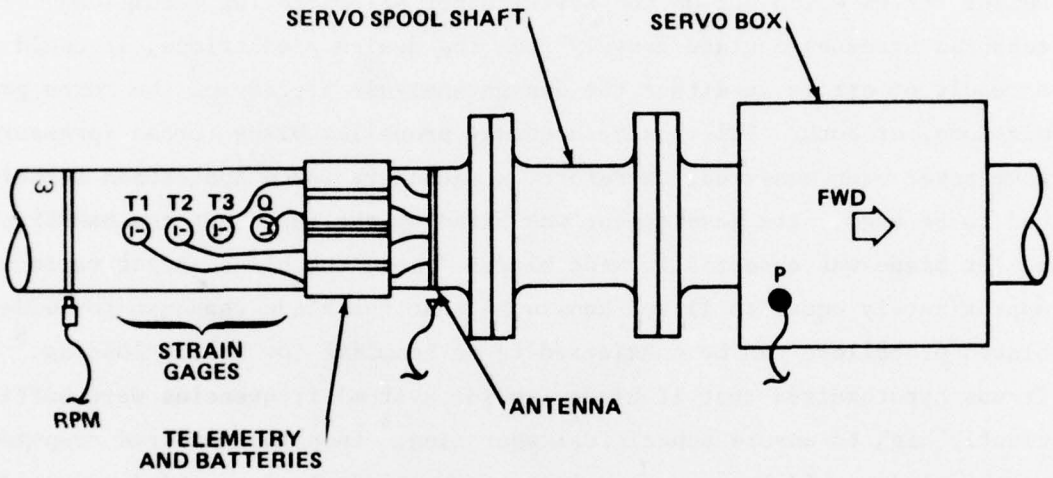

QUANTITIES MEASURED

- Q – MEAN AND ALTERNATING TORQUE
- T1 – MEAN AND ALTERNATING THRUST
- T2 – MEAN AND ALTERNATING THRUST
- T3 – MEAN AND ALTERNATING THRUST
- W – SHAFT RPM (INDEX PROP. BL.1 AT 12 O'CLOCK POSITION)
- P – PROPELLER PITCH
- R – RUDDER ANGLE (LOCATED IN AFT. STEERING RM.)

Figure 21 - Propeller Line Shaft Instrumentation

previously referred to) could be gross errors in the predicitions of mean (and/or alternating) propeller forces. Since one of the actual failures occurred during a crashback maneuver, there was considerable speculation regarding the actual propeller blade forces during this and other maneuvering conditions. Accordingly, the original CPP design (strength) calculations were reviewed to quantify the magnitude of the errors that could be tolerated in measuring the underway blade loads. These calculations showed that the component factors of safety (FS) ranged from 2 to 10; the failed parts — blade bolts and crank disks — had factors of approximately 6 and 5, respectively.* It was felt that considering all the vagaries involved in such design procedures, the proposed measurement technique would be capable of indicating ratios between "measured loads" and predictions on the order of the assumed FS (>2). Likewise, any ratios less than this (<2) would indicate that the actual underway loads would not significantly contribute to the failures, provided, of course, that the design calculations were correct.

TRIAL LIMITS/CRITERIA

In the interest of safety and to avoid jeopardizing the future trial schedule of the ship and the CPP system, decisions were made regarding the stress limits that should not be exceeded in the instrumented components during trials. In a sense, this was somewhat paradoxical to the objective of obtaining actual stress information on the CPP hub mechanism in a realistic (unrestricted) operating environment which at that time was practically nonexistent and sorely needed.

There was also the possibility that despite being accurate, the recorded information might not represent the areas of highest stress since the number of gage locations was somewhat limited. In addition, the nature of the individual series of test factors into the ability of evaluating the data for comparison against established criteria. For example, the incremental speed runs enabled the monitoring and evaluation of stress patterns

*As indicated by hub stress calculations of Liaaen Model D132/5 prepared by Propulsion System, Inc., under Job 1373-1 of 22 October 1969.

in a manner which allowed a reasonably accurate prediction of the results of subsequent runs to minimize the possibility that any established criterion would be exceeded. On the other hand, maneuvers or other nonsteady state conditions were not amenable to that treatment; because of their transient nature, they could not be controlled to meet any predetermined limits. Furthermore, it was the maneuvers per se, that yielded the most important information from a design point of view.

Other unpredictables such as structural flaws, component failures other than the blade-bolt-crank disk assembly, etc., that could cause maloperation of the CPP stystem, were statistically possible, thereby precluding any guarantee that some sort of a system failure would not occur during the trials.

The above discussion was intended to provide a background against which the utility of any full-scale trial limits could be viewed. Accordingly, specific limits were established for stresses in the blade-bolt-crank disk assembly, including the rationale behind their development.

Generally speaking, mechanical and structural failures are due to fatigue problems of one sort or another, i.e., low or high cycle fatigue. Therefore, the fatigue characteristics of the components in question were considered in setting the limits of stress that should not be exceeded during the conduct of the trials. More specifically, the limits were considered on the basis of a SODERBERG diagram in order to properly account for the combined effects of mean and alternating stress. Furthermore, consideration was given to the effects of saltwater corrosion and the nature of the trial event, i.e., whether it was steady state or a maneuver.

From a conservative standpoint, the fatigue limits were based on factors pertaining to high-cycle fatigue (10^8 cycles) which results in the lowest possible fatigue stress. Less than 10^6 cycles were accumulated during the trial period.

Such maneuvers as crashbacks and hard turns were viewed in terms of producing stresses that would tend to yield the components in question. Therefore, limiting stresses for maneuvers were based on the yield stresses

of pertinent materials. Limited results of the PG-100 propeller stress trials were used to estimate the effects of a crashback prior to its execution. Figure 22 graphically illustrates the radial stress of the PG-100 propeller at the 0.4 radius (midchord) as a function of the various phases of a crashback. In this case, the maximum stress was about twice that which occurred during full-power, steady ahead operation. Assuming that BARBEY would behave in a similar manner, the judgment on executing a crashback was based on the stress levels that occurred during full-power ahead conditions. For example, if when multiplied by a factor of 2, the full-power, steady ahead stresses in the blade-bolt-crank disk assembly were less than the yield stresses of the respective materials, then crashback maneuvers were executed without reservations. If, on the other hand, they exceeded the yield stresses, then a somewhat restricted form of crashback was executed in order to gradually approach the stress levels.

Fatigue limits and yield point stress data used for developing stress limits for the various materials in the blade-bolt-crank disk assembly were obtained from DTNSRDC Code 2814; see the metallurgical properties indicated in Table 3.

1. The CPP on BARBEY was made of nickel-aluminum-bronze (Alloy 1). Since it operated in a saltwater environment, a corrosion fatigue stress of 12,500 psi was used for limiting the alternating stresses. The yield point for this material is 35,000 psi based on MIL-B-21230. The top graph in Figure 23 illustrates the relationship of the steady and alternating stresses used to establish the limiting conditions for propeller blades.

2. The propeller bolts were made of 17-4 PH stainless steel with a heat treatment at 1150F. The threaded portion of the bolts contained significant stress concentrations; therefore, a notched fatigue value of $K_t=3$ was used. Although the stressed portion of the bolts is theoretically in an "air" environment, there was a possibility of saltwater penetration on a long-term basis. However, since the trial was of relatively short term in nature, an in-air notched fatigue value of 30,000 psi was used for the

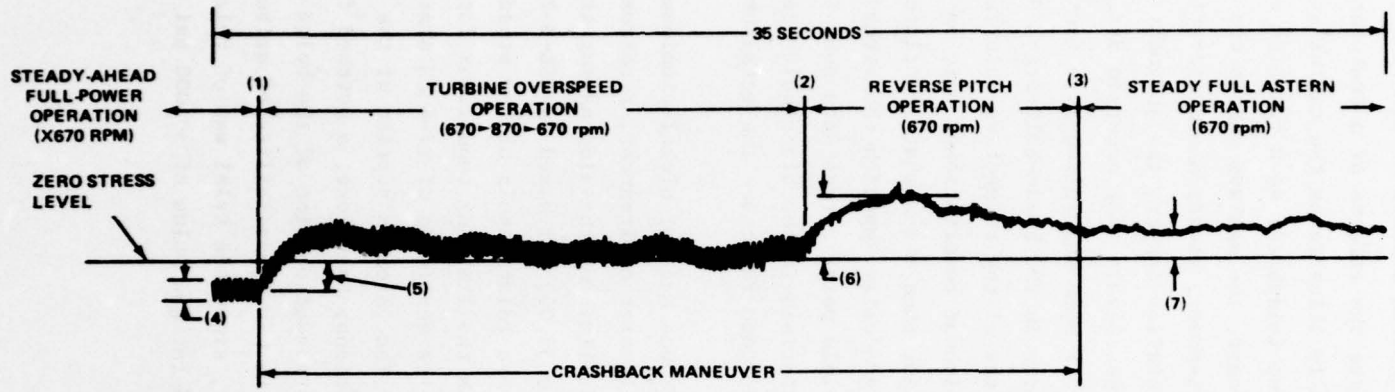

NOTES:
(1) EXECUTE CRASHBACK (FULL AHEAD PITCH TO ZERO PITCH, TURBINE OVERSPEEDS, GOVERNOR PREVENTS FURTHER PITCH CHANGE UNTIL SYSTEM IN CONTROLLED TO APPROX 670 rpm
(2) REVERSE PITCH OPERATION
(3) STEADY FULL ASTERN OPERATION
(4) STEADY FULL POWER ALTERNATING STRESS (±3,700 psi) SHAFT FREQ.
(5) STEADY FULL POWER MEAN STRESS (12,400 psi)
(6) MAXIMUM CRASHBACK MEAN STRESS (26,900 psi)
(7) AVERAGE STEADY ASTERN MEAN STRESS (10,600 psi)
(8) STRESSES INCLUDE HYDRODYNAMIC AND CENTRIFUGAL LOADS

Figure 22 - Radial Stress Measured on the DOUGLAS Propeller Blade at the 40-Percent Radius (Midchord)

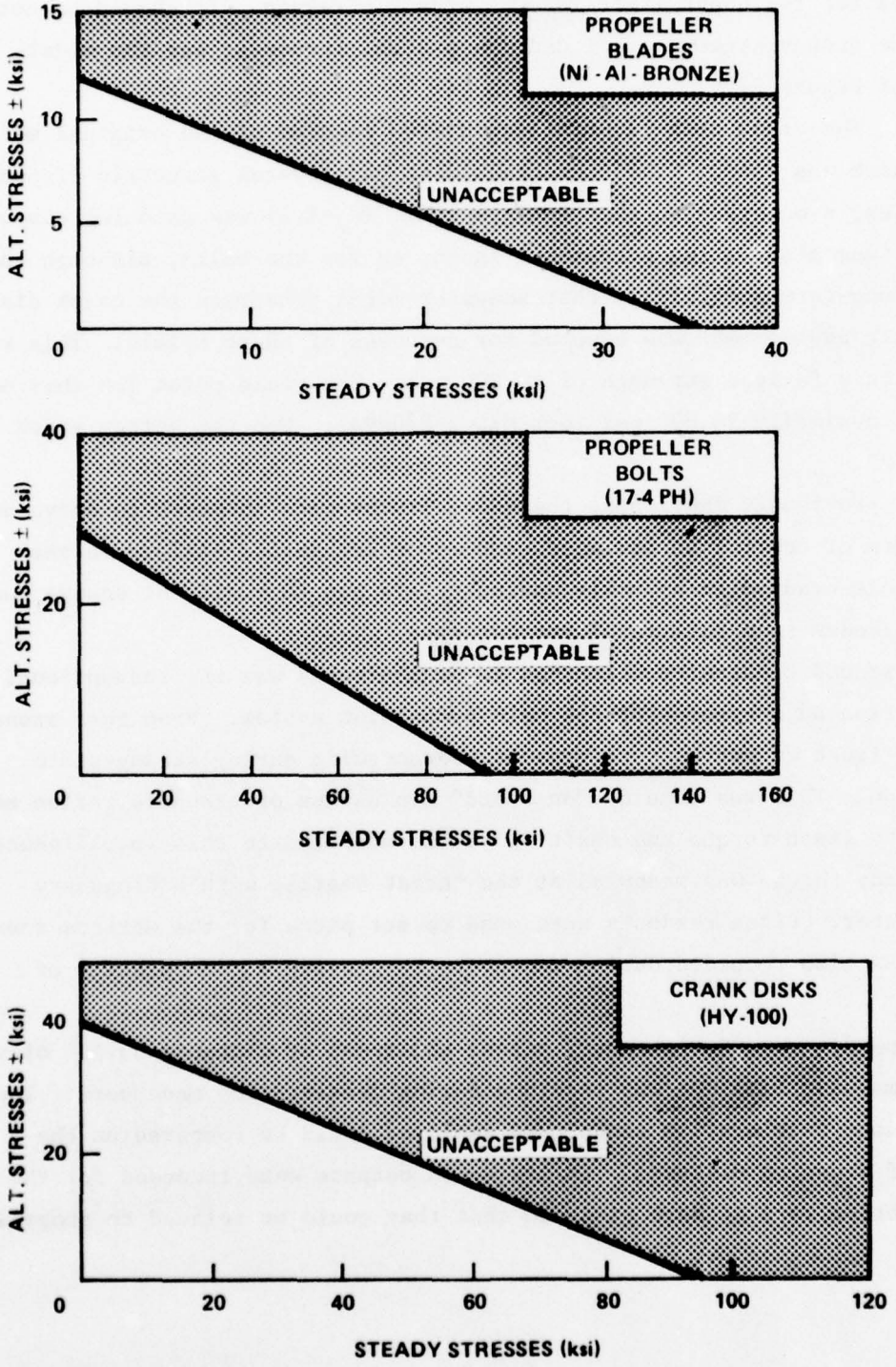

Figure 23 — Stress Limits for Propeller Blades, Bolts and Crank Disk for BARBEY Trials

alternating stress limits. A yield point of 94,400 psi (per MIL-S-81506A) was used for the upper limit for the steady stresses. It should be noted that the steady stresses included the preload stresses; see the middle graph of Figure 23.

3. The crank disk material was HY-100 instead of the original material which was 4340. Since the crank disk had several geometric discontinuities, a moderate notched fatigue limit (K_t=1.3) was used for computing the maximum alternating stresses. Again, as for the bolts, although there was a long-term possibility that seawater might penetrate the crank disk, an in-air environment was assumed for purposes of these trials. This resulted in a fatigue strength of 40,000 psi. The yield point for this material is nominally 94,000 psi (per MIL-S-23009A). See the bottom graph of Figure 23.

As previsouly mentioned, the above limits were intended to serve as some form of control to minimize chances of mechanical failure in the blade-bolt-crank disk assembly during trials but they did not ensure complete freedom from failure of another type.

A second constraint which had to be monitored was the conventional restriction on overtorquing the main propulsion system. From this standpoint, Figure 24 was used to prevent overtorquing during steady-state operation. This was done by "on-board" evaluation of standardization measurements (mean torque and shaft rpm). In addition to this intelligence, the steady thrust was measured at the thrust bearing with a Kingsbury thrustmeter. Pitch readouts were used to set pitch for the various runs. Pitch was also recorded during maneuvers to provide a time history of pitch.

Depending on the maneuver, either the speed or distance output of the electromagetic (EM) log was recorded during deceleration maneuvers. Thus, the various deceleration techniques employed could be compared on the basis of stopping distance. EM log speed outputs were recorded for the deceleration runs at zero pitch so that they could be related to propeller loads.

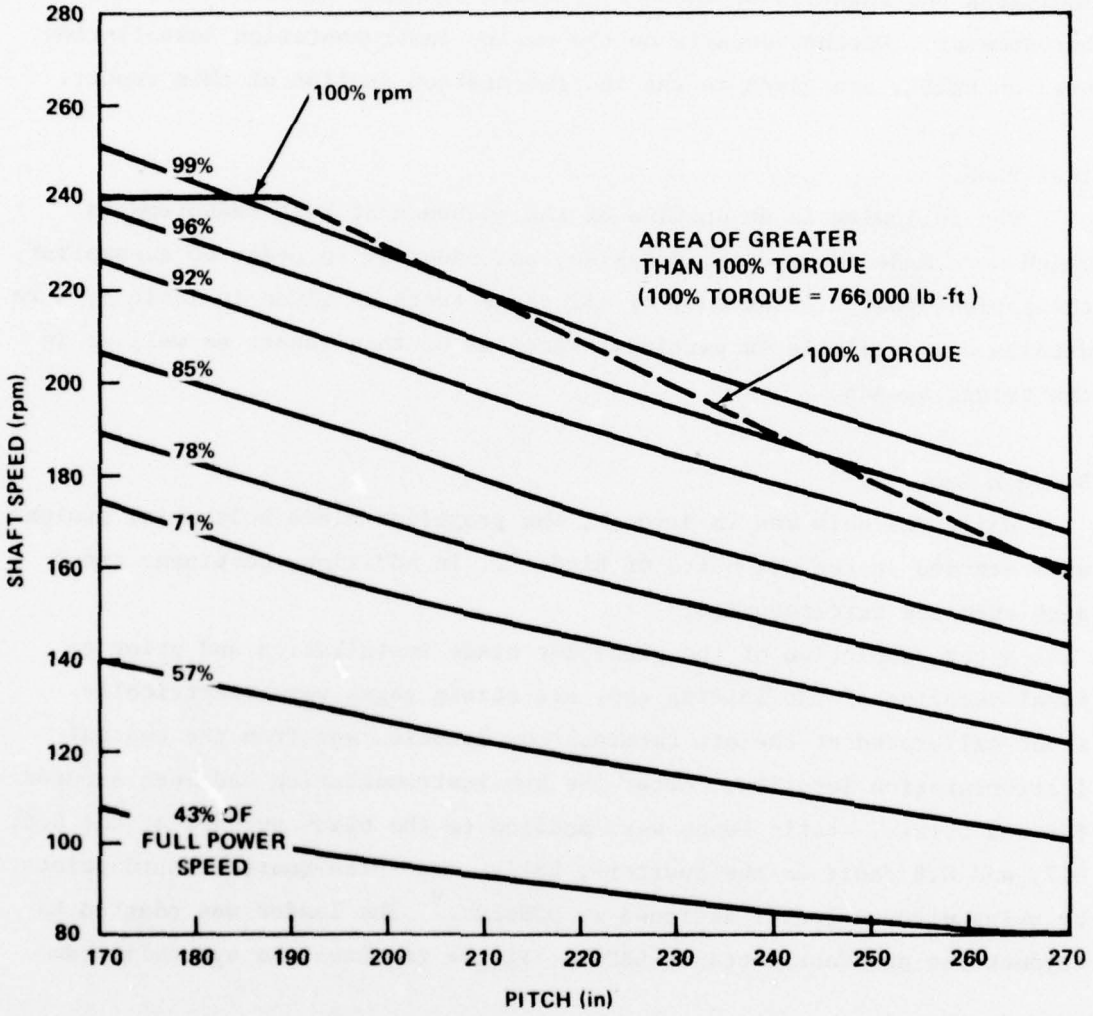

Figure 24 - BARBEY Operating Limits for Separate Mode of Control above Design Pitch of 190 Inches

The CPP hydraulic system was instrumented to measure main hydraulic pressure, Servo A pressure, and Servo B pressure. These pressures were measured external to the main propulsion shaft. The point of measurement was quite remote from the propeller hub in which the pitch changing mechanism is housed. Figure 25 is a sketch of the shafting arrangement and indicates the location of the CPP pressure pickups, torsionmeter, and thrustmeter. Further details on the entire instrumentation installation used on BARBEY are given in the instrumentation section of this report.

TEST PLAN

The following is an outline of the sequence of test measurements which were made in drydock, dockside, and underway in order to accomplish the project goals. A summary of all these tests is given in Table 5; more details are available in pertinent sections of this report as well as in the trials agenda.*

Drydock Test

While the ship was in drydock, the propeller blade bolt axial preload was recorded in the six bolts of Blade 2. In addition, pertinent crank disk stresses were recorded.

After completion of the propeller blade installation and prior to final securing of the fairing cap, all strain gages were electrically shunt calibrated at the aft terminal box location and from the central instrumentation location. After the hub instrumentation had been secured for sea trials, static loads were applied to the blade surface at the 0.6, 0.7, and 0.8 radii on the quarter-, half-, and three-quarter chord points by using a power loader designed at DTNSRDC.[9] The loader was adapted to drydock use and fabricated at LBNSY. Figure 26 shows the hydraulic ram

---

[9] "BARBEY Power Loader," DTNSRDC Drawings E-3280-1, -2, and -3 (20 Jan 1975).

* Enclosure (1) to DTNSRDC letter:1962:CJN:9870.1 dated 25 February 1975. (Agenda for CPP Mechanism Trials on the USS BARBEY (DE-1088)).

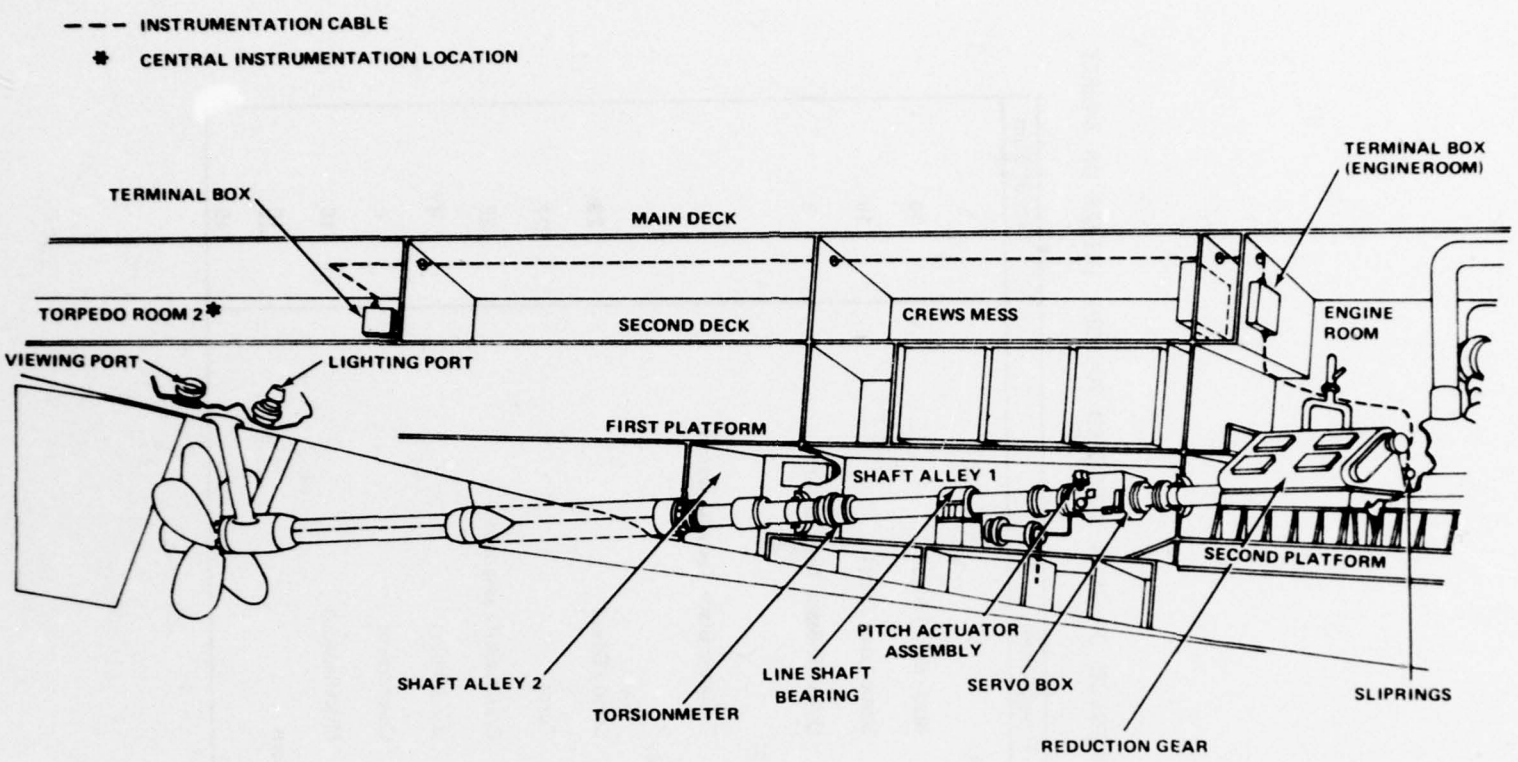

Figure 25 - Overall View of Propulsion System and Instrumentation

TABLE 5 - SUMMARY OF RUNS EXECUTED FOR CPP TRIALS ON BARBEY

Type of Run	No. of Runs
Drydock:	
Blade Bolt Torque	15
Static Load Tests	19
Dynamic Blade Tests (in air)	8
Dockside:	
Dynamic Blade Tests (in water)	2
Underway:	
Steady Speed	29
Turns	22
Crashback/Crashahead	22
Windmilling	4
Coastdowns	4
Miscellaneous	10
Calibrations	10
Total	145

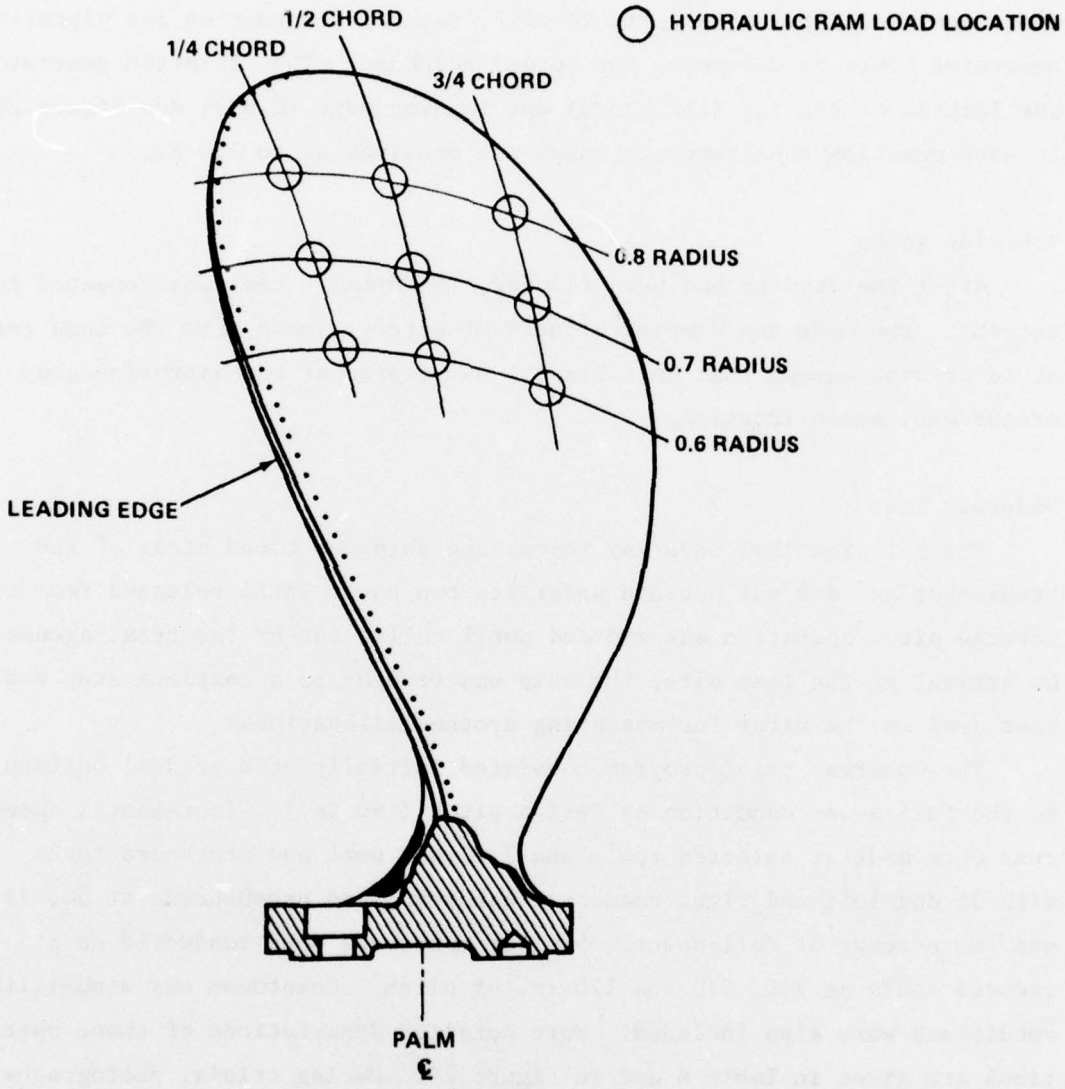

Figure 26 - Hydraulic Ram Load Matrix for Static Loads (Drydock Tests)

load matrix for the drydock tests and Figure 27 presents several photographic views of the loader. The loads were applied through hydraulic cylinders in various combinations to Blades 2, 4, and 5; see Table 6. Characteristics of the hydraulic loader are given in Table 7. Dynamic tests included impulse tests to identify natural frequencies and vibration generator tests to determine the forced response. The vibration generator was located at the tip (1/2 chord) and leading edge (0.8R); see Figure 28. In each position the frequency range was examined up to 100 Hz.

Dockside Tests

After the drydock had been flooded, the dynamic test was repeated to determine the mass and damping effects of water. These were the same tests as in drydock except that only Blade 4 was tested at one vibration generator excitation location.

Underway Test

Prior to initital underway tests, the ship was towed clear of the breakwater and did not operate under its own power until released from tow. Reverse pitch operation was avoided until called for by the trial agenda. On arrival at the test site, the ship was brought to a complete stop and kept dead in the water for measuring system calibrations.

The underway trial program consisted initially of a gradual buildup to the full power condition at design pitch (190 in.). Incremental speed runs were made at selected rpm's and included port and starboard turns with 35 deg left and right rudder, crashbacks, and crashaheads at 50, 75, and 100 percent of full power. Similar maneuvers were conducted on a reduced scale at 240, 210 and 170 in. of pitch. Coastdown and windmilling conditions were also included. More detailed descriptions of these operations are given in Table 8 and in Figure 29. During trials, photographs were taken through the propeller viewing ports in order to document the condition of the instrumentation protective coating system and the nature of the cavitation.

Figure 27 — Views of the Hydraulic Blade Loader

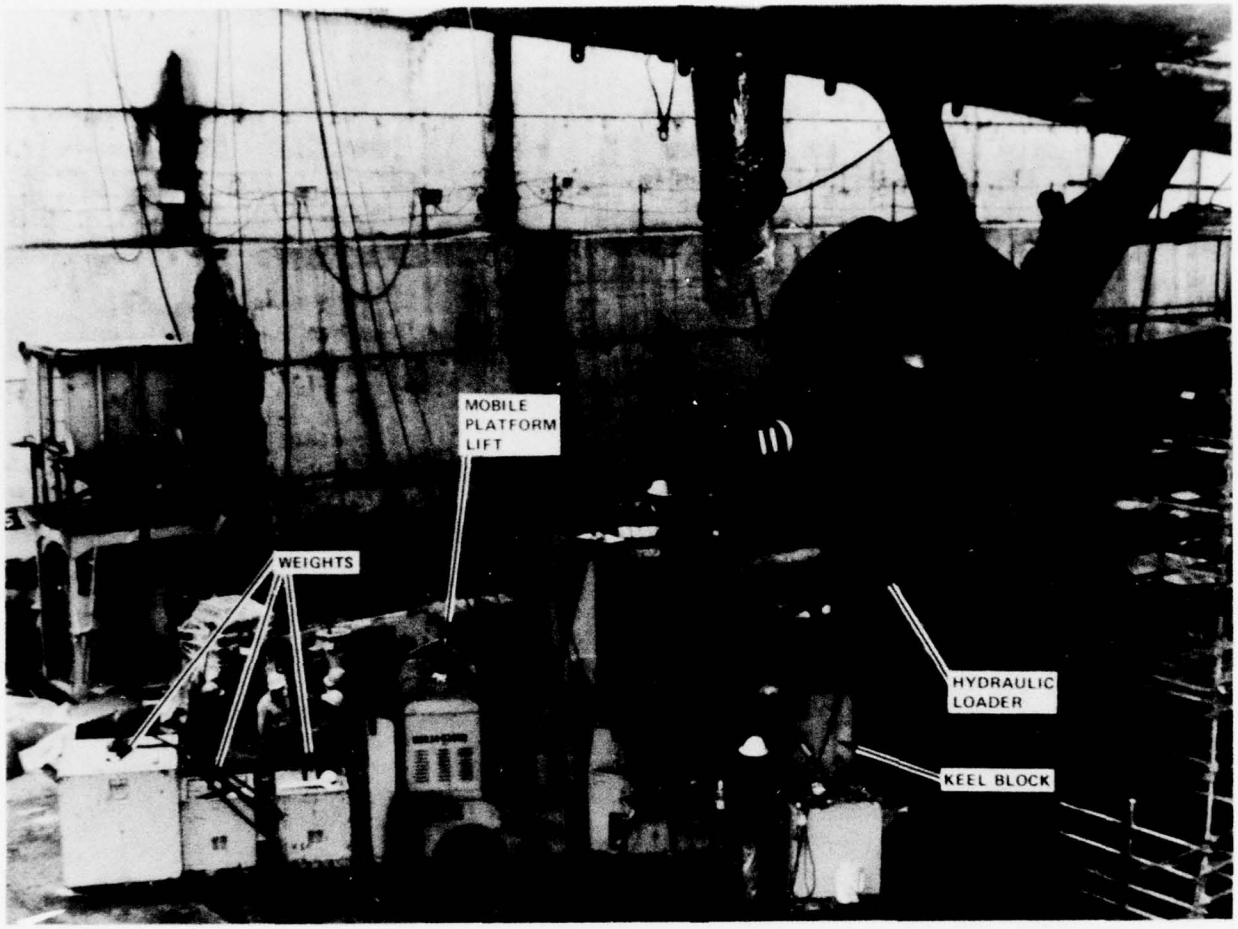

Figure 27a — Ahead Loading, General View

Figure 27 (Continued)

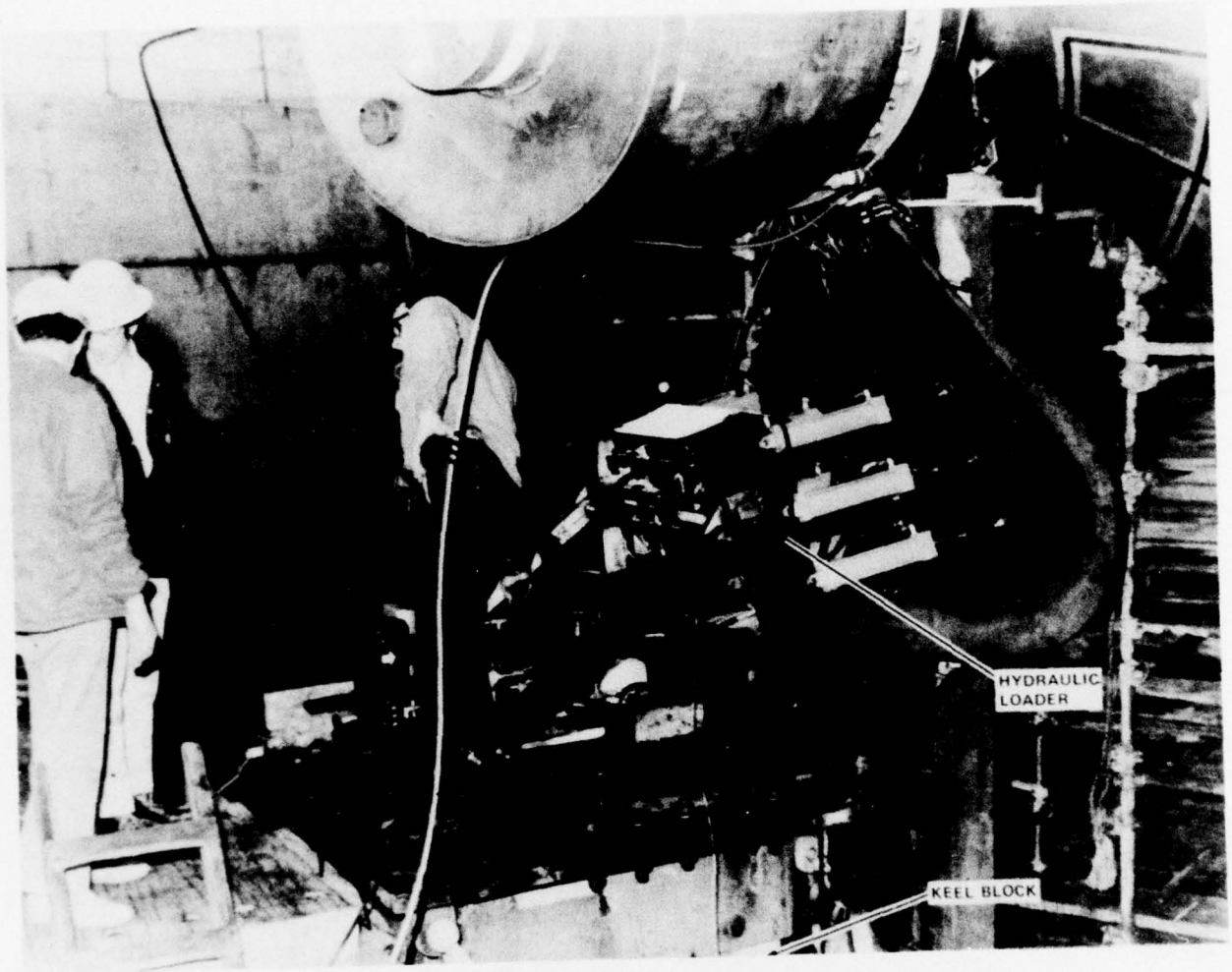

Figure 27b — Ahead Loading, Side View

Figure 27 (Continued)

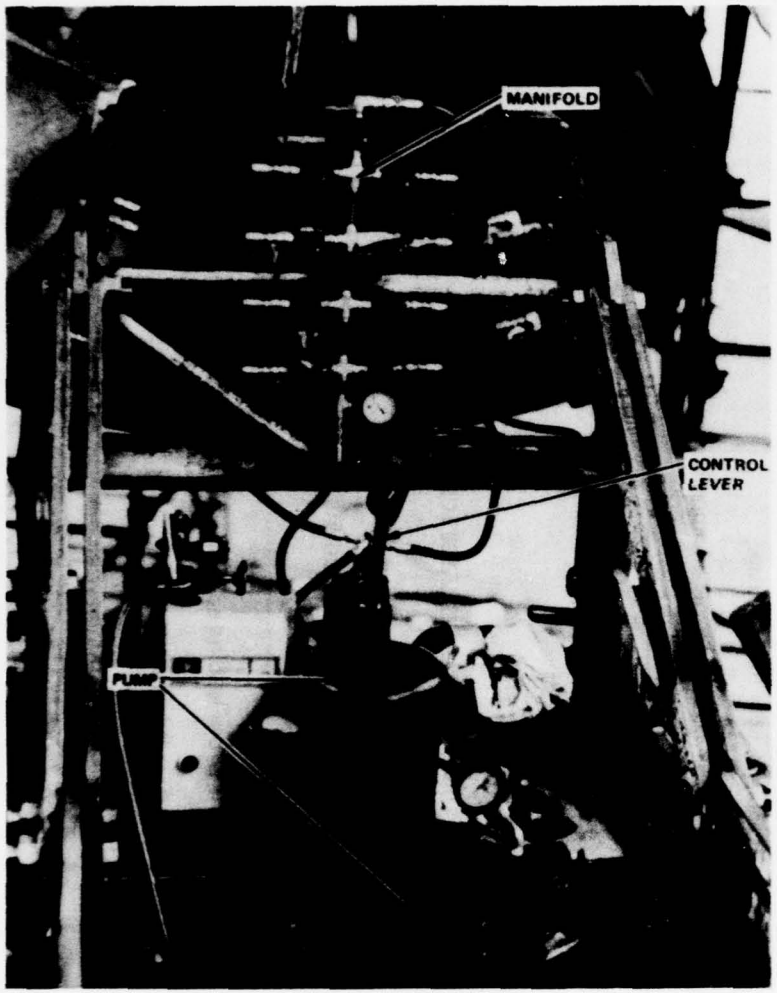

Figure 27c - End View Astern Loading

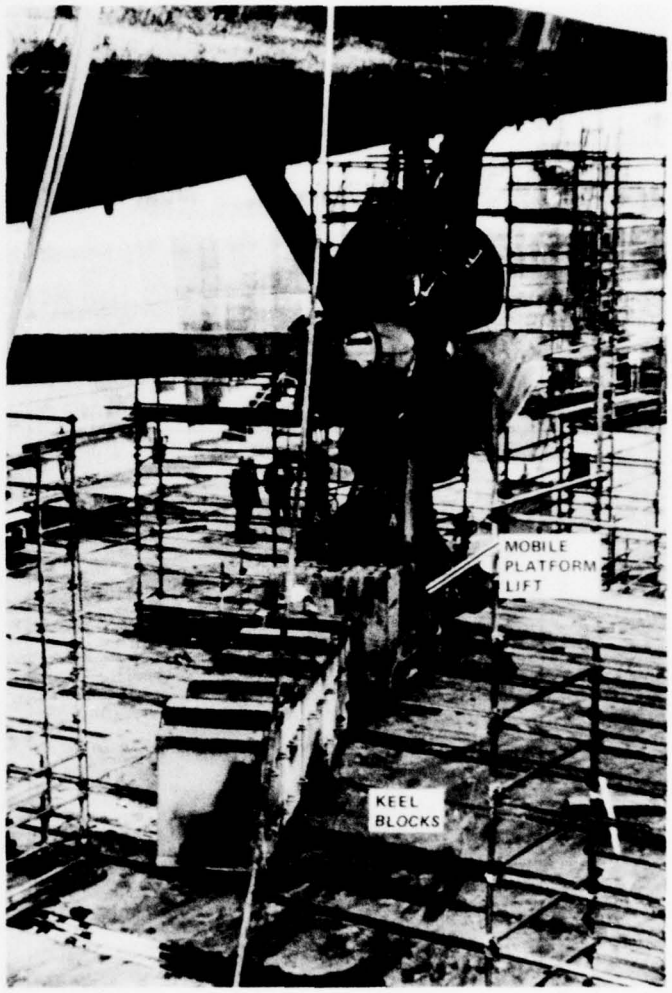

Figure 27d - Astern Loading (Detail)

TABLE 6 - DRYDOCK STATIC LOAD TESTS ON BARBEY

Run No.	Blade No.	Blade Pitch	Load Ahead	Load Astern
27	2	DAH	F(9)	X
28	2	DAH	C	X
29	2	DAH	C	X
30	2	DAH	C	X
31	2	0	F(9)	X
32	4	0	F(3)/C	X
33	5	0	F(6)/C	X
34	5	DAH	F(6)/C	X
35	4	0	X	F(7)/C
36	5	0	X	F(6)/C
37	2	0	X	F(9)/C
38	2	0	X	F(9)/C
39	2	DAH	F(9)	X
40	2	DAS	X	F(9)/C
41	4	DAS	X	F(7)/C
42	5	DAS	X	F(6)/C

Notes: DAH = Design Ahead
0 = Neutral (0) Pitch
DAS = Design Astern
F() = Full Load on ( ) Rams
C = Combinations of Ram Loadings

Full load (9 rams) was possible only on propeller Blade 2 since Blades 4 and 5 had instrumentation on their surfaces.

TABLE 7 - CHARACTERISTICS OF HYDRAULIC LOADER

No. of Rams	9
Ram Locations (on Propeller Blade):	
% Radius	60, 70, 80
% Chord (from leading edge)	25, 50, 75
Maximum Ram Pressure, psi	1,000
Maximum Force Ram, lb	8,000
Maximum Total Loader Force (9 Rams), lb	72,000

Figure 28 - Instrumentation Installation for Dynamic Propeller Blade Tests on BARBEY

TABLE 8 - SCHEDULE OF DRYDOCK AND UNDERWAY RUNS

Run	Type
1	Exp. Bolt 1 Torque Test
2	Bolt 1 Torque Test
3	Bolt 2 Torque Test
4	Bolt 3 Torque Test
5	Bolt 4 Torque Test
6	Bolt 5 Torque Test
7	Bolt 6 Torque Test
8	Torque Release on Crank 2
9	Bolt 1 Torque Test
10	Bolt 2 Torque Test
11	Bolt 3 Torque Test
12	Bolt 4 Torque Test
13	Bolt 5 Torque Test
14	Bolt 6 Torque Test
15	Cal
16	Shaker Sweep in Air Blade 4
17	Shaker Sweep in Air Blade 4
18	Shaker Sweep in Air Blade 4
19	Shaker Sweep in Air Blade 2
20	Shaker Sweep in Air Blade 5
21	Trans Excit Blade 5
22	Trans Excit Blade 5
23	Re-Null Values
24	Static Load Test Blade 2
25	Design Ahead Pitch Stat Load Blade 2
26	Design Ahead Pitch Stat Load Blade 2
27	Design Ahead Pitch Stat Load Blade 2
28	Design Ahead Pitch Stat Load Blade 2
29	Design Ahead Pitch Stat Load Blade 2
30	Design Ahead Pitch Stat Load Blade 2
31	Neutral Pitch Stat Load Blade 2
32	Neutral Pitch Stat Load Blade 4
33	Neutral Pitch Stat Load Blade 5
34	Design Ahead Pitch Stat Load Blade 5
35	Neutral Pitch Fwd Side Stat Load Blade 4
36	Neutral Pitch Fwd Side Stat Load Blade 5
37	Neutral Pitch Fwd Side Stat Load Blade 2
38	Neutral Pitch Fwd Side Stat Load Blade 2
39	Design Ahead Stat Load Blade 2
40	Design Astern Fwd Side Stat Load Blade 2
41	Design Astern Fwd Side Stat Load Blade 4
42	Design Astern Fwd Side Stat Load Blade 5
43	Neutral Pitch Trans. Excit by Diver Blade 4 Underwater
44	Shaker Sweep Blade 4
45	Underway 49-55 rpm
46	Underway 98 rpm
47	Underway 122 rpm
48	121 rpm
49	50 rpm Rezeroed
50	50 rpm Zero Level
51	*On Jack Gear from* Jack Shaft to Mar
52	Rpm to Zero
53 (103)	120 rpm
54 (106)	150 rpm
55 (110)	180 rpm/Turns Crashback Ahead
56 (118)	220 rpm/turns Crashback
57 (115)	Not Run Boiler Problems 190 in Man. Mode
58 (415)	100 rpm
59 (414)	110 rpm
60 (413)	120 rpm
61 (412)	130 rpm
62 (411)	140 rpm
63 (410)	150 rpm
64 (409)	160 rpm
65 (408R)	170 rpm (Rezeroed)
66 (408)	170 rpm Phase A Only
67 (407)	180 rpm
68 (407R)	180 rpm
69 (406)	190 rpm
70 (405)	200 rpm
71 (403)	220 rpm
72 (801)	200 rpm 5 deg Turns Crashback/Ahead Phase A
73 (802)	200 rpm 5 deg Turns Crashback/Ahead Phase B
74 (803)	200 rpm 10 deg Turns Crashback/Ahead Phase A
75 (804)	200 rpm 10 deg Turns Crashback/Ahead Phase B
76 (805)	200 rpm 20 deg Turns Crashback/Ahead Phase A
77 (806)	200 rpm 20 deg Turns Crashback/Ahead Phase B
78 (807)	200 rpm 30-35 deg Turns Crashback/Ahead Phase A
79 (808)	200 rpm 30-35 deg Turns Crashback/Ahead Phase B
80 (402)	225 rpm
81 (809)	223 rpm 190 deg Pitch Phase A F.P. Crashback
82 (820)	Accel. from DIW to F.P. Phase A
83 (810)	F.P. Crashback Phase B
84 (821)	F.P. Accel. *Phase B*
85 (811)	240 in P 100 rpm
86 (812)	240 in P 120 rpm
87 (813)	240 in P 140 rpm
88 (814)	240 in P 160 rpm
89 (815)	240 in P 180 rpm Phase A 35 deg
90 (186)	240 in P 160 rpm Turns Phase B 35 deg
91 (817)	240 in P 160 rpm Turns Incl. Crashback A 5 deg
92 (818)	240 in P 180 rpm Turns Incl. Crashback B 5 deg
93 (819)	240 in P 180 rpm Turns Prog. Mode Ahead Pitch 'A'
94 (822)	Crashahead/back Prog. Mode Ahead Pitch 'B'
95 (823)	Crashahead/back
96 (609)	170 in Pitch - Phase A 200 rpm 35 deg Turns
97 (610)	170 in Pitch - Phase B 200 rpm 35 deg Turns
98 (611)	170 in Pitch Phase A 220 rpm 35 deg Turns
99 (612)	170 in Pitch Phase B 220 rpm 35 deg Turns
100 (118R)	190 in Pitch A-B 299 rpm 100 Turns & Crashback
101 (301)	Drag Blade from 80 rpm Phase A
102 (302)	Drag Blade from 120 rpm Phase A
103 (303)	Drag Blade from 160 rpm A-B
104 (304)	Drag Blade from 202 rpm A-B
105 (305)	Drag Blade from 150 rpm Phase A
106 (701)	20 in Pitch (DIW) 100 rpm A-B
107 (702)	7 in Pitch (DIW) 140 rpm A-B
108 (703)	7 in Pitch (DIW) 180 rpm A-B
109 (704)	7 in Pitch (DIW) 220 rpm A-B

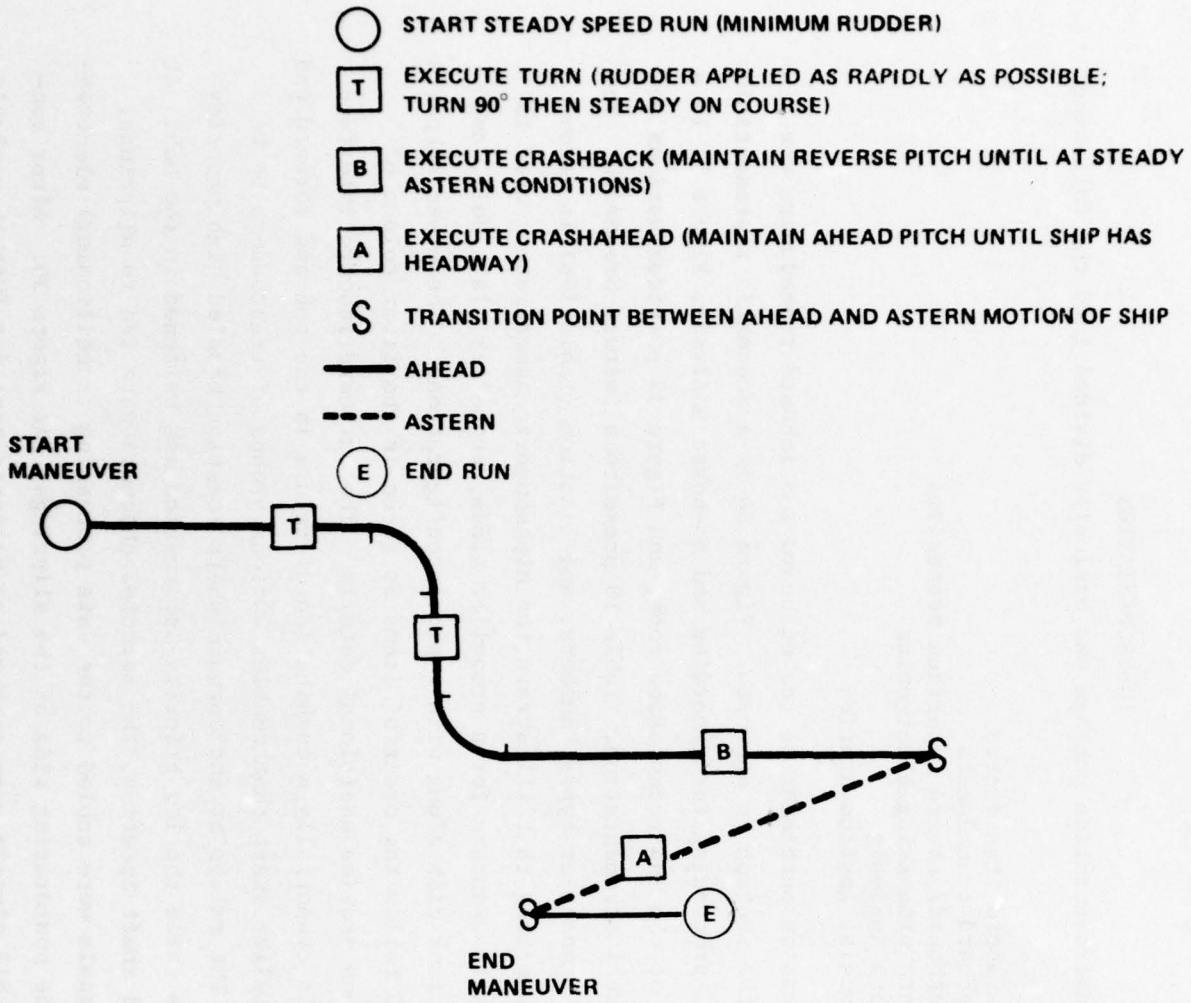

Figure 29 - Run/Turn/Crashback (RTC) Maneuver

Sea trials were conducted off the coast of Long Beach, California on 6–13 April 1975. Table 9 gives pertinent information on environmental conditions during the tests. Smooth trial conditions were generally experienced during that period.

INSTRUMENTATION

The instrumentation package was basically divided into the following areas:

1. Outboard transducers
2. Inboard transducers
3. Outboard/inboard interface mechanisms
4. Data processing electronics
5. Data analysis
6. Special instrumentation

Information pertinent to the outboard and inboard transducers was discussed in the section on approach. Figure 30 is a schematic representation of the data processing for recording and on-board analysis, Figure 31 is a photograph of the instrumentation room, and Figure 32 provides various details of the instrumentation. Table 10 presents a further breakdown. The summary of transducer types, numbers, and location (Table 10a) is accompanied by sketches that illustrate the alphanumeric nomenclature used in designating transducers for a propeller blade, propeller blade bolt, and propeller crank disk along with typical configurations. The other subparts of Table 10 follow the order of items as given in the first column of Table 10a and provide additional details. The outboard/inboard interface mechanism is essentially a combination of relays in the hub and forward end of the propeller shaft that enables various groups of transducers to be selected. The relays at the forward shaft location handled high priority transducers while the low priority information was switched in the hub. At the forward shaft location, the selected channels were fed to sliprings, and the signals were cabled to the data processing (conditioning) electronics from the nonrotating side of the sliprings; see Figure 30. After conditioning, all signals were recorded on magnetic tape for further analysis at DTNSRDC. Selected gages were processed for "on-board" analysis. With few exceptions, all strain gage transducers functioned well throughout the tests. A further analysis of continuing performance characteristics is given in the section on gage protection.

TABLE 9 - AVERAGE ENVIRONMENTAL TRIAL DATA FOR UNDERWAY TESTS

Parameter	Trial Day				
	1	2	3	4	5
Date	6 Apr	9 Apr	11 Apr	12 Apr	13 Apr
Sea State	3	1	1	2	0
Wave Height, ft	4	2	2	2	1
Water Depth, fathoms	300	300	300	300	300
Wind Speed, knots	17	7	10	12	5
Displacements					
Fwd, ft-in	14-6	14-3	14-8	14-8	14-8
Aft, ft-in	15-6	15-7	15-6	15-6	15-6

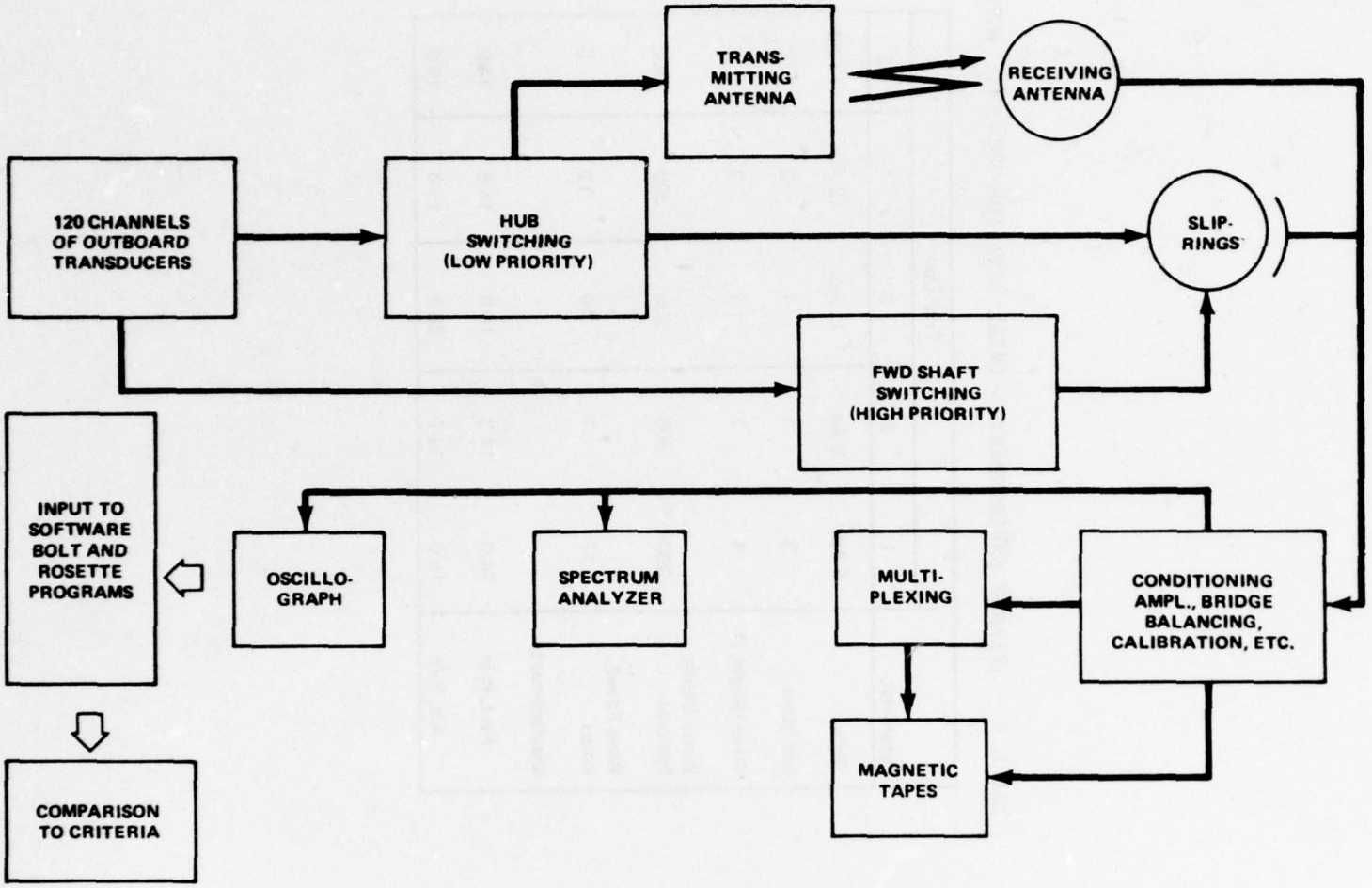

Figure 30 - Data Processing for Recording and On-Board Analysis

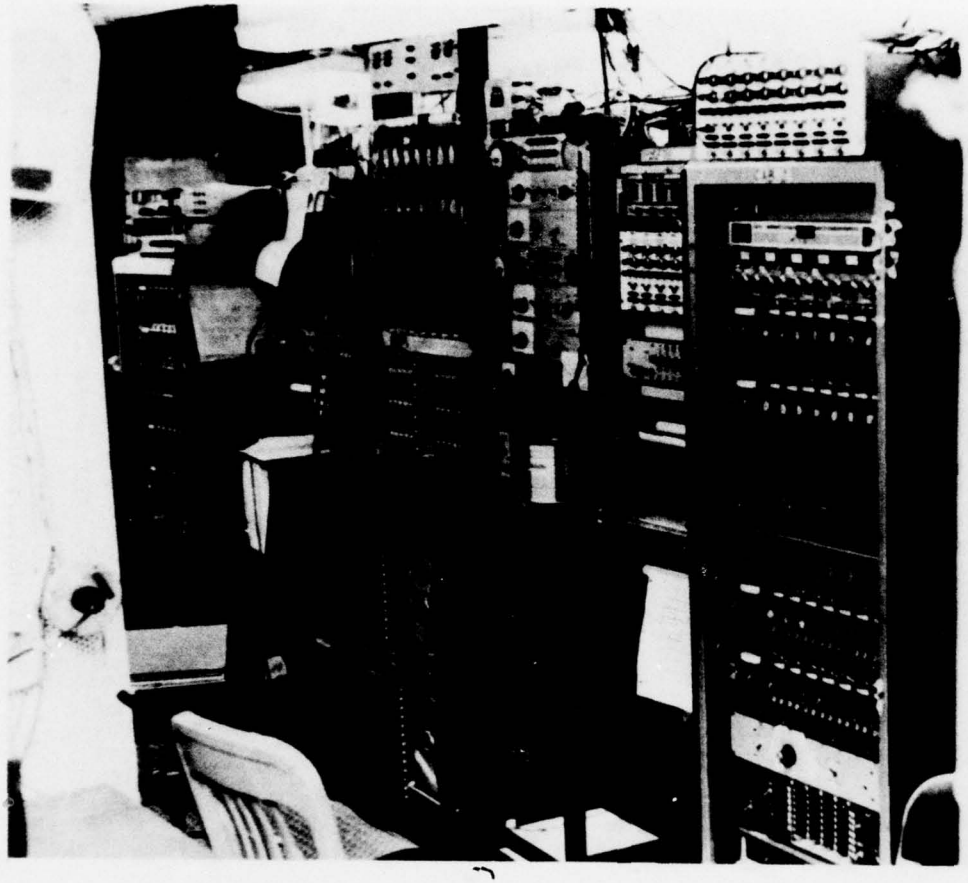

Figure 31 — Instrumentation Detail, Conditioning and Recording Electronics in Instrumentation Room

Figure 32 - Details of the Instrumentation

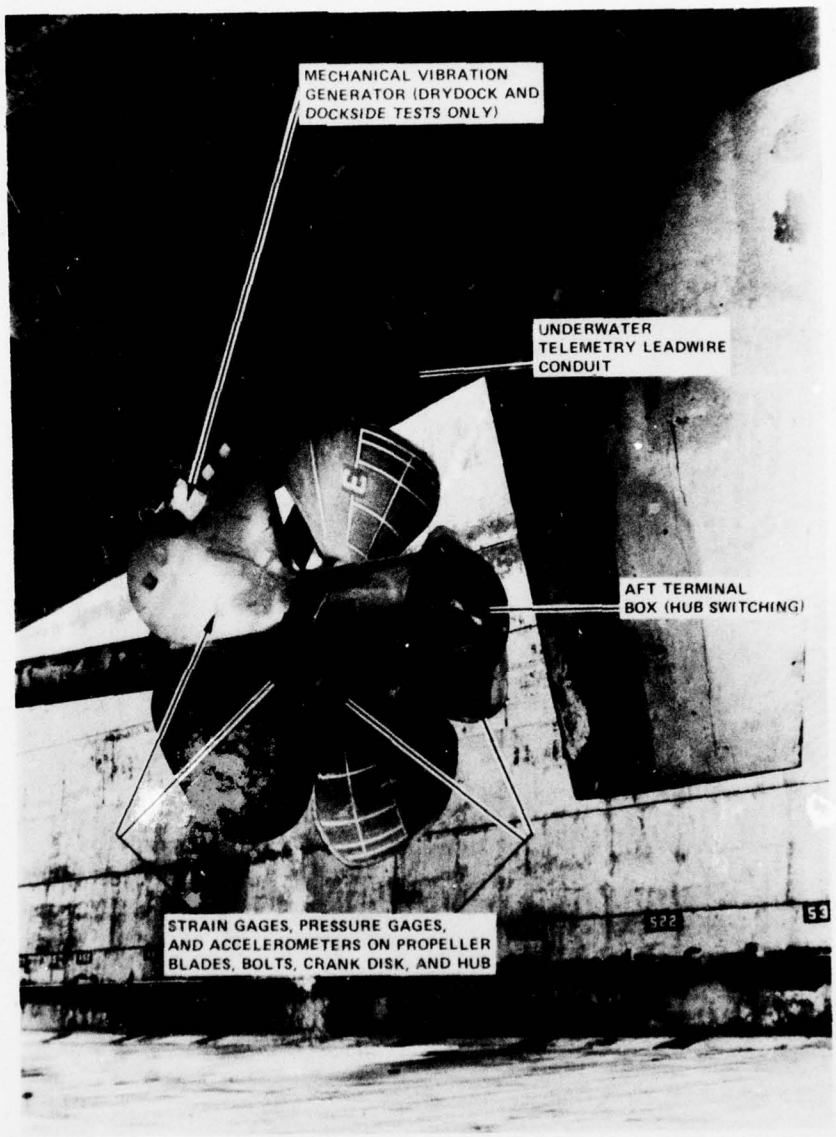

Figure 32a — Overall View of Outboard Gages

Figure 32 (Continued)

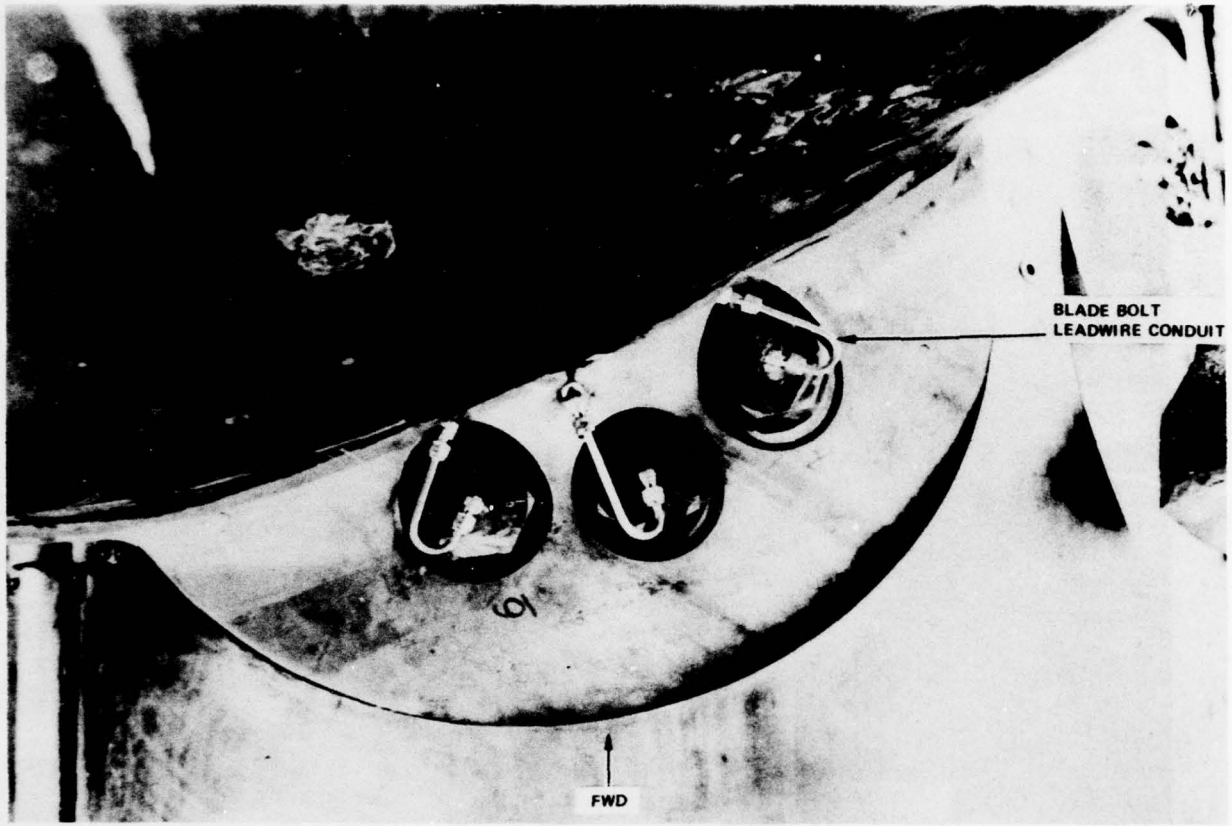

Figure 32b — Blade Bolts, Propeller Blade 2

Figure 32 (Continued)

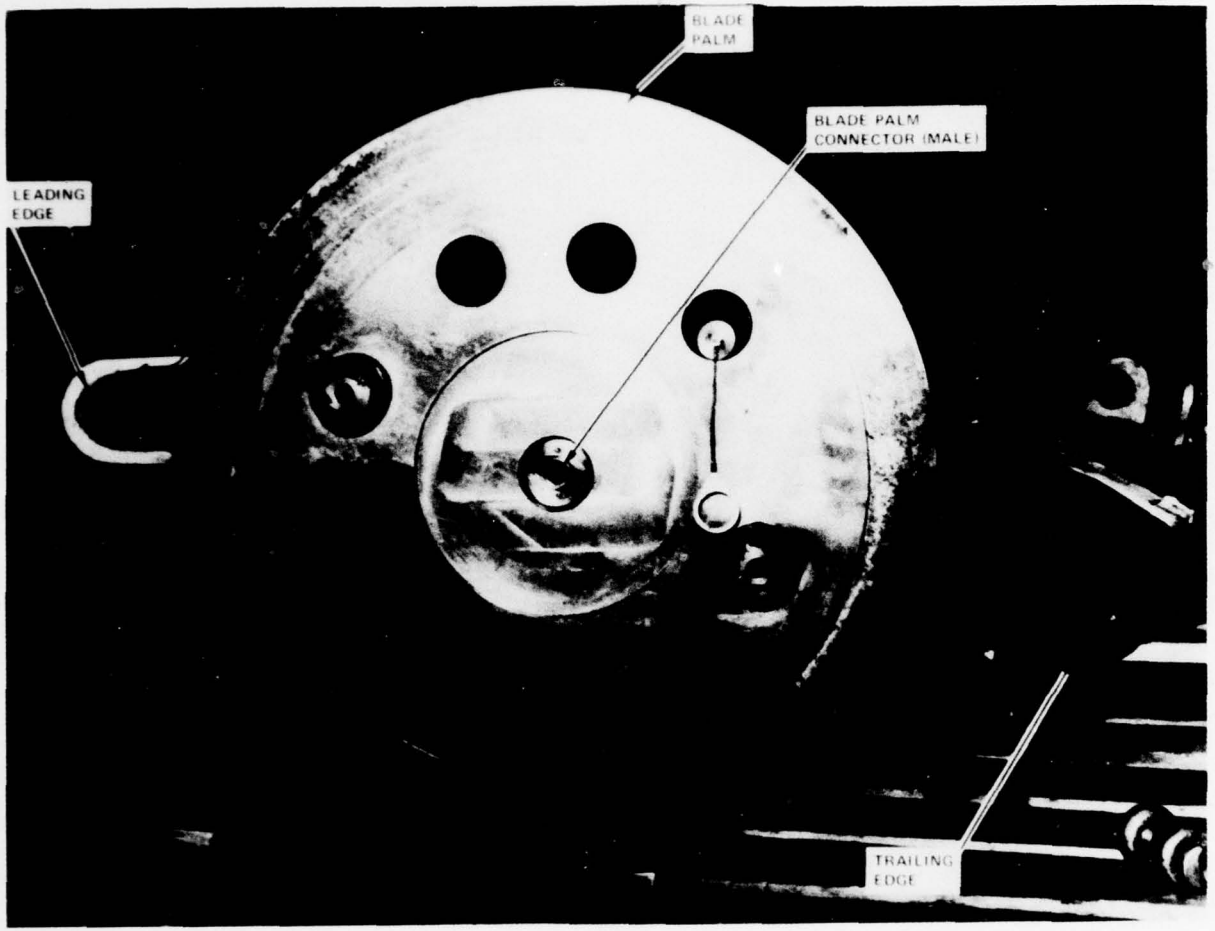

Figure 32c — Propeller Blade Palm

Figure 32 (Continued)

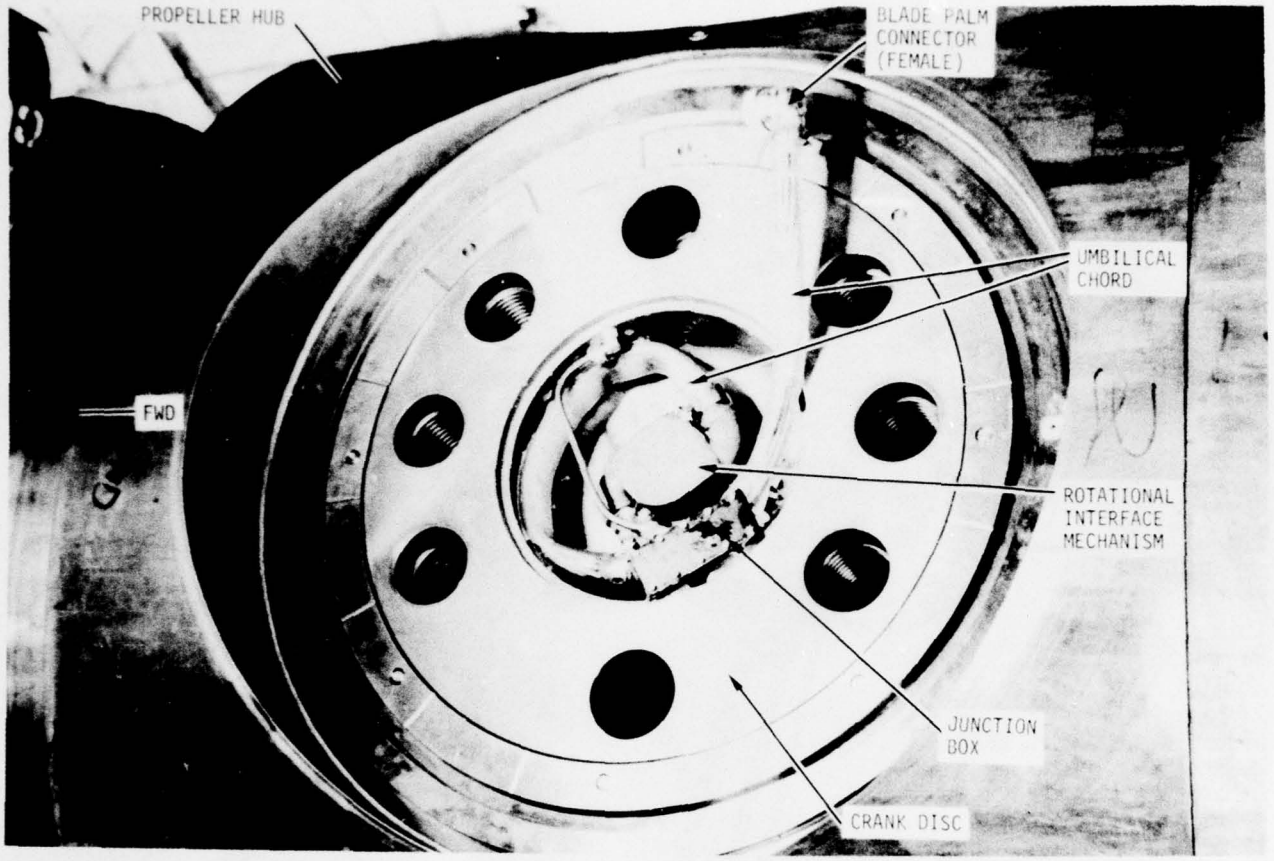

Figure 32d — Crank Disk 2

Figure 32 (Continued)

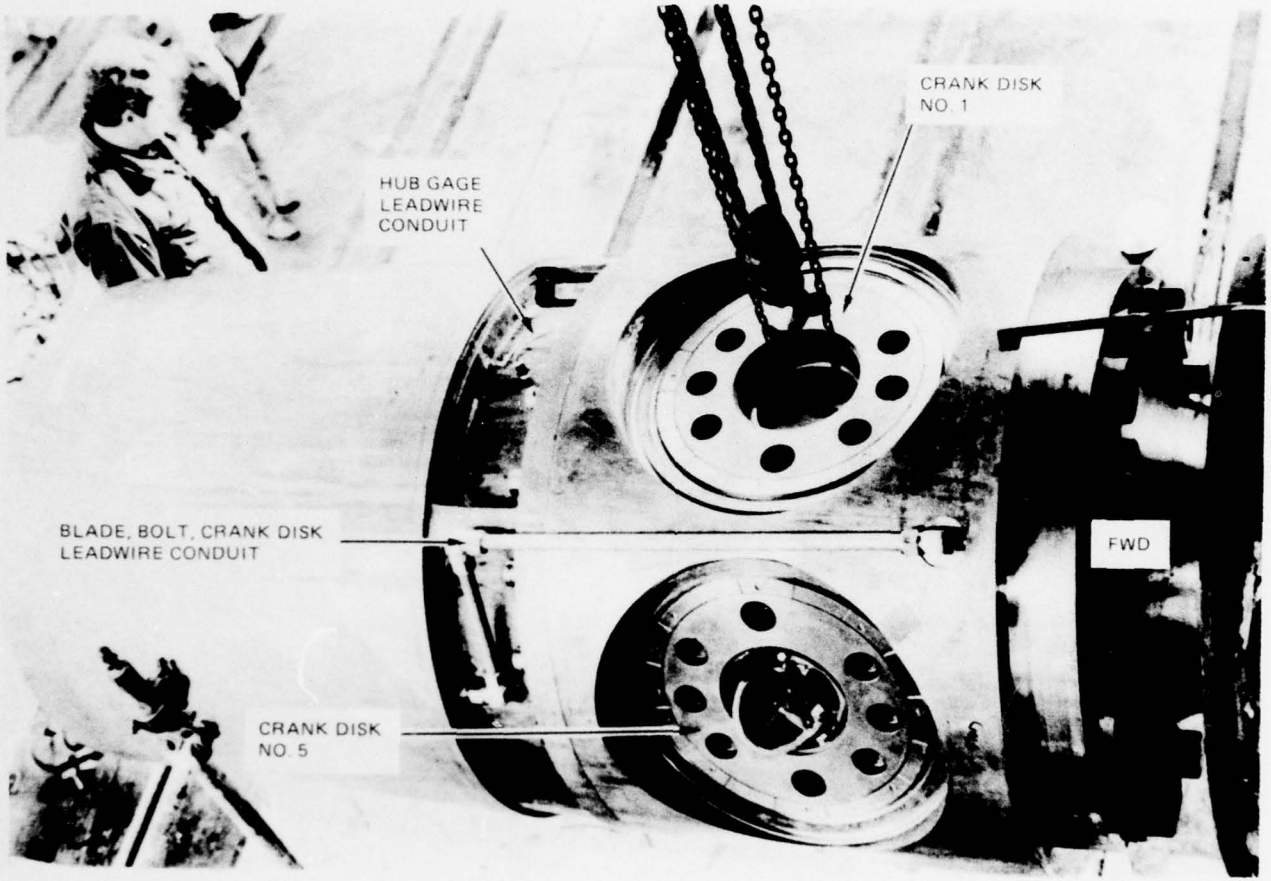

Figure 32e — Propeller Hub, External

Figure 32 (Continued)

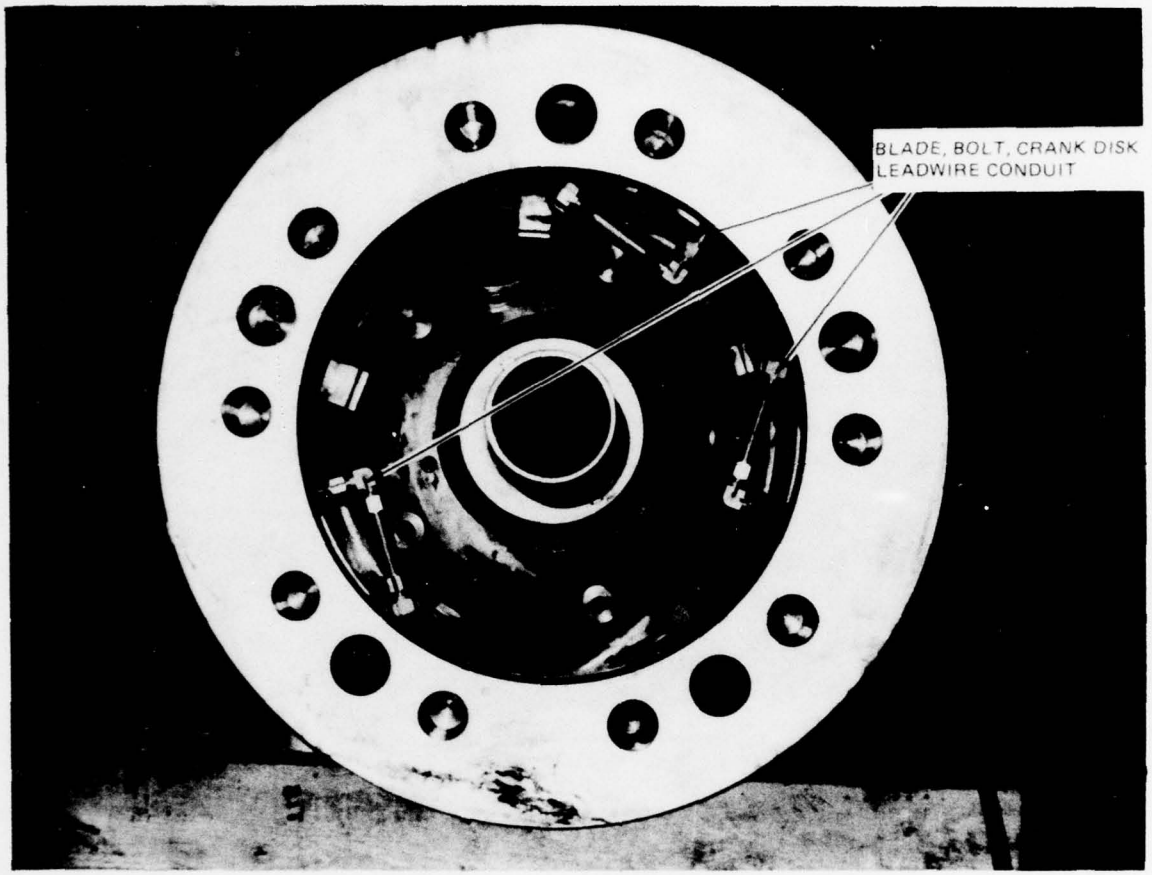

Figure 32f — Propeller Hub, Internal Looking Aft

Figure 32 (Continued)

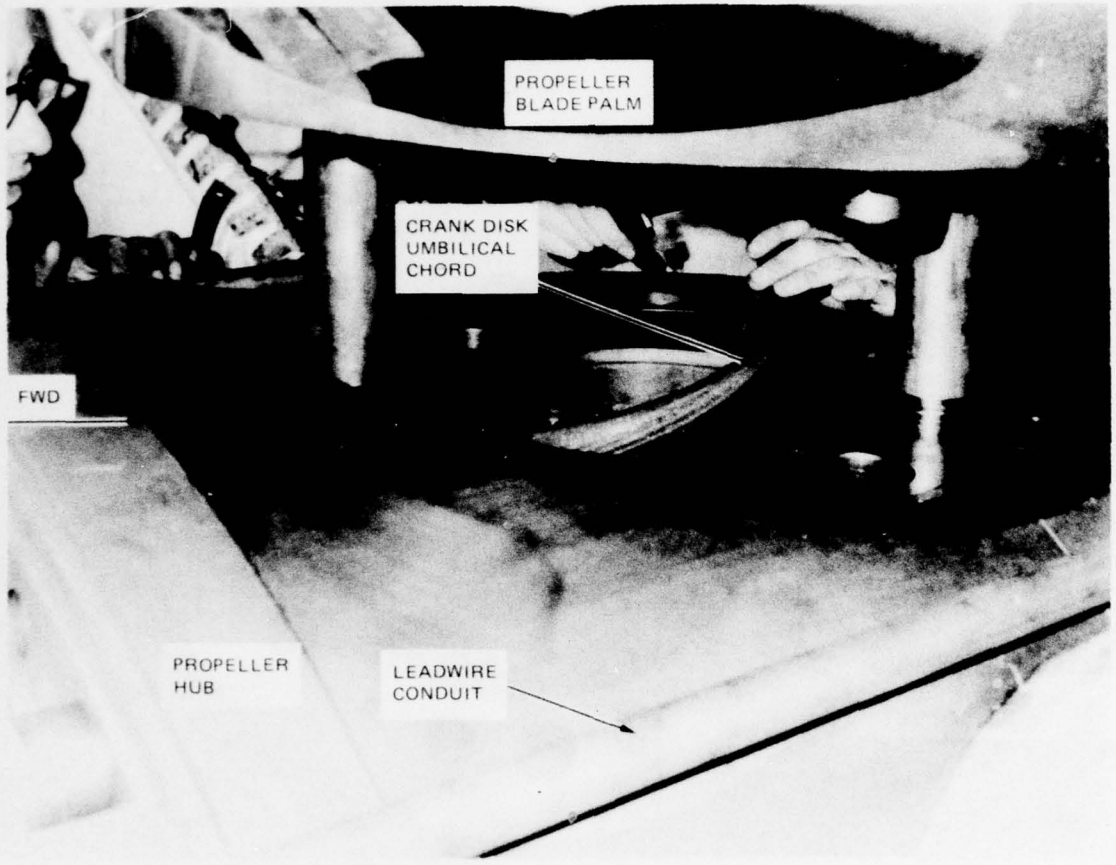

Figure 32g — Propeller Installation

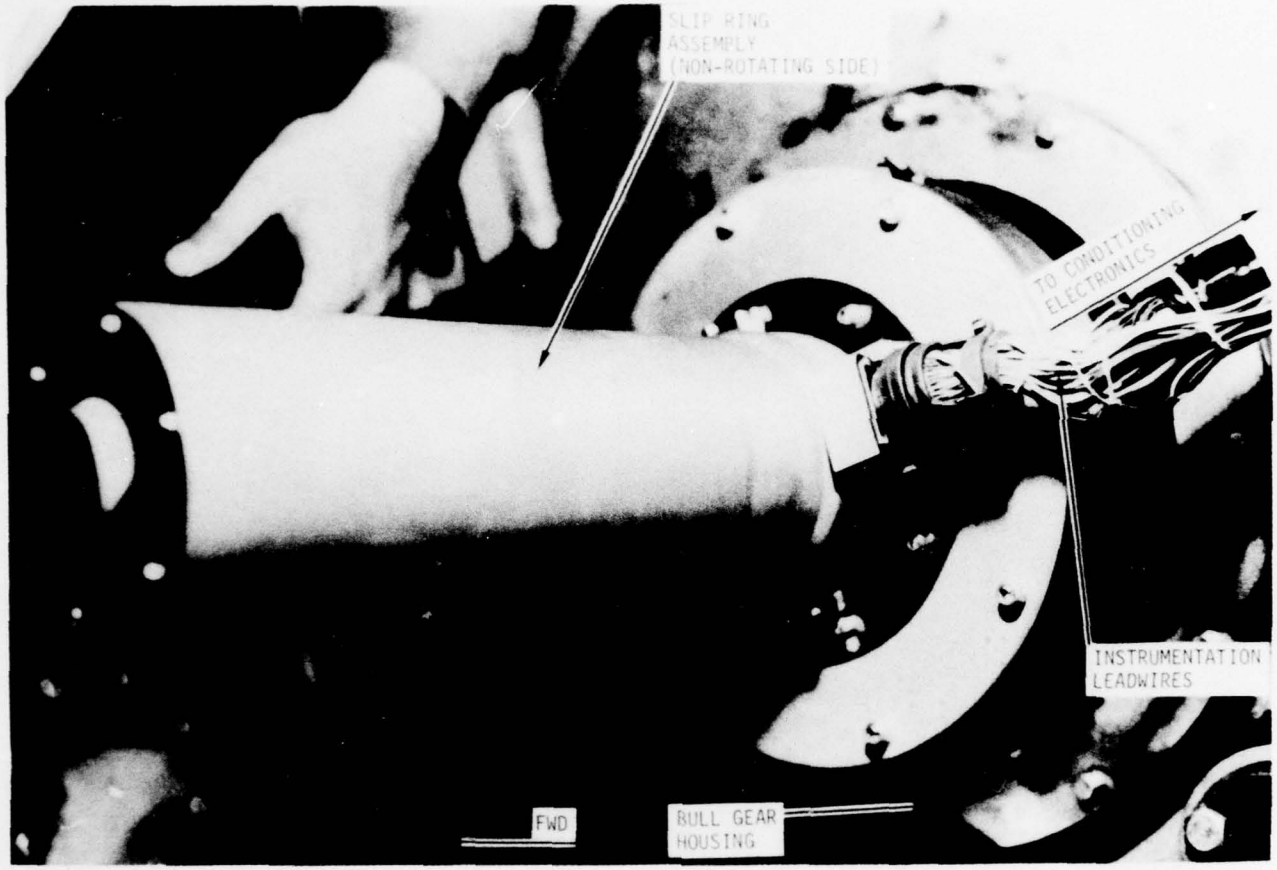

Figure 32h - Slipring Assembly, Forward End of Propeller Shaft at Bull Gear

Figure 32 (Continued)

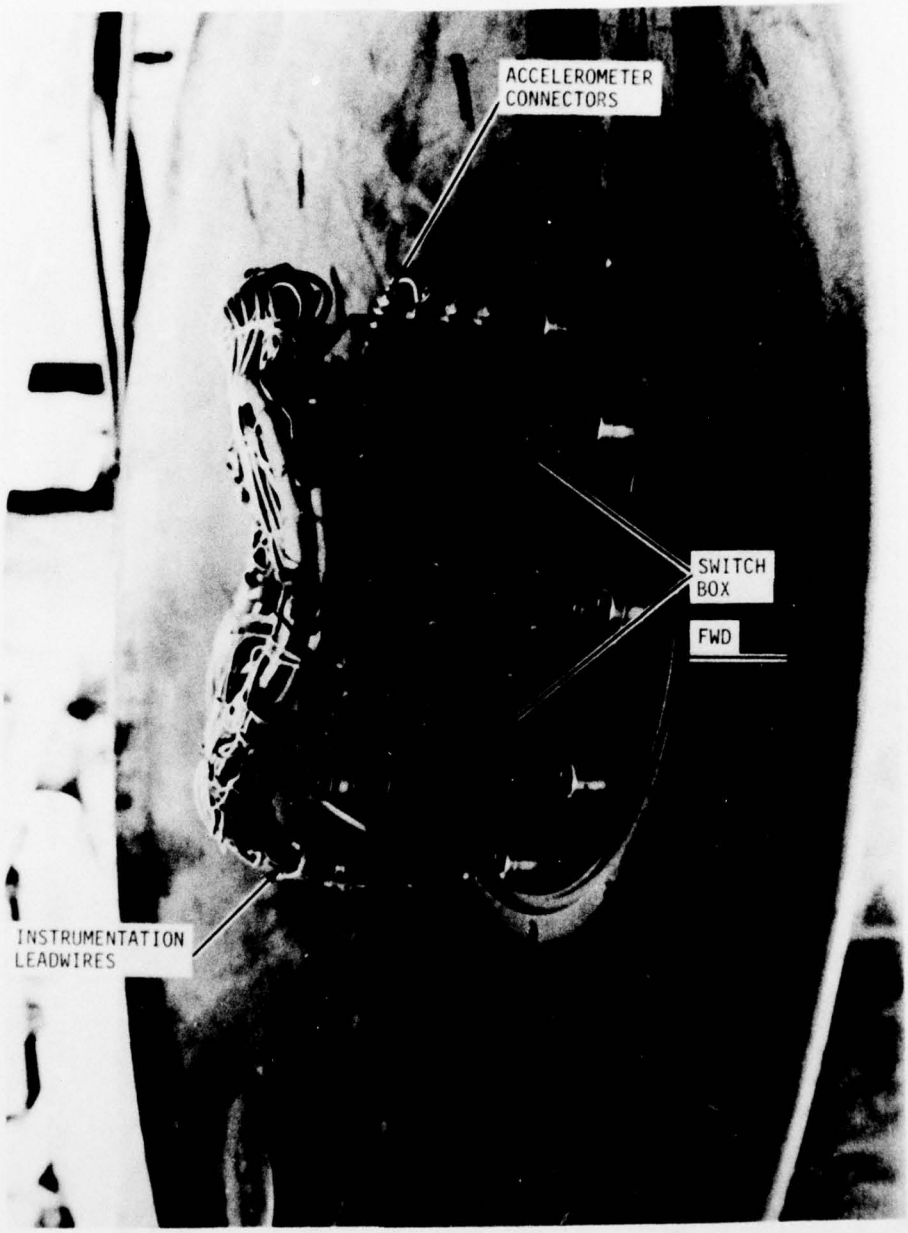

Figure 32i — Aft Terminal Box, Waterproof
(waterproof cover not installed)

TABLE 10 - TRANSDUCERS UTILIZED IN INSTRUMENTATION OF BARBEY CPP SYSTEM

TABLE 10A - SUMMARY LIST

Gage Location	Type of Transducer	No. of Gages	
		Pretrial	Trial
Prop. B1. 2 (Bolts and Crank Disk)	Strain Gages	49	39
Prop. B1. 4 (Blade and Crank Disk)	Accelerometers	3	3
	Pressure Gages	2	2
	Strain Gages	38	38
Prop. B1. 5	Strain Gages	32	32
Prop. Hub	Accelerometer	1	1
	Strain Gages	4	4
	Mag. Field Det	1	1
Shaft Alley	Strain Gages	4	4
	RPM	1	1
	Pitch	1	1
Aft. Steer Rm.	*Rudder Angle*	*1*	*1*
	Totals	137	127

NOTES:

(1) FOR AHEAD OPERATION, FORWARD SIDE OF BLADE SURFACE IS SUCTION AND AND AFT SIDE OF BLADE SURFACE IS PRESSURE.
(2) LEADING EDGE (IN PRARIE AIR CHANNEL) FOR ACCELEROMETERS AND ON THE 1/4 CHORD FOR STRAIN GAGES.
(3) TRAILING EDGE FOR ACCELEROMETERS AND 3/4 CHORD FOR STRAIN GAGES.

△ ACCELEROMETER

○ STRAIN GAGE

□ PRESSURE GAGE

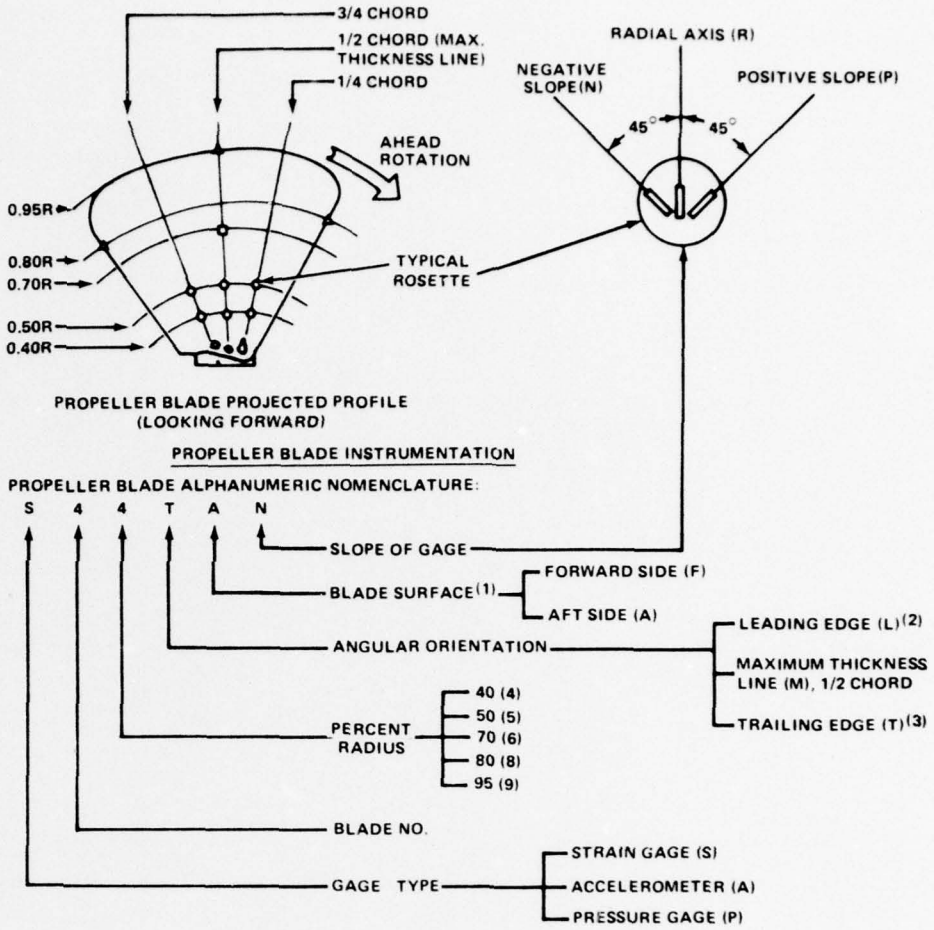

TABLE 10 (Continued)

TABLE 10A (Continued)

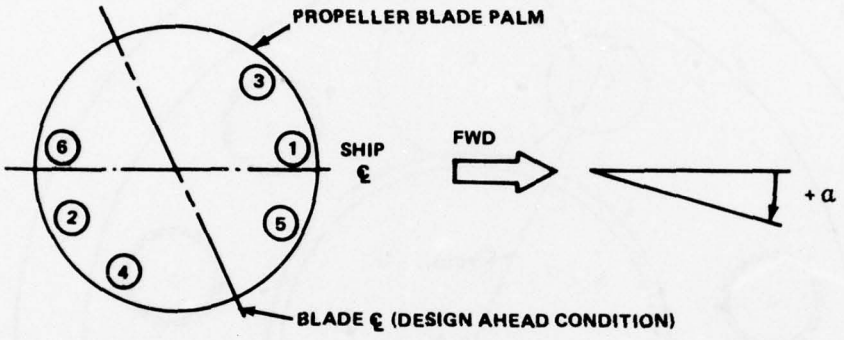

Propeller Blade Bolt Arrangement (Bolt Numbering System Assigned by LBNSY)

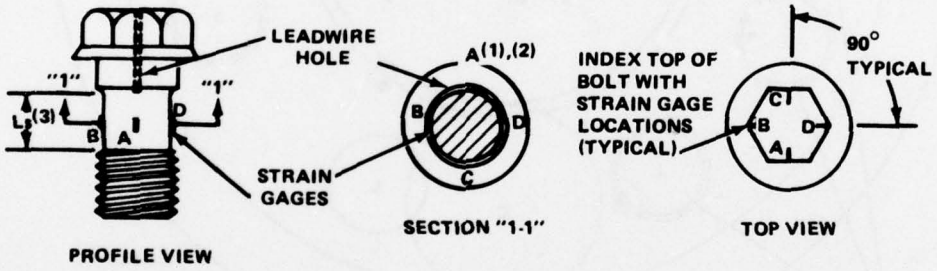

NOTES:

1. **LETTERS A–D DESIGNATE STRAIN GAGE LOCATIONS.**
2. **GAGE A IS ALIGNED WITH ℄ OF LEADWIRE HOLE.**
3. **GAGES ARE LOCATED AT CENTER OF SHANK LENGTH (Ls).**

Typical Instrumented Propeller Blade Bolt (Waterproofing and Leadwires not shown)

TABLE 10 (Continued)

TABLE 10A (Continued)

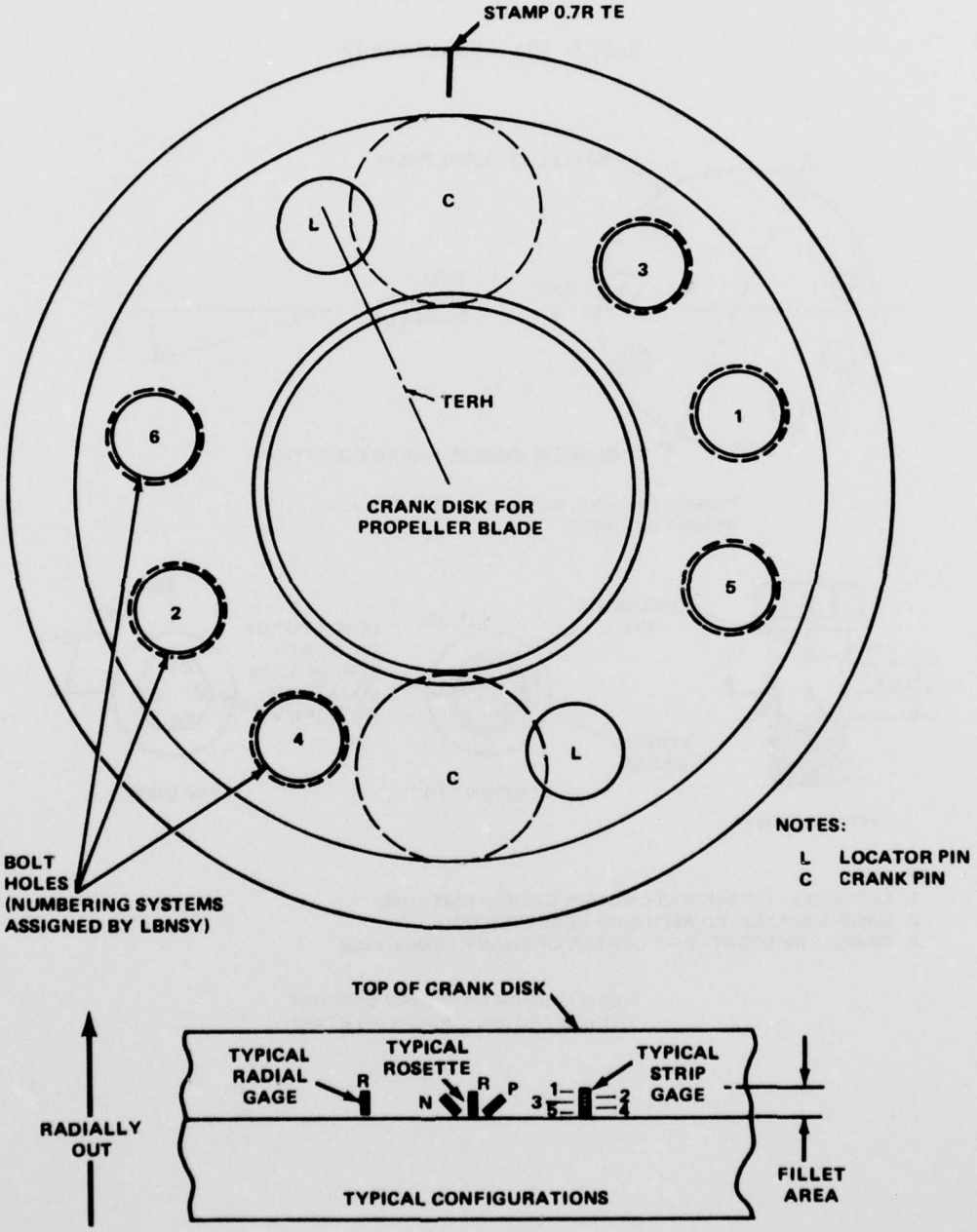

TABLE 10 (Continued)

TABLE 10A (Continued)

Propeller Blade Bolt Alpha-Numeric Nomenclature:

(See Figure on page 69)

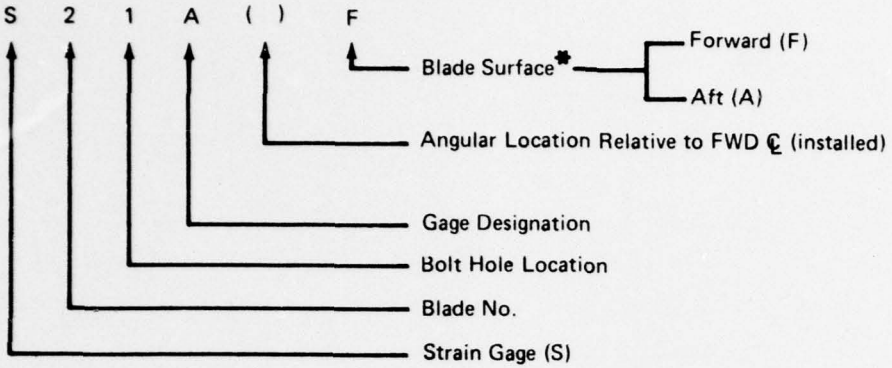

Propeller Crank Disk Alpha-Numeric Nomenclature:

(See Figure on page 70.)

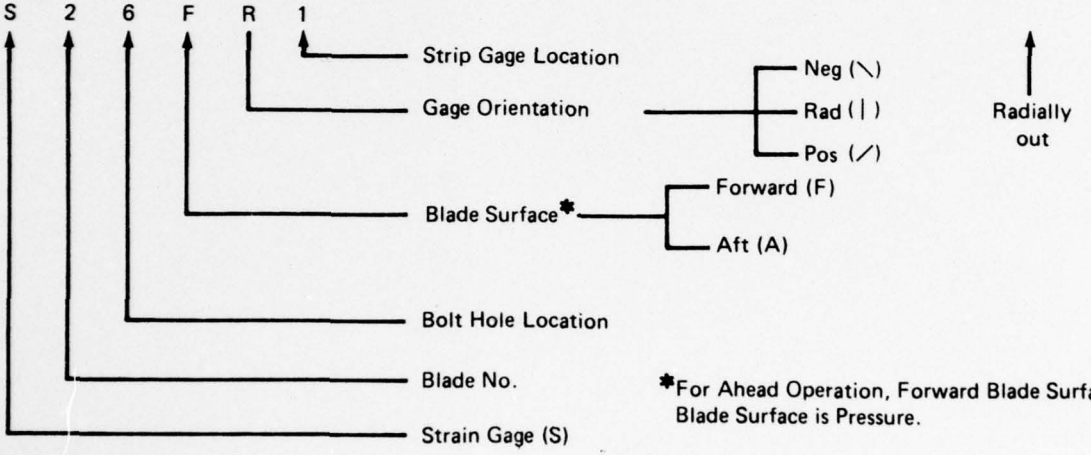

*For Ahead Operation, Forward Blade Surface is Suction and Aft Blade Surface is Pressure.

Seq. No.	Location	Configuration	Designation
3	Bolt 1	Axial	S 21A(23°)F
*	↓	↓	S 21B(113°)F
4	↓	↓	S 21C(203°)F
*	Bolt 1	↓	S 21D(293°)F
13	Bolt 2	↓	S 22A(3°)A
*	↓	↓	S 22B(93°)A
14	↓	↓	S 22C(183°)A
*	Bolt 2	↓	S 22D(273°)A
5	Bolt 3	↓	S 23A(155°)F
*	↓	↓	S 23B(245°)F
6	↓	↓	S 23C(335°)F
*	Bolt 3	↓	S 23D(65°)F
7	Bolt 4	↓	S 24A(202°)A
*	↓	↓	S 24B(292°)A
8	↓	↓	S 24C(22°)A
*	Bolt 4	↓	S 24D(112°)A
1	Bolt 5	↓	S 25A(214°)F
*	↓	↓	S 25B(304°)F
2	↓	↓	S 25C(34°)F
*	Bolt 5	↓	S 25D(124°)F
9	Bolt 6	↓	S 26A(199°)A
10	↓	↓	S 26B(239°)A
11	↓	↓	S 26C(329°)A
12	Bolt 6	Axial	S 26D(39°)A

*Drydock Trials Only

Seq. No.	Location	Configuration	Designation
15	Bolt Hole 1	Radial	S 21FR
16	Bolt Hole 2	Radial	S 22AR
17	Bolt Hole 3	Radial	S 23FR
18	Bolt Hole 4	Radial	S 24AR
19	Bolt Hole 5	Rosette	S 25FN
20	↓	↓	S 25FR
21	↓	↓	S 25FP
22	Bolt Hole 6	Rosette (with Radial Strip Gage)	S 26AN
23	↓	↓	S 26AR1**
24	↓	↓	S 26AR2**
25	↓	↓	S 26AR3**
26	↓	↓	S 26AR4**
27	↓	↓	S 26AR5**
28	↓	↓	S 26AP
29	Crank Pin (C)	Rosette	S 2CFN
30	↓	↓	S 2CFR
31	↓	↓	S 2CFP
32	Locator Pin (L)	Rosette	S 2LFN
33	↓	↓	S 2LFR
34	↓	↓	S 2LFP
35	Betw. Bolt Hole 1 and 5	Radial	S 21/5FR
36	Betw. Bolt Hole 2 and 4	Radial	S 22/4AR
37	Betw. Bolt Hole 2 and 6	Rosette	S 22/6AN
38	↓	↓	S 22/6AR
39	↓	↓	S 22/6AP

NOTE:

■ SIN(

▬ ROS

ROS
RAD

AD-A047 851 DAVID W TAYLOR NAVAL SHIP RESEARCH AND DEVELOPMENT CE--ETC F/G 13/10
THE BARBEY REPORT. AN INVESTIGATION INTO CONTROLLABLE PITCH PRO--ETC(U)
AUG 77 C NOONAN, G ANTONIDES, A ZALOUMIS

UNCLASSIFIED DTNSRDC-77-0080 NL

2 OF 4
AD A047851

TABLE 10 (Continued)

TABLE 10B - PROPELLER BLADE 2

Seq. No.	Location	Configuration	Designation
5	Bolt Hole 1	Radial	S 21FR
6	Bolt Hole 2	Radial	S 22AR
7	Bolt Hole 3	Radial	S 23FR
8	Bolt Hole 4	Radial	S 24AR
9	Bolt Hole 5	Rosette	S 25FN
0	↓	↓	S 25FR
1	↓	↓	S 25FP
2	Bolt Hole 6	Rosette (with Radial Strip Gage)	S 26AN
3	↓	↓	S 26AR1**
4	↓	↓	S 26AR2**
5	↓	↓	S 26AR3**
6	↓	↓	S 26AR4**
7	↓	↓	S 26AR5**
8	↓	↓	S 26AP
9	Crank Pin (C)	Rosette	S 2CFN
0	↓	↓	S 2CFR
1	↓	↓	S 2CFP
2	Locator Pin (L)	Rosette	S 2LFN
3	↓	↓	S 2LFR
4	↓	↓	S 2LFP
5	Betw. Bolt Hole 1 and 5	Radial	S 21/5FR
6	Betw. Bolt Hole 2 and 4	Radial	S 22/4AR
7	Betw. Bolt Hole 2 and 6	Rosette	S 22/6AN
8	↓	↓	S 22/6AR
9	↓	↓	S 22/6AP

NOTE:

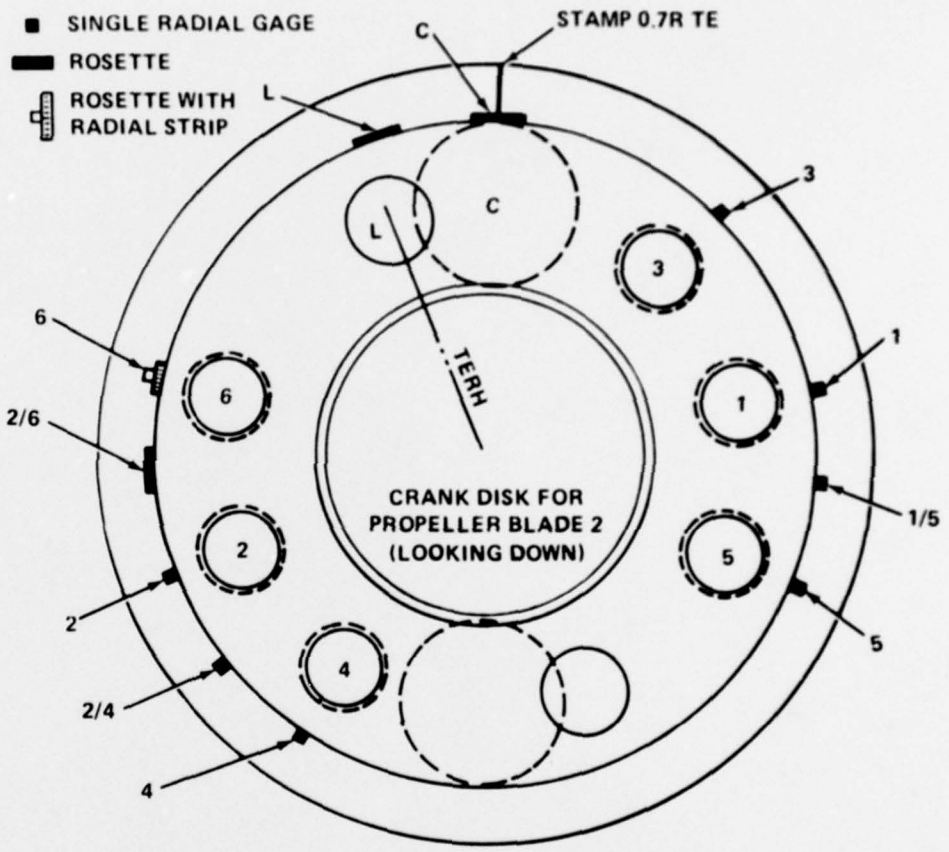

BLADE GAGES

Seq. No.	Location	Configuration	Designation
40	0.80R, LE	Normal to Surf	A48LF
41	0.95R, MT		A49MF
42	0.80R, TE		A48TF
43	0.70R, MT		P47MF
44	0.70R, MT		P47MA
45	0.5R, TE	Rosette	S45TAN
46			S45TAR
47			S45TAP
48	0.5R, MT		S45MAN
49			S45MAR
50			S45MAP
51	0.5R, LE		S45LAN
52			S45LAR
53			S45LAP
54	0.4R, TE		S44TAN
55			S44TAR
56			S55TAP
57	0.4R, MT		S44MAN
58			S44MAR
59			S44MAP
60	0.4R, LE		S44LAN
61			S44LAR
62		Rosette	S44LAP

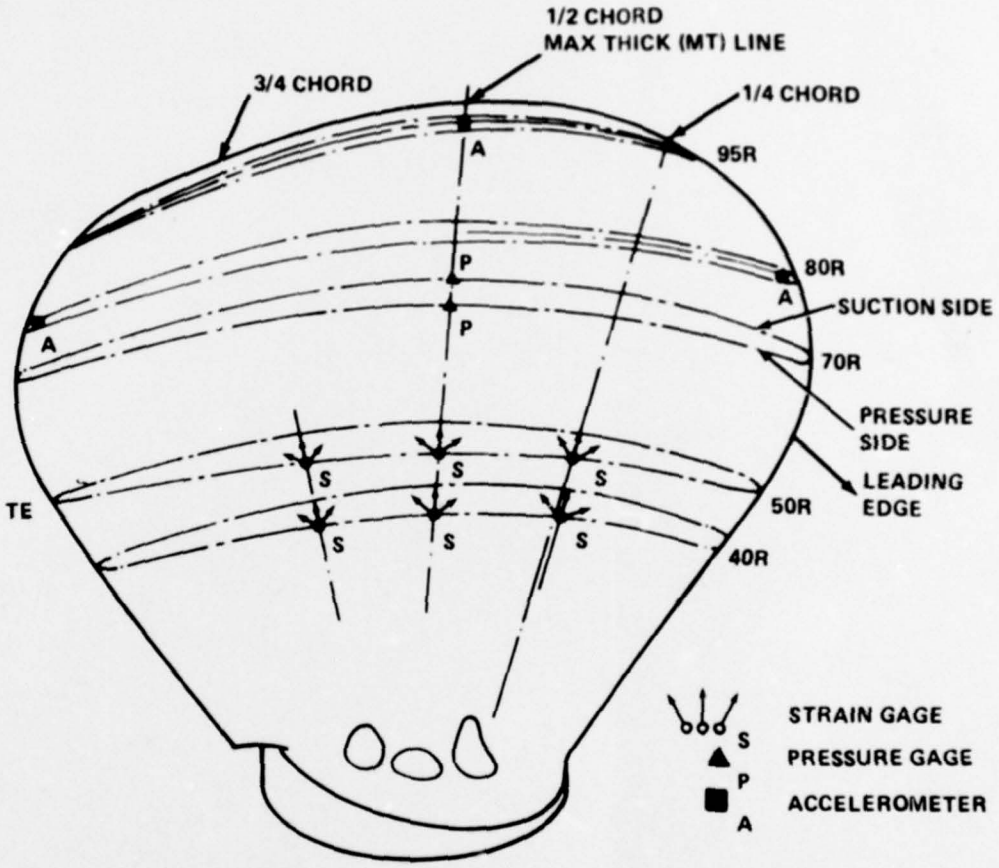

PROPELLER BLADE 4 (BLADE GAGES)

TABLE 10 (Continued)

TABLE 10C - PROPELLER BLADE 4

CRANK DISK GAGES

Seq. No.	Location	Configuration	Designation
63	Bolt Hole 1	Radial	S41FR
64	Bolt Hole 2	Radial	S42AR
65	Bolt Hole 3	Radial	S43FR
66	Bolt Hole 4	Radial	S44AR
67	Bolt Hole 5	Radial	S45FR
68	Bolt Hole 6	Rosette	S46AN1
69			S46AN2
70			S46AN3 *
71			S46AN4
72			S46AN5
73			S46AR1
74			S46AR2
75			S46AR3 *
76			S46AR4
77			S46AR5
78			S46AP1
79			S46AP2
80			S46AP3 *
81			S46AP4
82	Bolt Hole 6	Rosette	S46AP5

NOTE:

■ SINGLE RADIAL GAGE

STRIP ROSETTE

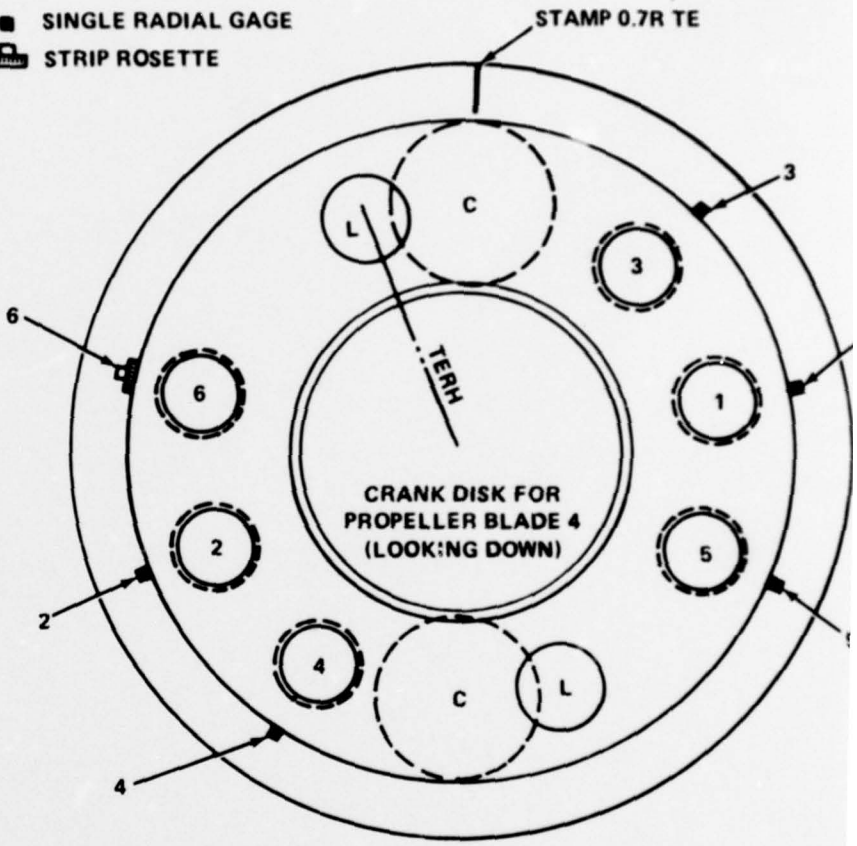

TABLE 10 (Continued)

TABLE 10D - PROPELLER BLADE 5 BLADE GAGES

Seq. No.	L[illegible]	Configuration	Designation
83	0	Radial	S55TAR
84	0.5[illegible]	Rosette	S55MAN
85	↓	Rosette	S55MAR
86	↓	Rosette	S55MAP
87	0.5R, LE	Radial	S55LAR
88	0.4R, TE	Rosette	S54TAN
89	↓	↓	S54TAR
90	↓	↓	S54TAP
91	0.4R, MT	↓	S54MAN
92	↓	↓	S54MAR
93	↓	↓	S54MAP
94	0.4R, LE	↓	S54LAN
95	↓	↓	S54LAR
96	↓	↓	S54LAP
97	0.5R, LE	↓	S54LFN
98	↓	↓	S55LFR
99	↓	↓	S55LFP
100	0.5R, MT	↓	S55MFN
101	↓	↓	S55MFR
102	↓	↓	S55MRP
103	0.5R, TE	↓	S55TFN
104	↓	↓	S55TFR
105	↓	↓	S55TFP
106	0.4R, LE	↓	S54LFN
107	↓	↓	S54LFN
108	↓	↓	S54LFP
109	0.4R, TE	↓	S54MFN
110	↓	↓	S54MFR
111	↓	↓	S54MFP
112	0.4R, TE	↓	S54TFN
113	↓	↓	S54TFR
114	↓	Rosette	S54TFP

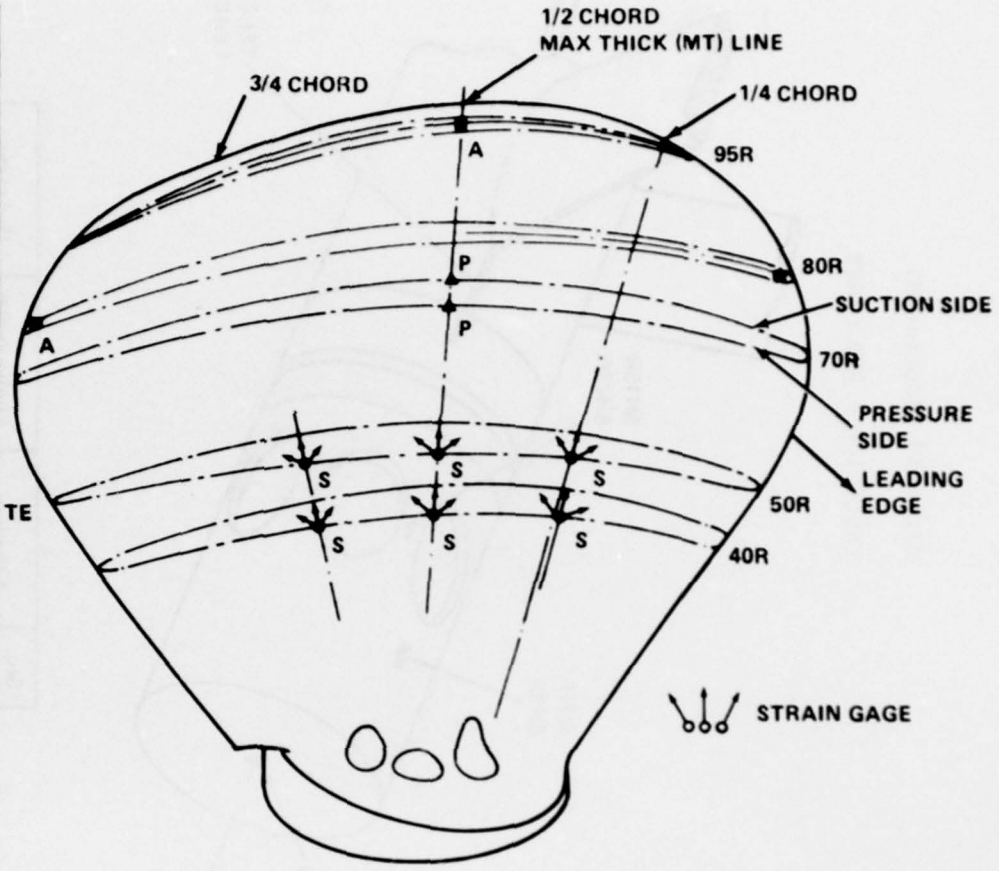

TABLE 10 (Continued)

TABLE 10E - HUB GAGES

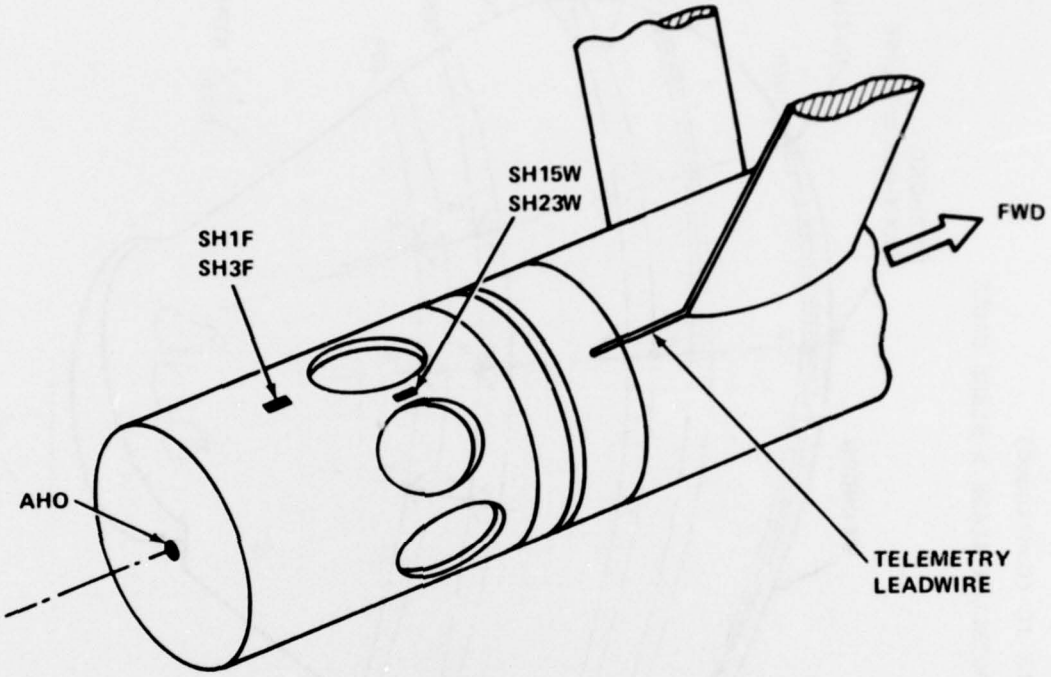

Seq. No.	Location	Configuration	Designation
115	Crank Disk (Flange)	Bending	SH1F
116	Crank Disk (Flange)	Bending	SH3F
117	Hub Web	Axial	SH15W
118*	Hub Web	Axial	SH23W
119	Hub ℄	Axial	AHO
120	Hub	Mag. Field	MF

AHO = ACCELEROMETER ℄ (IN AFT TERMINAL BOX)
SH1 = HUB STRAIN GAGE ON CRANK DISK BEARING FLANGE
SH2 = HUB STRAIN GAGE ON WEB BETWEEN PROPELLER BLADE HOLES

TABLE 10 (Continued)

TABLE 10F - SHAFT ALLEY GAGES

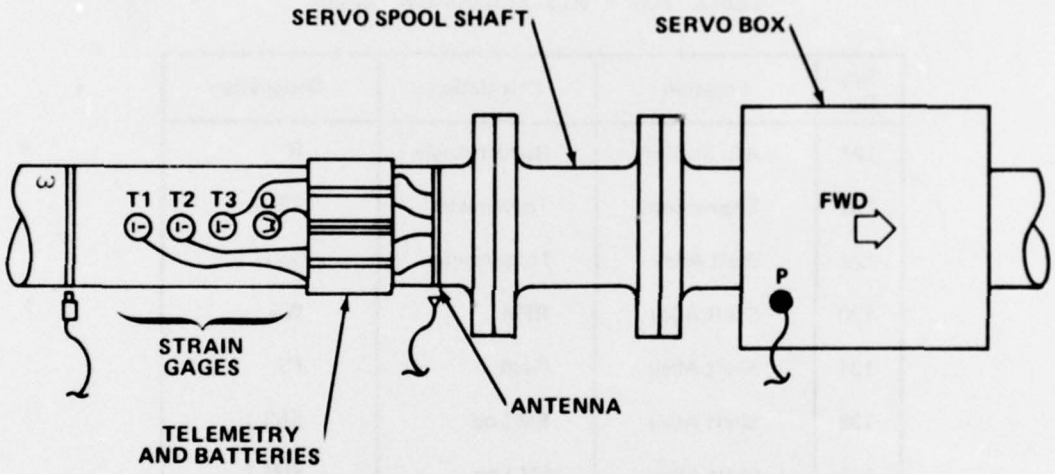

Seq. No.	Quantities Measured
121	Q – Mean and Alternating Torque
122	T1 – Mean and Alternating Thrust
123	T2 – Mean and Alternating Thrust
124	T3 – Mean and Alternating Thrust
125	ω – Shaft RPM
126	P – Propeller Pitch

TABLE 10 (Continued)

TABLE 10G - MISCELLANEOUS GAGES

Seq. No.	Location	Orientation	Designation
127	Aft. St. Rm.	Rudder Angle	R
128	Engineroom	Thrustmeter	TS
129	Shaft Alley	Torquemeter	QS
130	Shaft Alley	RPM	WS
131	Shaft Alley	Pitch	PS
132	Shaft Alley	EM Log	EML1
133	Shaft Alley	EM Log	EML2
134	Shaft Alley	Hy. Press A	Servo A
135	Shaft Alley	Hy. Press B	Servo B
136	–	Voice	–

The accelerometers and pressure gages were considered as special instrumentation because the transducers were adapted to the propeller environment. Output from these gages was limited, as discussed later.

One of the major costs associated with a project of this nature is the disassembly, modifications, and reassembly of the main propulsion system in order to accommodate the transducer leadwires aboard ship. This is especially true in a complex system like a controllable pitch propeller. DTNSRDC has been concerned about this problem for quite some time and has been developing an alternate technique for transmitting transducer signals. Some preliminary conceptual groundwork had already been done on a telemetry designed to investigate the peculiarities of transmission of a modulated RF carrier through the saltwater medium.* The conceptual representation of this system is shown in Figure 33. This concept was extended as a special instrumentation project on BARBEY by coupling an outboard strain gage bridge input to a Bendix TOE-304-mV VCO. The FM output (center frequency of 3.0 KHz) was buffered and used to amplitude-modulate a transmitter (carrier frequency of 72.080 MHz). The output of the transmitter was fed into a loop antenna about 4 ft in diameter that was mounted on the propeller hub (bolt flange cover). A similar loop was mounted to the rope guard, about 3/4 in. away, and served as the receiving antenna;[10] see Figure 34. Signals were detected by a NEMS-CLARK receiver and fed into a subcarrier discriminator.

The experimental underwater system proved that it is possible to transmit transducer intelligence through water from a rotating shaft. The results were disappointing, however, because of the many unanswered questions regarding the proper transmission link required (antenna design) for such data. At this time the transmission characteristics of the system in saltwater are not completely understood.** A redesign is currently being evaluated.

---

*DTNSRDC letter:964:CJN, 9870.1 dated 5 February 1970.

**Indicated by the project summary reported as DTNSRDC letter 7300.1, 296 BLZ:jam dated 11 June 1975.

[10]"Project BARBEY Antenna Sensor," DTNSRDC Drawings D-3272-1 through -6 (16 Jan 1975).

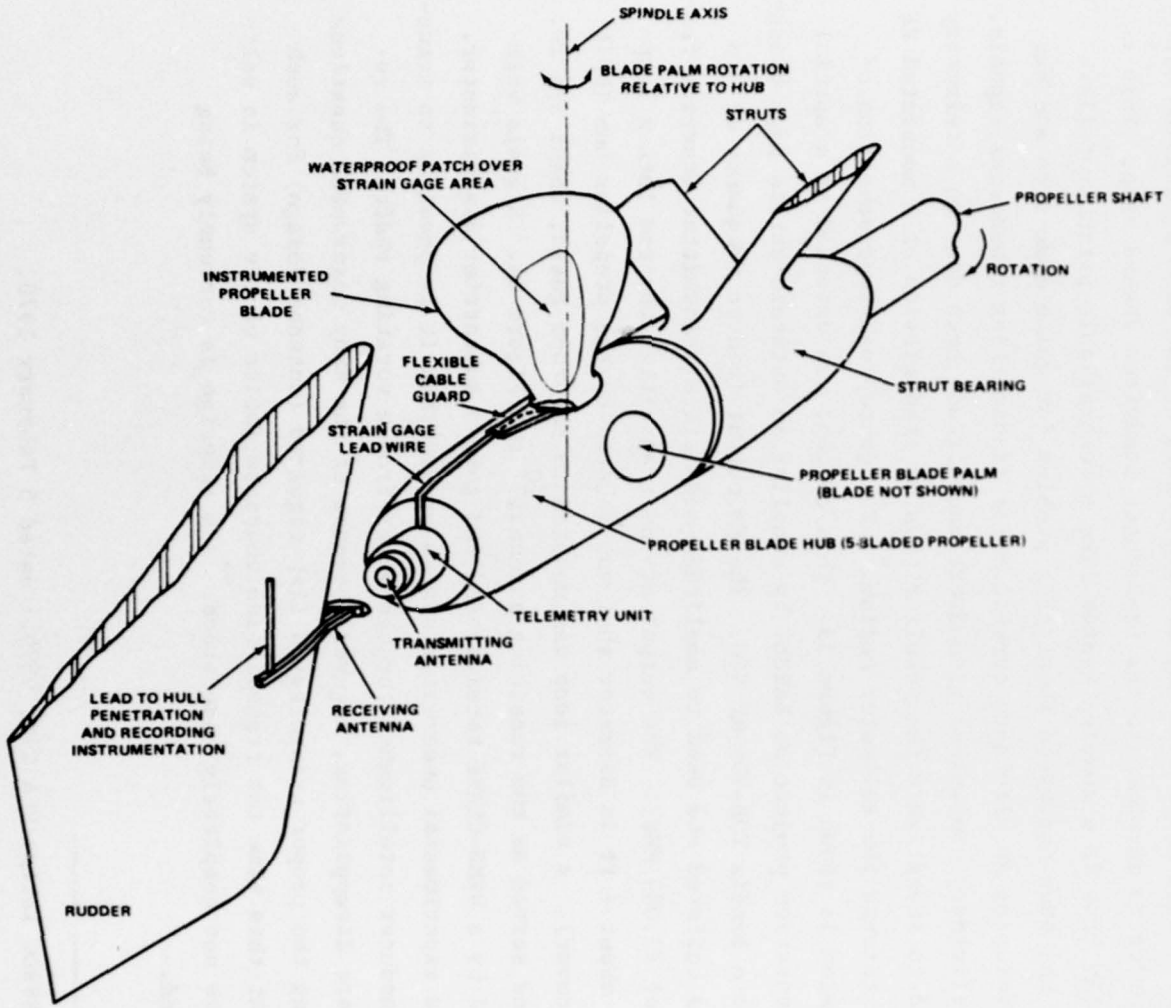

Figure 33 - Conceptual View of Underwater Telemetry System for Measurement of Outboard Propeller Shaft Data

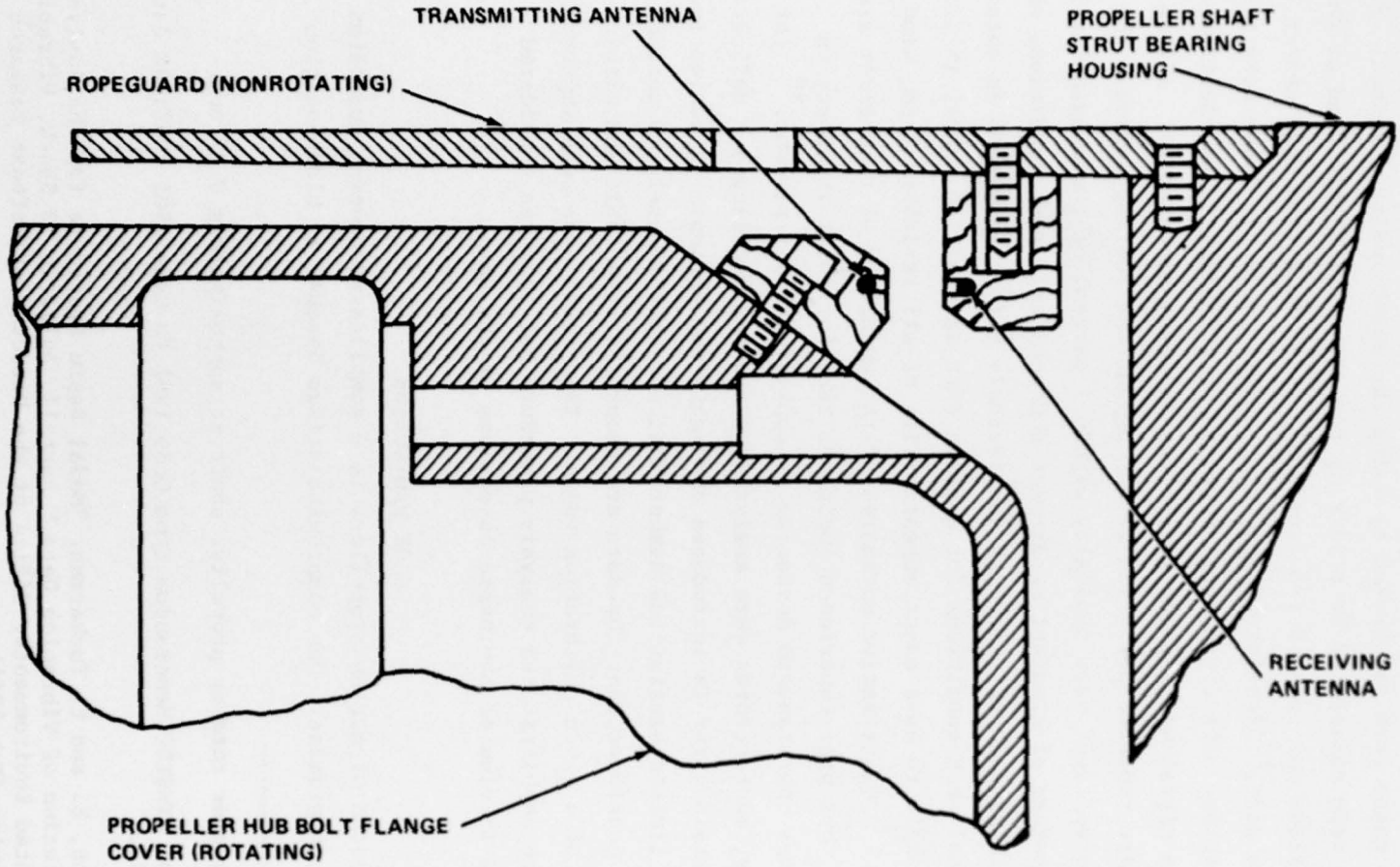

Figure 34 - Detail of Underwater Telemetry Antenna

Measurement errors for the instrumentation were carefully estimated. All strain gages were calibrated by using the shunt resistor method. Pressure gages were calibrated by utilizing the change in static head as the propeller blade was rotated from top dead center to bottom dead center with the jacking gear.* Accelerometers were calibrated in the laboratory prior to installation. After the accelerometers were installed, an electronic calibration signal was applied to the conditioning electronics. All calibrations were repeated periodically throughout the testing period. The calibration voltages were typically within 1 percent of the original values.

The sources of greatest error were nonrepeatable test conditions and the analysis procedure. Although considerable effort is placed in obtaining identical test conditions for a given data acquisition phase, it is highly unlikely to have exact repeatability of all variables (rpm, wind, speed, etc.). Quantitative estimates of the magnitude of this error are subjective, but past experience indicates that for shaft frequency on surface ships one standard deviation is approximately 5 percent.** For expendiency, most records were analyzed by reading oscillograph deflections. Again a certain error is introduced and again the estimate is subjective. Tests on a limited statistical number indicate approximately 10 percent.[11]

It is concluded that the data are generally repeatable and within 20 percent of a given calibration value. This could have been improved by using a more sophisticated analysis procedure but that was considered unwarranted in view of the basic objectives of the trial.

GAGE PROTECTION

The design of marine propellers is a complicated process and often results in compromise. One compromise arises because of blade-section

---

*Jacking gear rotates propeller shaft at approximately 0.07 rpm.

**Internal DTNSRDC Memorandum from Code 1962 to Code 1901 1962:CJN dated 27 June 1972.

[11]Buchmann, E. and E. Tuckerman, "Model Basin Procedure for the Analysis and Presentation of Vibration Data," Part II, Bulletin 33 Shock, Vibration and Associated Environments, Office of the Director of Defense Research and Engineering (Feb 1964).

thickness. The hydrodynamist desires thin blade sections on high-speed ships to optimize cavitation performance and efficiency, but strength considerations require propellers with thick blade sections in order to avoid catastrophic failure. The proper resolution of these conflicting criteria has occasionally evaded the propeller designer and blade failures have occurred. Until recently, it has not been technically feasible to experimentally evaluate the full-scale hydrodynamic and strength characteristics of a marine propeller. As a result, propeller strength design often consists of an updated version of the Taylor beam theory which was developed about 1909.[12] As late as 1968, an evaluation of the various methods for the calculation of stress in marine propellers concluded that without further empirical input, the use of more sophisticated techniques could not be justified.[13]

This lack of empirical guidance from full-scale measurements has apparently not hindered hydrodynamists in escalating design calculations to a high degree of sophistication. There is enough latitude in the torque, rpm, and speed variables to satisfy most propeller designs so far as performance characteristics are concerned.

The advent of the strain gage in 1938 made reliable field evaluation of the static and dynamic characteristics of structural design technically feasible.[14] However, a marine propeller operates in a saltwater environment which is further complicated by propeller cavitation. The intensity of the latter causes severe metal errosion and is probably the primary reason why the evaluation of marine propeller blade stress was delayed for an additional 20 years. Conolly[15] was the first (1956) to make full-scale, underway stress measurements on a propeller. Since that time,

---

[12]Taylor, D.W., "The Speed and Power of Ships," Ransdell, Inc., Washington, D.C. (1933), pages 216–241.

[13]Atkinson, P., "On the Choice of Method for the Calculation of Stress in Marine Propellers," Royal Institute of Naval Architects, Vol. 110 (1968).

[14]Tatnall, F.G., "Tatnall on Testing," American Society for Metals, Metals Park, Ohio (1966).

[15]Conolly, J., "Strength of Propellers," Royal Institute of Naval Architects (1960).

several trials have considerably increased the data base of information on this subject. A sampling is listed in References 16 – 19.*

Experience at DTNSRDC has shown that reliability of the gage protection system constitutes the most difficult phase of this type of data acquisition. Several successful trials of this type have been conducted at DTNSRDC. However, when the BARBEY trial came up, the state-of-the-art of gage protection was such that it was difficult to guarantee a successful trial. For this reason, several gage protection systems were selected for full-scale underway evaluation on BARBEY. Basically, three systems were considered:

1. Vulcanization (primary system).
2. Spray polyurethane (secondary system).
3. Epoxy bonded neoprene patch (reference system).

The vulcanization and urethane were used for actual gage protection. Having been used on previous trials of this type,[20,21] neoprene patch was applied to serve as the basis for judgment of the other two.

---

[16]Antonides, G., "Propeller-Stress Trials on USS FRANKLIN D. ROOSEVELT (CVA-42)," NSRDC Report 2562 (1968).

[17]Wereldsma, I.E., "Stress Measurements on a Propeller Blade of a 42,000-Ton Tanker on Full Scale," Netherlands Research Center T.N.O. for Shipbuilding and Navigation (1963).

[18]Dashnaw, F.J. and F.E. Reed, "Propeller Strain Measurements and Vibration Measurements on the USS MICHIGAN," presented to Chesapeake Section of SNAME (1970).

[19]Keil, H.G. et al., "Stresses Blades of a Cargo Ship Propeller," Schifibautechnische Gesellschaft (1970).

[20]Hanson, D.B., "Development of Strain Gage Protection Systems for Marine Propellers and Application to USS F.D. ROOSEVELT (CVA-42)," Hamilton-Standard Division of United Aircraft Corporation Report HSER-4704 (25 Aug 1967).

[21]Valentine, R.C., "Marine Propeller Strain Gage and Signal Transmission System for the USS DOUGLAS (PG-100)," Hamilton-Standard Division of United Aircraft Corporation Report HSER-5829 (16 Mar 1971).

*Reported informally as NSRDC letter report 9870.1 (Preliminary Report on Propeller Stress and Hull/Superstructure Vibration Measured on the USS DOUGLAS (PG-100)) in 1971.

All three systems have good and bad features. It was generally agreed that the vulcanization would be superior, but it was difficult to find adequate facilities which could handle the job and fit the project schedule. Spray urethane was relatively easy to apply, but its unevaluated performance characteristics in this application together with inconsistent bonding on test applications left much to be desired.

The location of adequate technical talent and facilities for vulcanizing permitted use of this technique as the primary protection system for all the propeller blade bolts and crank disk gages as well as the blade gages on Blade 5. It was eventually decided to also use urethane on Blade 4 since this technique would eliminate certain problems associated with heat of vulcanization effecting the pressure gages on that blade. In addition, the inconsistent bonding problem improved greatly with experience. Figures 35 – 37 show some of the developmental coatings during various stages of test. Basically, a number of bonding and/or coating techniques were evaluated for:

1. Bond strength as indicated by 180 deg (foldover) peel tests.
2. Waterproofing as indicated by gage leakage resistance.
3. Endurance characteristics in a realistic hydrodynamic environment as measured by the survival in a whirl rig or on outboard propellers.

Figure 38 shows typical preparation and gage installation on the propeller blades prior to waterproof coatings. After instrumentation the propeller blades were coated with waterproofing. Figure 39 shows the propeller blades as ready for/or installed on BARBEY. Coating sytems used are listed in Table 11, below.

TABLE 11 – PROPELLER BLADE WATERPROOF COATING SYSTEMS

Propeller Blade No.	Coating System
2	Vulcanized rubber*
4	Urethane (and epoxy-bonded neoprene)
5	Vulcanized rubber

*Trial patch; no instrumentation on blade surfaces.

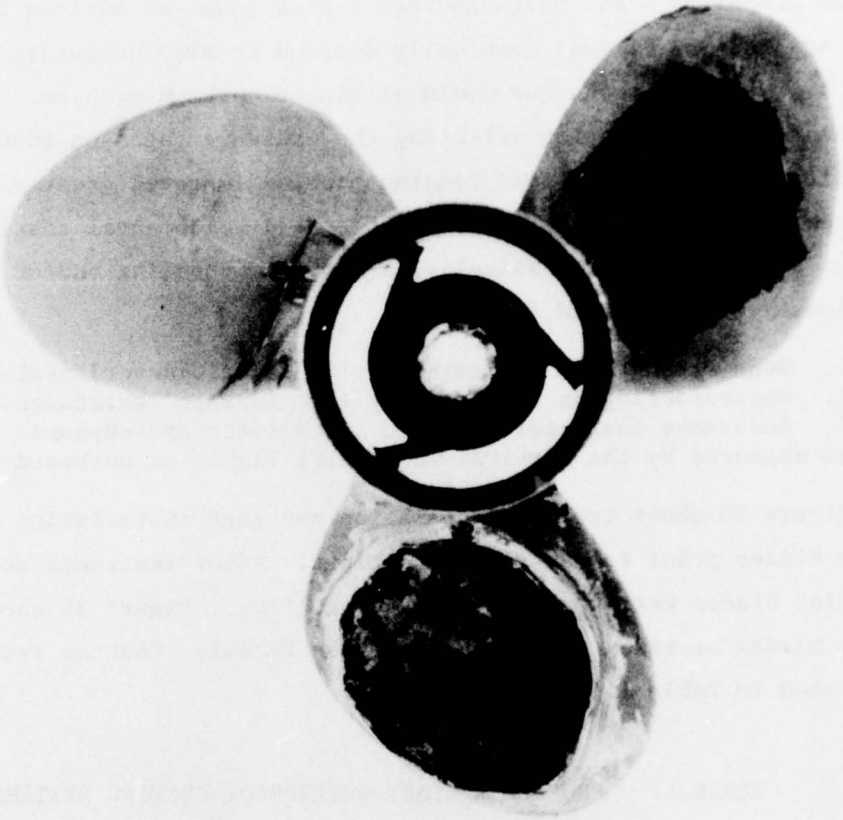

Figure 35 - Typical Test Coatings on Outboard Motor Propeller Blade

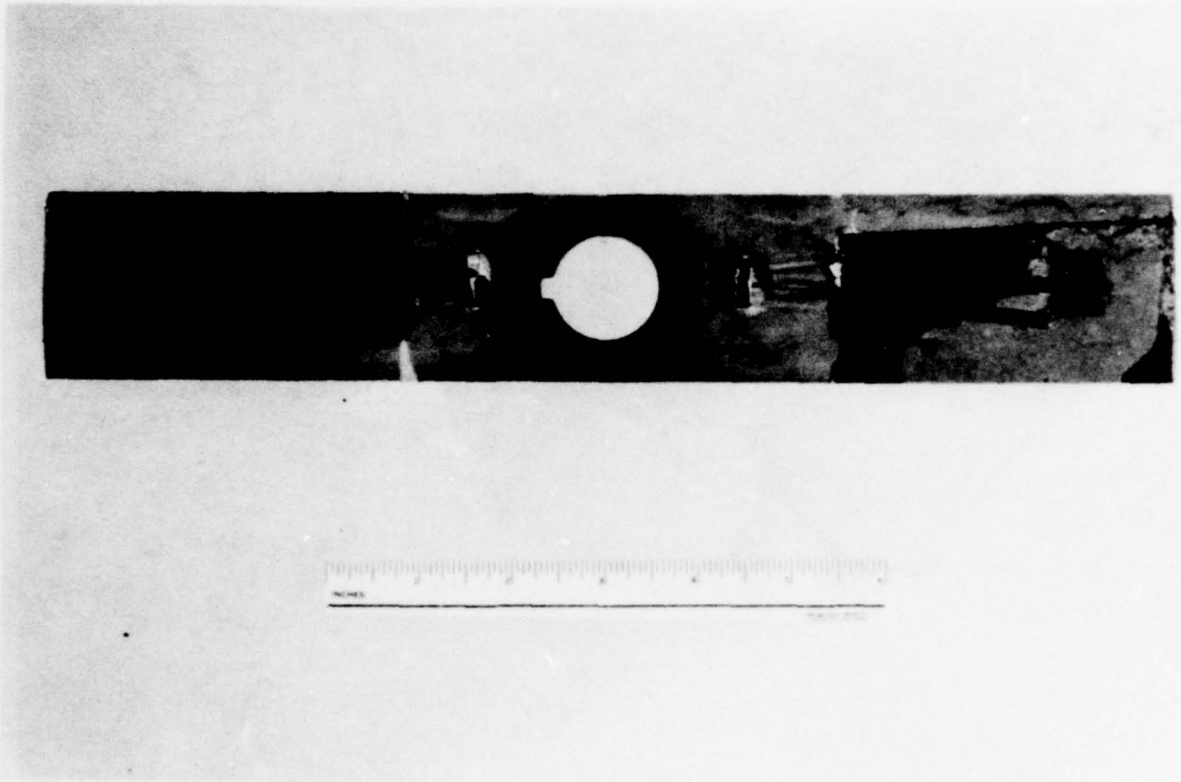

Figure 36 - Typical Test Coatings on Whirl Rig Blade

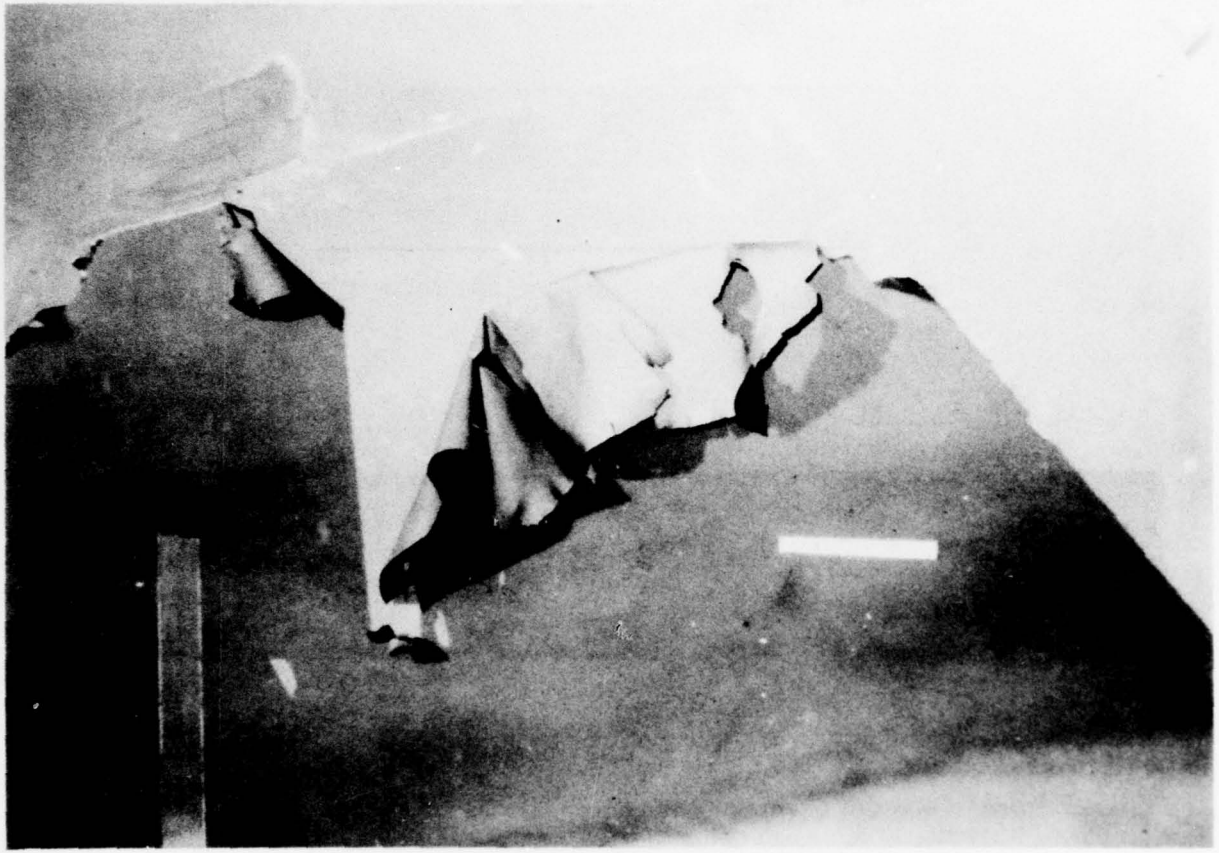

Figure 37 - Full-Scale Test Application of Urethane Coating
(Early applications did not meet peel strength tests)

Figure 38 - Typical Preparation and Gage Installation Prior to Waterproofing

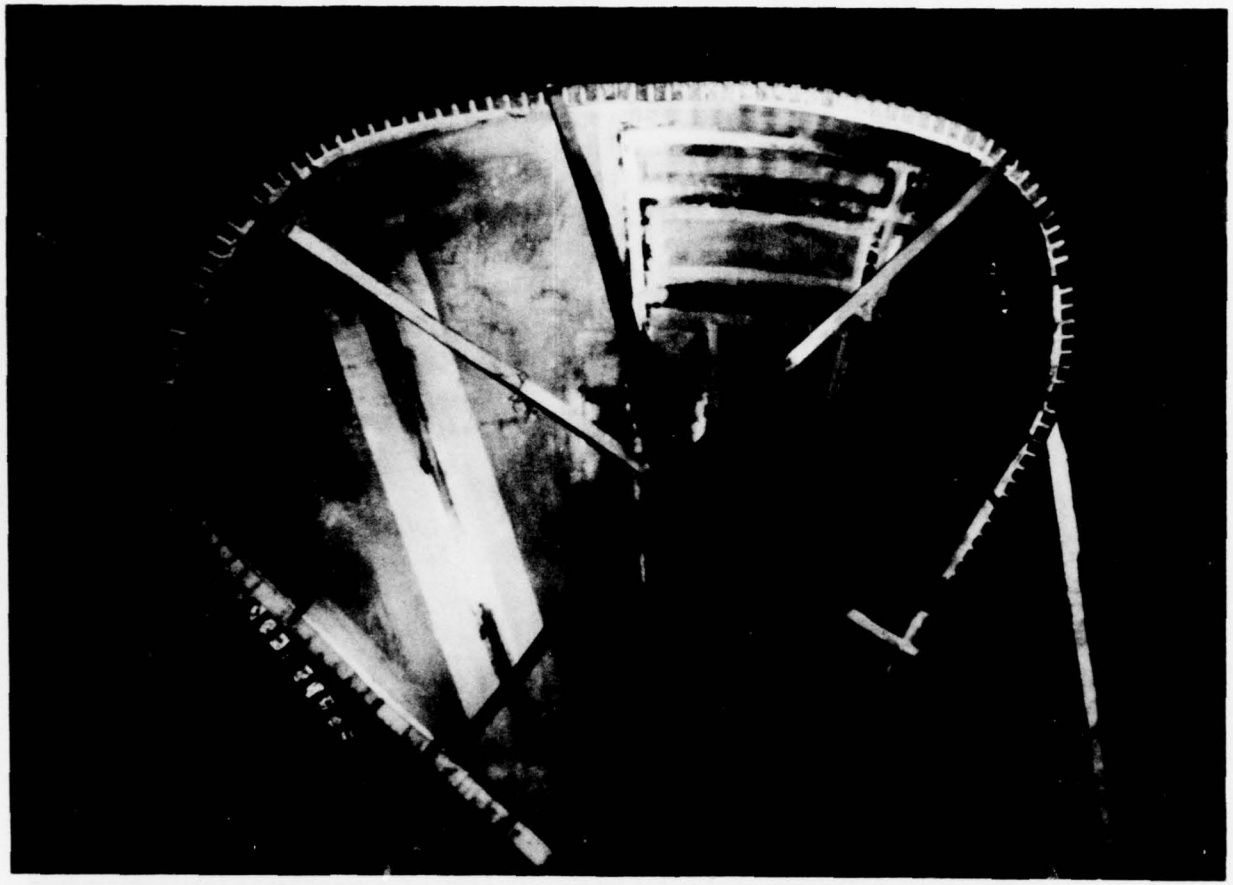

Figure 38a — Typical Propeller Blade as Received at DTNSRDC

Figure 38 (Continued)

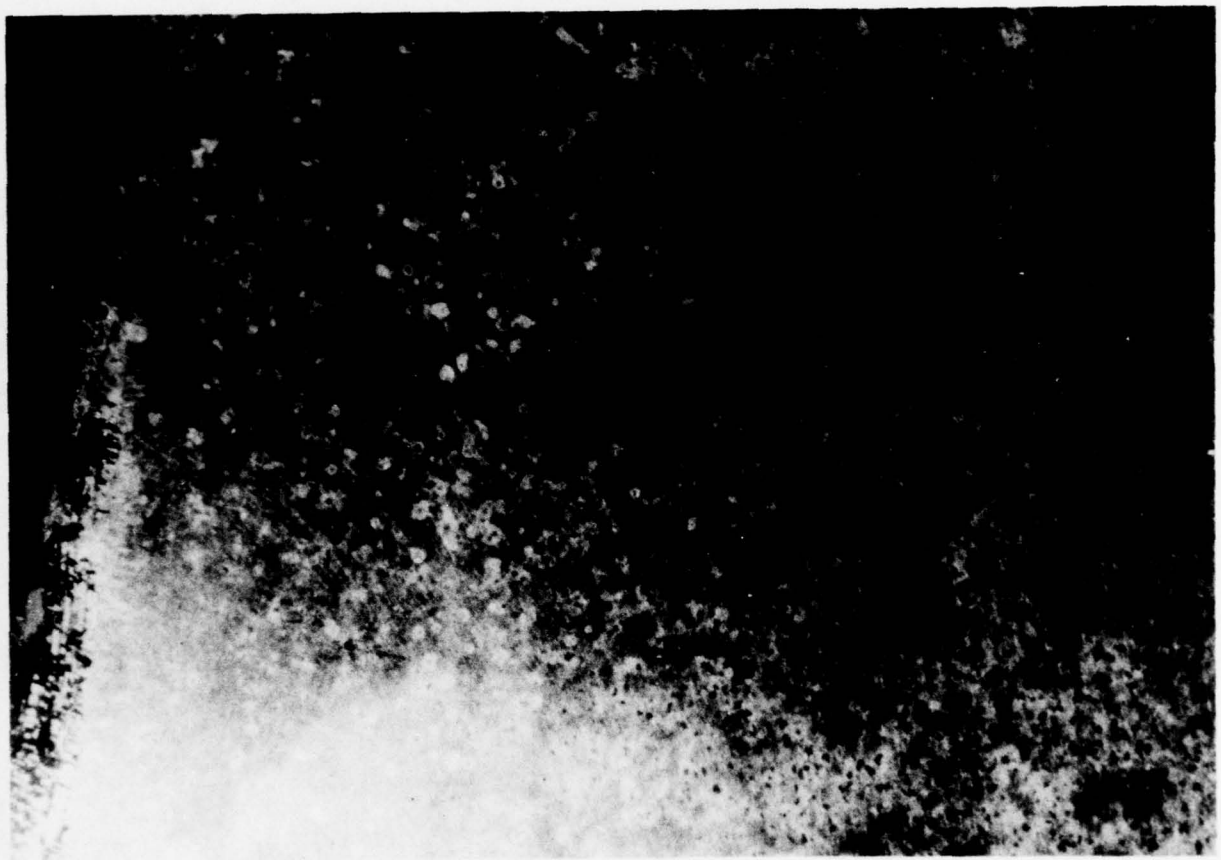

Figure 38b - Typical Surface of Propeller Blade As Received
(Note porous holes were filled with oil used for
blade machining process)

Figure 38 (Continued)

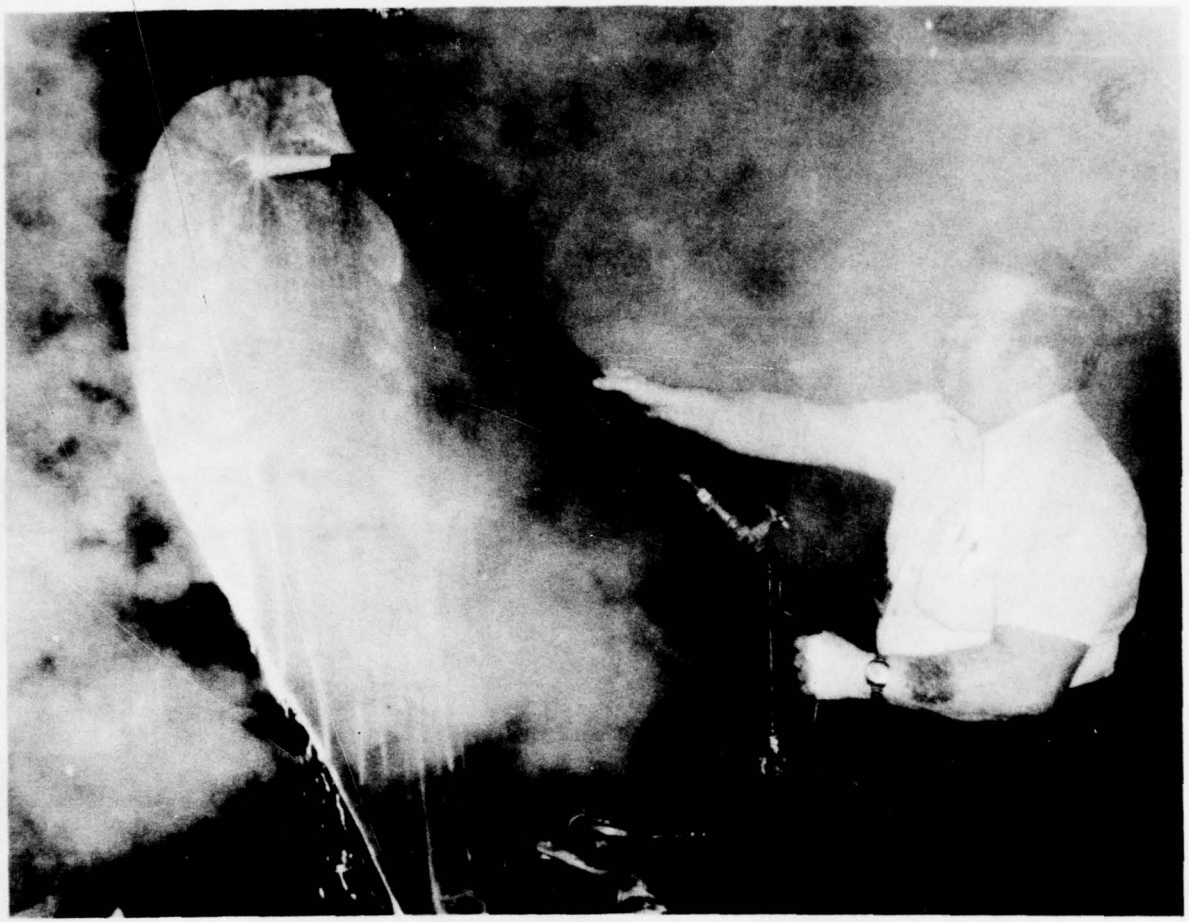

Figure 38c — Steam Cleaning Blades to Remove Oil

Figure 38 (Continued)

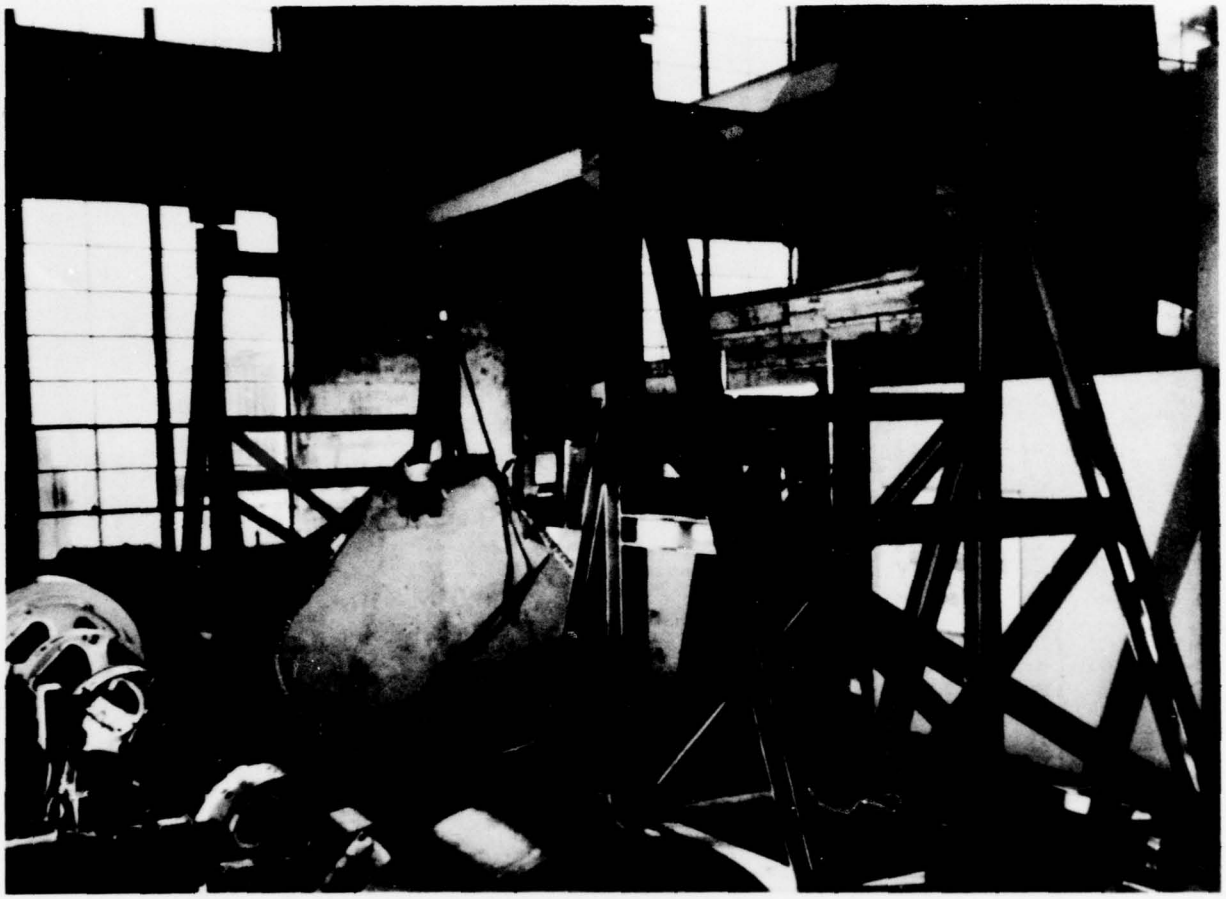

Figure 38d — Typical Propeller Blade Ready for Instrumenting

Figure 39 - Propeller Blades Ready for or Installed on BARBEY

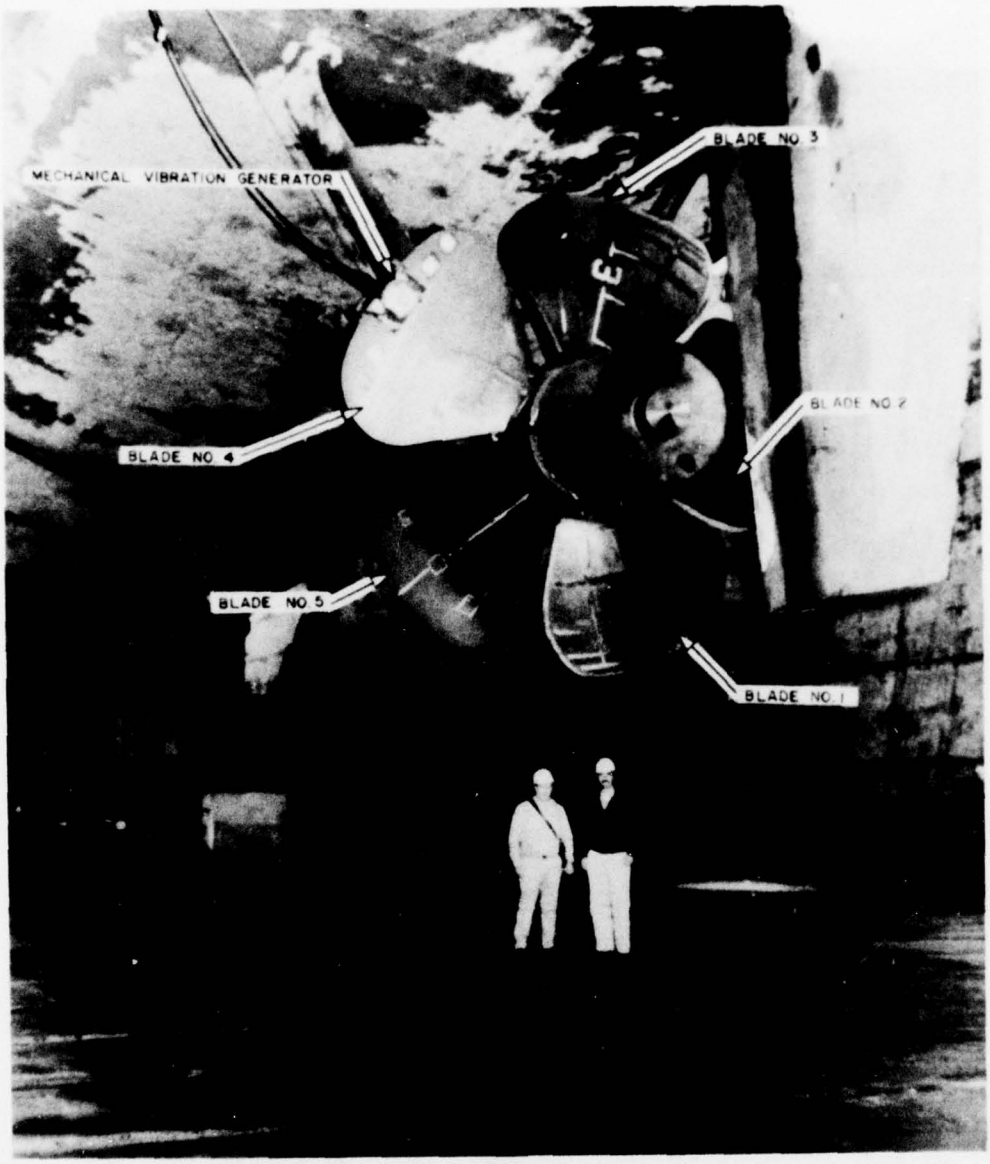

Figure 39a — General View of Instrumented CPP Propeller
Prior to April 1975 Sea Trials

Figure 39 (Continued)

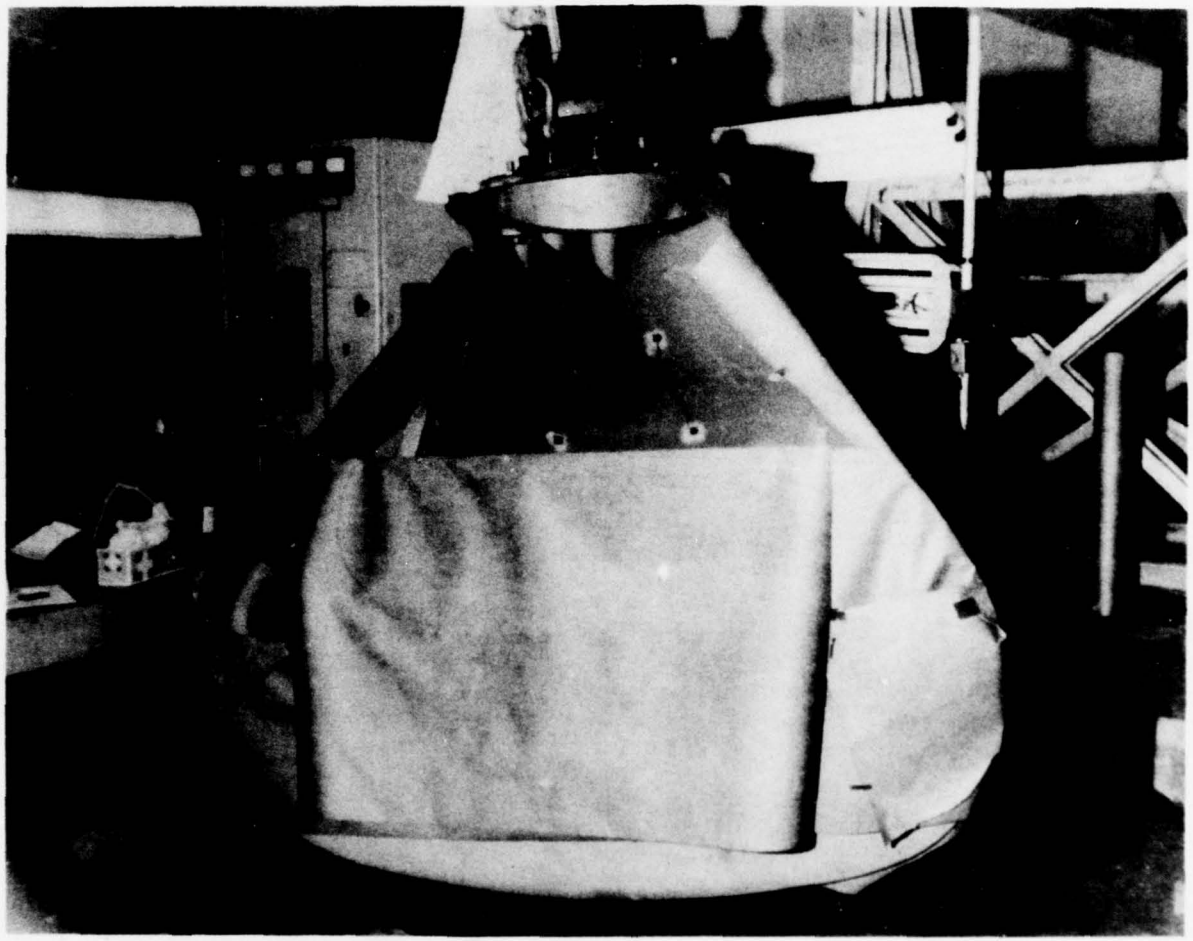

Figure 39b — Typical Strain Gage Rosettes on 40- and 50-Percent Radius

Figure 39 (Continued)

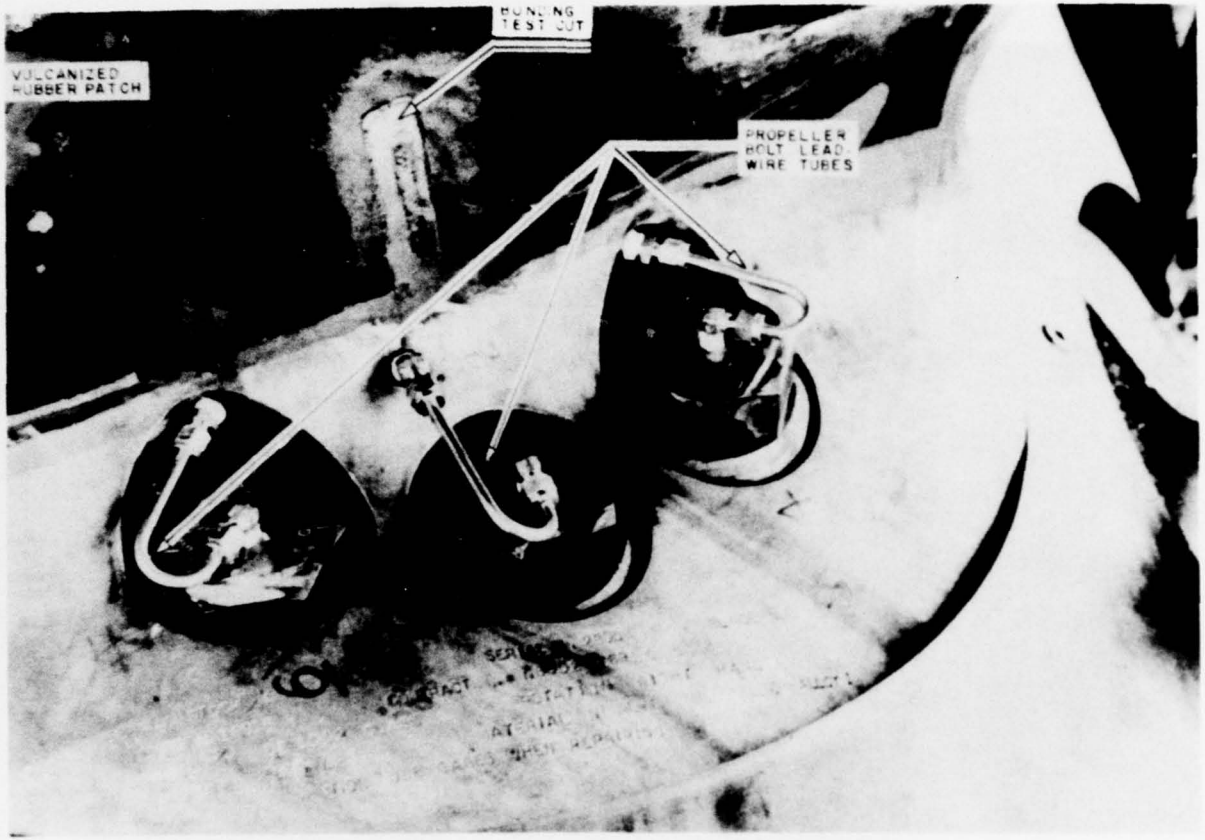

Figure 39c - Propeller Blade 2, March 1975 Pretrial Final Bolt Installation (Blade Face)

Figure 39 (Continued)

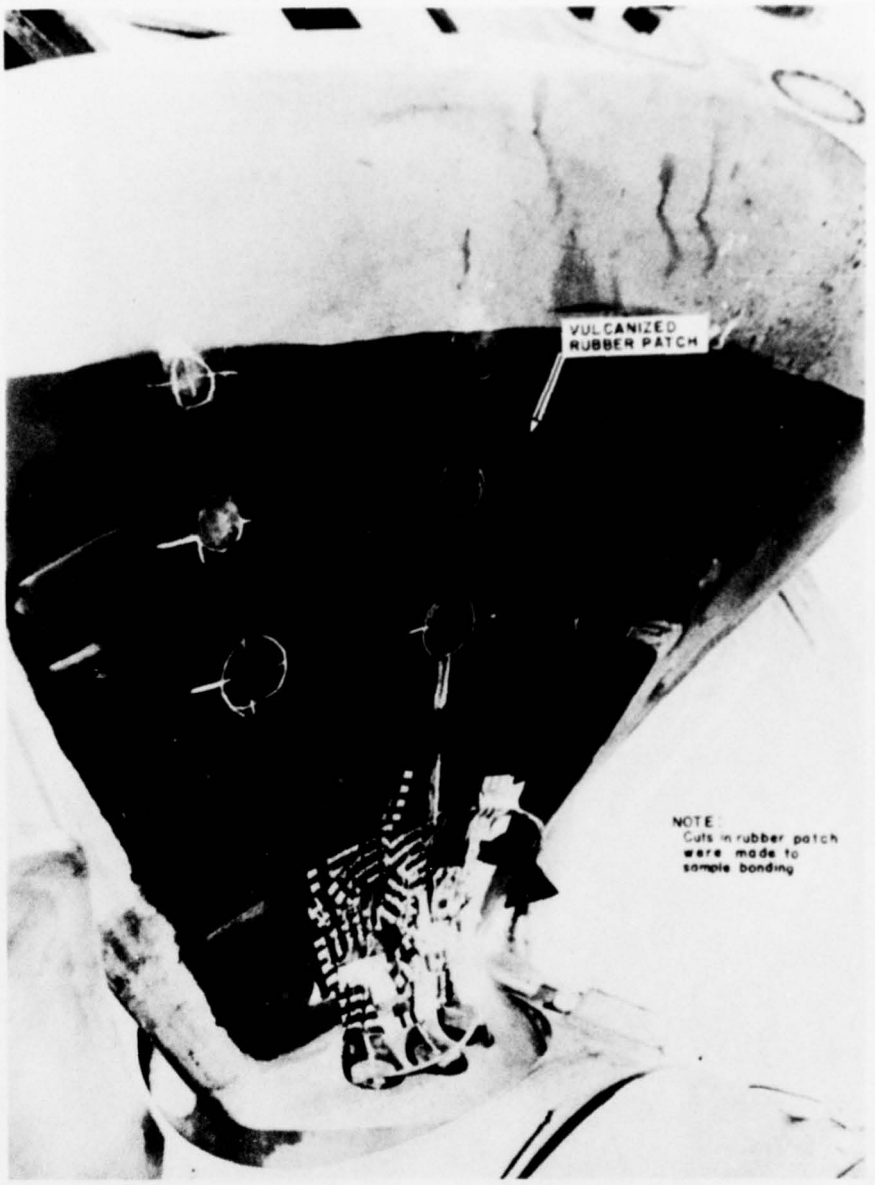

Figure 39d - Propeller Blade 2, March 1975 Pretrial (Blade Back)

Figure 39 (Continued)

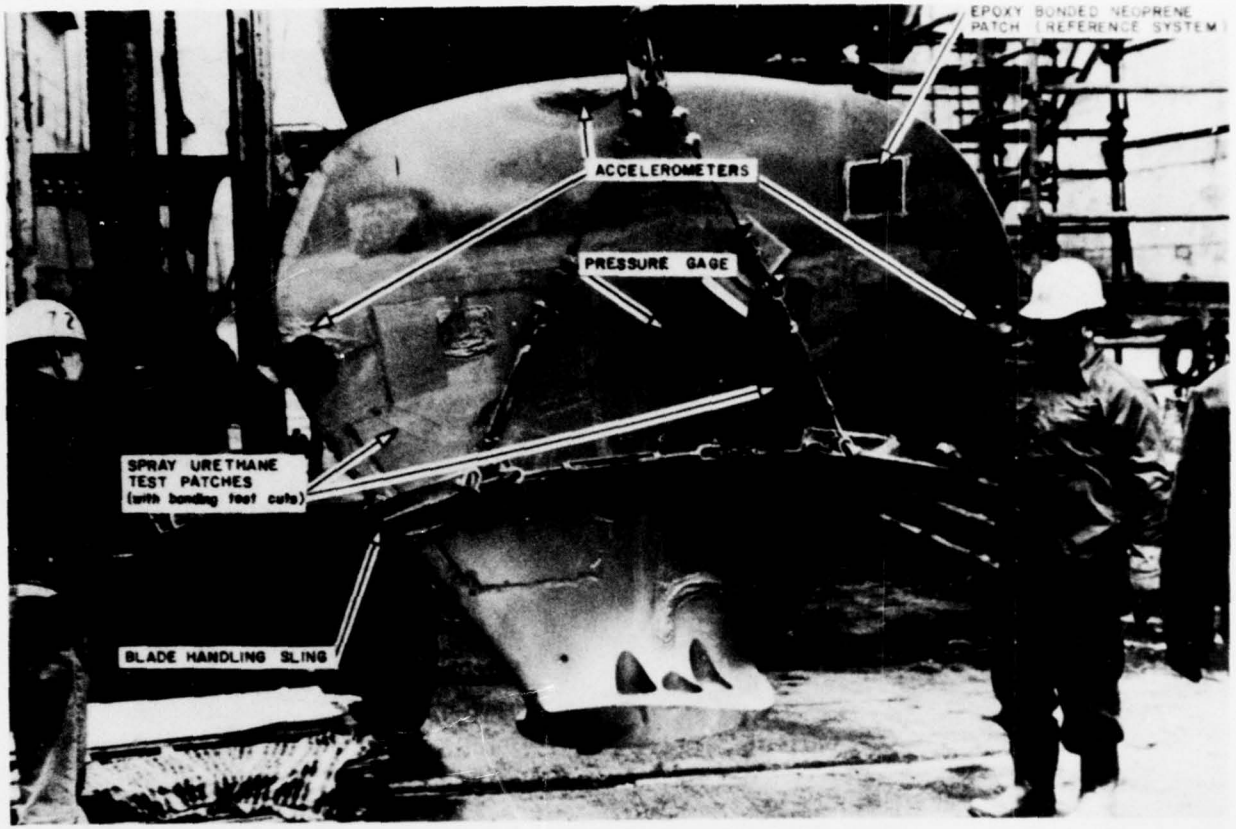

Figure 39e - Back of Propeller Blade 4, March 1975 Pretrial

Figure 39 (Continued)

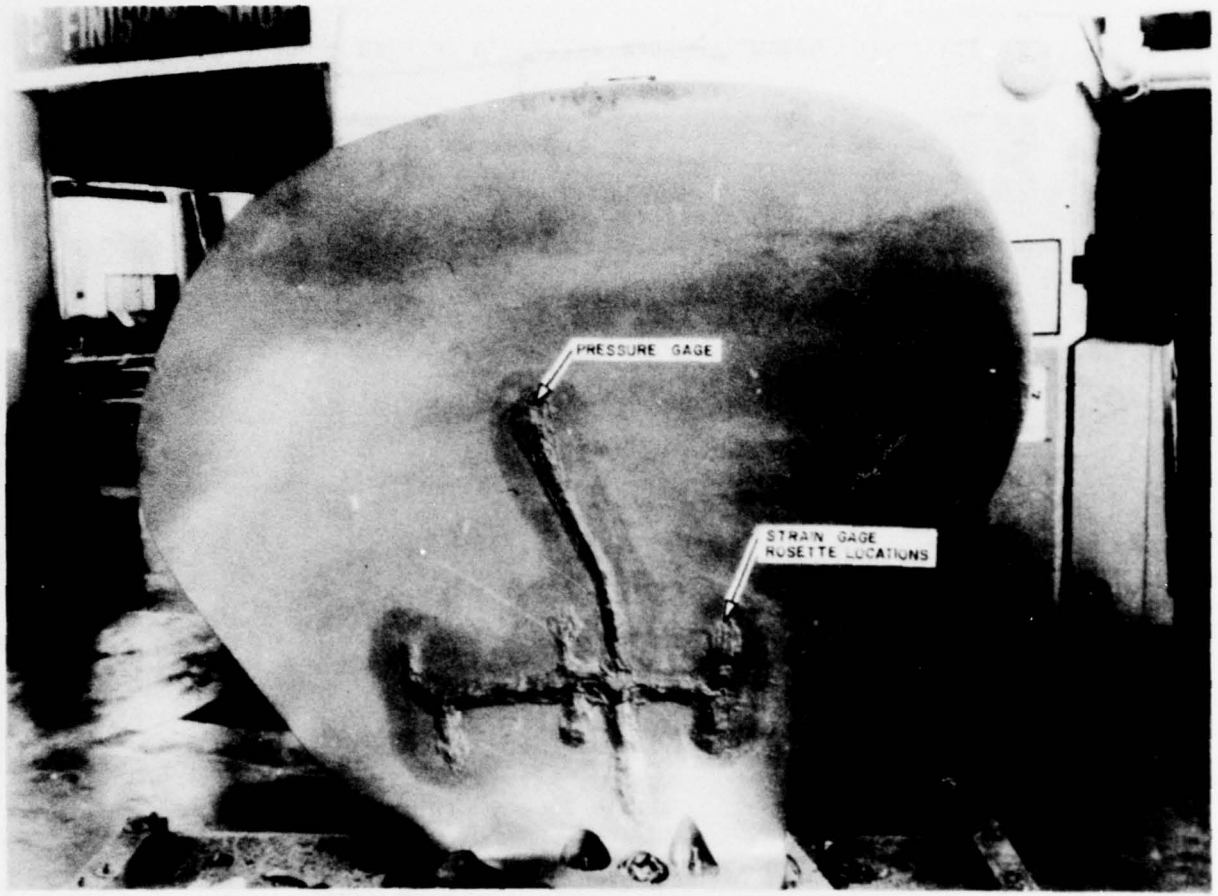

Figure 39f - Face of Propeller Blade 4, Jan 1975 Pretrail

Figure 39 (Continued)

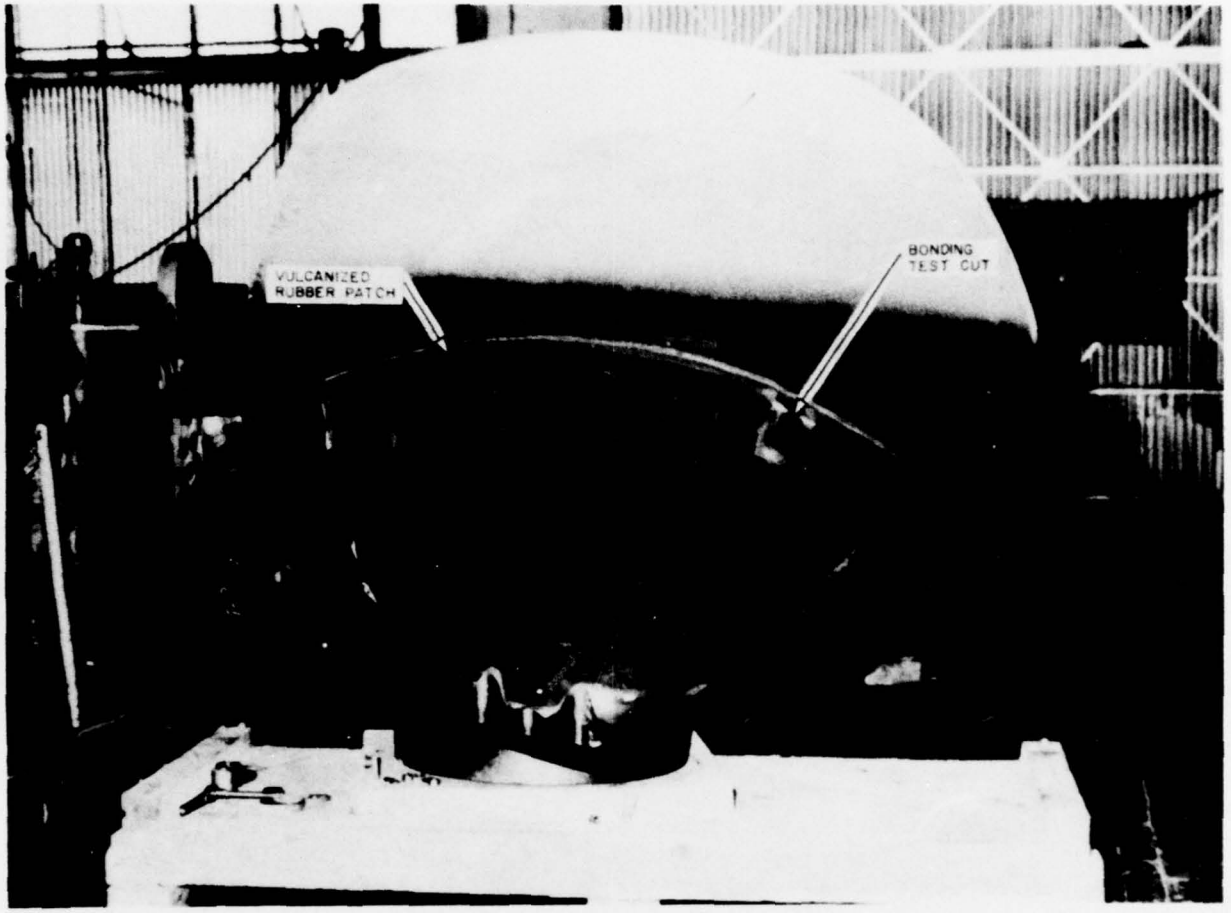

Figure 39g - Back of Propeller Blade 5, March 1975 Pretrial

Figure 39 (Continued)

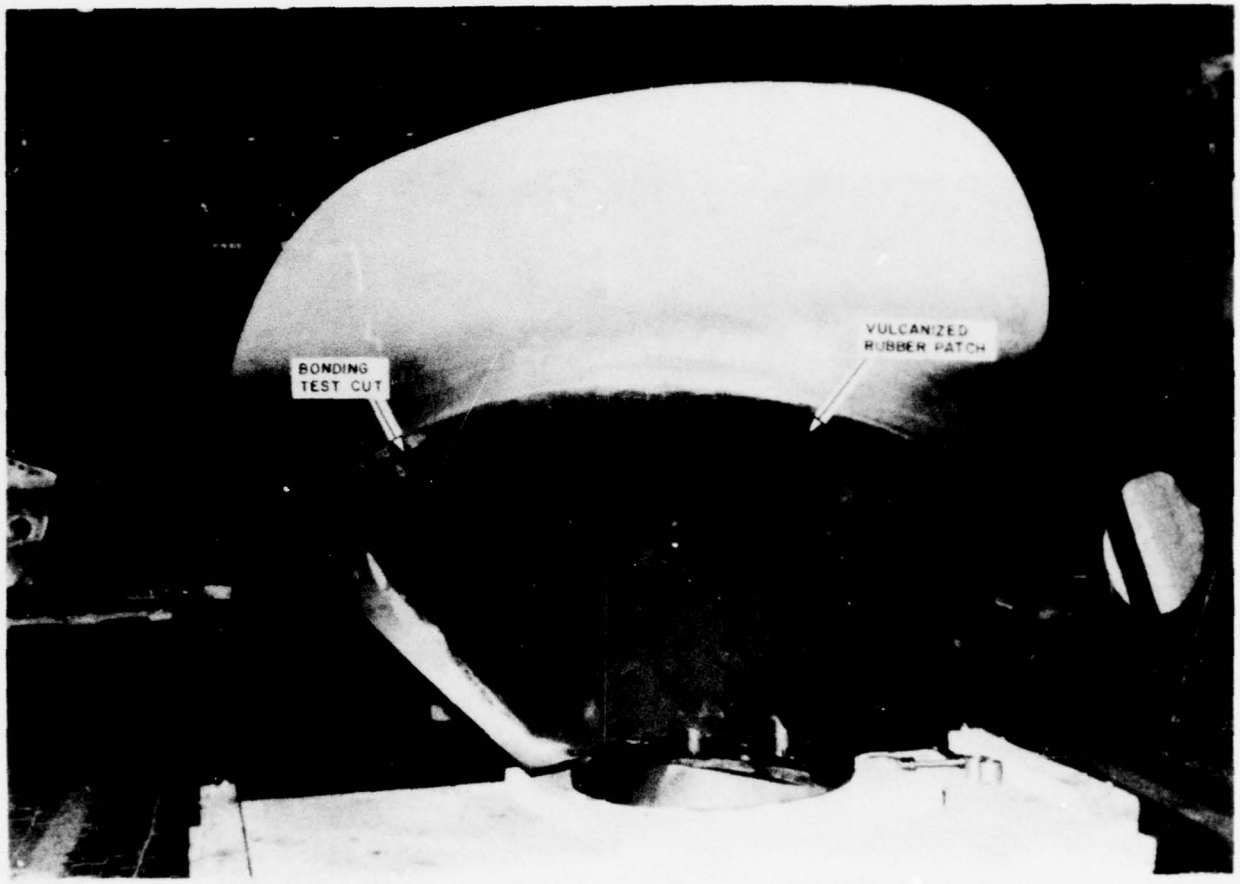

Figure 39h – Face of Propeller Blade 5, March 1975 Pretrial

The deep cuts in the patches (both sides of Blades 2 and 5, and blade back of Blade 4) were made to test the bond of the finished product.

Figure 40 shows the typical instrumentation and waterproofing of the propeller blade bolts and crank disk.

After completion of all instrumentation, the drydock was flooded on 2 April 1975. The performance of the gage protection system was monitored periodically in order to evaluate the long-term effects of submersion and cavitation. A final evaluation was made in January 1976 when BARBEY was drydocked for conversion back to a conventional propulsion system. The results are tabulated in Table 12. It is obvious from this table that virtually all gages under the primary protection system (vulcanized rubber) were intact;* the rubber showed no wear or damage after 287 days of submersion and approximately 1400 hours of main propulsion plant operation.

The condition of the various coating systems after this operational period (April 1975 – Jan 1976) are shown in Figure 41. This figure generally showed that:

1. All vulcanized patches on propeller Blades 2 and 5 were virtually intact with no damage on either the blade face or back.

2. Spray urethane patch on propeller Blade 4 was completely gone on the blade face and only partially intact on the blade back.

3. The epoxy-bonded neoprene patch (reference system) which was placed on the 80-percent radius (3/4 chord, back side) of propeller Blade 4 was partially intact.

It is concluded that vulcanized rubber coating provides excellent, long-term, mechanical and immersion protection for underwater instrumentation

---

*All gages were checked at their nominal resistance value and had a resistance-to-ground of better than 20μΩ. Details of CPP propellers, bolts, and crank disk strain gage installation and waterproofing development can be found in References 22 and 23.

[22]Dean, Mills, "Strain Gage Installation and Waterproofing on Propeller Blades and Associated Components on the USS BARBEY (FF-1083)," DTNSRDC Report (in preparation).

[23]Dean, Mills, "Vulcanized-Rubber Protection for Strain Gages in a Seawater Environment," Experimental Mechanics, Vol. 17, No. 8, pp. 303-307, (Aug 1977).

Figure 40 - Typical Instrumentation and Waterproofing

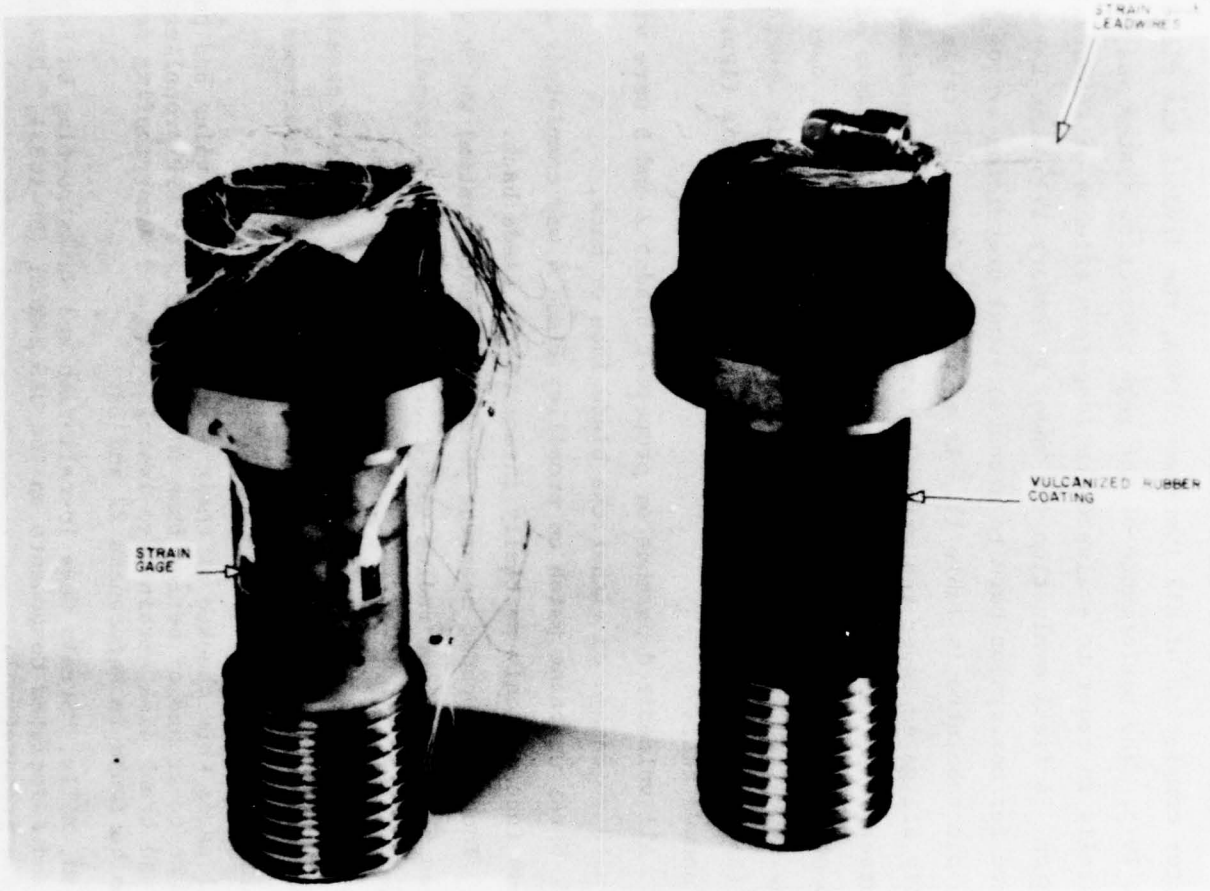

Figure 40a — Instrumented Propeller Blade Bolts

Figure 40 (Continued)

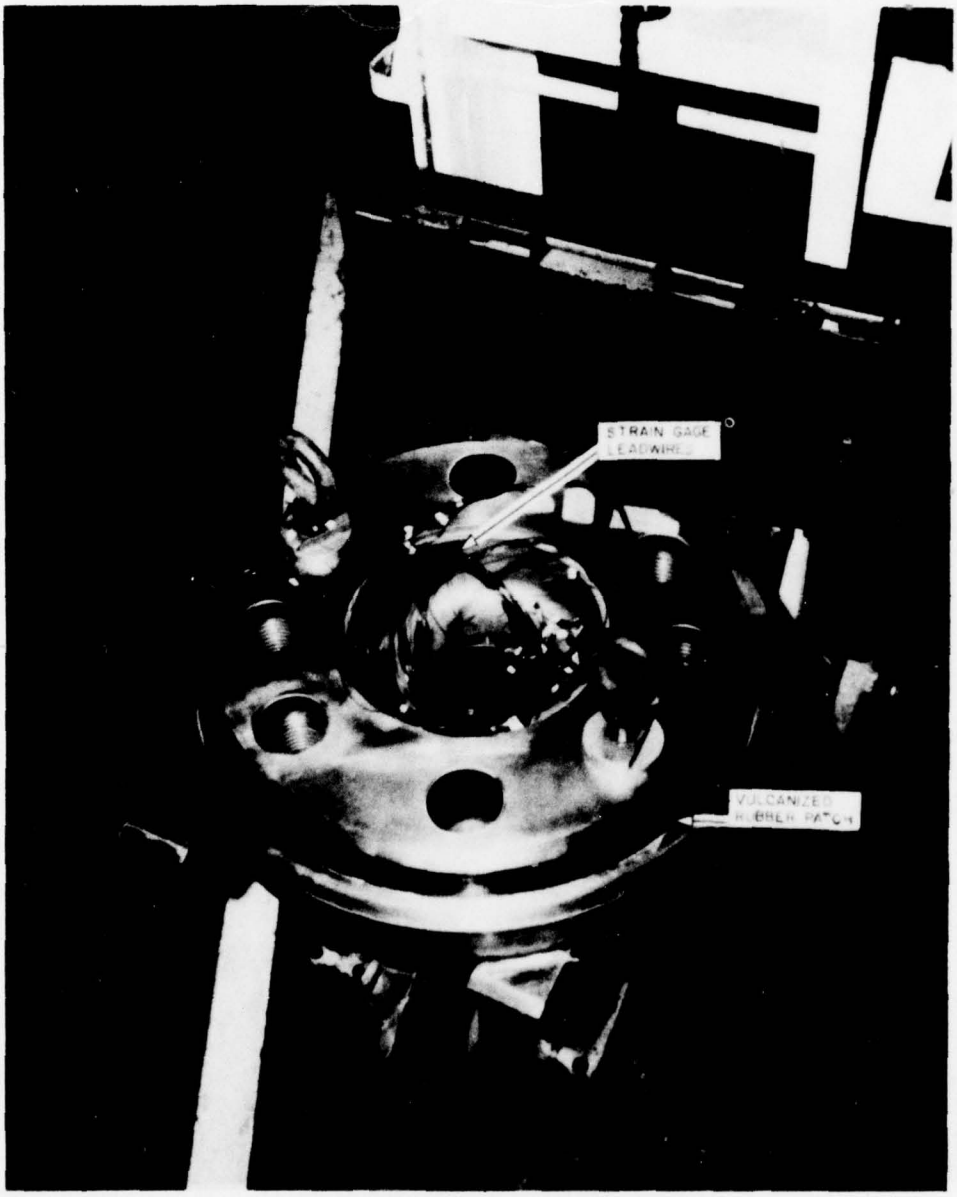

Figure 40b — Disk Ready for Installation

Figure 40 (Continued)

Figure 40c — Strain Gage Installation for Crank Disk

TABLE 12 - LONG-TERM EFFECTS OF SUBMERSION AND CAVITATION ON OUTBOARD INSTRUMENTATION

Period	Surviving Gages No. (%) of Surviving Gages						Total No. of Days Submerged	Operation Total No. of Main Propulsion Plant** hr
	Vub. Rubber		Spray Methane		Total			
	No.	Percent	No.	Percent	No.	Percent		
Original Flooding (4/2/75)	96	(100)	24	(100)	120	(100)	0	0
Completion of Sea Trials (4/12/75)	96	(100)	18	(75)	114	(95)	11	100
Dockside (8/8/75)	96	(100)	0	(0)	96	(80)	125	700
Drydocking to Remove CPP System (1/13/76)	80*	(83)	0	(0)	80	(67)	287	1371

*Gages lost inboard at sliprings: further investigation showed gages to be good at installed location.

**Total operating time for CPP system since original installation (November 1973) was 3439 hours.

Figure 41 - Condition of Various Coating Systems After Operational Period

Figure 41a – Forward View of Instrumented CPP Propeller After Sea Trials

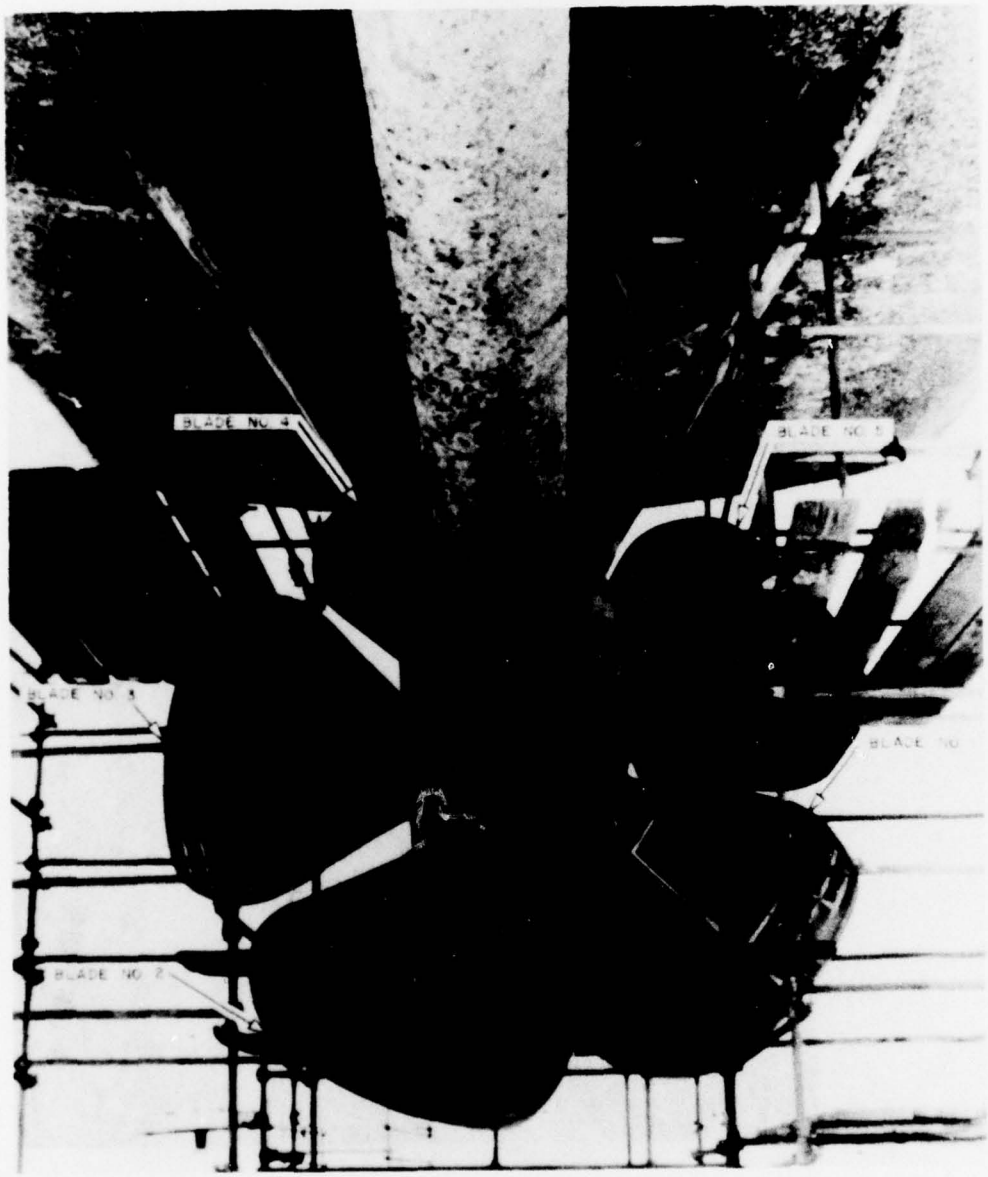

Figure 41b -- Looking Aft

Figure 41 (Continued)

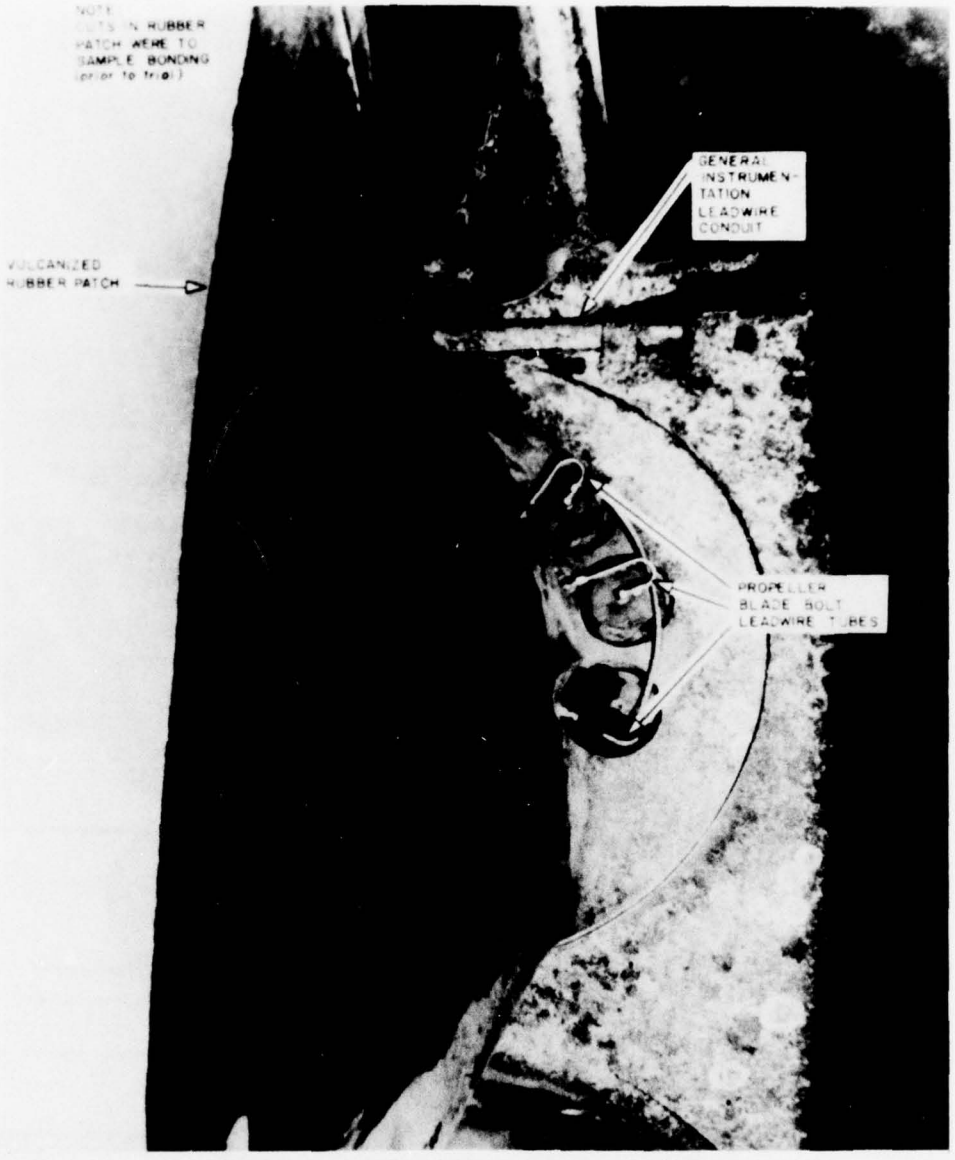

Figure 41c — Propeller Blade 2

Figure 41 (Continued)

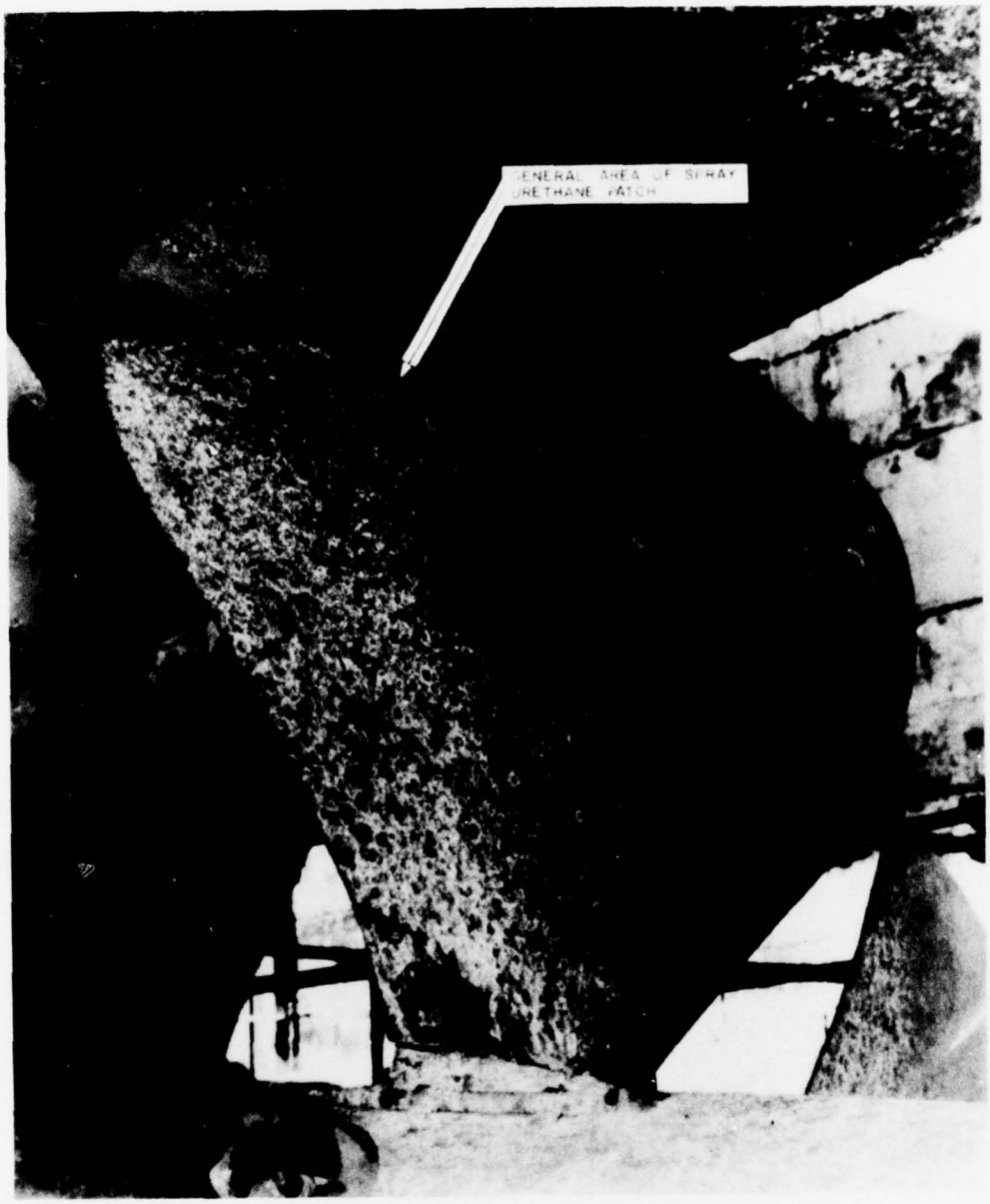

Figure 41d — Face of Propeller Blade 4

Figure 41 (Continued)

Figure 41e — Back of Propeller Blade 4

Figure 41 (Continued)

Figure 41f — Face of Propeller Blade 5

Figure 41 (Continued)

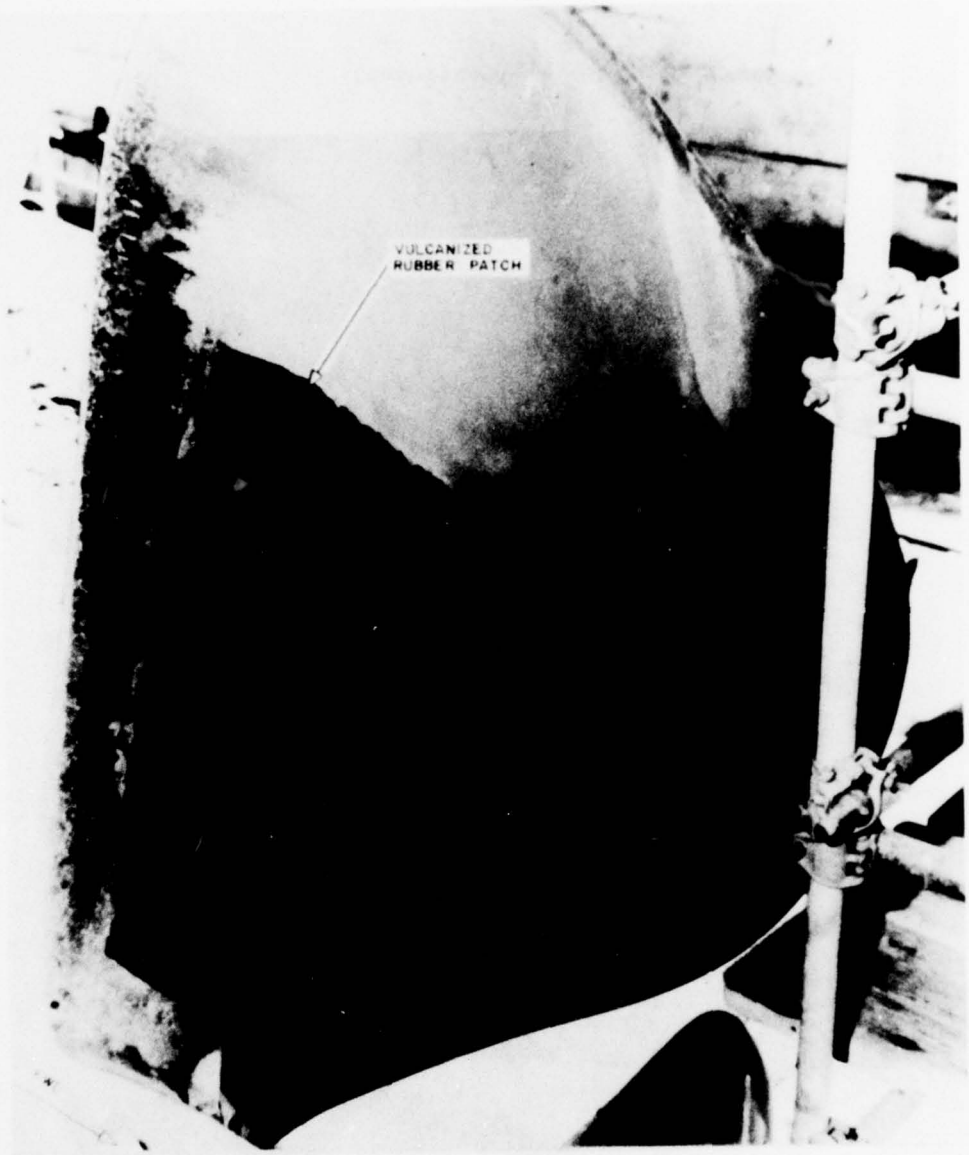

Figure 41g – Back of Propeller Blade 5

Figure 41 (Continued)

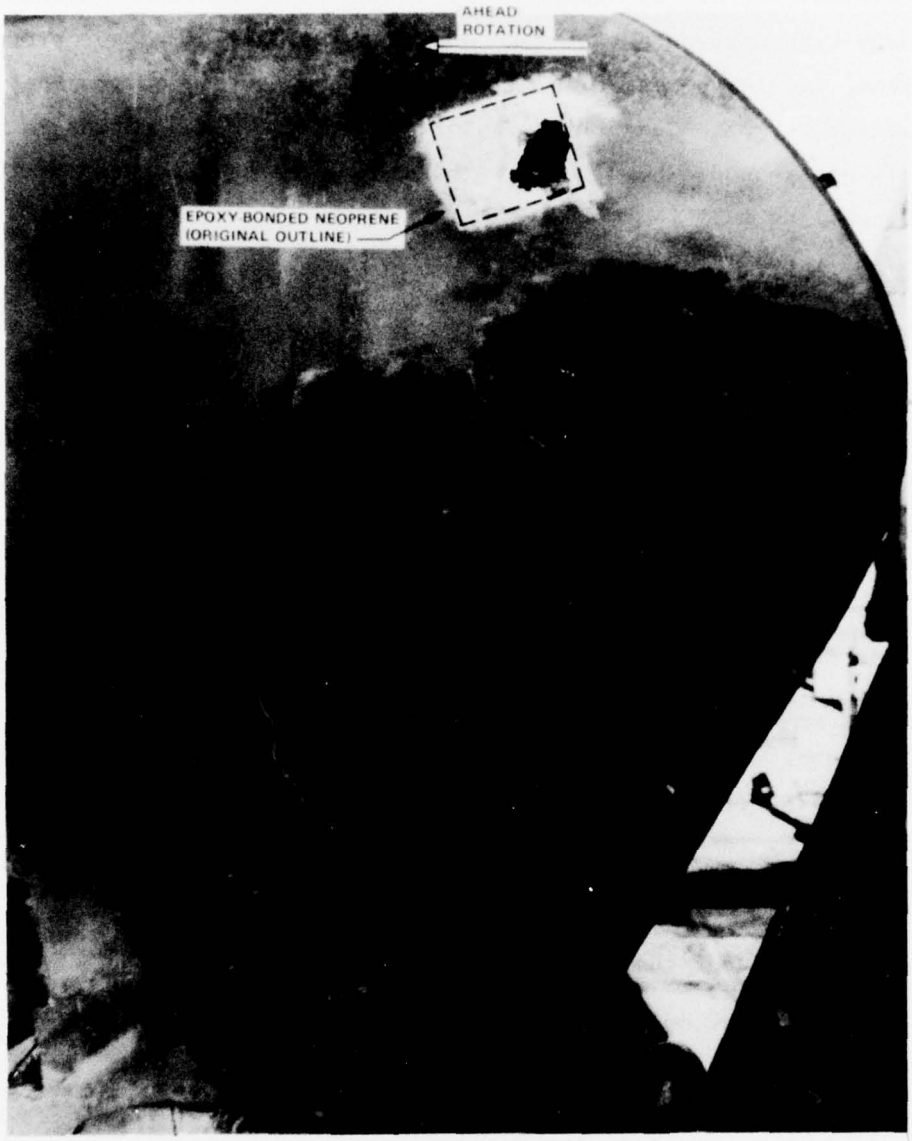

Figure 41h - Epoxy-Bonded Neoprene Patch (Reference System)
(On back of Blade 4, 80 percent R, 3/4 Chord)

even in the most hostile environments. The more easily applied spray urethane is useful in short-term applications.

In summary, it can be concluded that underway propeller measurements can be made with assurance that when used with vulcanized rubber protection system, the instrumentation will survive the adverse environment of the propeller for extended periods. In cases where vulcanization is not practical, epoxy-bonded neoprene or urethane can be used on a short-term (1- or 2-week) basis.

TEST PROCEDURE AND RESULTS

The large number of gage locations (Table 10) and trial runs (Table 8) together with the almost infinite variety of data processing and presentation techniques make it impractical from the standpoint of time and economy to cover all aspects of the recorded material. For this reason, most of the data presented in this report will be primarily limited to addressing the immediate problem involving the mechanical suitability of the BARBEY CPP mechanism as related to future design considerations involving a CPP installation. Test procedure and results will be presented under the following subheadings:

1. Drydock Tests
2. Dockside Tests
3. Underway Tests

DRYDOCK TESTS

The objectives of the drydock tests were:

1. To develop a measurement technique which would define bolt preload.
2. To determine the final residual preload after trials and extended operational period.
3. To measure the stresses induced in the bolts and crank disk by preloading.
4. To measure the static response of the blades, bolts, and crank disk to a known load.

5. To determine the dynamic characteristics of the propeller blades and the resulting effect on system response.

Bolt Preloading

The theory of bolted joints for use in a dynamic load environment has been covered by many authors.[24-30] It is generally recognized that if the preload characteristics (induced preload versus some measureable parameter) and the external loads (both static and dynamic) can be defined, then the appropriate bolt preload can be applied which will effectively minimize the cyclic bolt load, thereby minimizing the possibility of bolt fatigue failure. Although the concept of how this is accomplished is relatively simple theoretically, variables involved (joint geometry, thread load distribution, etc.) make the actual determination of preload characteristics difficult.*

---

[24]Faires, V.M., "Design of Machine Elements," Third Edition, MacMillan Company, New York (1955) Chapter 5.

[25]Horger, O.J., "Metals Engineering Design," ASME Handbook (1965).

[26]Snow, A.L. and B.F. Langer, "Low Cycle Fatigue of Large Diameter Bolts," ASME Papter 66-Pet-8 (Sep 1966).

[27]Fazekas, G.A., "On Optimal Bolt Preload," Journal of Engineering for Industry, Trans. SNAME (Aug 1976).

[28]Motosh, N., "Determination of Joint Stiffness in Bolted Connections," Journal of Engineering for Industry, Trans. ASME (Aug 1976).

[29]Stephenson, J. and R. Callander, "Engineering Design," John Wiley & Sons, New York (1974), Chapter 13.

[30]Meyer, G. and D. Strelow, "Simple Diagrams Aid in Analyzing Forces in Bolted Joints," Assembly Engineering, Vol. 15, No. 1 (Jan 1972).

*For example, calculations of bolt stiffness for the bolts used for trials range from 17 x 10^6 lb/in. to 28 x 10^6 lb/in. depending on the actual value of length which participates in elongation under load (effective length). Calculations for joint (blade palm to crank disk) stiffness are even more obscure since both the effective area and the effective length of both members are unknown.

In the case of BARBEY, the bolts on Propeller Blade 2 were instrumented with strain gages so the average* stress in the bolt shank could be measured directly during installation. The bolt preload on the other blades (Nos. 1, 3, 4, and 5) was determined from measured bolt elongation. The relationship between average stress in the bolt shank and bolt elongation was determined with a specially instrumented bolt which enabled simultaneous measurements of strain (stress) and elongation during drydock installation. Two other control parameters (torque and angular rotation) were recorded during initial evaluation as a secondary verification of the results. These tests were repeated about five times to check repeatability. Results (Figures 42 – 44) of these tests indicate that:

1. Individual bolt response was linear either in tension or compression.

2. When a load was directly applied to the bolt in making up (preloading) the blade, the palm/crank disk interface produced a linear** response.

3. Bolt effective length $L_{(EFF)}$ was approximately 4.6 in.***

4. The ratio of bolt stress (in kips per square inch) to elongation (in mils) was ≈ 6.2.

---

*In discussing bolt stresses, the following definitions are appropriate:
Average Stress $(\sigma_{Avg}) = (\sigma_1 + \sigma_2 + \sigma_3 + \sigma_4)\ /4$
where σ_1, σ_2, σ_3 and σ_4 are the individual axial midshank stresses determined by four gages spaced 90 deg apart around the shank circumference.

$$\text{Maximum Stress } (\sigma_{max}) = \left[\left(\frac{\sigma_1 - \sigma_3}{2}\right)^2 + \left(\frac{\sigma_2 - \sigma_4}{2}\right)^2\right]^{1/2} + \sigma_{Avg}$$

where $\frac{\sigma_1 - \sigma_3}{2}$ and $\frac{\sigma_2 - \sigma_4}{2}$ are orthogonal bending stresses.
Note that all bolt stresses, average and maximum, refer to stresses measured at the bolt midshank.

**Examination of Figures 43 and 44 indicates a nonlinearity in the low load ranges. This is attributed to the initial bolt seating torque, after which the response is linear. Measurement of bolt elongation would inherently eliminate this unknown and therefore this parameter was used to determine preload on the noninstrumented bolts.

***Assumes effective diameter of 2 1/8 in.

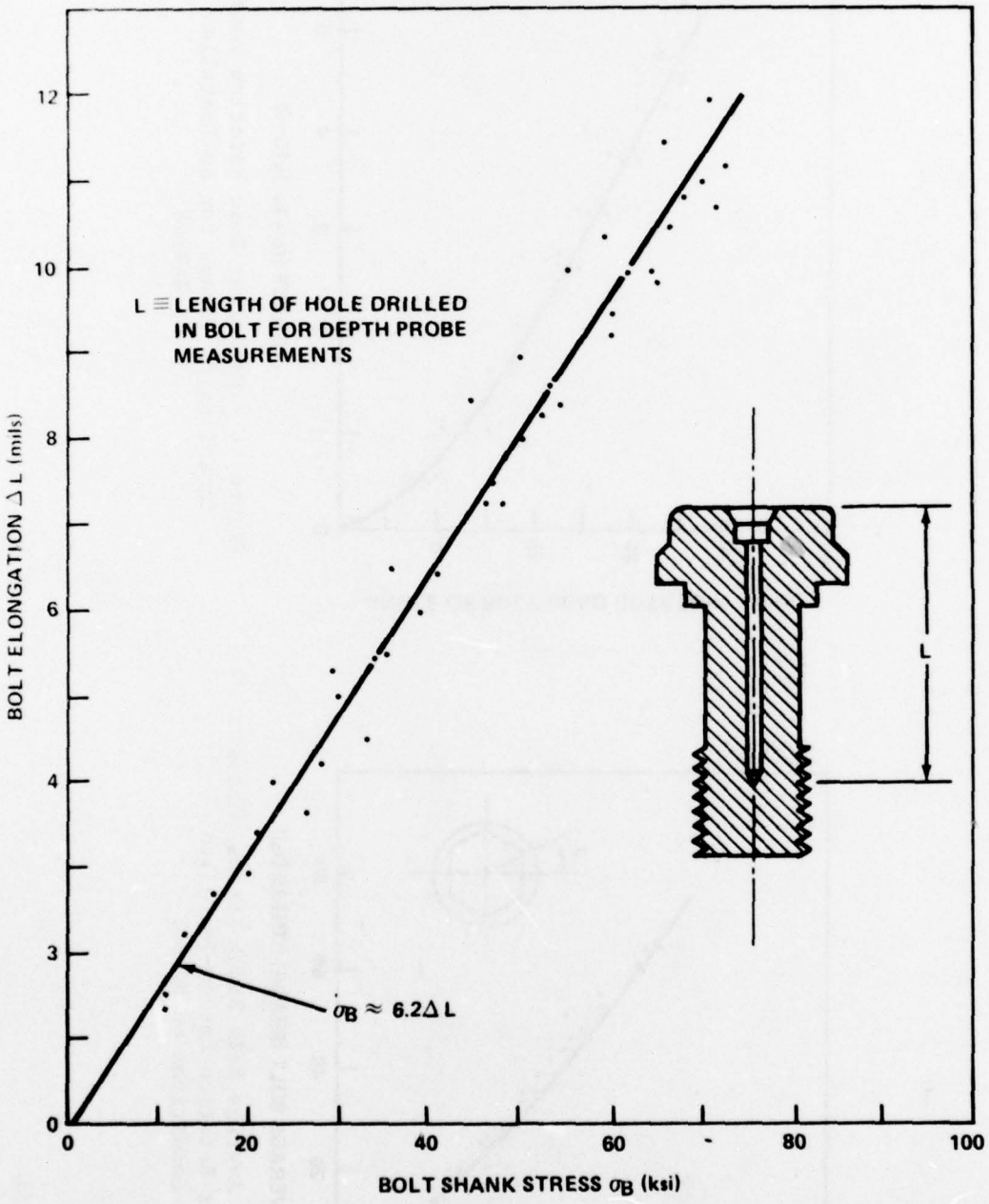

Figure 42 - Average Bolt Shank Stress versus Elongation for As-Installed Conditions on BARBEY

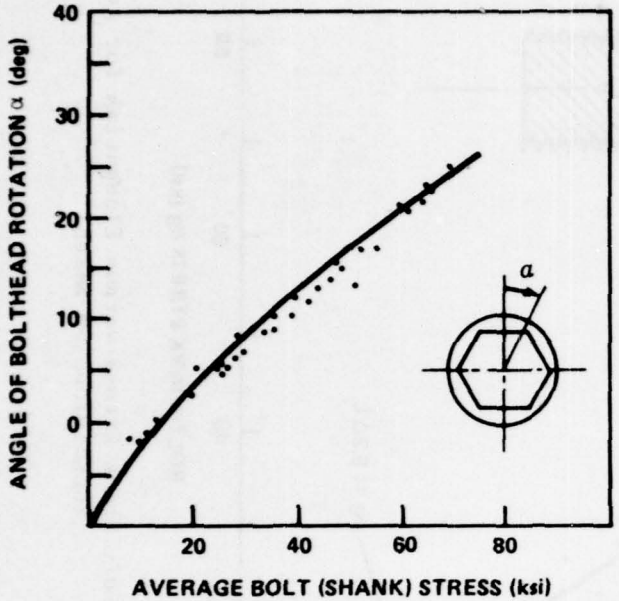

Figure 43 - Average Bolt Shank Stress versus Angular Rotation for As-Installed Conditions on BARBEY

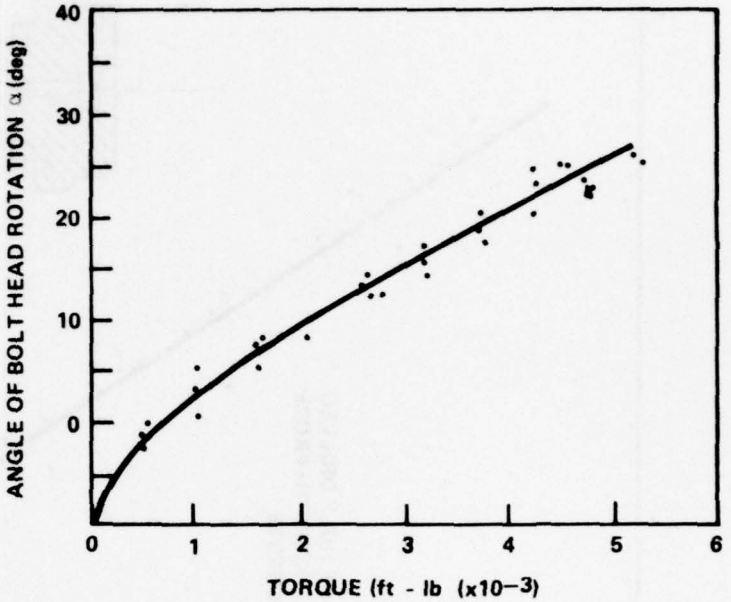

Figure 44 - Propeller Bolt Rotation versus Installation Torque for As-Installed on BARBEY

Following determination of bolt preload characteristics, there was still the problem of the proper amount of preload to be applied. Since it is not possible to define the service loads which a marine propeller will experience under all operating conditions, a value of 55 ksi was established more or less arbitrarily. However, this value was felt to be a pragmatic compromise between preload sufficient to avoid bolt fatigue and yet insufficient to cause gross yielding in the bolt.* The final (pre-trial) preload stresses on all bolts are given in Tables 13 and 14. Values in Table 13 indicate that the bolts on Blade 2 had essentially the same axial preload (approximately 56 ksi). However, a certain amount of bending occurred in each bolt. Although preload bending averaged only about 15 percent, it must be pointed out that this was 15 percent of a load which was more than one-half the yield strength of the bolt material. Actual values ranged from approximately 4 to 11 ksi. It is noted that bending stress for the bolts on the face of Blades 6, 2, and 4 averaged approximately 66 percent higher than for bolts on the back of Blades 3, 1, and 5.

The axis about which being occurred on each bolt** on Blade 2 is shown in Figure 45 together with final bolt gage orientations. Observe that blade face bending axes tended to align with decreasing palm thickness contour, with the bolts bending away from the blade. The opposite was true for the blade back. The bending axes were generally perpendicular to decreasing blade contours, with the bolts bending toward the propeller blade. Certainly, it is recognized that the reason for bolt bending could be and usually is attributable to geometric differences within the assembled structure (allowable manufacturing tolerances in parallelism, perpendicularity, etc.). The amount of bending induced by geometric tolerance allowances is impossible to calculate since the amount and kind of tolerance are unknown. However, it seems reasonable that this type of bending would occur in a random fashion.

---

*It was recognized that local yielding would occur in the bolt threads because of the high stress concentrations in that area.

**Bolt bending axis can be determined for all preload and drydock data, but limitations in the underway trial installation cabling prevented determination of this parameter on all but Bolt 6 for underway operation.

TABLE 13 - MEAN STRESS IN BOLTS OF PROPELLER BLADE 2 AFTER PRELOADING

Location	Bolt No.	Bolt Stress (ksi)				Percent Bending Stress S_B
		$S_{Max.}$	$S_{Min.}$	S_{Avg}	S_B	
Blade Face	6	+67.2	+46.1	+56.6	±10.6	19
Blade Face	2	+63.3	+48.4	+55.9	±7.4	14
Blade Face	4	+66.1	+43.2	+54.7	±11.4	21
Blade Back	5	+61.3	+47.8	+54.6	±6.8	13
Blade Back	1	+61.6	+53.3	+57.5	±4.1	7
Blade Back	3	+63.9	+46.9	+55.4	±8.5	16

Notes:

1. Bending Stress (S_B) = ($S_{Max} - S_{Avg}$)
2. Percent S_B = (S_B/S_{Avg}) 100
3. No load on propeller blade (bolt preload only)
4. Four-gage average

TABLE 14 - SUMMARY OF PROPELLER BLADE BOLT ELONGATION AND SHANK STRESS DUE TO PRELOAD

Propeller Blade No.	Blade Bolt No.	Bolt Elongation* in. x 10^{-3}		Average Bolt Shank** Stress ksi	
		Mar 1975***	Jan 1976†	Mar 1975***	Jan 1976†
1	1	8.2	2.5	50.46	15.5
	2	8.5	6.5	52.31	40.3
	3	8.5	10.0	52.31	62.0
	4	9.0	8.0	55.38	49.6
	5	8.5	8.0	52.31	49.6
	6	9.0	5.0	55.38	31.0
2	1	9.3	8.6	57.45	52.87
	2	9.1	8.8	55.88	54.23
	3	9.0	9.0	55.41	55.58
	4	8.9	8.9	54.68	54.65
	5	8.9	8.5	54.58	52.09
	6	9.2	8.4	56.60	51.95
3	1	8.0	6.0	49.23	37.2
	2	9.0	7.5	55.38	46.5
	3	8.2	7.8	50.46	48.4
	4	8.5	11.5	52.31	71.3
	5	8.5	8.0	52.31	49.6
	6	8.8	8.0	54.15	49.6
4	1	7.8	7.5	48.00	46.5
	2	8.6	8.0	52.92	49.6
	3	8.5	9.5	52.31	58.9
	4	9.3	8.0	57.23	49.6
	5	8.5	8.0	52.31	49.6
	6	8.5	8.5	52.31	52.7
5	1	8.2	8.0	50.46	49.6
	2	9.0	7.0	55.38	43.4
	3	8.7	8.0	53.54	49.6
	4	9.0	8.0	55.38	49.6
	5	9.0	8.0	55.38	49.6
	6	9.0	8.5	55.38	52.7

*Bolt Elongations were measured on propeller Blades 1, 3, 4, and 5. Bolt shank stresses for these bolts were calculated from the emperical relationship established in Figure 42.

**Bolt shank stresses were measured on propeller Blade 2. Bolt elongations for these bolts were calculated from the emperical relationship established in Figure 42.

***Date of original installation prior to sea trial.

† Date of drydocking for removal of CPP system.

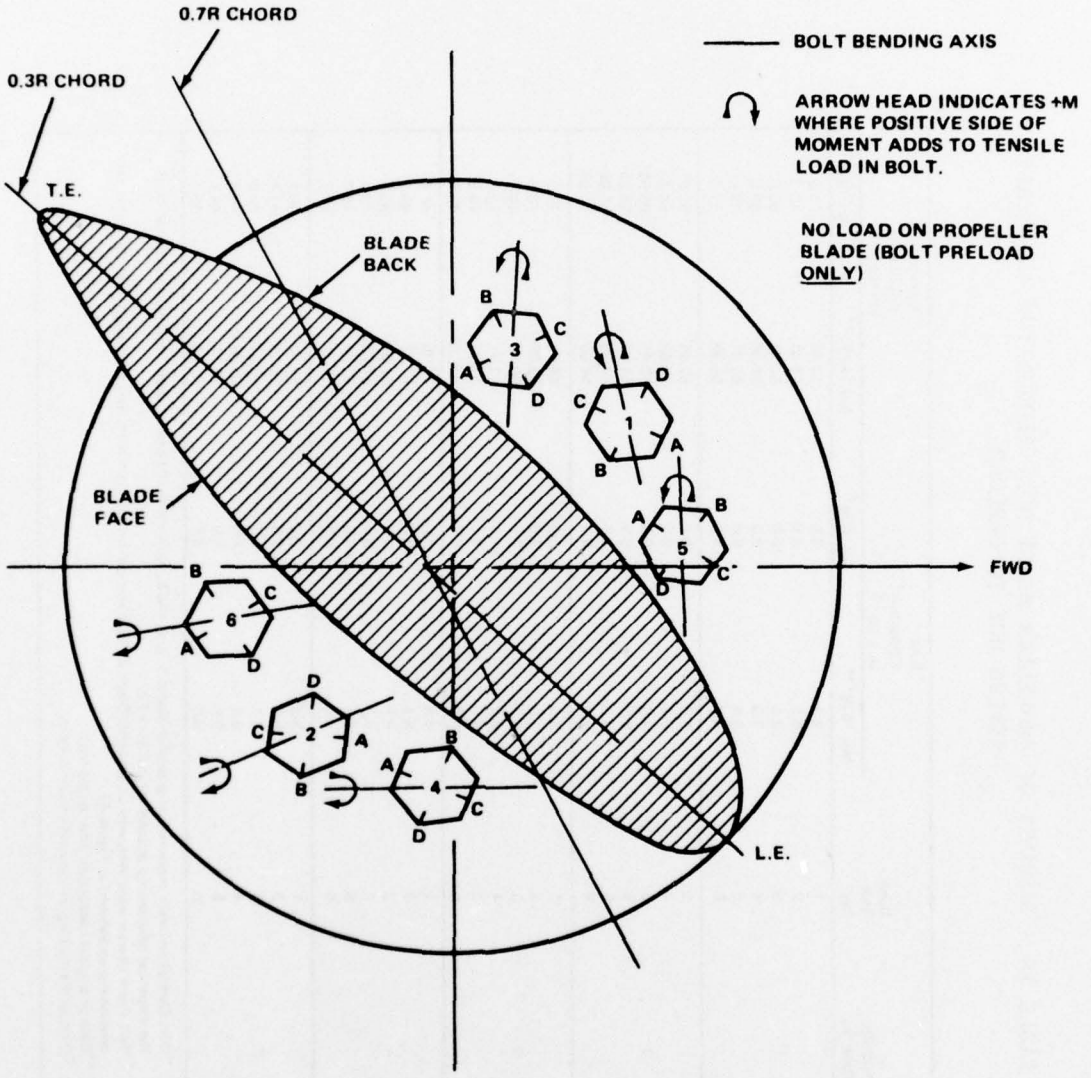

Figure 45 - Bolt Gage Final Orientation and Bending Axis Orientation after Preload (Propeller Blade 2, looking down)

Although there is hardly enough information (statistical or otherwise) in Figure 45 to draw a conclusion, there does seem to be a preferential orientation of the bending axis. The point made here is that other possible causes could contribute to or even dominate the bolt bending mechansim and that none should be overlooked. In particular, the contoured stiffness of the propeller blade palm and bearing rigidity of the clamped surfaces should be considered. Bolt bending and bending axis orientation will be discussed further in later sections.

When BARBEY was reconverted to a fixed-pitch propeller (in January 1976), readings were taken on the propeller blade bolts for the purpose of determining the residual prestress. These values are also included in Table 14. Both strain and dial gage readings gave good collabrative readings on the instrumented bolts (Blade 2). The prestress was generally unchanged except for a slight (10 percent) reduction in Bolts 1 and 6.* This was generally verified by the other bolt reading (made with dial gage only). Some of the posttrial dial gage readings were obviously affected by damage (corrosion, etc.) to the measuring surfaces. Overall results indicated that no loss of bolt preload occurred as a result of the trials or subsequent operational experience with the possible exception of Bolt 6.

Bolt preloading results in an induced stress in the crank disk. The measured values to bolt preload-induced crank disk stresses are given in Table 15. Figure 46 presents stress conventions for gages located on the crank disk. Generally, Table 15 shows a compressive radial stress of approximately 7 to 8 ksi in the fillet in the vicinity of the bolt holes. The stress state became more complex around the crank pin and locator pin. It is assumed that unknown boundary conditions at these latter locations complicated the structural interaction of the assembled parts.

---

*The values given in Tables 13 and 14 are stresses as each bolt was installed or removed. It was noted that if readings were taken after all bolts were installed, a certain amount (~10 percent) of stress relaxation took place in some bolts.

TABLE 15 - PRINCIPAL STRESSES INDUCED IN CRANK DISK 2 BY BOLT PRELOADING
(All Bolts Tight, with Approximately 55-ksi Preload; see Table 13)

Location \ Parameter (See Figure 46)		Radial Stress* σ_r(CD) ksi	Angle θ(CD) deg	Principal Stress σ_1(CD) ksi	Principal Stress σ_2(CD) ksi	Maximum Shear Stress τ(CD) ksi
Aft Side (Ahead Operation)	Locator Pin	−1.8	+108	+0.9	−1.6	+1.2
	Bolt Hole 6	**	**	**	**	**
	6/2	−6.8	+88	−2.4	−6.9	+2.3
	Bolt Hole 2	−10.1	***	***	***	***
	2/4	−5.7	***	***	***	***
	Bolt Hole 4	−8.9	***	***	***	***
Fwd Side (Ahead Operation)	Bolt Hole 5	−11.0	+90	+12.6	−6.2	+9.4
	5/1	−6.3	***	***	***	***
	Bolt Hole 1	−7.0	***	***	***	***
	Bolt Hole 3	−7.6	***	***	***	***
	Crank Pin	+2.7	−27	+3.4	+.12	+1.1

*$\sigma_r = E\,\epsilon_r/(1\cdot\mu^2)$, where ϵ_r is strain measured on single radial gage

**Record gains not recorded

***Radial gage only (no rosette)

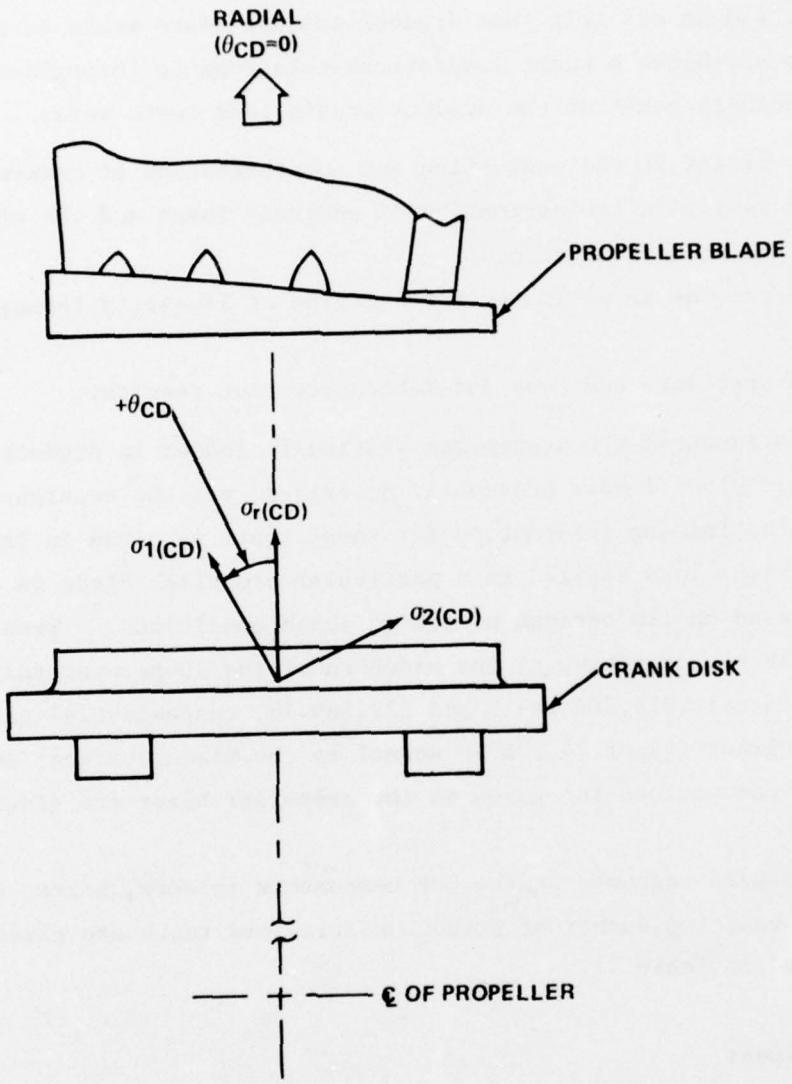

σ_r(CD) = RADIAL STRESS IN CRANK DISK FILLET

σ_1(CD),σ_2(CD) = MAXIMUM AND MINIMUM STRESSES IN CRANK DISK FILLET

θ_{CD} = ANGLE MEASURED FROM σ_r(CD) TO σ_1(CD) POSITIVE CCW

Figure 46 - Stress Conventions for Gages Located in the Crank Disk Fillet

Static Response of Propeller Blade, Bolts, and Crank Disk

The difficulties involved in simulating propeller blade loads were recognized, and it was felt that drydock loading tests would be necessary in order to establish a known load/stress relationship throughout the system. The primary goals of the drydock static load tests were:

1. To assist in the evaluation and interpretation of underway results.
2. To assist in the estimation of underway loads and the effect of variation in load distribution.
3. To provide an estimate of the degree of linearity throughout the system.
4. To correlate underway and laboratory test results.

The instrumented CPP system was statically loaded in drydock by using the hydraulic blade loader previously described; see the section on approach. The loading information for these tests is given in Table 16.

The maximum load applied to a particular propeller blade in drydock tests was based on 120 percent of design ahead conditions.* When resolved into a single vector acting at the midchord of the 70-percent radius, this torque and thrust (919,200 ft-lb and 327,600 lb, respectively) gave in an applied resultant (R) of 74,300 lb normal to the blade surface; see Figure 47. Stress conventions for gages on the propeller blade are given in Figure 48.

The measured response of the CPP components (blades, bolts, and crank disk) for a selected number of drydock static load tests are given in Figure 49 and in Table 17.

Propeller Blades

Propeller blade stress is linear with applied load, Figure 49. The principal stress at this location is essentially radial, Table 18. Even though the geometry of the propeller blade itself is complex, certain approximating assumptions can be made which allow a relatively simple

---

*Reported informally as hub stress calculations on Liaaen Model D132/5 by Propulsion Systems Inc., dated 22 October 1969.

TABLE 16 - DRYDOCK STATIC LOAD APPLICATION FOR PROPELLER BLADES

Run No.	Location of Applied Load*						Total Load+ lb
	Spanwise**			Chordwise***			
	0.6R	0.7R	0.8R	1/4	1/2	3/4	
SC1	X	X	X	X	X	X	66,600
SC2	X			X			7,400
SC3	X				X		
SC4	X					X	
SC5		X		X			
SC6		X			X		
SC7		X				X	
SC8			X	X			
SC9			X		X		
SC10			X			X	
SC11	X			X	X	X	22,000
SC12		X		X	X	X	
SC13			X	X	X	X	
SC14	X	X	X	X			
SC15	X	X	X		X		
SC16	X	X	X			X	
SC17	X	X	X	X	X		44,000
SC18	X	X	X		X	X	
SC19	X	X	X	X	X		14,800
SC20		X			X	X	

*Loads were applied first to pressure face of blades and then to suction side of blades.

**Radial position from shaft centerline.

***Chord position from leading edge of blade.

+Distributed equally over all loading points and applied normal to blade surface.

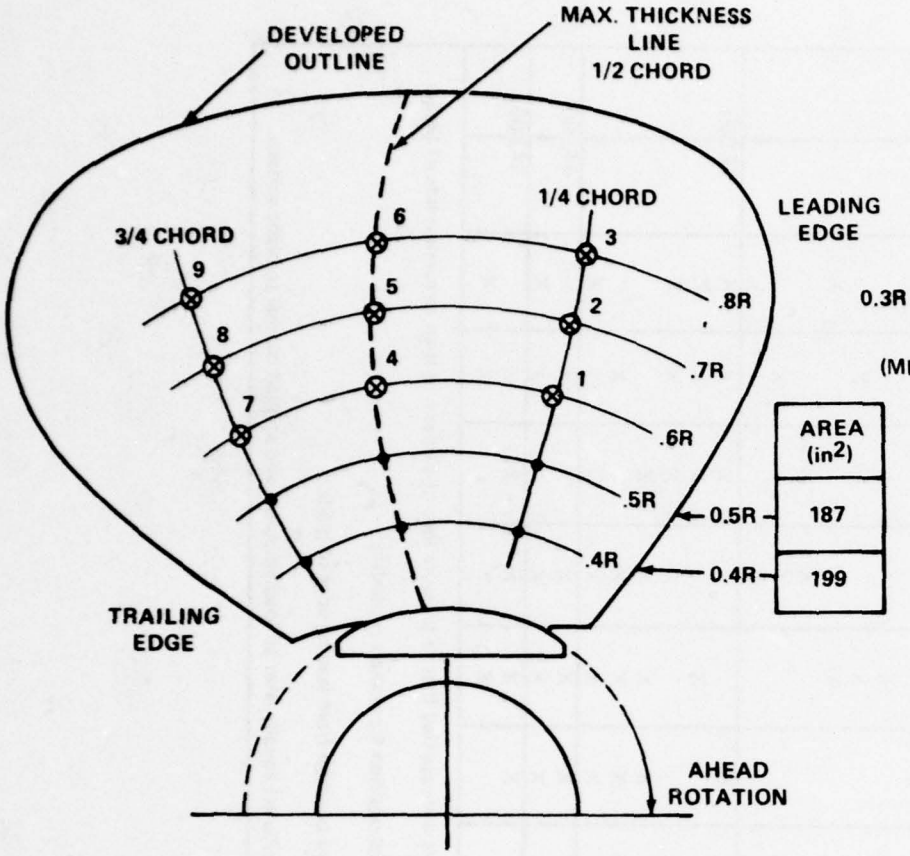

Figure 47a - Hydraulic Loader Matrix

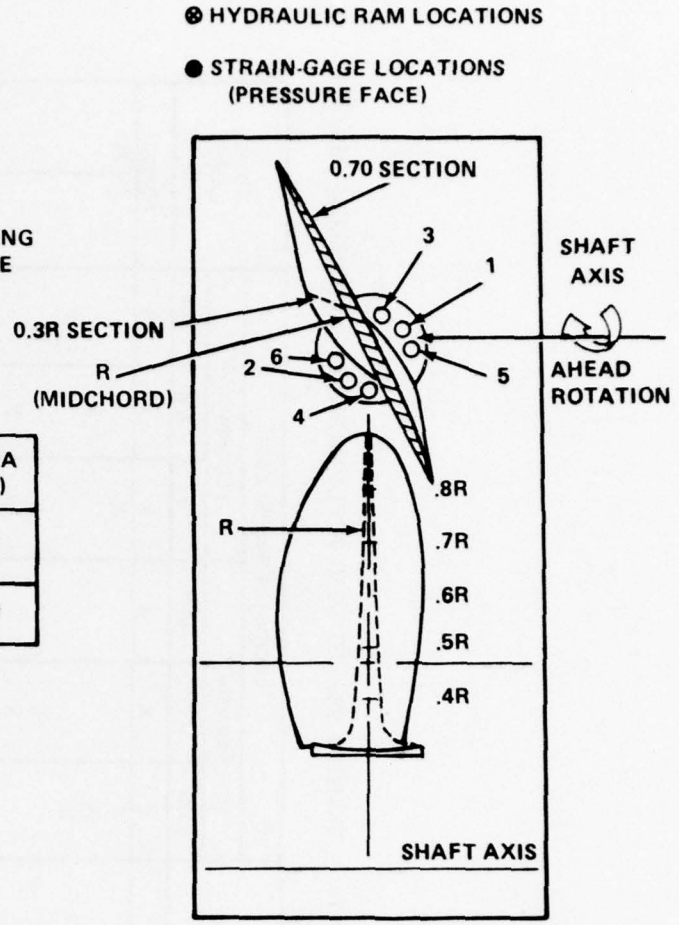

Figure 47b - Resultant Load Vector for 9-Ram Loading

Figure 47 - Static Drydock Load Matrix/Resultant Vector Relationship for Nine Ram Loading

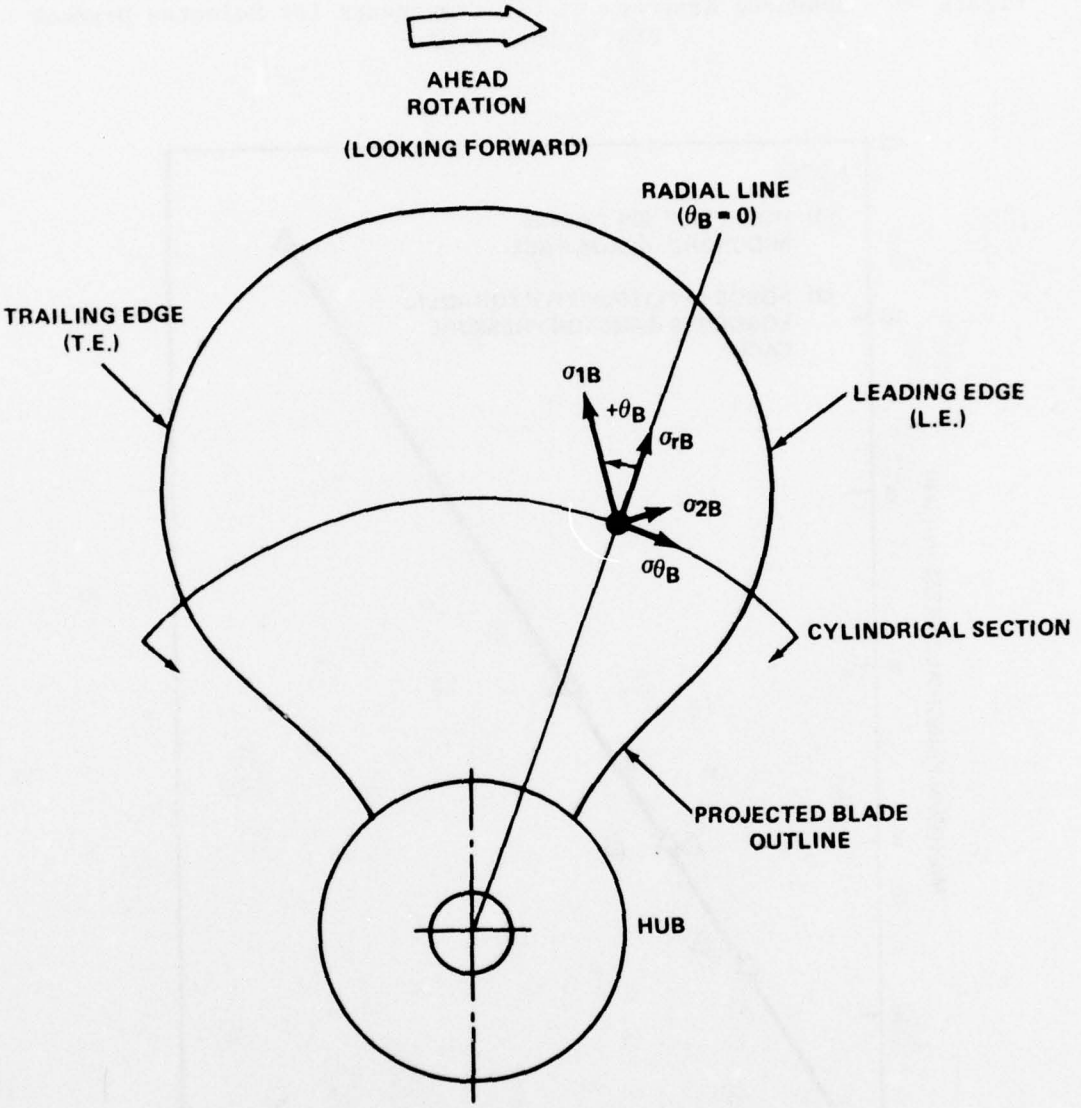

CYLINDRICAL SECTIONS: σ_{rB}, $\sigma\theta_B$ = RADIAL AND CIRCUMFERENTIAL STRESSES

σ_{1B}, σ_{2B} = MAXIMUM AND MINIMUM PRINCIPAL STRESSES

θ_B = ANGLE BETWEEN σ_1 AND σ_r, POSITIVE TOWARD T.E.

Figure 48 - Stress Conventions for Gages Located on Cylindrical Blade Sections

Figure 49 - Measured Response of CPP Components for Selected Drydock Static Load Tests

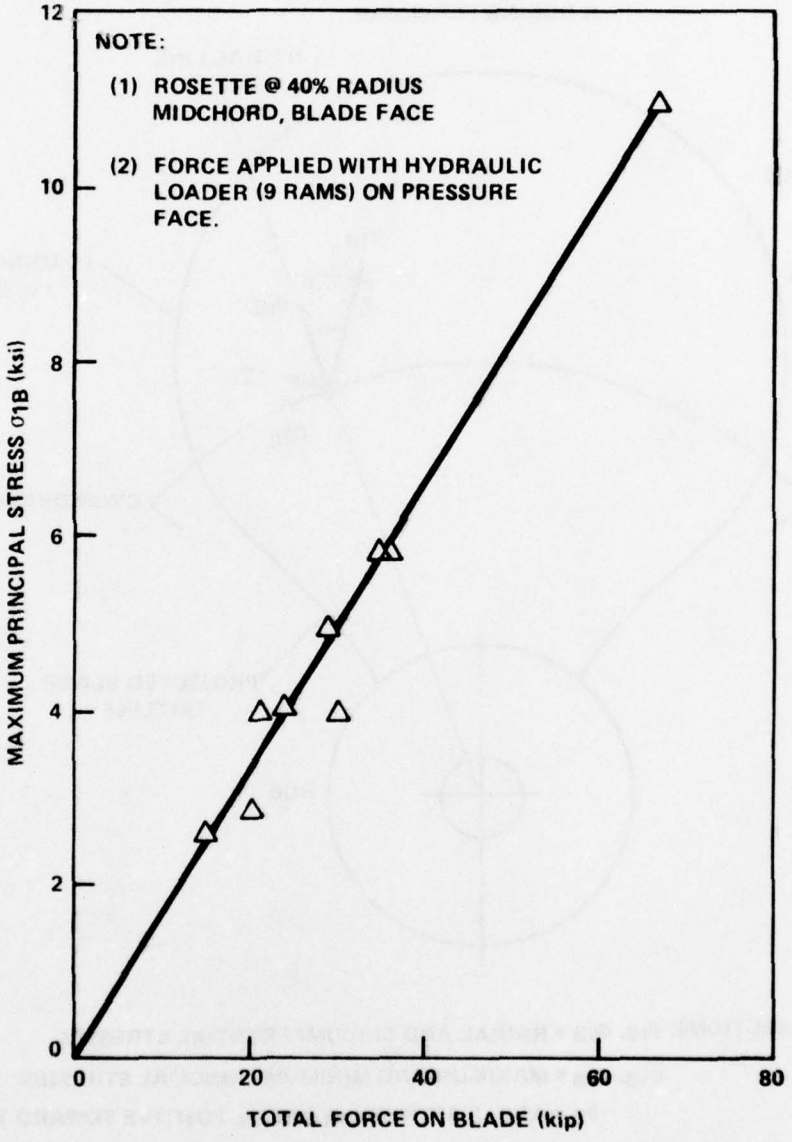

Figure 49a - Principal Stress on Propeller Blade 2

Figure 49 (Continued)

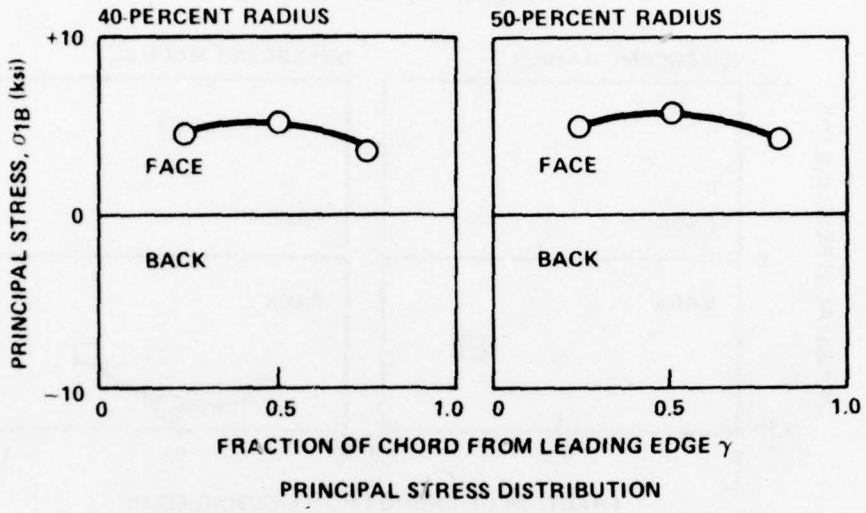

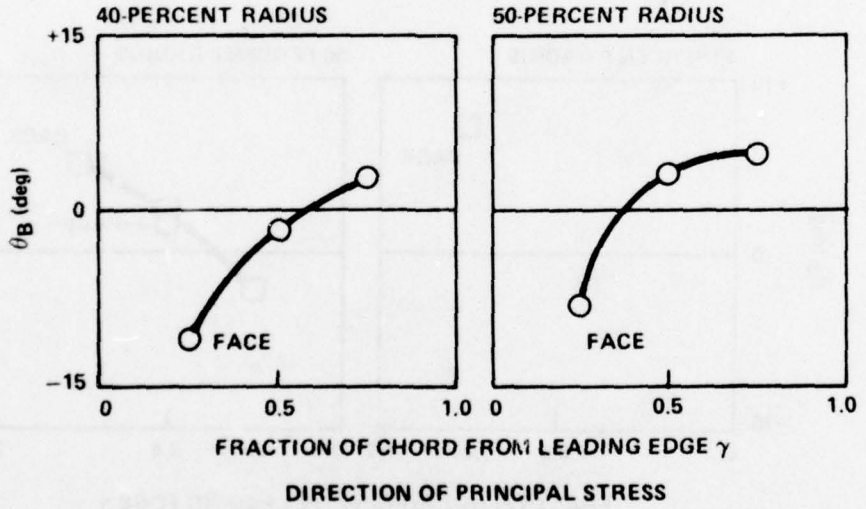

Figure 49b - Principal Stress on Propeller Blade 4 (Loading Condition: See Notes in Table 4)

Figure 49 (Continued)

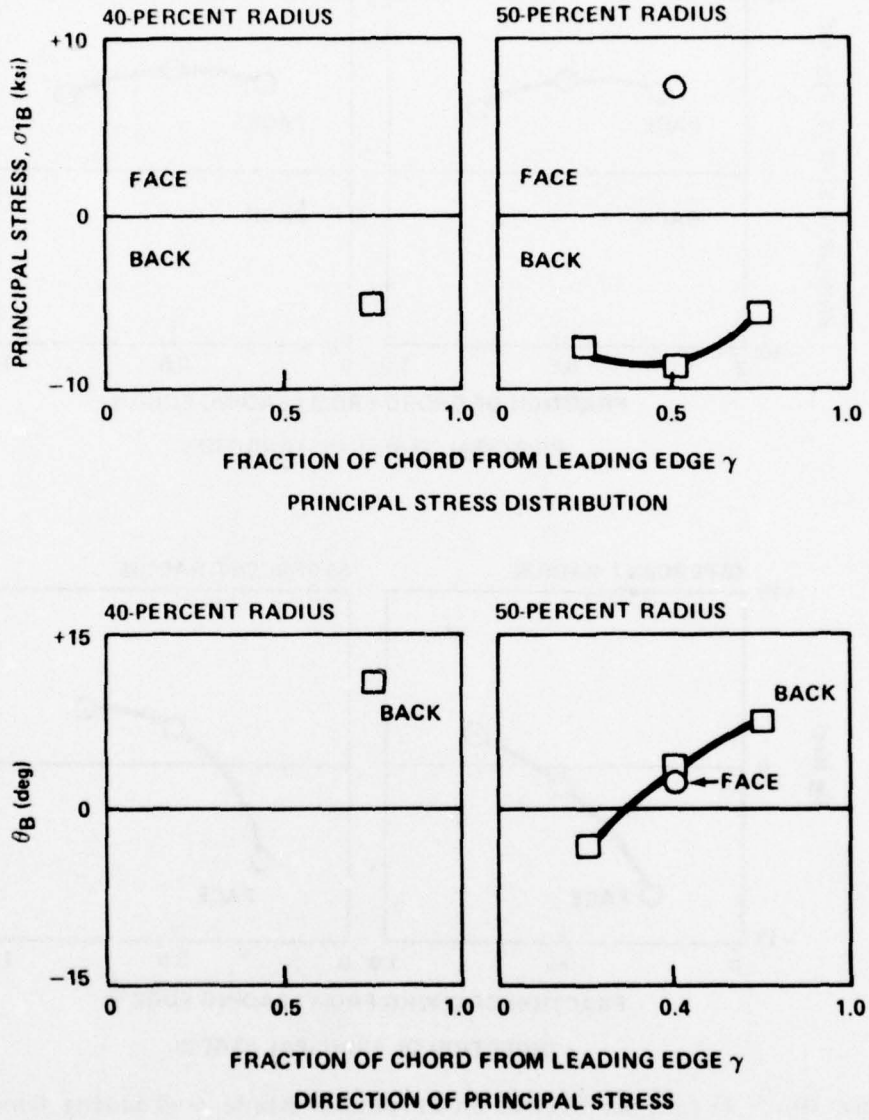

Figure 49c - Principal Stress on Propeller Blade 5 (Loading Condition: See Notes in Table 5)

Figure 49 (Continued)

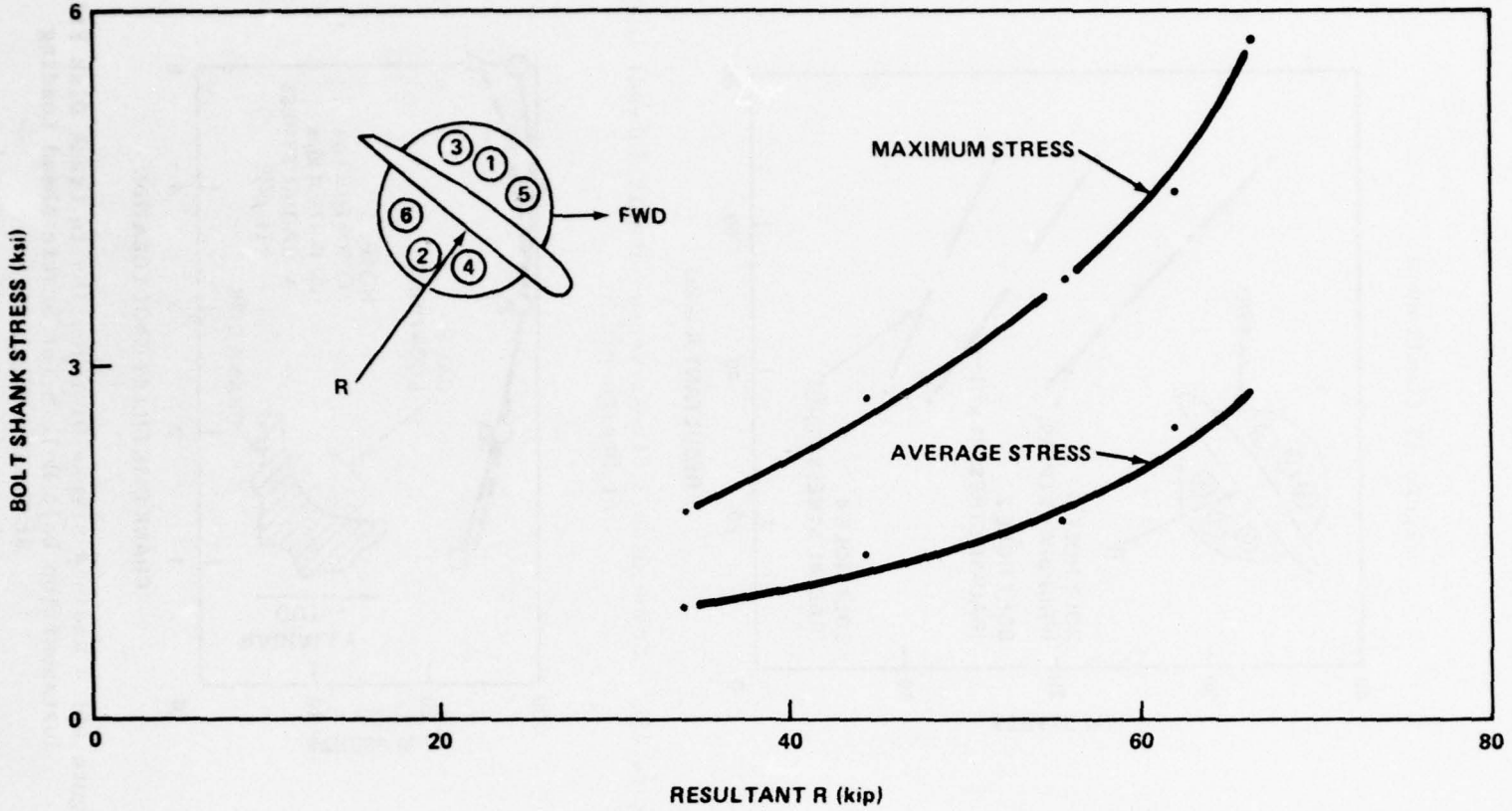

Figure 49d - Propeller Blade Bolt 6 Stress Variation for Static (Ahead) Loading at Design Pitch (Stresses above Prestress)

Figure 49 (Continued)

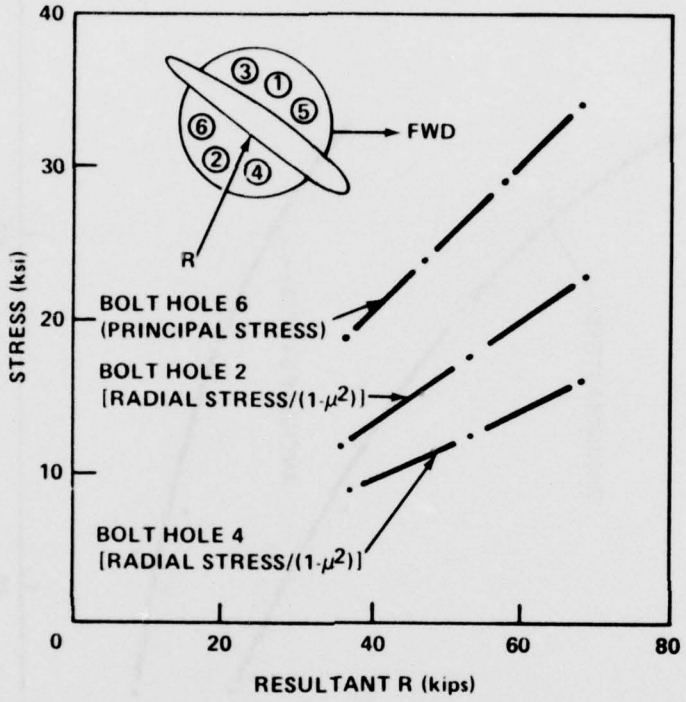

Figure 49e - Crank Disk 2 Stress versus Static (Ahead) Loading at Design Pitch

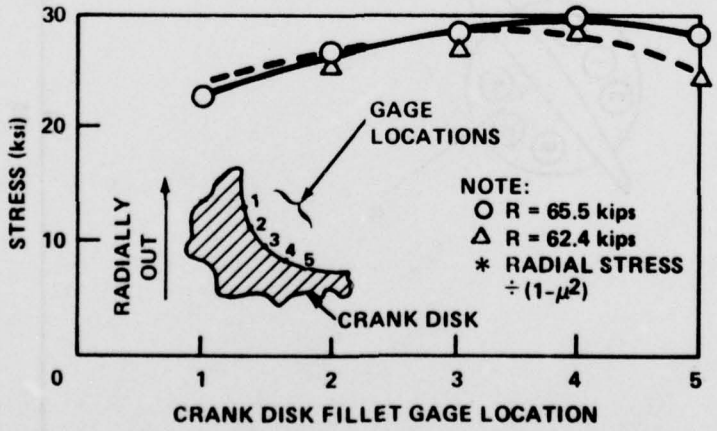

Figure 49f - Radial* Stress Distribution in Crank Disk Fillet Juxtaposition Bolt Hole 6 for Static Ahead Loading at Design Pitch

Figure 49 (Continued)

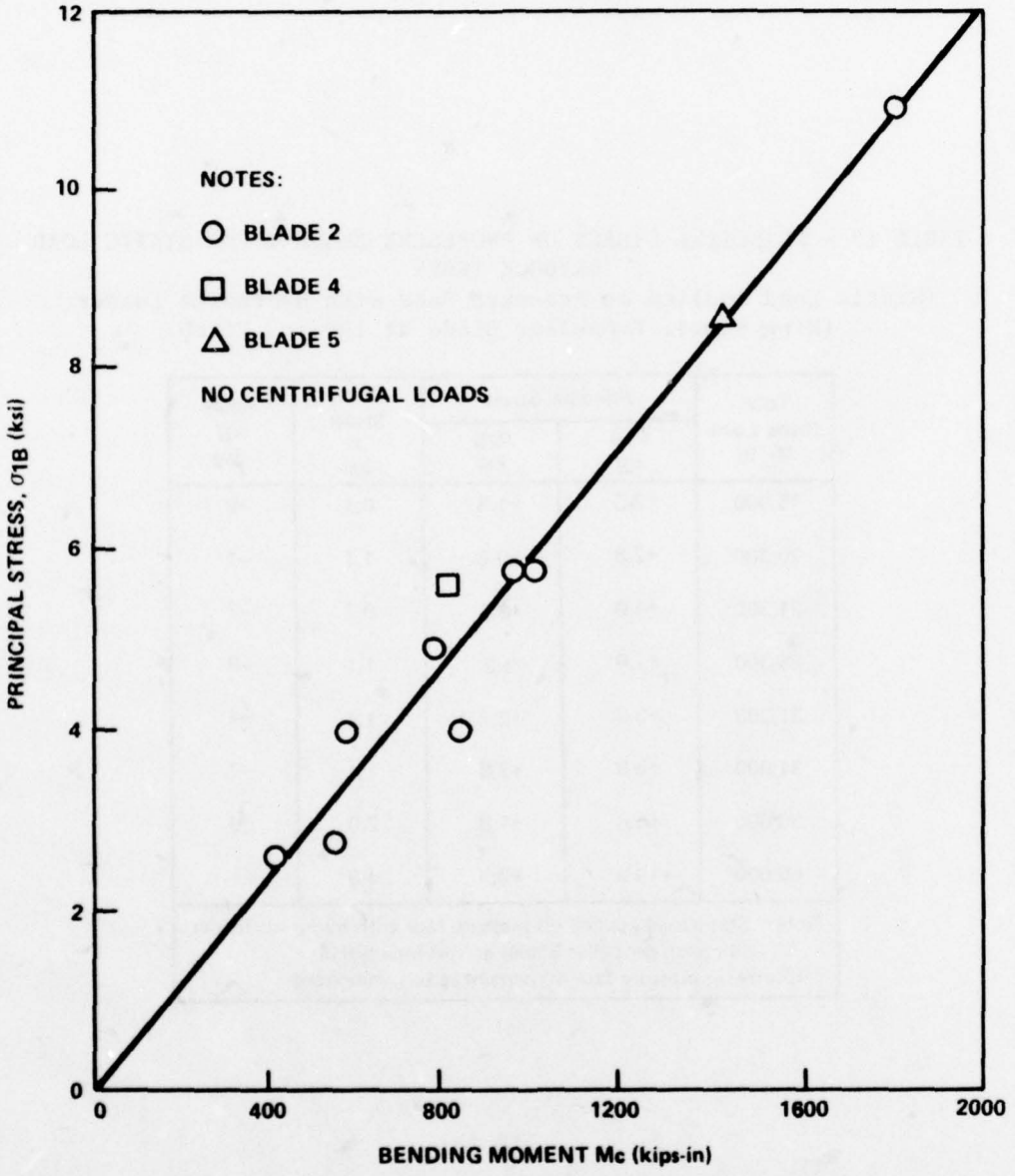

Figure 49g - Principal Stress Measured at Maximum Thickness, 40-Percent Radius, Pressure Face

TABLE 17 - PRINCIPAL STRESS ON PROPELLER BLADE 2 FOR STATIC LOAD DRYDOCK TESTS
(Static Load Applied on Pressure Face with Hydraulic Loader (Nine Rams), Propeller Blade at 190-in. Pitch)

Total Blade Load R_L lb	Principal Stress*		Shear Stress τ ksi	Angle θ_B deg
	σ_{1B} ksi	σ_{2B} ksi		
15,000	+2.6	+1.8	0.4	+9
20,300	+2.8	+0.6	1.1	−1
21,300	+4.0	+2.5	0.7	−7
28,300	+4.9	+1.2	1.1	−9
31,300	+3.9	+2.7	1.4	−4
34,900	+5.8	+3.0	1.4	−7
36,600	+5.8	+1.8	2.0	0
66,600	+10.9	+2.3	4.3	−1

Note: Static load applied on pressure face with hydraulic loader (9 rams), propeller Blades at 190 inch pitch.
*Rosette on pressure face 40 percent radius, midchord.

TABLE 18 - PRINCIPAL STRESS DISTRIBUTION ON PROPELLER BLADES 4 AND 5 FOR STATIC LOAD DRYDOCK TESTS

($\sigma_r = E\varepsilon_r/1-\mu^2$ where ε_r is strain measured on single radial gage)

Location / Parameter (See Figure 48)		Radial Stress σ_{rB} ksi	Angle θ_B deg	Principal Stress σ_{1B} ksi	Principal Stress σ_{2B} ksi	Radial Stress σ_{rB} ksi	Angle θ_B deg	Principal Stress σ_{1B} ksi	Principal Stress σ_{2B} ksi	Radial Stress σ_{rB} ksi	Angle θ_B deg	Principal Stress σ_{1B} ksi	Principal Stress σ_{2B} ksi
Propeller Blade 4:													
40% Radius	Precent Chord from Leading Edge	← 25 →				← 50 →				← 75 →			
	Face	+4.5	−11	+4.5	+0.8	+5.7	−2	+5.6	+1.2	+4.1	+3	+3.8	+0.1
	Back	← No Stress Gages on Back (Suction Face) →											
50% Radius	Precent Chord from Leading Edge	← 25 →				← 50 →				← 75 →			
	Face	+4.9	−8	+4.7	+0.5	+5.4	+3	+5.4	+1.3	+4.4	+5	+4.1	+0.2
	Back	← No Stress Gages on Back (Suction Face) →											
Propeller Blade 5:													
40% Radius	Precent Chord from Leading Edge	← 25 →				← 50 →				← 75 →			
	Face	*	*	*	*	+8.5	**	**	**	+6.4	**	**	**
	Back	*	*	*	*	*	*	*	*	−4.5	+101	−1.3	−4.7
50% Radius	Precent Chord from Leading Edge	← 25 →				← 50 →				← 75 →			
	Face	+8.2	**	**	**	+7.4	+2	+7.6	+2.5	+6.4	**	**	**
	Back	−7.9	+87	−1.4	−7.7	−8.6	+94	−2.4	−8.6	−5.5	+98	−1.1	−5.5

Load Matrix (kips)

	% Radius	% Chord from L.E. 25	50	75	Total Load	Blade Pitch (in)
Blade 4	80 (Bl. Face)	7.4	7.4	7.4	22.2	190
Blade 5	70 (Bl. Face)	7.4	7.4	7.4	44.4	191
	80 (Bl. Face)	7.4	7.4	7.4		

*No gages recorded

**Radial gage only

analysis to reasonably describe the stress which would result from a known load. Basically these assumptions presume a "beamlike" structure which is rigidly fixed at its base (approximately 0.3 radius). For the other components, such as the bolts and crank disk, the complexity of the load path, nonlinear response characteristics, and the geometric properties of these components makes the prediction, or the accountability of these stresses considerably more difficult. This became evident from model and prototype studies conducted at NSRDC.* Therefore, the blade stresses will be used in connection with the estimation of underway loads on the propeller. This is considered desirable not only as a verification of design predictions but also to estimate "off-design" load characteristics.

The BARBEY propeller is modified NACA 16 section (Navy Type I) with the following properties[31] (see Figure 50):

Blade Section Area (A):

$$A = CbT \ (in^2)$$

where T = maximum blade section thickness at x/b = 50 percent

b = blade section width

$C = 0.7466$

Section Modulus Coefficient $Zx_0(C,t)$:

$$Zx_0(C,t)\ \frac{bT^2}{B_c} = \frac{bT^2}{B_t}$$

where B_c = coefficient for compressive bending stress due to Mc at point Y, about $X_o - X_o$ axis

B_t = coefficient for tensile bending stress due to Mc at Point Yz about Xo - Xo axis

---

*Reported informally by G. Lauver and J. Rodd as Enclosure 1 (USS BARBEY (DE-1088) Propeller Stress Analysis (Bolt Load Distributions from Strain Gaged Photoelastic Model)) to DTNSRDC letter 173:GL5605 75-173-65 dated 2 June 1975.

[31]"Propeller Blade Section Design Coefficients for Type I Sections," NAVSEA Drawing 203-1737514 (21 Jul 1958).

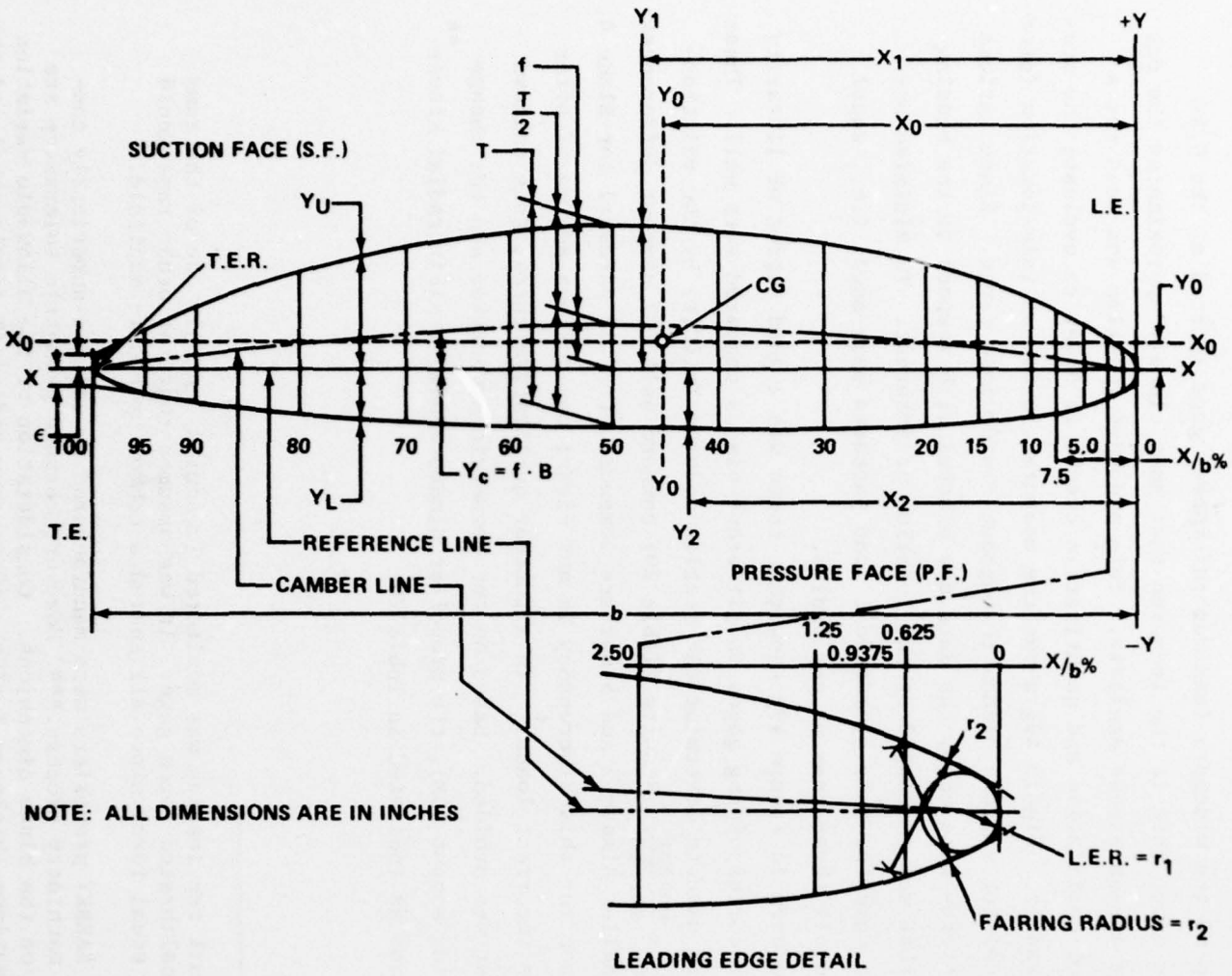

Figure 50 - Propeller Blade Sections, Type I Nomenclature

Pertinent values for the 40 and 50 percent radius for the BARBEY propeller are given in Table 19.

Of particular interest in the drydock tests is the load/stress relationship of the midchord (maximum thickness) gage located at the 0.4R position since this is the location that most closely approximates the one used for design stress analysis. This midchord location was used for a number of qualitative and quantitative checks in order to evaluate the measured results. Figure 49g shows the measured stress at this location (pressure face) for various blades throughout a wide load range. Since various load patterns were used, the data are plotted with respect to the bending moment that was developed at the location of interest. To minimize any twisting moments, only symmetrical load patterns were used, i.e., equal loads on all three rams at any radius.

The data in Figure 49g show that there was a good degree of linearity and that corresponding gages on different blades compared very well. These data were used to determine the section modulus $Zx_0(C,t)$ by the relationship $Zx_0 = \frac{\text{moment}}{\text{stress}}$. Results (Table 20) compare well (<7 percent differences) for Propeller Blades 2 and 5 but are somewhat off (~22 percent) for Blade 4. The reason for this discrepancy is not clear; one obvious source of error could be incorrect loads.* In a further qualitative check, this unknown parameter was avoided. Based on the geometric properties and the change in bending moment (ΔM), the propeller blades should exhibit radial stress** variations as indicated in Table 20.

---

*Actual ram loading was monitored (measured) on only one of the rams with a calibrated force gage. It was assumed that the other rams would have an equal force since all shared a common hydraulic manifold.

The BARBEY propellers were manufactured by using a numerically controlled machinery process.* However, certain geometric tolerances are allowed on the blade dimensions. Consideration of the allowable variation in the maximum thickness T of the 40 percent radius (T + tolerance) and the 50 percent radius (T - tolerance) gives approximately a 6 percent error in the calculated stress.

***Documented in a DTNSRDC classified report by T. Brockett.

TABLE 19 — GEOMETRIC PROPELLER BLADE PARAMETERS

Percent Radius	T in	b in	ϵ* in	f** in	Bc	Bt	A in^2	Section Modulus (in.)	
								Blade Face	Blade Back
								$ZX_{o(t)}$	$Zx_{o(C)}$
40	6.10	44.68	0.20	1.35	12.16	9.88	199	168	132
50	4.54	56.00	0.20	1.57	11.95	8.88	187	130	97

*Thickness used to add metal thickness at the trailing edge
**Maximum camber at x/b = 50 percent

TABLE 20 — COMPARISON OF PROPELLER BLADE SECTION MODULUS BASED ON MEASURED (DRYDOCK) DATA AND CALCULATIONS FROM PROPELLER DESIGN DRAWING

Blade No.	Percent Radius	Section Modulus (in^3)					
		$Z_{xo(t)}$		Ratio M/C	$Z_{xo(c)}$		Ratio M/C
		M	C		M	C	
2	40	160	168	0.95	–	132	–
4	40	132	168	0.79	–	132	–
5	40	158	168	0.94	–	132	–
4	50	104	130	0.80	–	97	–
5	50	130	130	1.00	112	97	1.15

This shows approximately 10 percent and 1 percent comparisons between calculated and measured results on Blades 4 and 5, respectively. Generally, it would appear that a reasonable estimate of static blade "loading" can be obtained by using the calculated section properties if the following assumptions can be made:

1. Chordwise hydrodynamic blade loads are symmetric about the mid-chord.

2. Radial variations of the hydrodynamic blade loads do not significantly alter the response characteristics (chordwise response distribution is essentially radial).

3. Beam theory is applicable.

During normal operation, a propeller blade is subjected to two types of loads: one is the net resultant load due to the developed thrust and torque which acts normal to the blade surface (causing bending stresses) and the other is the centrifugal load which acts radially outward (causing tensile stresses*). Although the drydock load tests did not simulate the centrifugal load, this effect may be accounted for by calculation. Figure 51 contains information on the centers of gravity of the palm and blade.

W_B = BLADE WEIGHTS = 2,565 lb

W_p = PALM WEIGHT = 451 lb

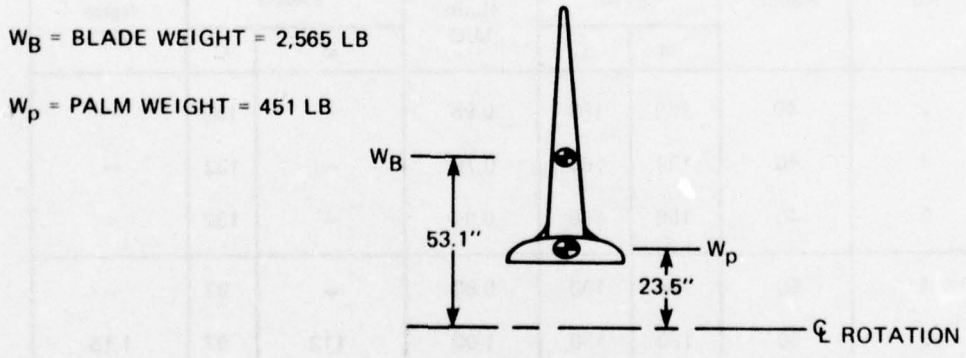

Figure 51 — Radial Locations for Approximate Center of Gravity for Propeller Blade and Palm

*This assumes that the propeller has no significant skew or rake angle.

Since the section of interest is just above the palm at 0.4R, palm weight is neglected and the centrifugal force F_c at full power (226 rpm) is:

$$F_c = 2\pi \left(\frac{226}{60}\right)^2 (53.1) \left(\frac{2565}{386}\right) = 197{,}640 \text{ lb}$$

The resulting tensile stress at the 0.4R location will be $\frac{197{,}640}{199 \text{ psi}}$ ≈1.0 ksi. At any other shaft speed N, the tensile stress due to the centrifugal force will be $\left(\frac{N}{266}\right)^2$ ksi.

The individual effects of the bending (S_b) and tensile (S_t) stress are shown in Figure 52 for normal ahead operations.

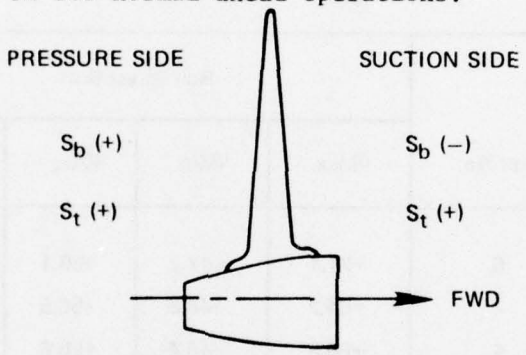

Figure 52 — Face/Back Distribution of Hydrodynamic and Centrifugal Stresses

Therefore, the difference in magnitude of underway data for the pressure and suction sides should be equivalent to twice the value of the tensile stress due to the centrifugal force.

Propeller Blade Bolts

The response of the blade bolts to the static load applied to the propeller blade is complex; see Table 21 and Figures 49d and 53. The bolt stress including prestress (Table 21) indicates that bolt load is dominated by preload conditions since there is very little change in the maximum or average stress of bolt bending axis due to an applied load simulating the full power resultant. Removal of the prestress component permits a clearer

TABLE 21 - STRESS IN PROPELLER BOLTS (BLADE 2) FOR STATIC LOAD DRYDOCK TESTS

TABLE 21A - STRESS* INCLUDING PRESTRESS

Including Prestress*

Location	Bolt No.	Bolt Stress (ksi)				Percent Bending Stress ($\%\sigma_B$)
		$\sigma_{Max.}$	$\sigma_{Min.}$	σ_{Avg}	σ_B	
Blade Face	6	+71.1	+47.2	+59.1	±12.0	20
Blade Face	2	+64.2	+48.8	+56.5	±7.7	14
Blade Face	4	+66.8	+44.4	+55.6	±11.2	20
Blade Back	5	+64.2	+44.5	+54.3	±9.9	18
Blade Back	1	+64.6	+50.5	+57.6	±7.0	12
Blade Back	3	+64.7	+45.1	+54.9	±9.8	18

*Blade Load: R = 66,600 lb (nine rams), applied to blade face, blades at 191 in. pitch.

Notes:

$\sigma_B = (\sigma_{Max} - \sigma_{Avg})$

Percent $\sigma_B = (\sigma_B/\sigma_{Avg})\ 100$

TABLE 21 (Continued)

TABLE 21B - STRESS ABOVE PRESTRESS

Location	Bolt No.	Bolt Stress (ksi)				Percent Bending Stress ($\%\sigma_B$)
		σMax.	σMin.	σAvg.	σ_B	
Blade Face	6	+4.4	+0.6	+2.5	±1.9	76
Blade Face	2	+1.8	−0.5	+0.7	±1.1	157
Blade Face	4	†2.8	−0.9	+1.0	±1.8	180
Blade Back	5	+3.0	−3.5	−0.3	±2.7	900
Blade Back	1	+3.0	−2.7	+0.6	±2.8	1400
Blade Back	3	+1.5	−2.4	−0.5	±2.0	400

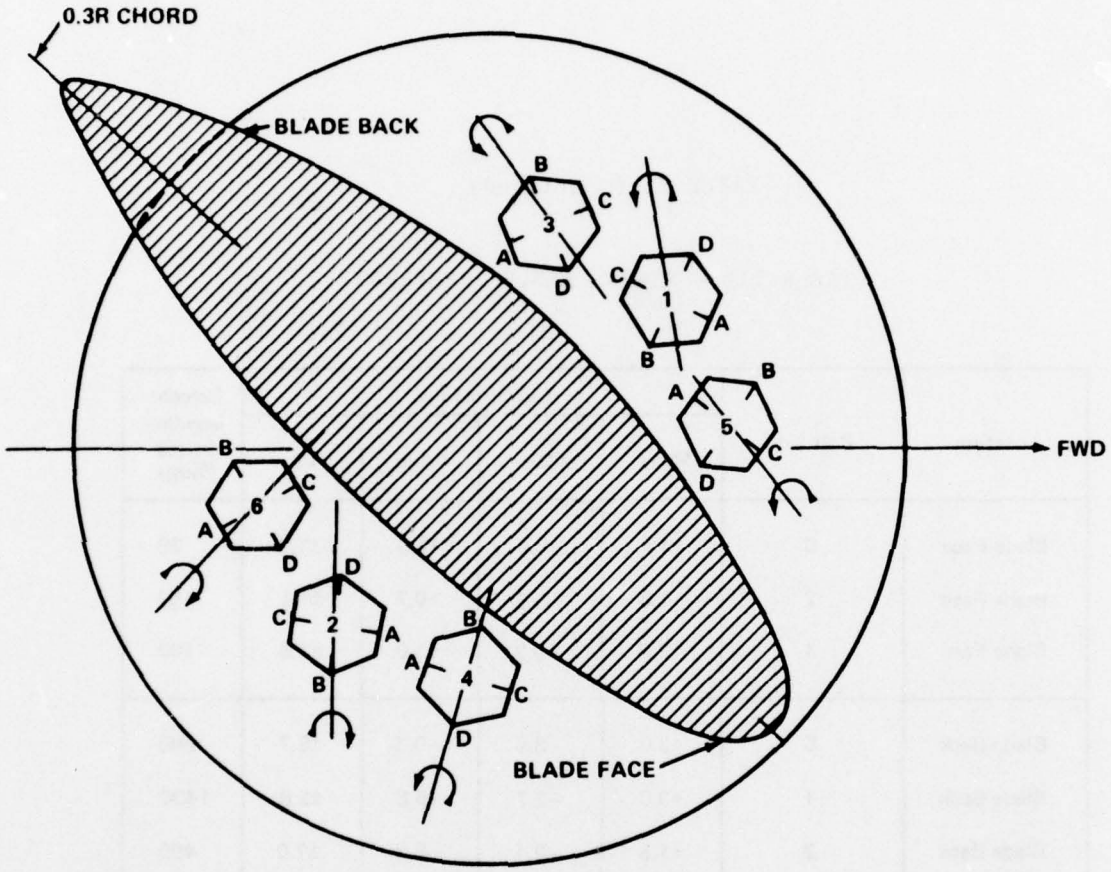

NOTES:

1. BENDING AXIS DUE TO APPLIED LOAD ONLY (NO PRELOAD)
2. ARROW HEAD INDICATES +M WHERE POSITIVE SIDE OF MOMENT ADDS TO TENSILE LOAD IN BOLT
3. BLADE LOADING:
   R = 66,600 lb (9 RAMS)

Figure 53 - Bolt Bending Orientation for Static Load in Drydock (Propeller Blade 2)

view of the effect of the external blade load on the bolts. Generally, it can be seen that the average bolt load was so distributed that tensile load increased for the blade face bolts and was essentially unchanged for the blade back bolts. Note the blade face bolt load was skewed toward Bolt 6. The percent of bending load in the bolts due to external load was considerably higher than that caused by preload. However, it should be noted that the highest average stress due to external load was less than 5 percent of the average axial preload stress. The bending stress in the blade face bolts was approximately equal to the tensile stress while the stress on the blade back bolts was mostly bending. In contrast to preload bending, the blade face bolts averaged approximately 56 percent lower bending than the bolts on the blade back. The bolt bending axes due to external load were generally aligned with those established in preloading with one notable exception, Bolt 4. Here the applied load axis had rotated almost 180 deg so that bending occurred opposite to preload bending.

The most heavily loaded bolt (Bolt 6) exhibited a nonlinear response which deviated considerably from the loading mechanism to the propeller blade and the response of the propeller blade. However, this response can be characteristic of the clamped blade palm/crank disk interface, as will be discussed later.

The stress distribution for crank disk response (Figure 49e) was similar to that of the bolts in that the higher stresses occurred juxtaposition Bolt 6. The stress distribution in the flange at this location varied only slightly with location; see Figure 49f. Response at all crank disk locations was linear with system forcing functions.

Dynamic Characteristics

Several tests were performed in drydock to determine the in-air dynamic characteristics of the assembly. The instrumented CPP system was excited with a mechanical (rotating mass) vibration generator in order to determine the response to a known dynamic load and to identify the propeller

blade frequencies and mode shapes. In addition, the system response to impulse loading was determined. Results of these tests indicate that the propeller blade was the only component which experienced any dynamic amplification within the range of interest; the propeller had a fundamental (bending mode) frequency of 31 Hz and a first torsional mode of 127 Hz (Table 22).

DOCKSIDE TESTS

The dynamic response of the propeller blades in water was obtained in order to determine the (nonrotating) added mass effect. Results are included in Table 22. The ratio of the in-air to in-water frequencies was approximately 1.6 for both the bending and torsional modes. Note that the first bending mode (in-water frequency of 19 Hz) was very close to the full-power (design) blade frequency of 20 Hz.

UNDERWAY TESTS

The objective of the underway tests was to determine actual operational stresses on the CPP system components. Table 8 indicates the considerable number of underway test conditions run in order to define stresses under all operating conditions. Selected tests have been analyzed and present a comprehensive picture of system response. Most of the emphasis was on the design-ahead condition (steady state operation) in order to directly correlate theory with experimental results. In addition, maneuvering tests results are presented to demonstrate the effects of off-design operation.

During all underway runs, standardization data were recorded and certain parameters monitored to avoid overloading the propulsion plant. Standardization data for steady state operation and maneuvers are given in Tables 23 – 25 and in Figure 54. A single blade hydrodynamic resultant (R_L) was determined by using the measured torque, thrust, and rpm; see Figure 55 for the input forcing function on each blade. This function follows a frequency square (ω^2) law. The magnitude of the resultant for

TABLE 22 — NATURAL FREQUENCIES OF PROPELLER BLADE IN AIR AND IN WATER

Frequency Hz			Ratio	Comments
Mode	In-Air(fa)	In-Water(fw)	fa/fw	
First Bending	31	19	1.6	Node line approx. on 0.4 radius
First Torsional	127	80	1.6	Node line approx. on 50-percent chord

TABLE 23 - INCREMENTAL RUNS FOR CPP SYSTEM ON BARBEY

Run No.	Norm* Speed (Ship Log)	Propeller Turns rpm	Pitch in.	Thrust lb	Torque lb-ft	Speed shp
415	.44	100.4	190	47000	162000	3098
414	.48	110.4	190	52500	192800	4053
413	.52	120.7	190	66200	231250	5316
412	.57	130.1	190	75800	271000	5714
411	.61	140.1	190	85200	325000	8668
410	.66	150.5	190	96200	337800	9680
409	.72	161.0	191	111200	385300	11800
408	.77	171.0	191	125400	435600	14180
408R	.77	170.3	191	121600	426900	13850
407	.82	181.0	191	138600	482500	16600
406	.87	191.3	191	151600	525600	19150
405	.88	200.6	191	176000	607450	23200
404	.93	211.0	191	199600	680850	27350
403	.93	219.4	191	213300	727600	30400
812	.66	120.7	242	88400	366600	8400
813	.76	139.7	242	111200	463800	13200
814	.88	160.4	242	150400	609100	18600
815	.95	179.0	242	200400	790700	26950
811	.52	100.2	242	58000	256800	4899

*Normalized to Fullpower (225 rpm, 191 in Pitch) Operation

TABLE 24 - PERCENT INCREASE OF MEAN TORQUE AND THRUST DURING MANEUVERING RUNS FOR CPP SYSTEM ON BARBEY

Run No.	Type of Run*	Approach						Turning				
		Norm.** Ships Log Speed	Prop. Shaft Rev srpm	Prop. Pitch in	Prop. Shaft Thrust lb	Prop. Shaft Torque lb-ft	Shaft Horse-Power shp	Rudder Angle deg	Thrust Increase		Torque Increase	
									Stbd Turn Percent	Port Turn Percent	Stbd Turn Percent	Port Turn Percent
110	RTC	.82	181	190	138300	478000	16500	–	78	56	26	19
118	RTC	.95	218	190	215900	743000	30800	–	33	–	25	–
118R	RTC	.98	221	190	234700	807000	34000	10	15	11	6	4
609	RTC	.86	200	170	153200	514500	19600	35	54	31	18	10
610	RTC	.87	201	170	147300	513000	19600	35	60	45	19	11
611	RTC	.91	218	170	190500	627000	26000	35	38	38	13	15
801	RTC	.89	200	191	176000	581500	22100	5	7	6	6	5
803	RTC	.90	200	190	177200	594000	22600	10	–	–	6	4
805	RTC		204	190	179900	613900	23800	20	23	15	8	5
807	RTC		200	190	175400	614000	23400	35	45	40	18	12
808	RTC		200	191	179200	615000	23400	35	23	34	18	11
809	CB	.98	225	193	226700	809000	34700					
810	CB	.96	221	192	217300	800000	33700					
816	RTC	.88	161	243	163300	620000	19000	35	32	37	16	13
817	RTC	.87	160	243	158000	615000	18700	35	30	21	13	8
818	RTC	.94	179	242	211100	812000	27700	5	6	4	2	1
819	RTC	.96	179	243	200600	761200	25900	5	13	9	7	3
822	CAHD		–100	–71	–36000	–203000	–3900					

*RTC – Run, Turn, Crashback (See Figure 29)
CB – Crashback
CAHD – Crashahead
**Normalized to full power (225 rpm, 191 in. pitch) operation.

TABLE 25 - MAXIMUM MEAN TORQUE AND THRUST DURING CRASHBACK AND CRASHAHEAD RUNS FOR CPP SYSTEM ON BARBEY

Crashback					Crashahead				
Run No.	Pitch Inhibit rpm	Shaft rpm Astern srpm	Prop. Pitch in.	Shaft Torque lb-ft	Shaft Thrust lb	Shaft rpm Ahead srpm	Prop. Pitch in.	Shaft Torque lb-ft	Shaft Thrust lb
110	150	39	–71	223000	141300	71	+177	284400	142900
118R	210	83	–74	403300	208500				
609	210	86	–76	363100	208500				
610	210	82	–75	365300	180500				
611	210	83	–75	383300	214100				
801	150	79	–76	340100	163700	107	+208	607700	242500
803	150	78	–78	315400	132900	108	+204	743900	
805	150	83	–72	333900	166500	100	+144	592400	278700
807	150	81	–72	357600	200100	124	+150	616100	290200
808	150	101	–71	474500	197300	170	+150	642700	300800
809	210	86	70	371700	135700				
810	210	110	–67	383100	197300				
816	190	80	–72	366100	219700				
817	190	84	–73	383300	180500				
818	190	82	–75	375600	208500				
819	190	81	–74	375600	186100				
822	190	42	–74	243600	219700	140	+185	751100	276900

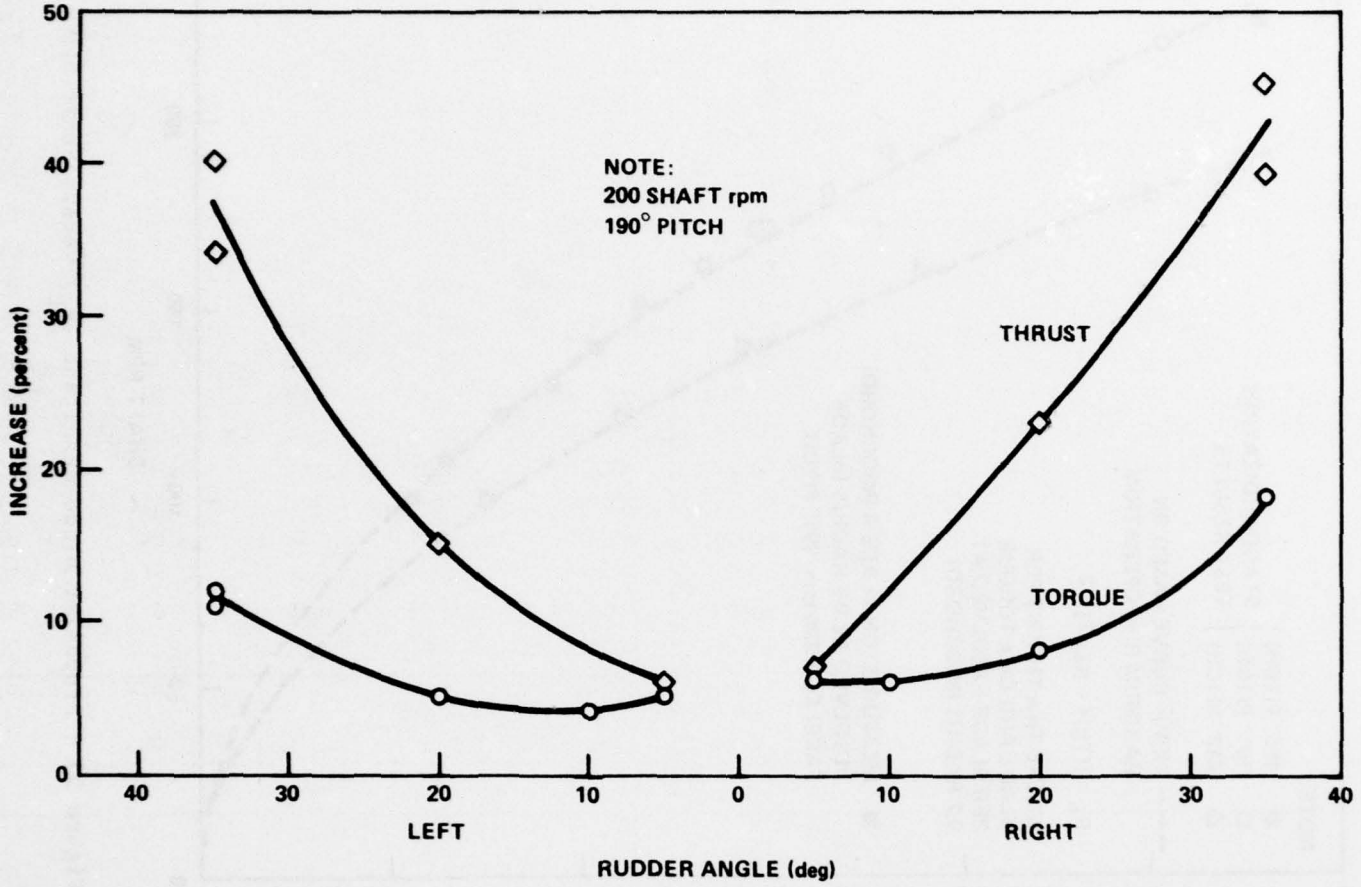

Figure 54 - Percent Increase of Mean Thrust and Torque for Various Rudder Angles

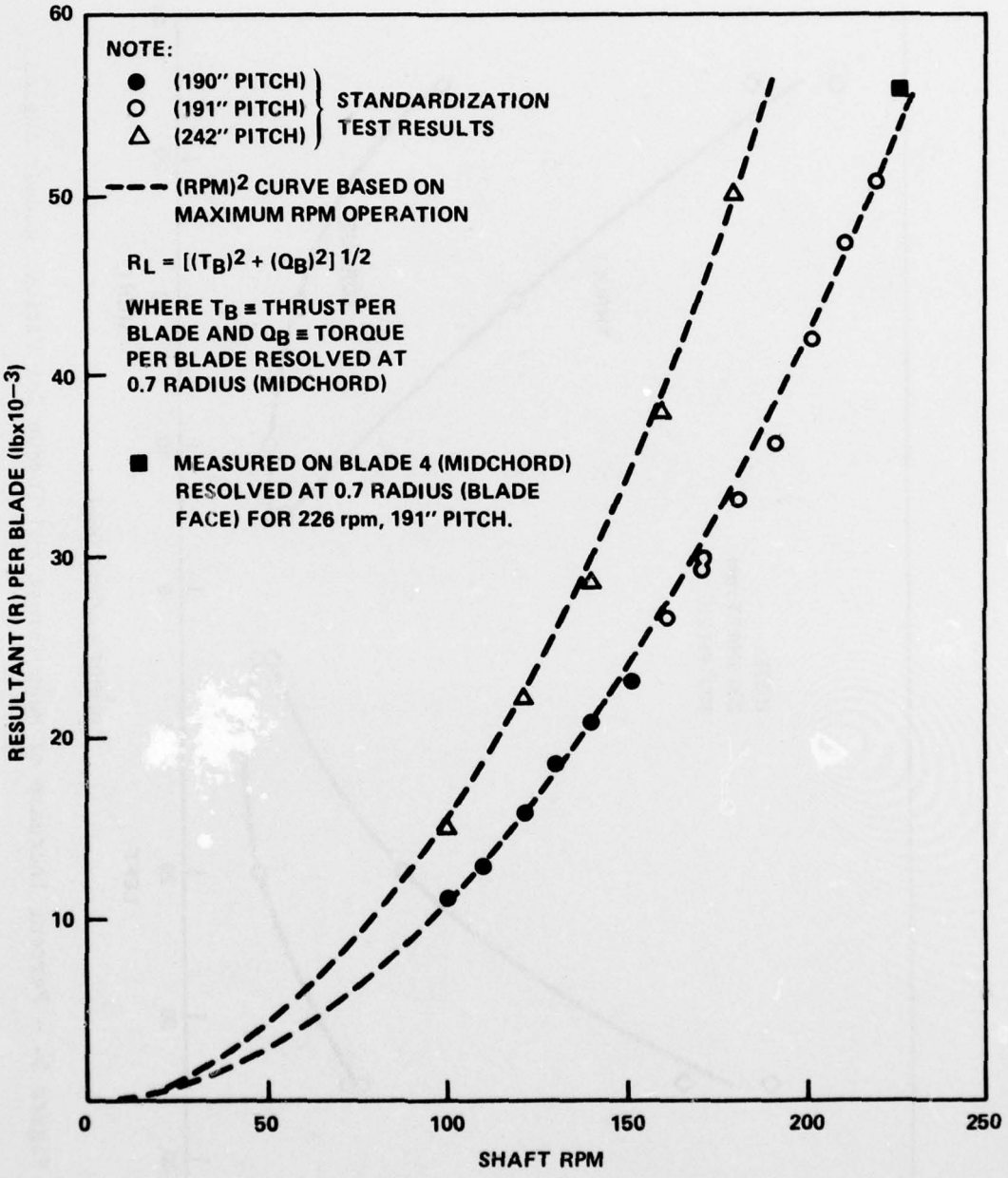

Figure 55 - Propeller Blade Resultant (R_L) versus Shaft RPM

full-power (226 rpm) steady operation is approximately 54,000 lb per blade.* All standardization data were under the cognizance of DTNSRDC Code 1536.

Steady State Operation

Response of the propeller blade, bolts, and crank disk to steady, incremented steps in powering are shown in Figure 56. This figure presents an overall view of both the mean and alternating stresses for steady-state operation. Details of the mean and alternating stress response of the individual CPP components at full power (226 rpm, 190-in. pitch) operation are shown in Tables 26 — 43 and Figures 57 — 64. Figure 58 shows typical transducers time history responses relative to angular rotation of the propeller at 210 rpm.

As in the case of drydock test results, the response of each CPP component will be discussed in relation to significant data charactersitics.

Propeller Blades. Figures 55 and 56 indicate that the qualitative and quantitative mean response of the propeller blades correlate well with both drydock and standardization results. Propeller blade "loads" were calculated by using the measured stress** at the root (40-percent radius, mid-chord) and the previously determined geometric properties. The calculated resultant (R_L) was 56,000 lb. This is shown in Figure 55 together with standardization data. The blade response was linear with load function*** (Figure 56) and the mean response of the propeller blades for full power operation (226 rpm) showed that both measured blades (Nos. 4 and 5) had

---

*Calculated 120 percent of R_L was 74,300 lb at 240 rpm. Extrapolation of the measured R_L at 226 rpm to 240 rpm showed that agreement between calculated and measured results was within 2 percent.

**Accounting for centrifugal loads as per discussion in the section on drydock tests.

***Dashed curves in Figure 56 are presented in order to compare the measured CPP component responses with that of one which is proportional to ω^2 (arbitrarily referenced to data at 180 rpm, 191-in. pitch). The minor deviations on the propeller blade and crank disk response is within measurement error.

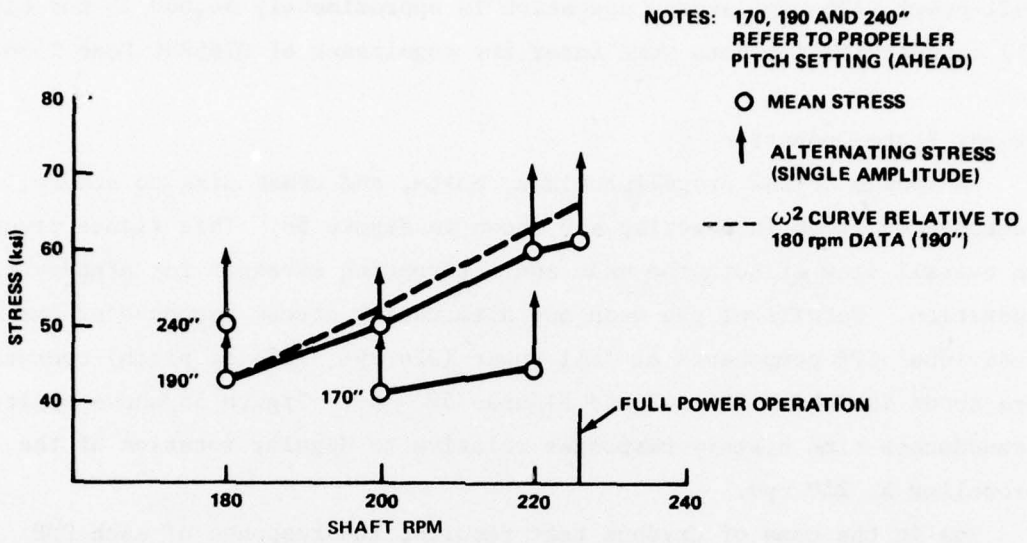

Figure 56a - Principal Stresses on Crank Disk 4 Juxtaposition Bolt Hole 6

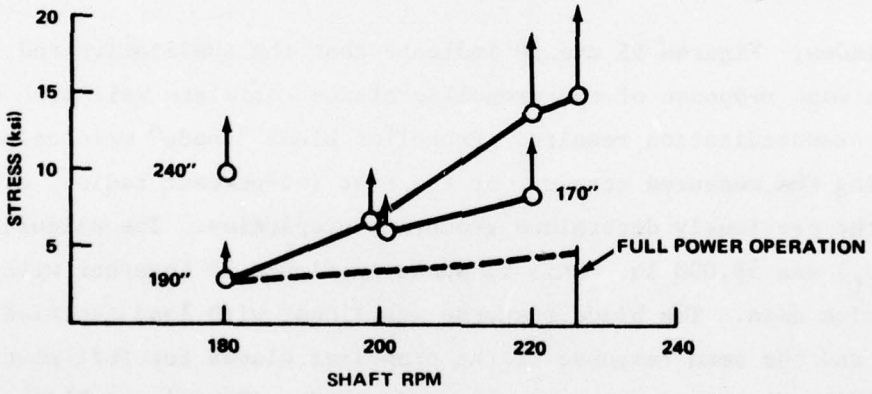

Figure 56b - Maximum Stress (above Prestress) on Blade Bolt 6

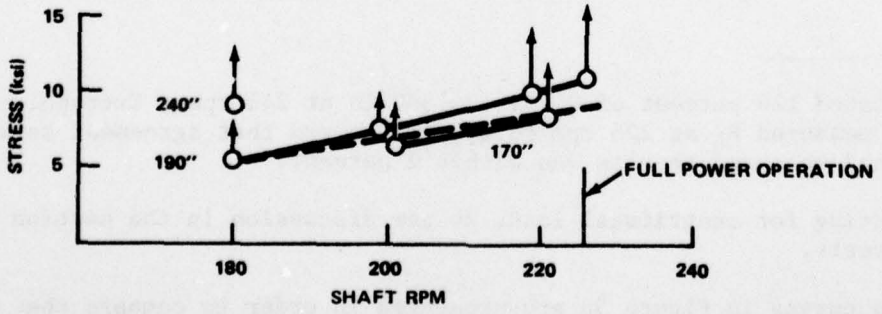

Figure 56c - Principal Stress on Blade 5 at 40-Percent Radius, Midchord (Blade Face)

Figure 56 - Stresses in the CPP Components for Various Pitch Settings and Shaft RPM

approximately the same stress levels* and distribution (see Table 26 and Figure 57). The mean response on Blade 4 showed the same characteristic as observed in the drydock test results. That is, the stresses at the 50-percent radius were consistently higher (≈5 percent) than those at the 40-percent radius. This tends to strengthen the speculation that this is caused by within-tolerance blade geometry.

Alternating stresses on Propeller Blades 4 and 5 are given in Table 27. The complex signal of blade strain is shown in Figure 58 and the relative content of each harmonic function in Figure 59. The decibel scale was used to highlight the large number of higher frequency components which made up the dynamic response.

Generally, it can be seen that alternating stress increased chordwise from trailing edge to leading edge. This is consistent with hydrodynamic blade theory which predicts a concentration of dynamic loads at the leading edge. Alternating stress on the blade face was lower than on the blade back. The average (percent of mean) alternating stress over the entire blade is shown in Table 28. The percentage of alternating stress which represents the average overall measuring points on the propeller blade (45 percent)** is shown later in Table 34 together with representative values for other underway measurements on a variety of ships. This table indicates that a considerable data base of underway propeller blade measurements is now available.

Propeller Blade Bolts. The mean response of the blade bolts for full-power underway operation was almost identical to characteristics exhibited in the drydock data. Bolt preload dominated the total signal; however, there appeared to be more of a tendency for external loads to burden Bolt 6

---

*Stress levels were within 15 percent with Blade 5 being slightly higher. It was noted earlier that this blade had a slightly higher pitch setting than the other blades.

**Using the total blade average is more indicative of the actual hydrodynamic wake-induced fluctuating loads since this averaging of both the blade face and back stresses essentially eliminates centrifugal effects.

TABLE 26 - MEAN PRINCIPAL STRESS DISTRIBUTION ON PROPELLER BLADES 4 AND 5 FOR FULL-POWER, UNDERWAY OPERATION

(Stresses Include Effect of Both Hydrodynamic and Centrifugal Loads. Centrifugal Stress on the Propeller Blades at the 40- and 50-Percent Radii was Estimated to be Approximately 1.0 ksi at Full Power. Conditions for Full-Power Underway Operation Include Shaft Power at 226 rpm and Pitch of 191-inches. $\sigma_{rB} = E\varepsilon_r/1-\mu^2$ Where ε_r is Strain Measured on Single Radial Gage.)

	Location	Parameter (See Figure 48)	Radial Stress σ_{rB} ksi	Angle θ_B deg	Principal Stress ksi σ_{1B}	Principal Stress ksi σ_{2B}	Radial Stress σ_{rB} ksi	Angle θ_B deg	Principal Stress ksi σ_{1B}	Principal Stress ksi σ_{2B}	Radial Stress σ_{rB} ksi	Angle θ_B deg	Principal Stress ksi σ_{1B}	Principal Stress ksi σ_{2B}
BLADE 5	40 Percent Radius	Percent Chord from Leading Edge	← 25 →				← 50 →				← 75 →			
		Face	+9.3	−4	+8.8	+0.9	+10.0	−4	+10.0	+2.6	+7.0	−8	+7.0	+1.4
		Back	← No Strain Gages on Back (Suction) Side of Blade →											
	50 Percent Radius	Percent Chord from Leading Edge	← 25 →				← 50 →				← 75 →			
		Face	+9.5	−5	+9.4	+2.2	+10.6	+9	+11.5	+4.9	+7.6	+1	+7.2	+0.9
		Back	← No Strain Gages on Back (Suction) Side of Blade →											
BLADE 4	40 Percent Radius	Percent Chord from Leading Edge	← 25 →				← 50 →				← 75 →			
		Face	+10.4	*	*	*	+11.7	+3	+11.4	+2.2	+8.4	−2	+8.0	+0.9
		Back	−9.1	−17°	−3.6	−10.2	−9.5	−1°	−3.6	−9.8	−5.9	*	*	*
	50 Percent Radius	Percent Chord from Leading Edge	← 25 →				← 50 →				← 75 →			
		Face	+10.0	*	*	*	+10.6	+4	+10.6	+2.5	+7.7	*	*	*
		Back	−8.7	+2	−3.5	−9.1	−8.7	+4	−3.6	−9.2	−5.3	−5	−0.1	−4.3

*Radial gage only

Figure 57 - Mean Principal Stress on Propeller Blades 4 and 5

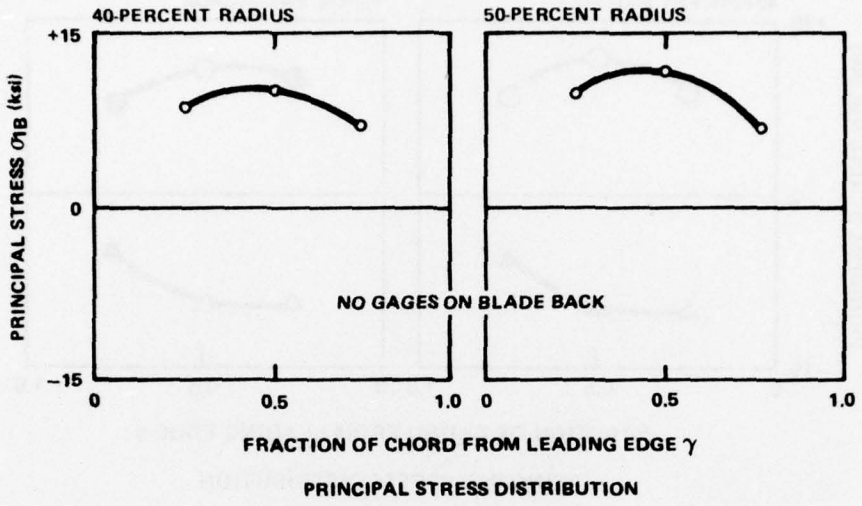

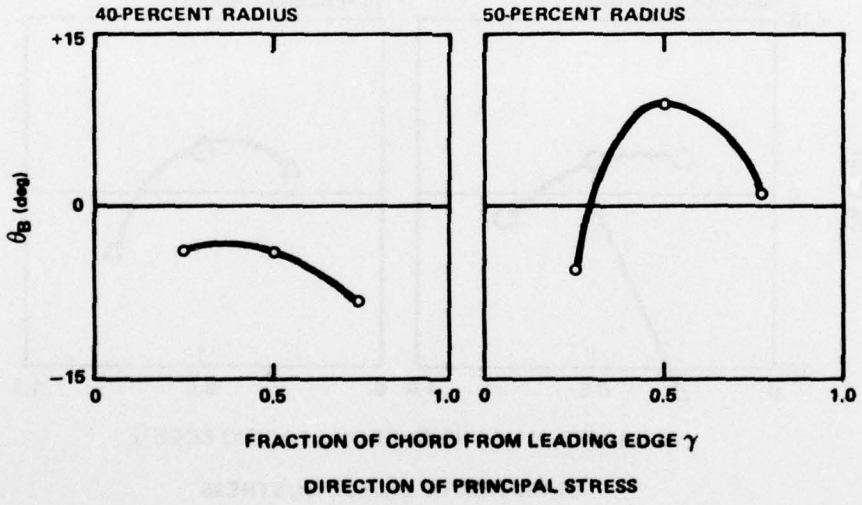

NOTES:

- ○ PRINCIPAL STRESS
- ● RADIAL STRESS/(1-μ^2) } PROPELLER FACE
- △ PRINCIPAL STRESS
- ▲ RADIAL STRESS/(1-μ^2) } PROPELLER BACK

Figure 57a - Propeller Blade 4

Figure 57 (Continued)

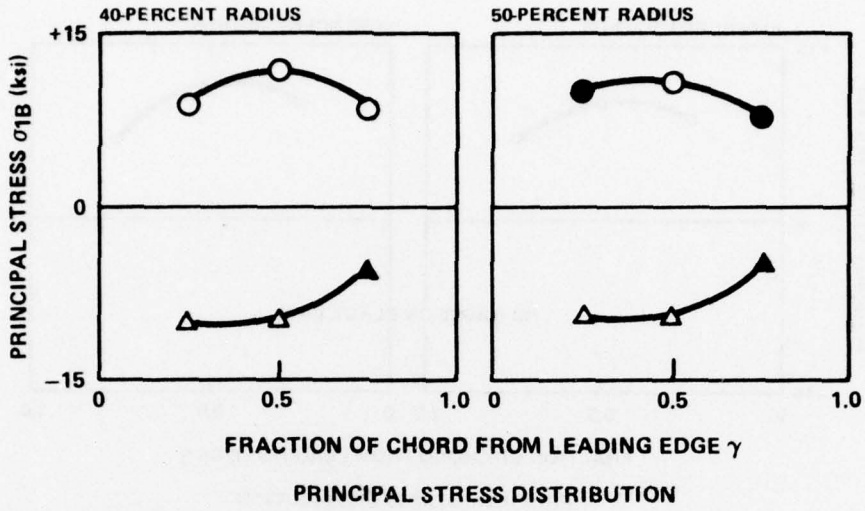

PRINCIPAL STRESS DISTRIBUTION

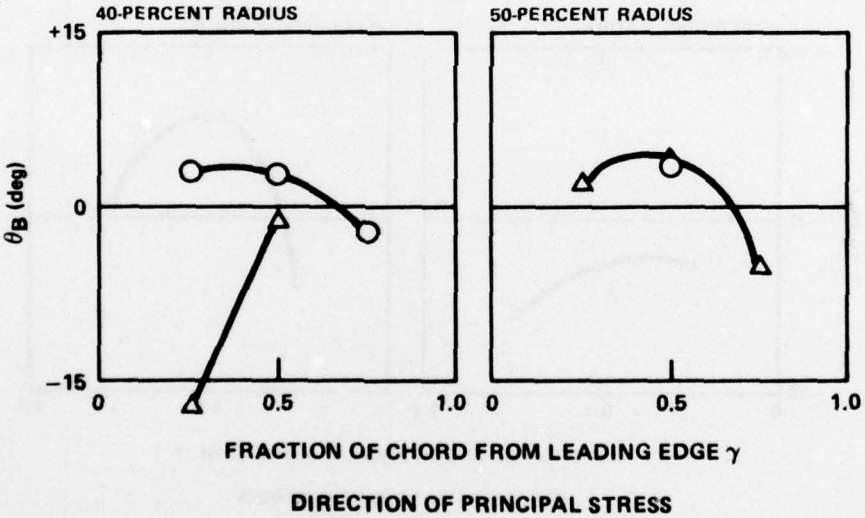

DIRECTION OF PRINCIPAL STRESS

NOTES:

- ○ PRINCIPAL STRESS
- ● RADIAL STRESS/(1-μ^2) } PROPELLER FACE
- △ PRINCIPAL STRESS
- ▲ RADIAL STRESS/(1-μ^2) } PROPELLER BACK

Figure 57b - Propeller Blade 5

TABLE 27 - ALTERNATING PRINCIPAL STRESS DISTRIBUTION ON PROPELLER BLADES 4 AND 5 FOR FULL-POWER, UNDERWAY OPERATION

(This Operating Condition Includes Shaft Power of 226 rpm and Pitch of 191 inches. Percent of Mean Equals Alternating Stress Divided by Mean Stress and Multiplied by 100; Mean Stress Includes the Effect of Both Hydrodynamic and Centrifugal Loads.)

Location		Alt. Stress ksi	Percent of Mean	Alt. Stress ksi	Percent of Mean	Alt. Stress ksi	Percent of Mean
(Blade 4)							
40 Percent Radius	Percent Chord from Leading Edge	← 25 →		← 50 →		← 75 →	
	Face	4.7	53	3.5	35	2.5	36
	Back		No Stress Gages on Blade Back				
50 Percent Radius	Percent Chord from Leading Edge	← 25 →		← 50 →		← 75 →	
	Face	5.3	56	5.4	47	2.1	29
	Back		No Stress Gages on Blade Back				
(Blade 5)							
40 Percent Radius	Percent Chord from Leading Edge	← 25 →		← 50 →		← 75 →	
	Face	4.4	42	4.3	38	3.1	39
	Back	4.8	47	4.1	42	2.5	42
50 Percent Radius	Percent Chord from Leading Edge	← 25 →		← 50 →		← 75 →	
	Face	4.4	44	4.9	46	3.1	40
	Back	4.9	53	3.6	39	2.5	58

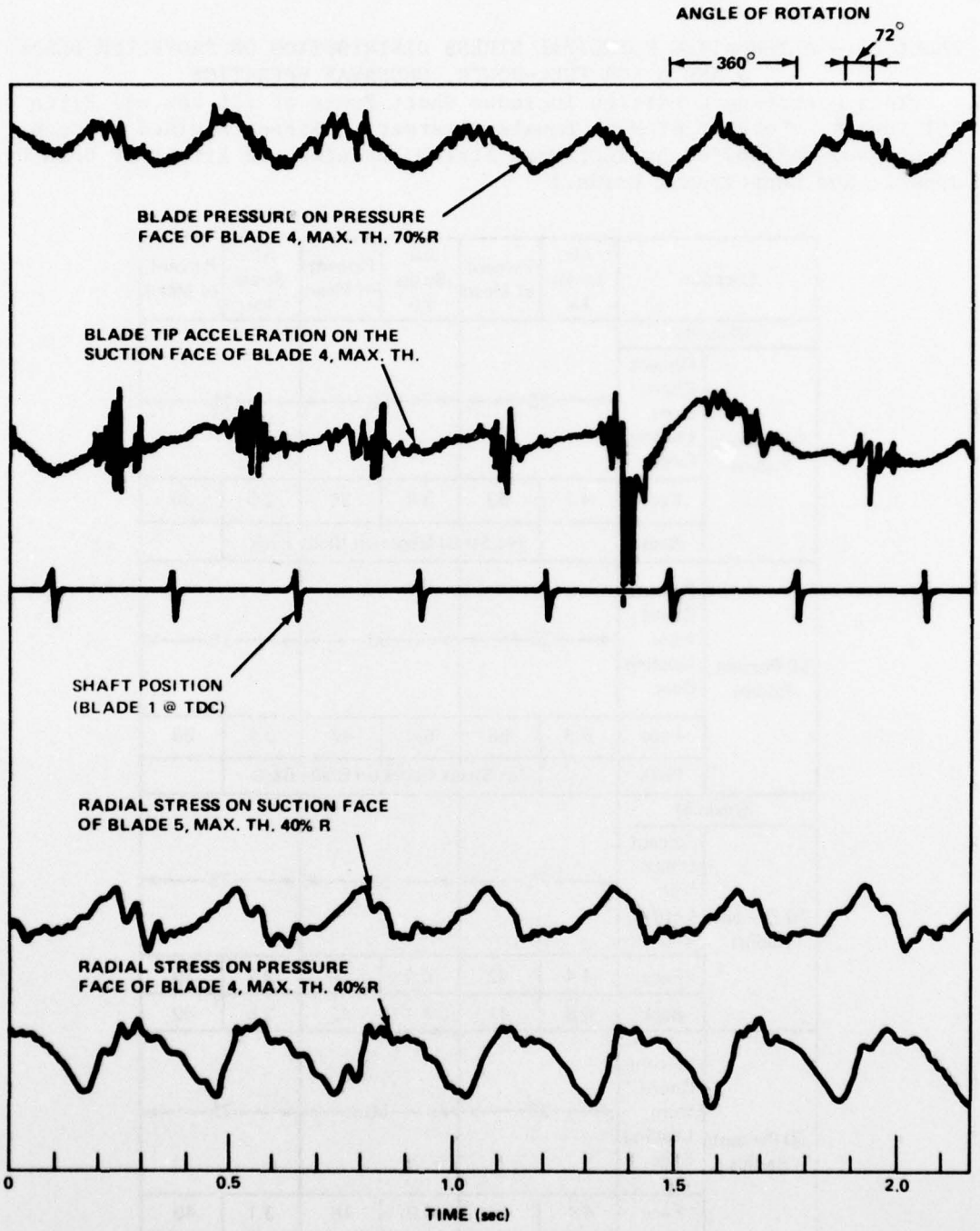

Figure 58 - Variation of Propeller Blade Pressure, Acceleration, and Strain with Blade Position at 210 Revolutions per Minute

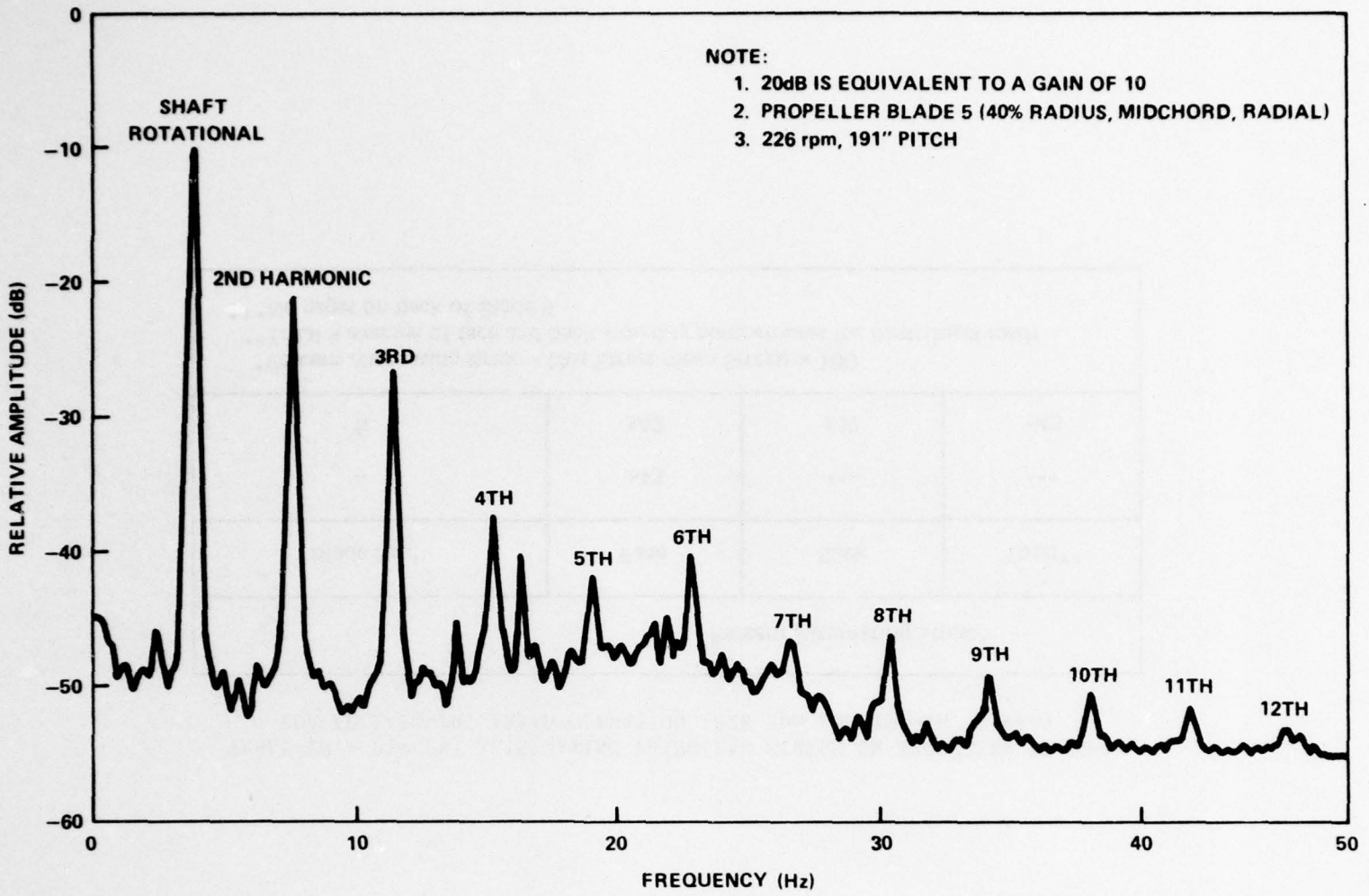

Figure 59 - Frequency Content of Propeller Blade Strain for Full-Power, Underway Operation

TABLE 28 - PERCENT ALTERNATING PRINCIPAL STRESS ON PROPELLER BLADES FOR FULL-POWER, AHEAD OPERATION (226 rpm and 191-in. Pitch)

	Percent Alternating Stress*		
Blade No.	Face	Back	Total**
4	±43	***	***
5	±42	±47	±45

*Percent alternating stress = (Alt Stress/Mean Stress) x 100
**Total = average of face and back (roughly compensates for centrifugal load)
***No gages on back of Blade 4.

(Table 29). This bolt remained the most heavily loaded by almost an order of magnitude; see Figure 60. Its response showed the now characteristic nonlinearity with even greater divation with more load, Figures 56 and 61. With increasing load, the bending axis changes from the original preload alignment to approximately perpendicular alignment to the propeller blade chord (0.3R section); see Table 30 and Figure 62. This suggests a variable loading mechanism on the bolts.

Alternating bolt stresses (Table 31) were less than 1.0 ksi for all but Bolt 6 (3.1 ksi). When compared with the mean applied load (load without preload), the alternating signal was significant. This is generally because the bolts experience very little of the applied load. When compared to the total bolt load (applied load including preload), the ratio of alternating load to mean was approximately 1 percent for all but Bolt 6 which was 4.8 percent. The alternating stress also exhibited a bending component. The pertinent values for the pressure face of Bolt 6 were $\alpha_{max} = \pm 5.1$, $\sigma_{min} \pm 1.1$, $\sigma_{av} = \pm 3.1$, $\sigma_{\beta} = \pm 2.0$, and percent $\sigma_{\beta} = 64.5$. The bending axis associated with this bending was approximately midway between the preload and external load bending axes.

Crank Disk. Mean stress measured at various locations in the crank disk fillet for underway, full-power operation is shown in Figure 63 and Table 32. Note that stress distribution was skewed toward the most heavily loaded bolt (No. 6). Response was linear with system forcing function (Figure 56) and principal axis was essentially radial.

Alternating crank disk stresses are shown in Table 33. Alternating stress distribution was also skewed toward Bolt Hole 6. The crank disks had an average of approximately 25 percent of alternating to mean stress on the "loaded" side (blade face). The percentage on the blade back was not calculated since the load path on the blade back did not pass through the bolts (1, 3, and 5) and crank disk flange, see Figure 64, and therefore the data would have no particular meaning.

Table 34 compares BARBEY propeller blade stress with that of a variety of other ships.

TABLE 29 - MEAN* STRESS IN BOLTS OF BLADE 2 FOR FULL-POWER, UNDERWAY OPERATION

TABLE 29A - INCLUDING PRESTRESS

Location	Bolt No.	Mean Bolt Stress (ksi)				Percent Bending Stress ($\%\sigma_b$)***
		σMax.	σMin.	σAvg.	σ_b*	
Blade Face	6	+80.8	+48.2	+64.5	±16.3	±25
Blade Face	2	†	†	+56.1	†	†
Blade Face	4	†	†	+55.8	†	†
Blade Back	5	†	†	+53.6	†	†
Blade Back	1	†	†	+57.2	†	†
Blade Back	3	†	†	+55.8	†	†

TABLE 29B - ABOVE PRESTRESS

Location	Bolt No.	Mean Bolt Stress (ksi)				Percent Bending Stress ($\%\sigma_b$)***
		σMax.	σMin.	σAvg.	σ_b**	
Blade Face	6	+14.6	+1.1	+7.8	±6.8	±87
Blade Face	2	†	†	+0.2	†	†
Blade Face	4	†	†	+1.1	†	†
Blade Back	5	†	†	−0.8	†	†
Blade Back	1	†	†	−0.0	†	†
Blade Back	3	†	†	−0.2	†	†

*Mean stress includes both hydrodynamic and centrifugal loads. Centrifugal bolt stress is complicated because of propeller palm distortion at full-power ahead operation. Based on unpublished test results at DTNSRDC (Code 1720.6) on the full-scale DD-963 model, it is estimated that centrifugal bolt stress on the most heavily loaded bolt was < 1.0 ksi; conditions of 226 rpm and 191 in pitch.

**$\sigma_b = (\sigma_{Max.} - \sigma_{Avg.})$

***Percent $\sigma_B = (\sigma_B/\sigma_{Avg.})\ 100$

†Underway trial instrumentation was limited to two diametrically opposed gages on Bolts 1, 2, 3, 4 and 5.

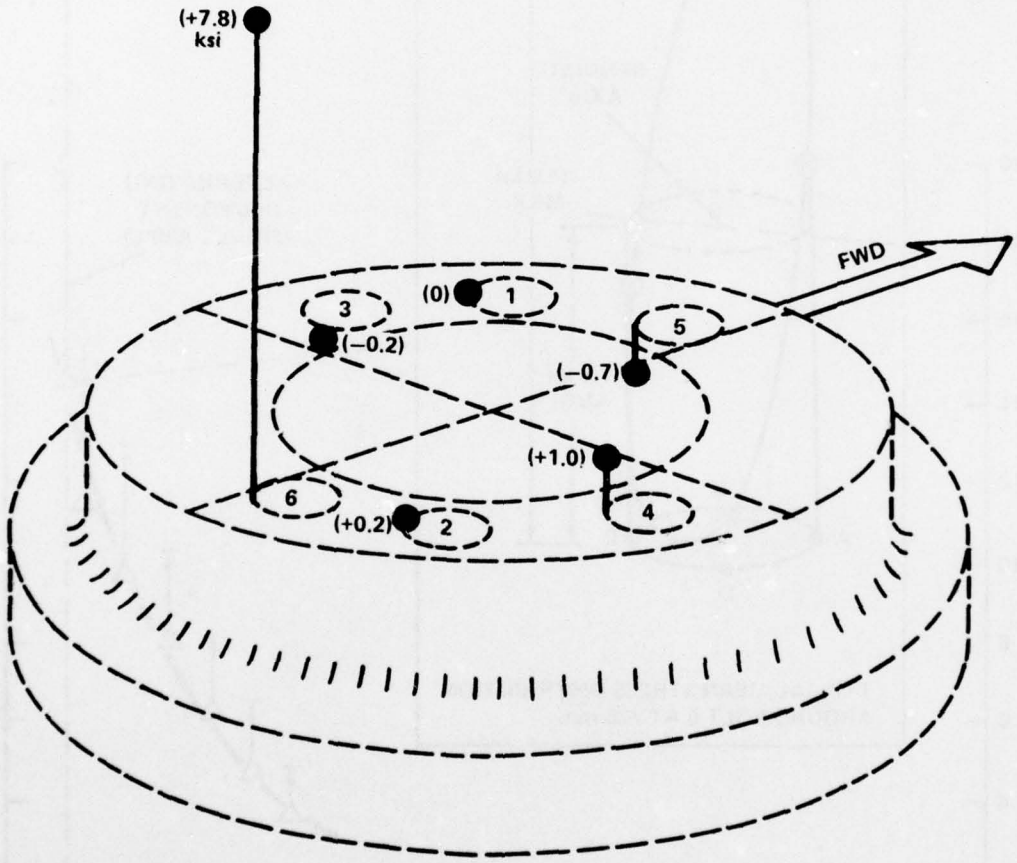

Figure 60 - Average Mean Stress (above Prestress) in Blade Bolts, Propeller Blade 2, for Full-Power, Underway Operation

AD-A047 851 DAVID W TAYLOR NAVAL SHIP RESEARCH AND DEVELOPMENT CE--ETC F/G 13/10
THE BARBEY REPORT. AN INVESTIGATION INTO CONTROLLABLE PITCH PRO--ETC(U)
AUG 77 C NOONAN, G ANTONIDES, A ZALOUMIS

UNCLASSIFIED DTNSRDC-77-0080 NL

3 OF 4
AD
AD47851

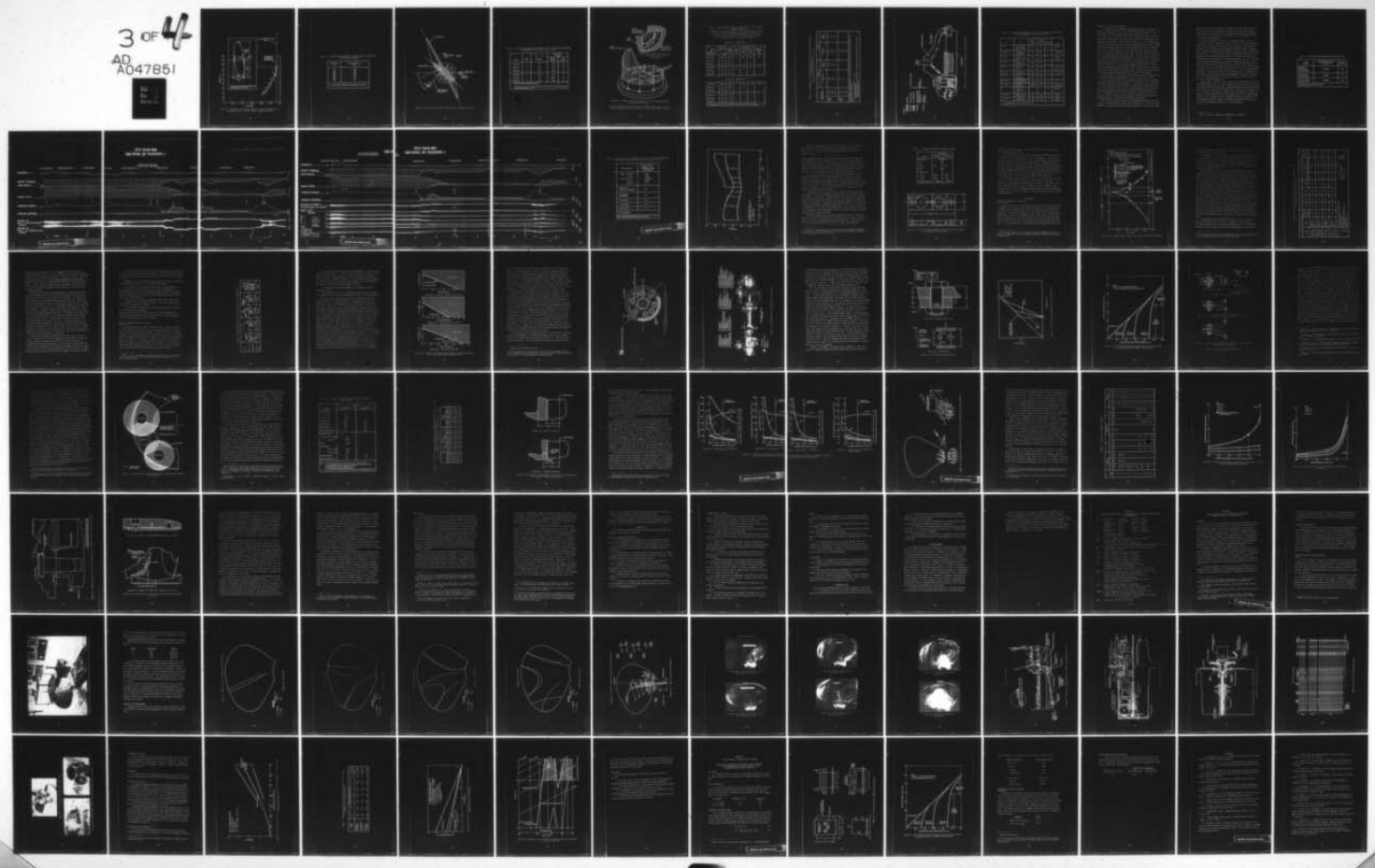

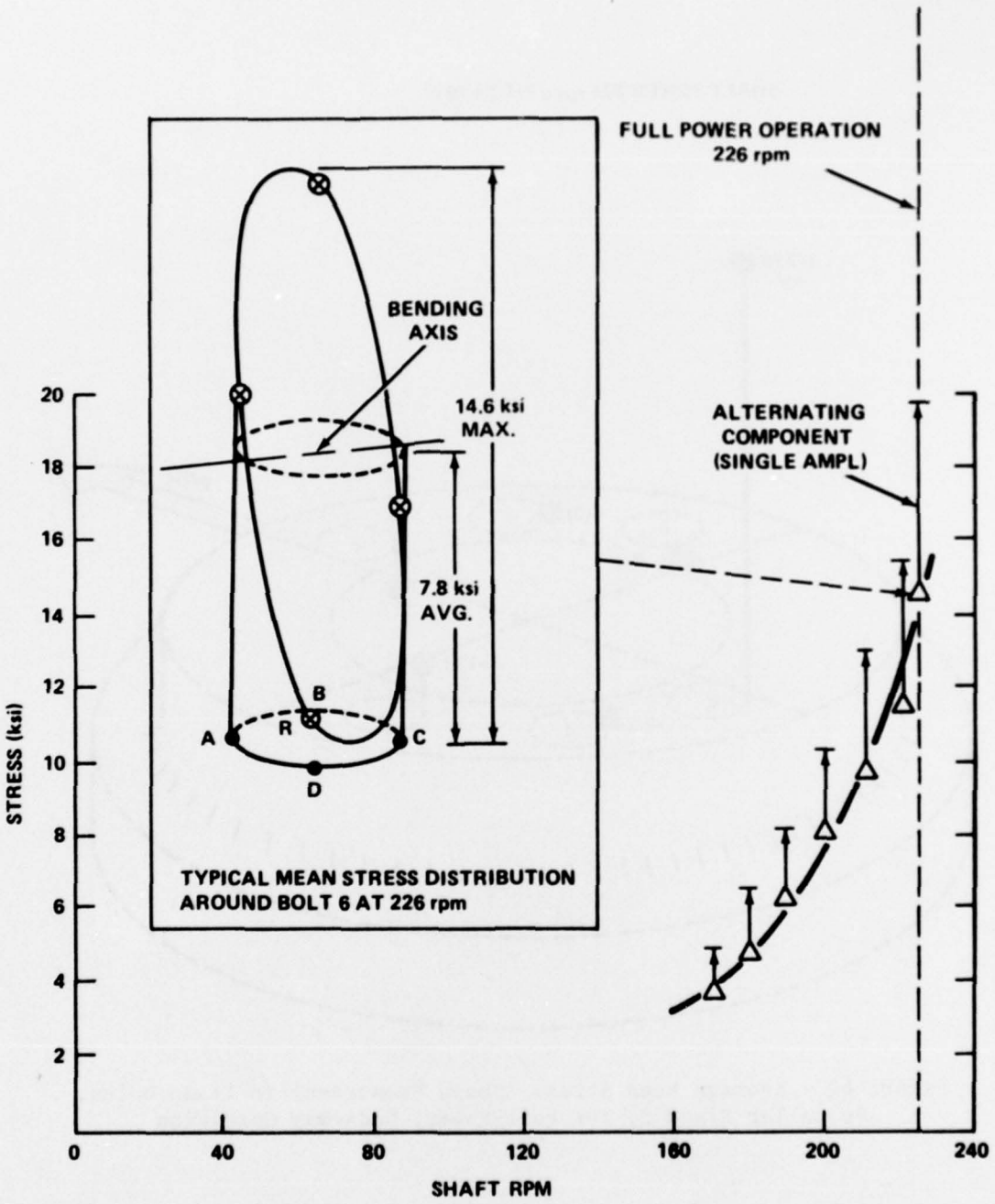

Figure 61 - Maximum Stress (above Prestress) in Shank of Blade Bolt 6, Propeller Blade 2, for Full-Power, Underway Operation

TABLE 30 - ANGULAR VARIATION OF BOLT 6 BENDING AXIS WITH SHAFT RPM FOR UNDERWAY OPERATION

Shaft Power rpm	Angular Variation α deg
170	28
180	38
190	33
200	46
210	45
220	47
226	45
α = angle between shaft $\mathbb{C}$ and bolt bending axis (CCW+)	

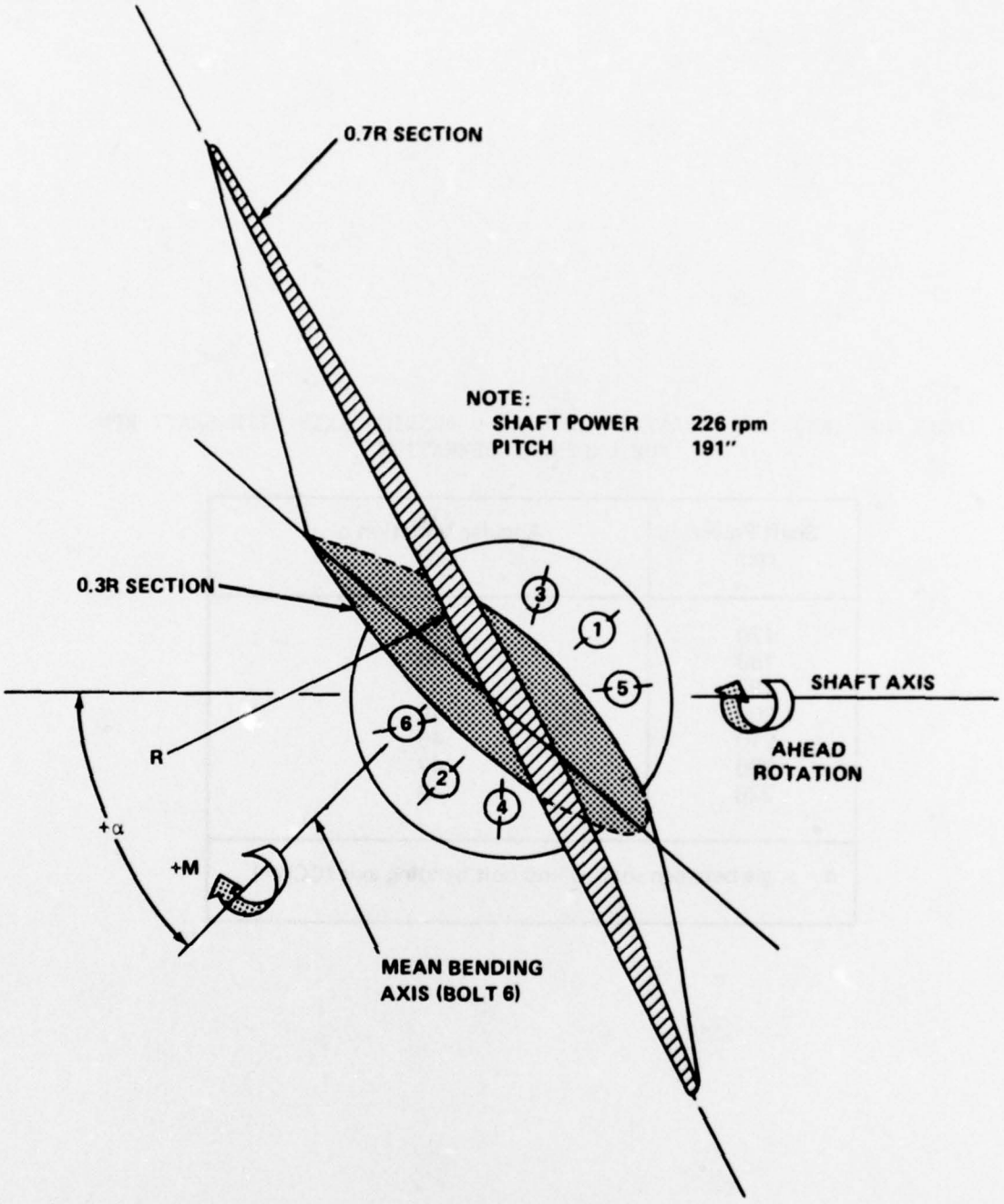

Figure 62 - Bending Axis of Bolt 6 for Full-Power, Underway Operation

TABLE 31 - AVERAGE ALTERNATING BOLT STRESS FOR FULL-POWER, AHEAD OPERATION
(Conditions of 226 rpm and 191-in. Pitch)

Location	Bolt No.	Avg.* Alt. Stress, S. A. ksi	Percent A/M** Stress	
			Without Prestress	With Prestress
Blade Face	6	±3.1	±39	±4.8
Blade Face	2	±0.4	±218	±0.8
Blade Face	4	±0.7	±68	±1.3
Blade Back	5	±0.6	±75	±1.1
Blade Back	1	±0.5	±5450	±1.0
Blade Back	3	±0.9	±415	±1.5

*Bolts also had an alternating bending load

**Percent A/M = ratio of (alt. stress/mean stress) x100, where mean stress includes centrifugal effects estimated to be $<$1.0 ksi.

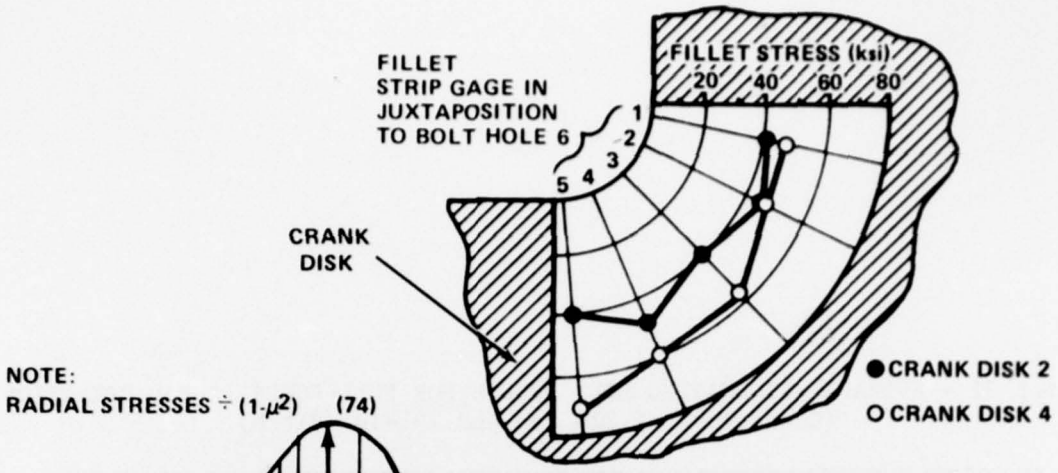

Figure 63b - Crank Disk Fillet Stress Distribution Juxtaposition Bolt Hole 6

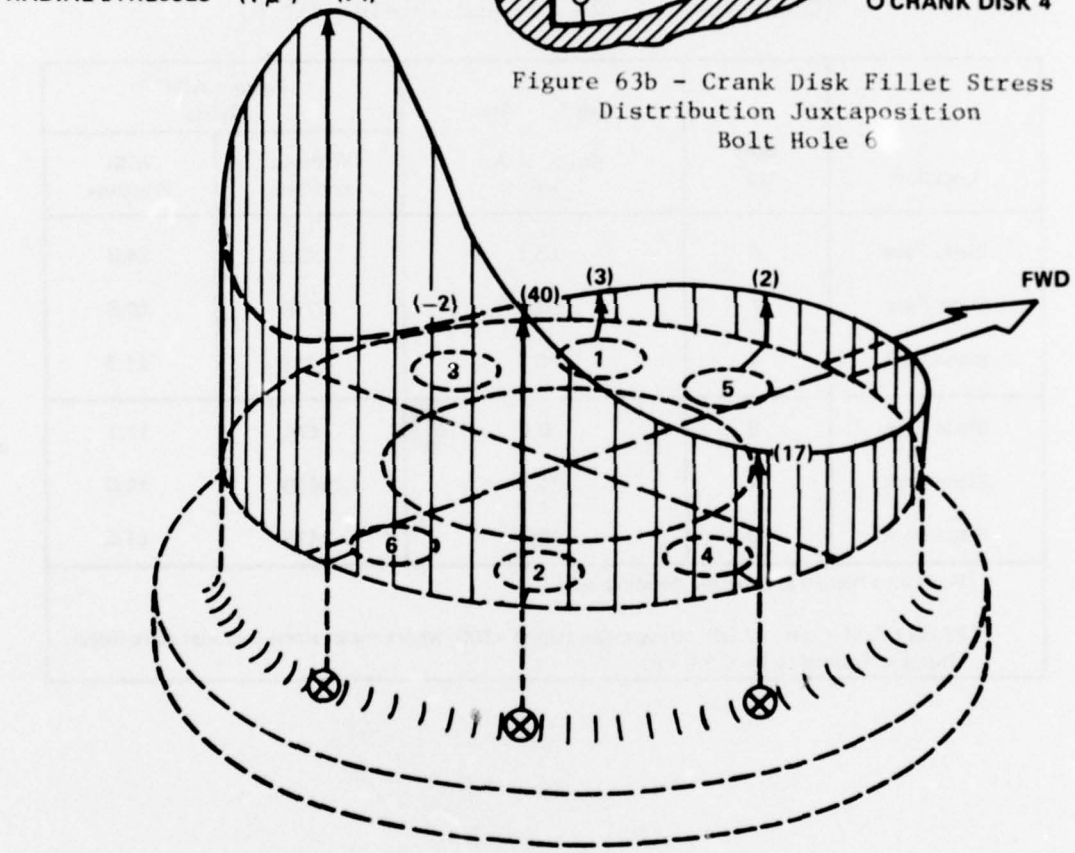

Figure 63a - General Stress Distribution in Fillet Including Maximum Values for Crank Disk 4

Figure 63 - Radial Stresses in Fillets of Crank Disks 2 and 4 for Full-Power, Underway Operation (Condition of 226 rpm and 191-in. Pitch)

TABLE 32 - MEAN PRINCIPAL STRESS ON CRANK DISKS FOR FULL-POWER, UNDERWAY OPERATION

(Conditions of 226 rpm and 191-in. Pitch. Mean Stress Includes the Effect of Both Hydrodynamic and Centrifugal Loads. Centrifugal Load on the Crank Ring Estimated to be Approximately 1.9 ksi. Stresses at Bolt Hole 6 were Computed on an Average Value of Strip Gage Output)

TABLE 32A - CRANK DISK 2

Gage Location and Bolt Hole No. / Parameter (See Fig. 46)		Radial Stress* σ_r(CD) ksi	Angle θ(CD) deg	Principal Stress σ_1(CD) ksi	Principal Stress σ_2(CD) ksi	Maximum Shear Stress τ(CD) ksi
Blade Face	BH6	+44.8	−2	+48.7	+26.2	+11.3
Blade Face	BH2	+41.0	•	•	•	•
Blade Face	BH4	+18.3	•	•	•	•
Blade Back	BH5	+6.1	+11	+5.2	−2.2	+3.7
Blade Back	BH1	+4.1	•	•	•	•
Blade Back	BH3	(8)	–	–	–	–

TABLE 32B - CRANK DISK 4

Blade Face	BH6	+58.0	−2	58.0	+17.3	+20.4
Blade Face	BH2	+40.2	•	•	•	•
Blade Face	BH4	+17.4	•	•	•	•
Blade Back	BH5	+2.1	•	•	•	•
Blade Back	BH1	+2.5	•	•	•	•
Blade Back	BH3	−1.8	•	•	•	•

*Radial gage only; $\sigma_r = E\,\epsilon_r/(1-\mu^2)$, where ϵ_r is strain measured on single radial gage.

TABLE 33 - ALTERNATING PRINCIPAL STRESSES[1] IN CRANK DISKS FOR FULL-POWER, UNDERWAY OPERATION
(Conditions of 226 rpm and 191-in. Pitch)

Gage Location and Bolt Hole No.		Crank Disk 2		Crank Disk 4	
		Alt Stress, SA[2] ksi	Percent A/M[3]	Alt Stress, SA ksi	Percent A/M[3]
Blade Face	BH6	±9.0	±19	±11.6	±21
	BH2	±11.5	±29	±11.3	±30
	BH4	±5.7	±35	±5.1	±33
Blade Back	BH5	±3.1	*	±3.7	*
	BH1	±3.1	*	±4.9	*
	BH3	–	*	±1.2	*

*Since load path for full-ahead operation does not pass through the forward flange of the crank disk, calculations of percent A/M are not applicable.

Notes:
1. Principal stress [or radial stress ÷ $(1-\mu^2)$]
2. SA = Single Amplitude
3. Percent A/M = Ratio of (Alt Stress/Mean Stress x 100 where mean stress is principal or (radial/$1-\mu^2$) minus estimated centrifugal stress.

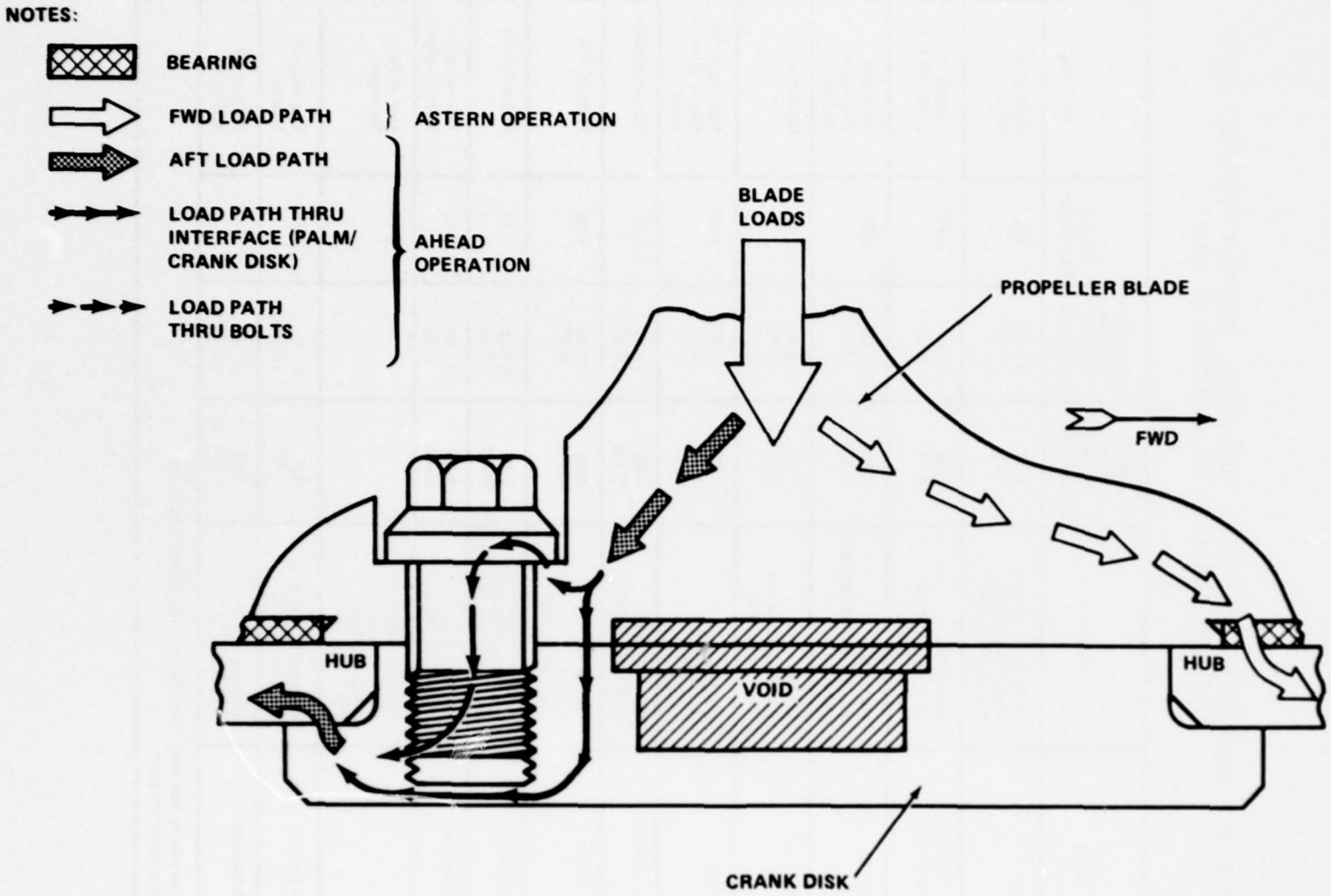

Figure 64 - Propeller Blade Load Flow Path for Ahead Operation

TABLE 34 - COMPARATIVE SUMMARY OF FULL-SCALE, UNDERWAY PROPELLER BLADE STRESS MEASUREMENTS ON A VARIETY OF SHIPS

Ship	Source	Average Stress tons/in^2 (kg/mm^2)	Fluctuation in Stress tons/in^2 (kg/mm^2)	Percent Fluctuation	Remarks
Viana	Wereldsma - International Shipbuilding Progress 133 1964	2.93 (4.61)	±0.84 (1.32)	±29	42,000-ton tanker
USS Franklin D. Roosevelt	Antonides DTNSRDC Report No. 2562 1968	3.88 (6.11)	±1.61 (2.54)	±47*	Aircraft Carrier quadruple screw
Neuenfels	Keil et al. Journal of Hydronautics 1972	1.79 (2.82)	±1.50 (2.36)	±84	Cargo ship (two failures in class)
Flinders Bay	Chirila Shipping World and Shipbuilder 1971	1.91 (3.01)	±0.76 (1.12)	±40	Container ship
Michigan	Brewer J.SESA 1971	4.68 (7.37)	±2.61 (4.11)	±56	Fast cargo ship (five failures in class)
Golar Nichu	Sontvedt et al. RINA Symp. 1973	4.00 (6.30)	±1.40 (2.20)	±35	Ducted propeller
Seiun Maru	Ueta et al. Mar. Eng. Soc. Japan 3/74	5.85 (9.21)	±2.76 (4.35)	±46	Training ship
Hakano Maru	Nakano - Shipbuilding Research Assoc. R.A. Japan No. 172, 1972	3.62 (5.70)	±1.33 (2.09)	±37	Container ship
USS Douglas	Noonan, C. J. DTNSRDC, 1971	5.64 (8.88)	±1.68 (2.65)	±33*	Twin-screw patrol gunboat
**	Conolly, Trans. Royal Inst. of *Naval Architects* 1960			±43	Twin-screw destroyer
USS Barbey	Noonan, C. J. et al. DTNSRDC 1975	4.8 (7.56)	±1.9 (2.99)	±45*	Single-screw frigate
USS Spruance	Antonides, G. P. DTNSRDC 1976	4.68 (7.38)	±1.77 (2.79)	±45*	Twin-screw destroyer

*Test results have been modified to exclude centrifugal loads.
**Ship name not given.

Maneuvers and Off-Design Operation

It is generally recognized that maneuvering (turns, crashbacks, etc.) operations change the levels of mean and alternating propeller forces. The prediction of propeller forces under these transient conditions is difficult even for a conventional (fixed pitch) propeller. The CPP propeller is even more complicated since there are variations of considerably more parameters (shaft power, pitch, inhibit control, etc.). For example, execution of a crashback maneuver was rather complicated and involved a number of interrelated parameters which were programmed together in the automatic control mode. Normal operation on the execution of a crashback command basically involved in iteration of the power and pitch control mechanisms about a preprogrammed 150 rpm inhibit point. In other words, on execution of a crashback, the shaft power would drop to 150 rpm, at which point the propeller pitch would decrease and result in increasing power. When power exceeded the inhibit point, a decrease in pitch would stop until power could be returned to the inhibit level (return from overshot). Iteration of these two parameters would continue until a decrease in pitch would not increase shaft power above the inhibit point. At this point, throttle and pitch would decrease simultaneously until zero pitch was reached.

In these tests, the throttle was then opened and pitch brought to design astern conditions (approximately 131 in. of pitch and 100 rpm).

Several runs were made at various inhibit points in order to examine crashback conditions of varing severity. In particular, the crashback at CPP system (crank disk) failure mode was repeated during the latter part of the test agenda in order to measure system response at this condition. The crashahead maneuver was usually initiated while making steady stern way. On command, the throttle was closed and propeller pitch was increased. When zero pitch point was passed, the throttle and pitch were increased together until desired conditions were reached.

Since the most dramatic failure of the BARBEY CPP mechanism occurred during a crashback, there was considerable speculation as to the existing magnitude of propeller blade forces during maneuvers in general and during

crashback operation in particular. Estimates were that a full-power turn would increase the mean hydrodynamic forces (above full-power ahead) by approximately 35 percent whereas a crashback would involve approximately 172 percent of full-power ahead loads (Table 35). No estimates of alternating loads were attempted.

Typical time-history response of the propeller blades, bolts, and crank disk for an RTC* maneuver is shown in Figure 65. Typical standardization data for maneuvers are given in Tables 24 and 25, and Figure 54. Included in these figures are pertinent main propulsion plant parameters which, together with measured CPP component response, give an operational/stress history. It can be seen from these figures and tables that in all maneuvers, the response varied depending on test conditions; however, a few generalities are appropriate to most measurements. In turns, the mean values increased approximately as predicted (Table 36); however, the dynamic stress levels increased considerably, reaching double (100 percent increased) the value of a steady ahead condition for a hard (35-deg rudder) turn, Figure 66. This resulted in an A/M ratio in turns of approximately 66 percent. Although the rudder was held over for only a 90-deg turn, it was found that the generally higher (approximately 100-percent increase) level of alternating stresses continued as long as the rudder was held over for a longer (360-deg) turn.

Higher levels of stress (torque, thrust, etc.) were predicted for the crashback maneuvers; however, none exceeded the values recorded for normal steady ahead full-power operation. Crashahead operation increased the mean by as much as 40 to 50 percent compared to full-power ahead operation and for a very short time (several seconds) more than doubled the dynamic response. The qualitative nature of the dynamic signal also changed during this burst as it appeared that the propeller blade was responding at its first bending frequency (19 Hz). The above observations were generally true for all measuring locations in the CPP mechanism.

---

*RTC ≡ run, turn, crashback (crashahead); see Figure 29.

TABLE 35 - PREDICTED MEAN HYDRODYNAMIC PROPELLER LOADS

Load Condition	Bending Moment* Due to Torque and Thrust ft - lb	Percent of Full Power
Design Full Power Ahead (No Alt Loads)	220,500	100
Crash Astern (No Alt Loads)	378,750	172
Full-Power Turn (No Alt Loads)	297,850	135
*Bending moment at crank disk fillet		

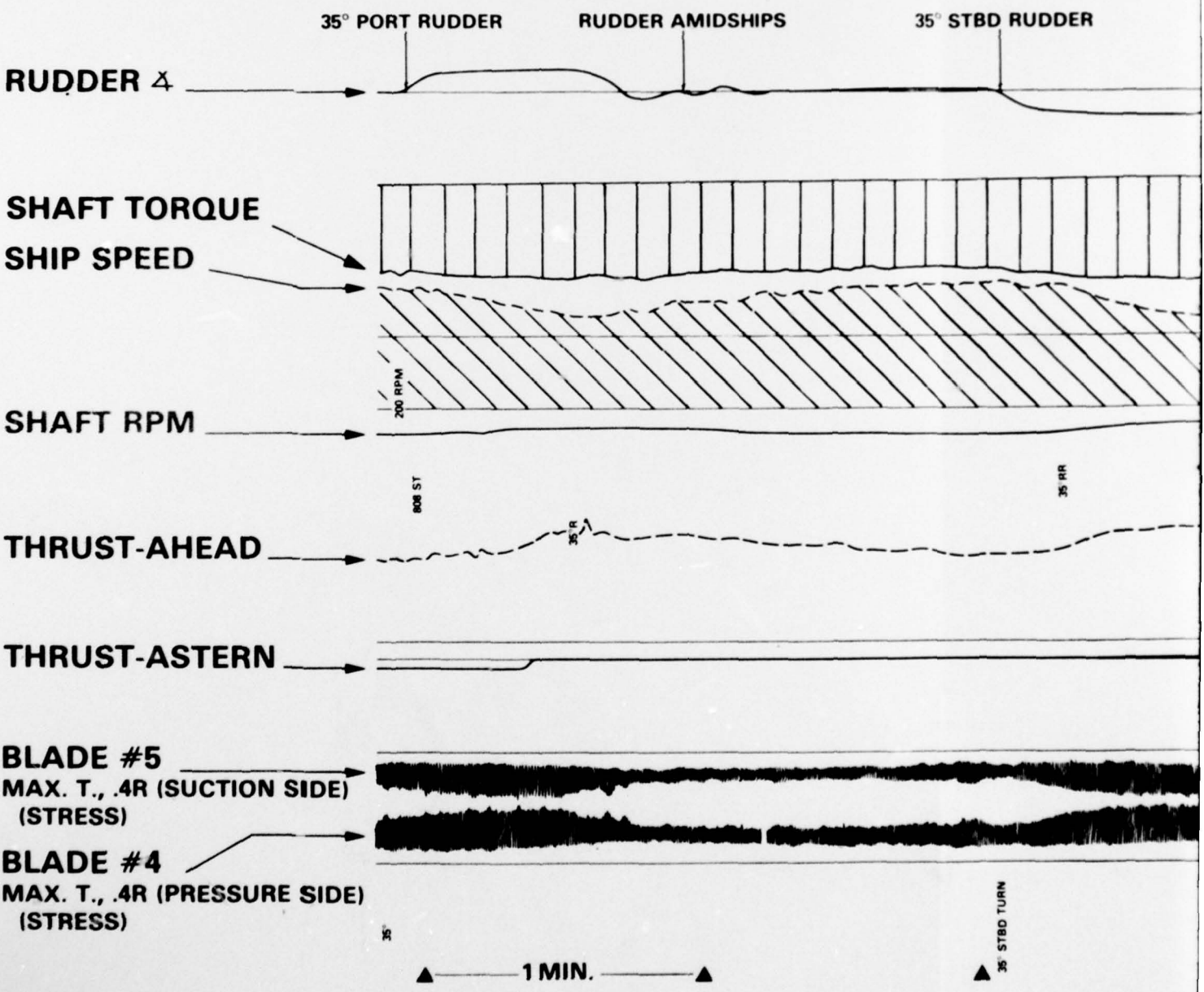

PRECEDING PAGE BLANK-NOT FILMED

RTC RUN 808
200 RPM, 35° RUDDER 4

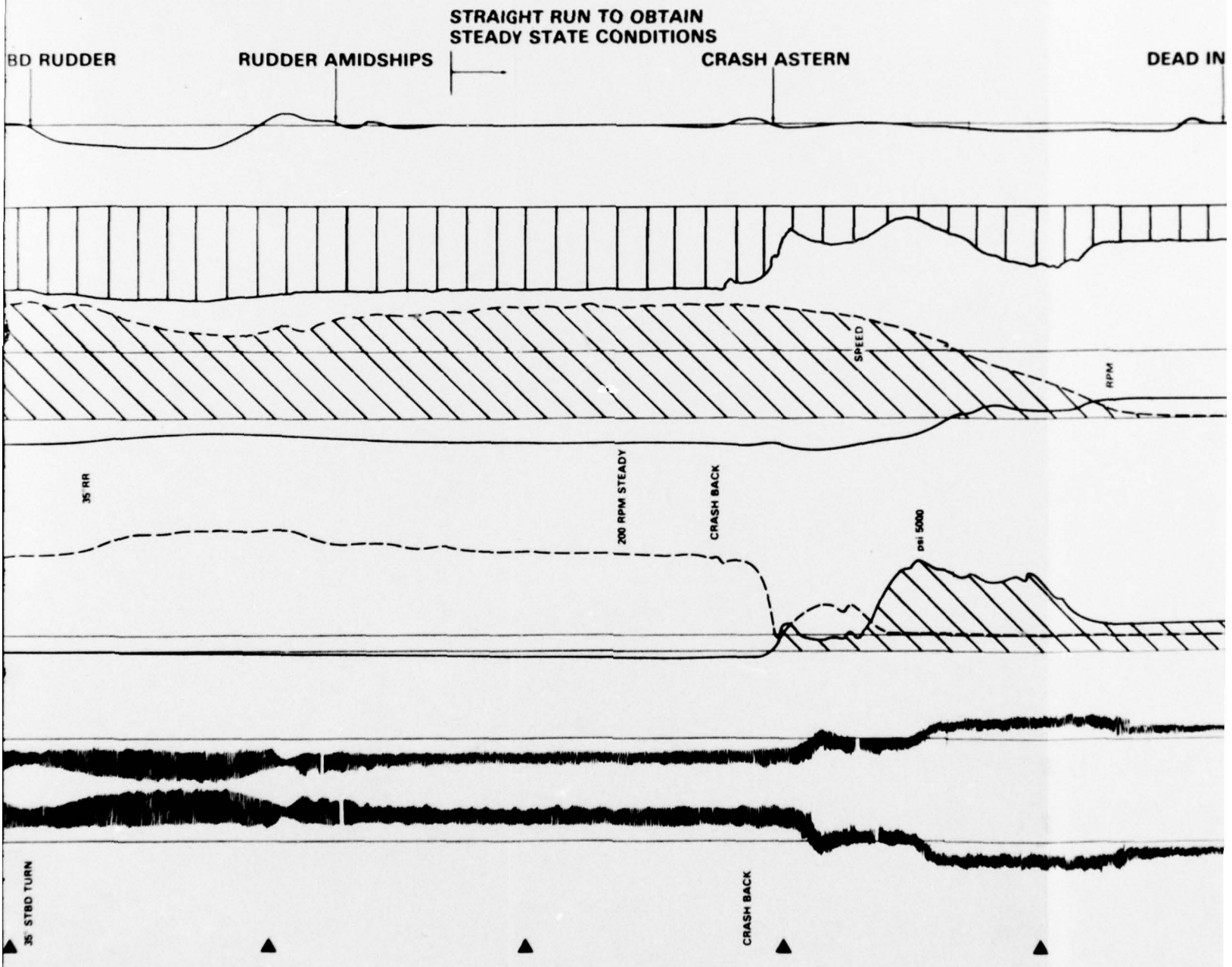

Figure 65 - Time/History of Measured Parameters for RTC Maneuvers

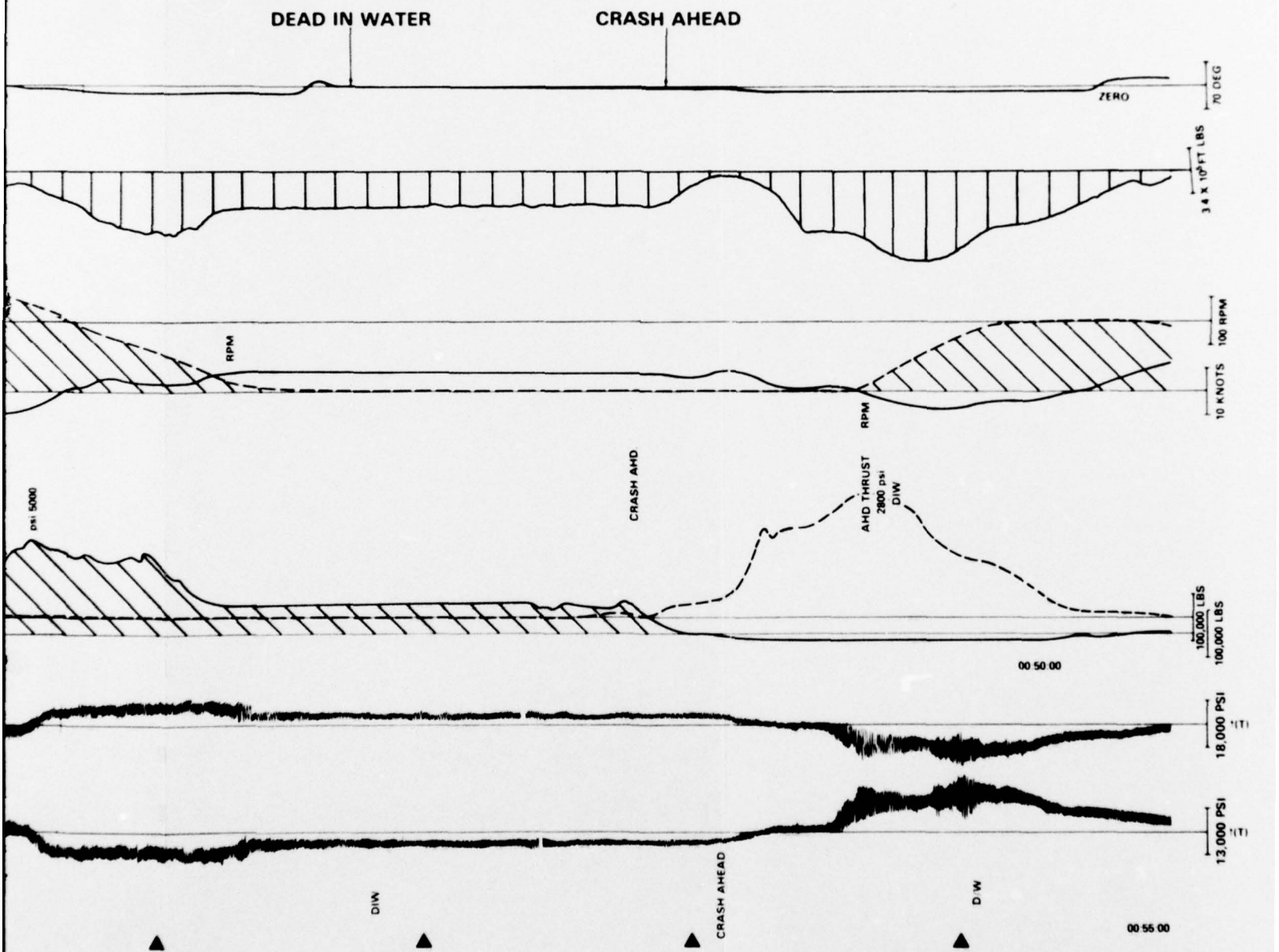

Figure 65a - RTC Run 808

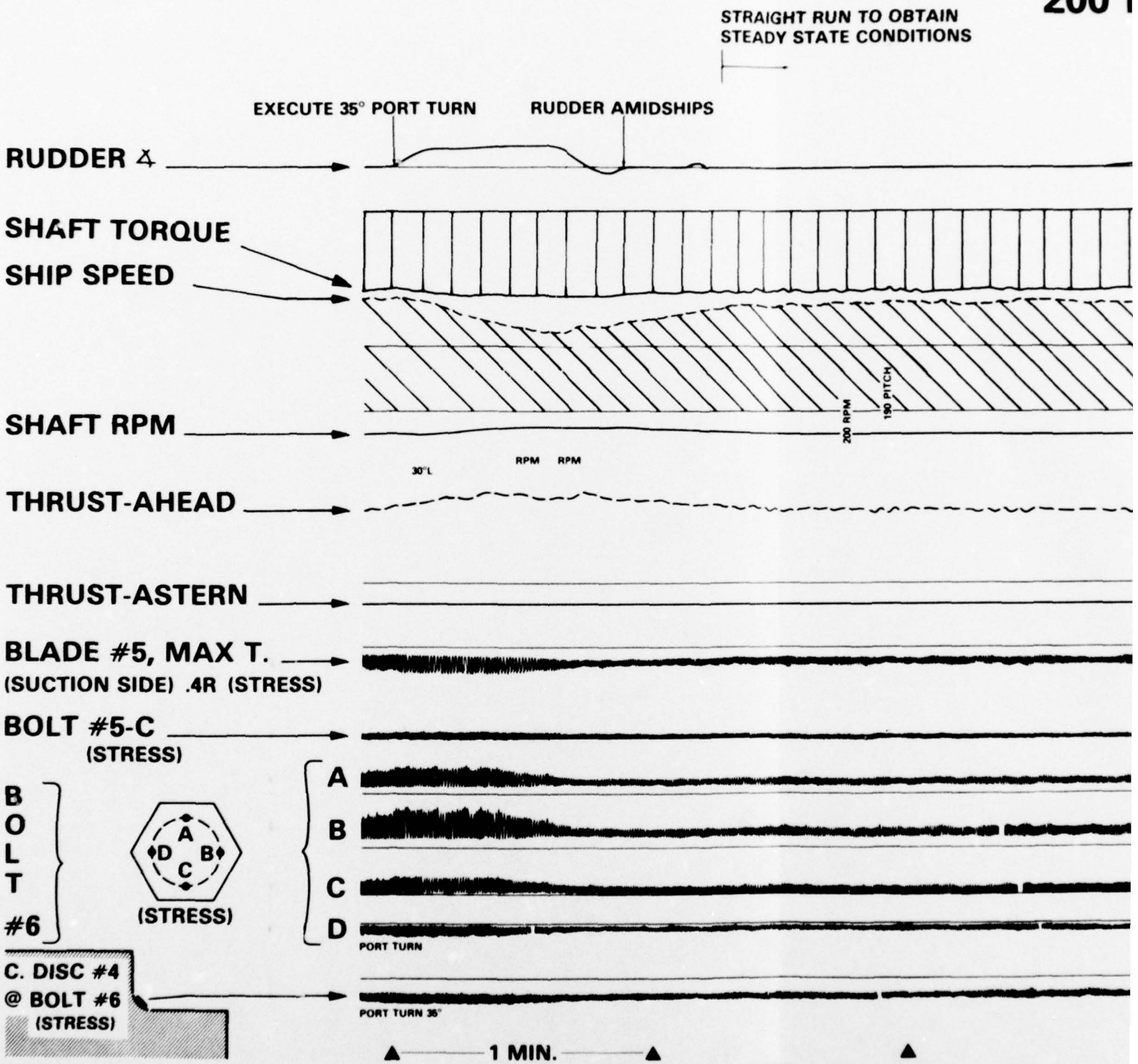

RTC RUN 807
200 RPM, 35° RUDDER 4

TAIN
TIONS

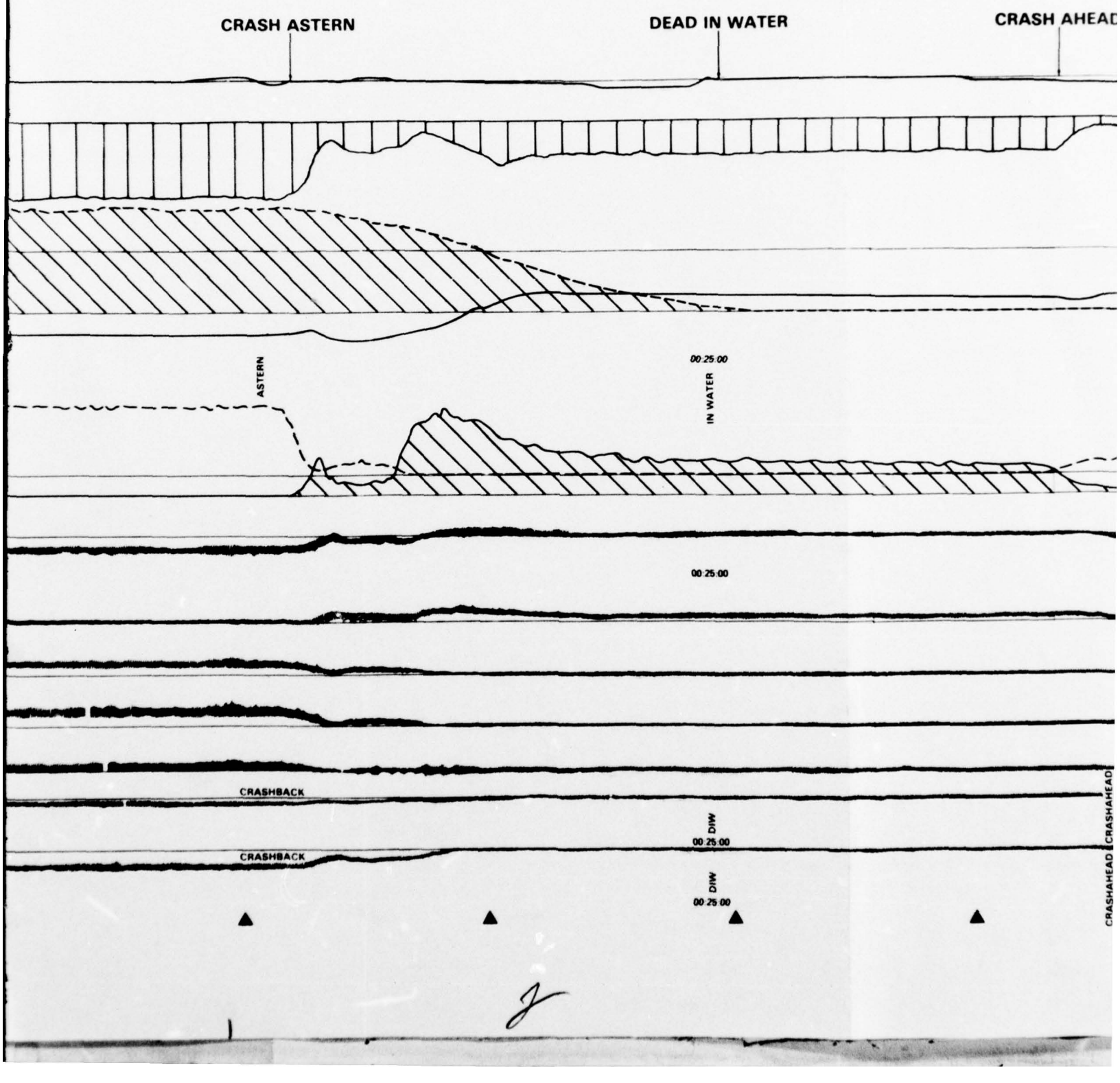

Figure 65 (Continued)

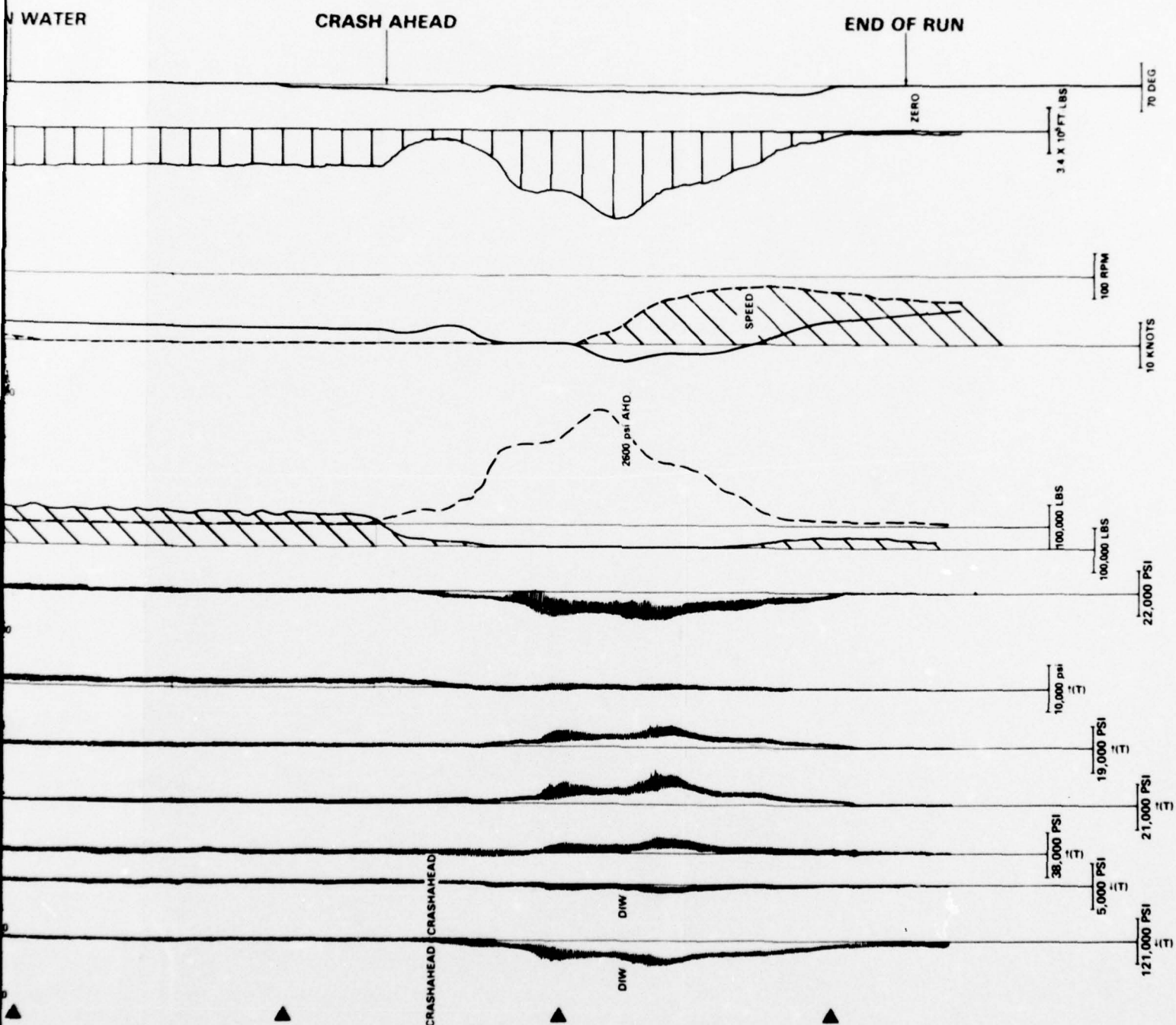

Figure 65b - RTC Run 807

TABLE 36 - RELATIVE EFFECT OF TURNS ON MEAN VALUES OF MEASURED PARAMETERS
(Conditions of 200 rpm, 191-in. Pitch, 35-deg Port Turns)

Quantity Measured	Percent Increase (+) or Decrease (−) Due to Turn Relative to Straight Ahead Operation
Bolt 6 (Strain)* Gage 1 (A)	+31
Gage 2 (B)	+35
Gage 3 (C)	+38
Gage 4 (D)	+40
	36 avg
Blade 5, 0.4R Radial, Suction Side (Strain)	+36
Crank Disk 4 at Bolt 6 (Strain)	+20
Thrust in Shaft	+35
Torque in Shaft	+15
Shaft Power, rpm	−8

*Above Preload Stress

Note: Relative differences determined from records similar to Figure 65. Table includes both hydrodynamic and centrifugal loads.

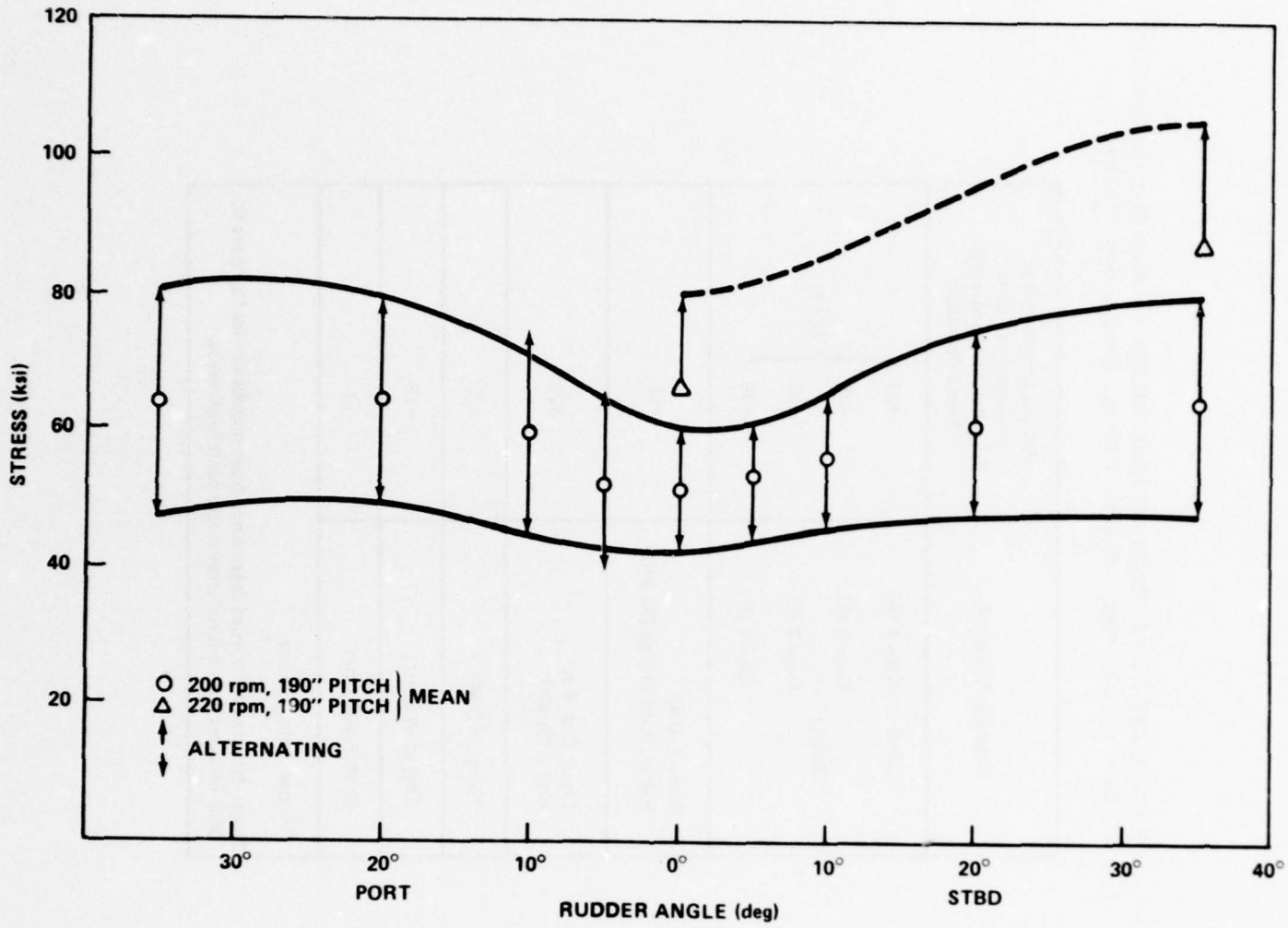

Figure 66 - Effect of Turns on Crank Disk Stresses in Juxtaposition to Bolt Hole 6
(Disk Stresses = Radial Stress ÷ $(1-\mu^2)$

Operation at underpitch (170 in.) and overpitch (240 in.) conditions were recorded but did not contribute any significant revelations; see Figure 56. It is noted that the overpitched operation did result in higher stresses.

Propeller Blade Pressure. As previously stated, one of the primary goals of the BARBEY trials was to define the state of stress which existed in the CPP propeller system. The philosophy was that the measured stresses would be (1) approximately the same as originally predicted, or (2) approximately the same as predicted by recent sophisticated (finite element) analysis, or (3) considerably different from all predicitions.

If (1) were true, then no further work would be required in view of the premise that some satisfactory explanation of the failure could be found. If (2) were true, then the system could be modified by using a fairly representative finite element model. If measurements indicated item (3) were true, then the CPP propeller program would require extensive theoretical reevaluation. This would mean reworking the mathematical model and/or the assumed loading conditions.

It was assumed that the drydock tests, together with measured underway component strains, could give reasonable empirical "correction factors" for modeling, if necessary. DTNSRDC proposed that an extensive investigation of blade pressure be conducted, but time and monetary constraints prohibted the execution of this phase of the program. However, it was decided to make some attempt at recording blade pressure only from the standpoint of feasibility. This type of measurement had not been attempted before and it was important to take advantage of this opportunity to explore the problems involved in doing this work.

Two pressure gages were installed in Propeller Blade 4. Both gages were located at the intersection of the midchord and 0.7 radius lines, one gage on the blade face and the other on the blade back. Gage characteristics are given by Dean[32] and in Table 37. Figure 67 shows gage

---

[32]Dean, M., "Miniature Pressure Gage (for use in Aerodynamic and Hydrodynamic Research Investigations)," presented at 8th Transducer Workshop, St. Louis, Missouri (22–24 Apr 1975).

TABLE 37 - PRESSURE TRANSDUCER CALIBRATION SUMMARY

Parameter	Gage Location	
	Blade Back	Blade Face
Manufacturer	– DTNSRDC –	
Type	– Bikini –	
Serial No.	272	273
Range	– 50 psi –	
Resistance, ohms		
Input	362.8	360.9
Output	362.6	360.8
Sensitivity, mV/V/psi	0.04800	0.0376

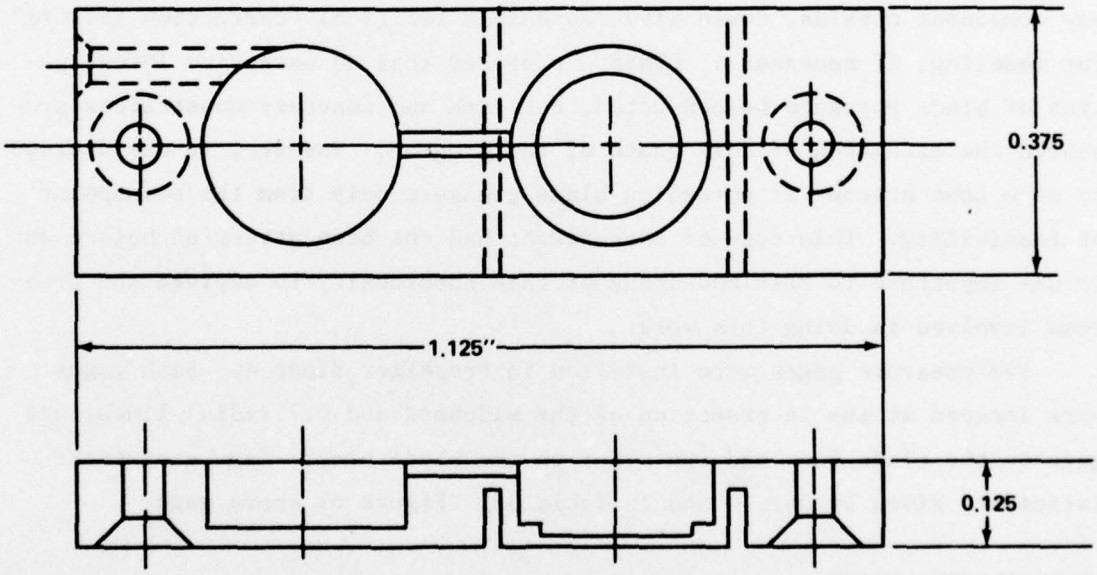

Figure 67 - Details of the Bikini Pressure Gage (Adapted from NSRDC Engineering Drawing E-3076-1)

construction and size details. Figures 39e and 39f show their location on the BARBEY propeller blade.

After installation, the gages were calibrated both electronically and by rotation of the propeller shaft with the jacking gear. Typical underway pressure data are shown in Figure 58. The predominant oscillary signal was static head rotation from TDC through 360 deg. Hydrodynamically induced pressures were superimposed on this. The mean pressure of the blade face and back versus shaft power is shown in Figure 68. Mean pressure at full-power (ahead) operation was about 3 psia on the blade back and 33 psia on the blade face. This gave a total pressure across the blade (ΔP) of approximately 30 psi at the 70-percent radius midchord location.

Both pressure gages were eventually lost, that on the blade back after about 12 hr of operation and the one on the blade face after 27 hr. It appears that both gages functioned well up to failure. The failure on both was by diaphragm implosion and was probably caused by transient, large bubble cavitation.* The information gained from this phase of the work was invaluable for the future development of gages for use in full-scale, underway measurements.

DISCUSSION

ANALYTICAL THEORIES AND FULL-SCALE TRIAL RESULTS

During the course of the investigation into the CPP crank disk failure on BARBEY, many different studies were conducted in order to maximize the accumulation of knowledge on the subject of load-stress behavior in CPP components. In addition to underway trials, these studies included stress calculations by several investigators, model studies, and full-scale component investigations. Most of this effort was directed toward the crank disk stresses since that was the component that suffered catastrophic failure. To a lesser extent, bolt stresses were also analyzed but very little

*Reported informally by M. Strasberg, (Cavitation Damage to Pressure Gages) in DTNSRDC Ship Acoustic Department Technical Memorandum TM-13-1901 in January 1977.

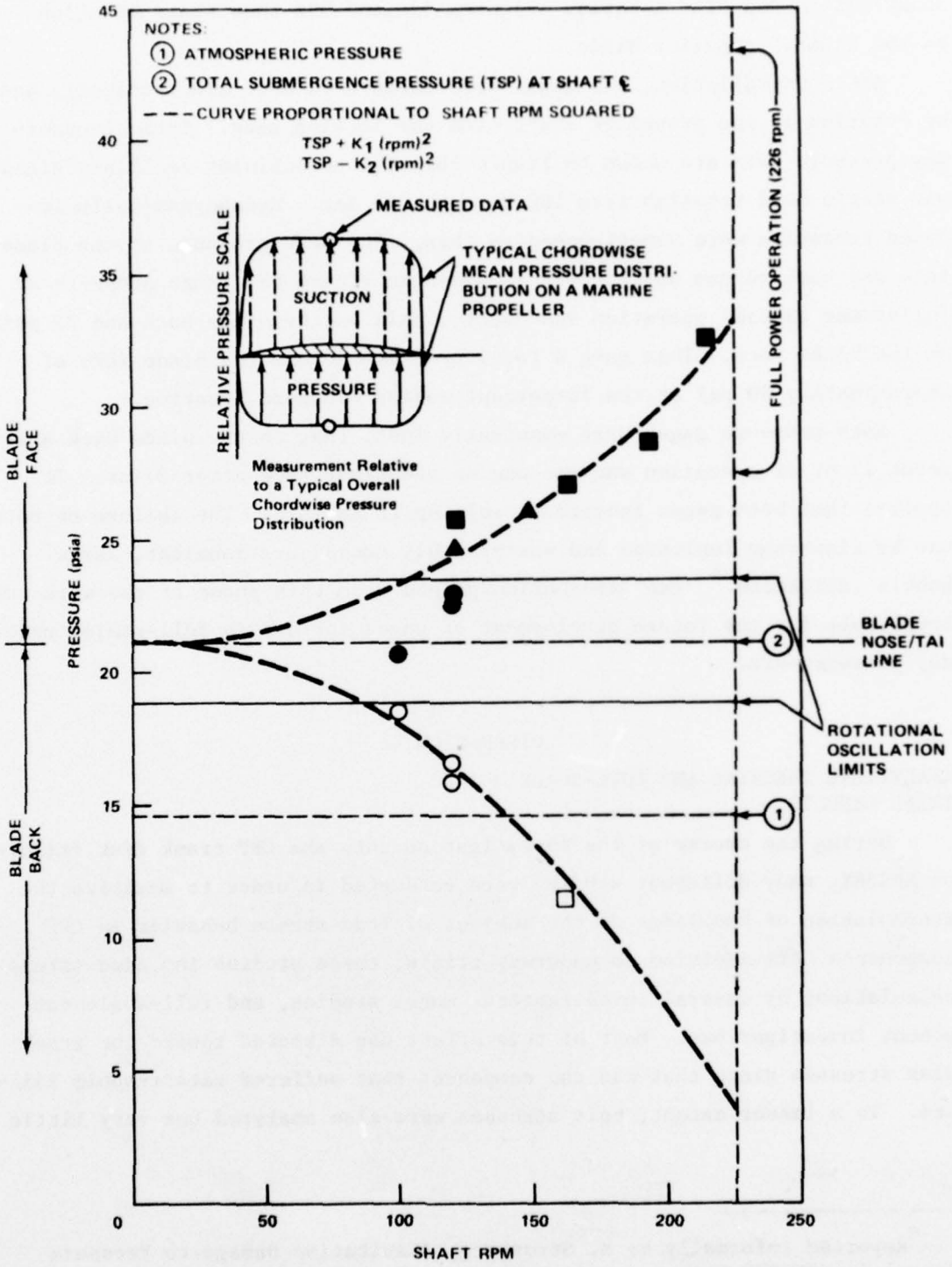

Figure 68 - Underway Mean Propeller Blade Pressure Measured on BARBEY

effort was placed on propeller blade stresses since there appeared to be no obvious deficiency in that area.

In attempting to relate the findings of some of these studies to the full-scale underway results, a rather cursory approach will be used since it is beyond the scope of this report to probe into the ramifications of the various investigations. The intent here is to highlight the results of the then existing capabilities and to compare them to one another and to the actual measured results.

Any comparison may be of a qualitative or quantitative nature or a combination of both. Input loads must be identical in order to properly compare results obtained by different methods for a load-stress relationship. In the event that the load parameters cannot be adequately reconciled, then only qualitative comparisons of the results can be made.

As previously mentioned, the underway trials with the instrumented propeller on BARBEY were conducted with a redesigned crank disk (and bolts). The crank disk changes are shown in Figure 14 and Table 4. The result of this redesign was to thicken the section between the bolt holes and the fillet, thereby reducing the stresses developed in the fillet area. Table 38 summarizes the results of calculations and full-scale measurements performed on the crank disk for either the original or new design. It should be noted that only the stresses due to action of the steady load on the propeller (thrust, torque, and centrifugal load) are shown for the calculated results of the condition designated "design full power ahead" in Table 38. The actual full power ahead condition includes a 20-percent allowance* for alternating thrust and torque loads. The crash astern and full power turns conditions do not contain any allowance for alternating loads.

In comparing the calculated and measured results, the actual full power ahead condition will be used as an example. The calculations assumed full power thrust, torque, and centrifugal force. In addition, a 20-percent factor was added to the thrust and torque to account for the

---

*This value represented the "best estimate" of percent alternating load prior to underway tests when calculations were done.

TABLE 38 - COMPARISON OF CALCULATED AND FULL-SCALE, UNDERWAY CRANK DISK FILLET STRESSES ON BARBEY

Assumptions Used for Calculations			Stress Predictions for Original Crank Disk Design, lb/m^2				New Crank Disk Design			
Load Condition	Blade Loading	Bending Moment Due to Thrust and Torque ft-lb[6]	Investigator A	Investigator B[2]	Investigator C[2]	Original Design Calculations[3]	Measured Full-Scale Stresses lb/in^2			Predicted by Intestigator[2] B lb/in^2
							Mean	Alternating	Peak	
Design Full Power Ahead (No Alt Load)	100% Thrust 100% Torque 100% F_C	220,500	52,000	48,000[1]	39,600[1]	21,920[1]	N/A	N/A	N/A	28,200
Actual Full Power Ahead (Includes 20% Alt. Loads)	120% Thrust 120% Torque 100% F_C	264,700	58,000	50,400	44,500	24,900	62,000[4]	±11,000[4]	73,000[4]	30,050
Crash Astern (No Alt Load)	Estimated Bending Moment Plus 100% F_C	378,750	72,000	59,300[1]	57,400[1]	32,515[1]	28,800[5]	±14,400[5]	43,200[5]	34,900
Full Power Turn (No Alt Load)	137% Thrust 127% Torque 100% F_C	297,850	62,000	53,400[1]	48,500[1]	27,190[1]	79,000[5]	±16,000[5]	95,000[5]	31,400

Notes:
[1] Stress calculated by using calculated stress levels for the actual full power ahead condition and proportioning them for different load conditions.
[2] Finite element analysis
[3] No stress concentrations factors considered
[4] 190 in pitch, 226 rpm (240 rpm = design full power)
[5] 190 in pitch, 200 rpm
[6] Bending Moment at crank disk

	Design Values	
	Per Ship	Per Blade
100% Thrust	273,000 lb	54,600 lb
100% Torque	766,000 ft-lb	153,200 ft lb
100% F_C (Centrifugal Force)		248,000 lb at 240 rpm

alternating load components. For the original crank disk design, the calculated stresses varied from a low of 24,900 psi to a high of 58,000 psi, greater than a 2:1 spread and well below the value of 73,000 psi which was subsequently measured on the considerably strengthened new crank disk. It would be expected that the original crank disk actually experienced much higher stresses than those measured on the new design. The only calculation of the new crank disk showed stresses that were less than one-half the measured values.

Obviously, this disparity between measured and calculated stresses is not fully accounted for in any differences that might exist between the assumed and actual input loads acting on the propeller. The steady state blade loading can be reasonably predicted within 10 percent. Therefore, the problem lies either in the path of the input load as it passes through the various components and/or in the mathematical modeling of the structure under analysis. In the case of the controllable pitch propeller, the load path through the components is much different and more complex than that assumed by conventional design approaches. This perhaps is the main reason for the gross underestimates of the crank disk stresses in the original design calculations and, to a lesser degree, the lower estimates of the other investigations as shown in Table 38. It should be emphasized that the underway stress measurements were made on a crank disk that was considerably strengthened over the original design and that some of the underway conditions, such as the full power levels, are less severe than those assumed in the calculations. In certain cases, therefore, the disparity is even greater than that indicated in Table 38.

The principal problem in predicting input loads acting on the propeller is determination of the alternating component rather than the mean or steady component, regardless of whether the load condition is for straight ahead operation or maneuvers. Not only was the alternating component of the load completely overlooked in the design stage for the original calculations, but it was underestimated by about 100 percent in subsequent analytical studies that attempted to diagnose the crank disk failure.

It is interesting to note that the crash astern maneuver was predicted to produce the greatest load on the propeller. Actually, the trials showed that the full power turns (performed at only 200 rpm) resulted in the greatest load.

In summary, it may be stated that the greatest weaknesses in predicting crank disk stresses appear to be (in order of importance):

1. Predicting the distribution of the input load throughout the CPP components, i.e., determining the path of the load between the propeller blade and the hub. Associated with this problem is the mathematical modeling of the various structural components in question (blade palm, bolts, crank disk, hub).

2. Predicting the alternating component of the input load acting on the propeller for any operating condition. This is especially important from the standpoint of fatigue.

3. Predicting the steady state input loads acting on the propeller for various operating conditions.

Obviously there is need to study these areas with proper emphasis on empirical interpretation of CPP system test results. Such an attempt is made in the following part of the discussion.

HEURISTIC INTERPRETATION OF FULL-SCALE TEST RESULTS

Existing CPP designs include a variety of pitch changing and blade attachment mechanisms. Because of its high power/volume ratio, hydraulic power is generally used in most designs to actuate the CPP pitch control mechanism. The hydraulics produce a translation in a piston in a cylinder which is converted to rotation (γ) via one of the elementary linkage mechanisms; see Table 39. The rotation around a radial axis varies the attitude of the blade sections to produce a pitch change for the propeller. Another important construction detail is the blade attachment. Generally there are two types, the trunnion and the collar (bolted) type.[33]

---

[33] Beek, G. and J. Heidemans, "Strength Considerations in Controllable Pitch Propeller Design," International Shipbuilding Progress, Vol. 23, No. 266 (23 Oct 1976).

TABLE 39 - SOME MECHANISMS USED IN CONTROLLABLE PITCH PROPELLERS[33]

Type	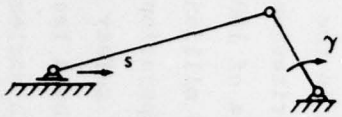		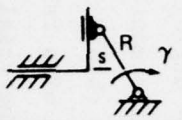	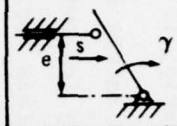	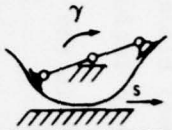
Realization		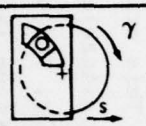	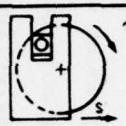	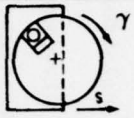	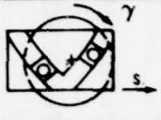
Name	Crank-Rod	Pin-Curved Slot	Crank-Slot	Pin-Slot	Cycloid

The experimental CPP test installation on BARBEY was a (double) crank-slot/collar blade design. In order to satisfy the project objectives, the BARBEY propeller system response was analyzed relative to requirements which were unique to BARBEY in addition to the more general design application which was pertinent to collar (bolted) blade type of CPP attachment. More explicitly, analyses were performed to include:

1. The operational needs for BARBEY in the immediate post-trial evaluation period.

2. Reconstruction of the first (propeller bolts) and second (crank disk) BARBEY failures and their relationship, if any, to other CPP designs.

The impact of the measured stresses on the operational needs was reported informally to NAVSEC immediately following completion of full-scale trials; only a brief summation of this topic will be included in this report. Basically, it was desirable during the trial (and the CPP operational evaluation period of about nine months thereafter) to avoid system failure while still being able to obtain realistic operating stresses. The rationale behind the selection of a failure criterion was developed (see Approach) and applied during the trial and the subsequent CPP operational/evaluation period. This criterion, Figure 69, was generally agreed to be the most readily applicable in the absence of a realistic operational profile. Essentially, the criterion was represented as a Soderberg diagram based on a fatigue life of 100 million cycles; it is conservative in some respects (e.g., 100 million cycles represents approximately 300 days continuous, full-power operation) whereas in other respects it is not (e.g., there are no factors of safety applied to any of the criteria; normal design practice would employ a factor of at least 2 for structural design of such complexity with unclearly defined forcing functions, and saltwater intrusion was not considered). It can be seen in Figure 69 that several maneuvers were "unacceptable" from the standpoint of propeller blade bolt and crank disk stresses. As a result, BARBEY was

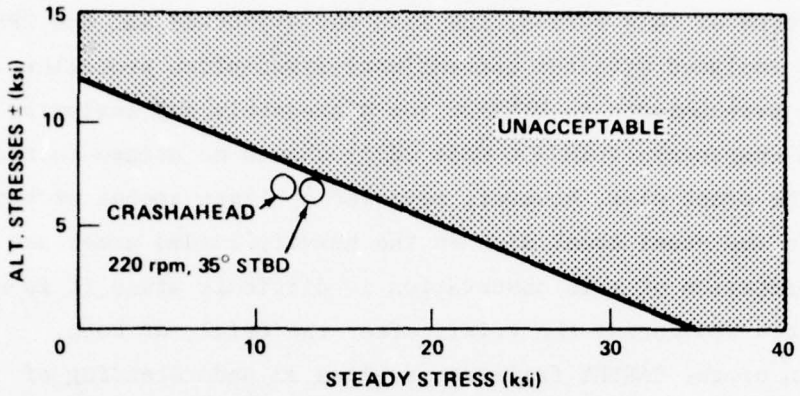

Figure 69a - Propeller Blades (Ni-Al-Bronze)

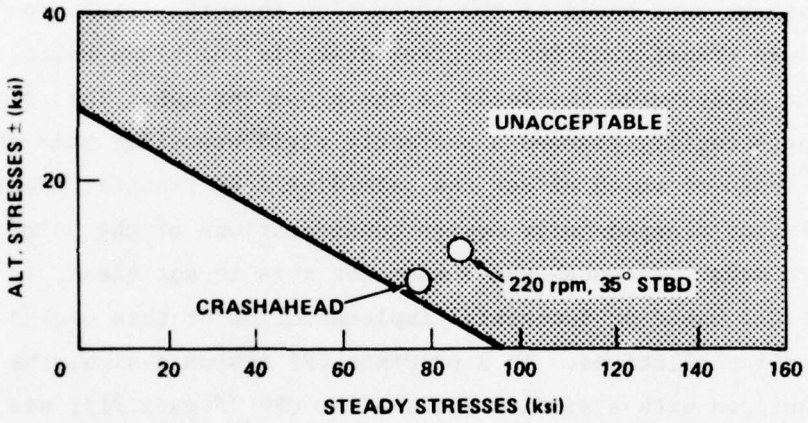

Figure 69b - Propeller Bolts (17-4 Ph)

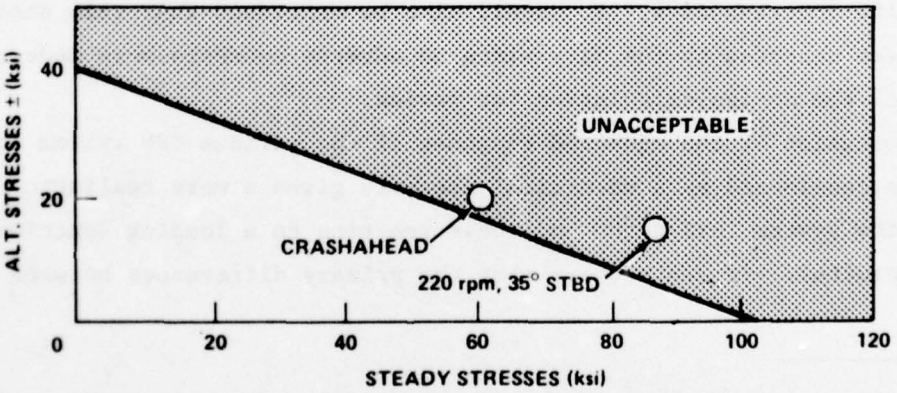

Figure 69c - Crank Disks (HY-100)

Figure 69 - General CPP Stresses versus Limits for Propeller Blades, Bolts, and Crank Disks for BARBEY Trials

placed on restricted operation* for the remainder of the CPP evaluation period. On completion of this period, the ship was drydocked and the CPP system removed and replaced with the conventional fixed-pitch propeller. The CPP components were shipped to DTNSRDC for disassembly and analysis. Examination of the components (DTNSRDC Code 2832) showed no damage to the blade or bolts. The crank disk, however, revealed a slight amount of bronze (HUB) transfer onto the steel crank disk in the heavily loaded area; see Figure 70. Interpretation of this observation is difficult since it is not known whether it occurred during the trial, after the trial, or both.

Reconstruction of the BARBEY failures requires an understanding of the mechanics of a bolted blade (joint design) CPP attachment. The original design calculations were based on the assumption that the total propeller blade load was transferred to the crank disk via the blade bolts. The crank disk then distributed the loads to the propeller hub. This concept of the load path tacitly assumed a perfectly rigid propeller palm and no bolt preload,** both of which affect the palm/disk load transfer characteristics. That is, no clamped-joint design considerations of the palm/disk interface were made. Although the reason for this is not clear, it is assumed that it was based on successful implementation of this design philosophy in other installations. In a previous CPP system design, the PG-84 class was equipped with a similar but smaller CPP (Figure 71); see Introduction. This class has never experienced any problems associated with the bolts or crank disk. It should also be mentioned that this design philosophy was accepted by the Navy since no adverse comments were made on submission of the design calculation for review.

An examination of the measured response of the various CPP system components when considered as a mechanical assembly gives a more realistic picture of the system load paths and their reaction to a loading function (see Test Results). It can be seen that the primary differences between

---

*NAVSEC message 011855Z May 1975.

**Even though it was not explicitly called for in the design, the propeller blade bolts were "slugged up" (see Introduction) during installation. This resulted in an unknown amount of random preload.

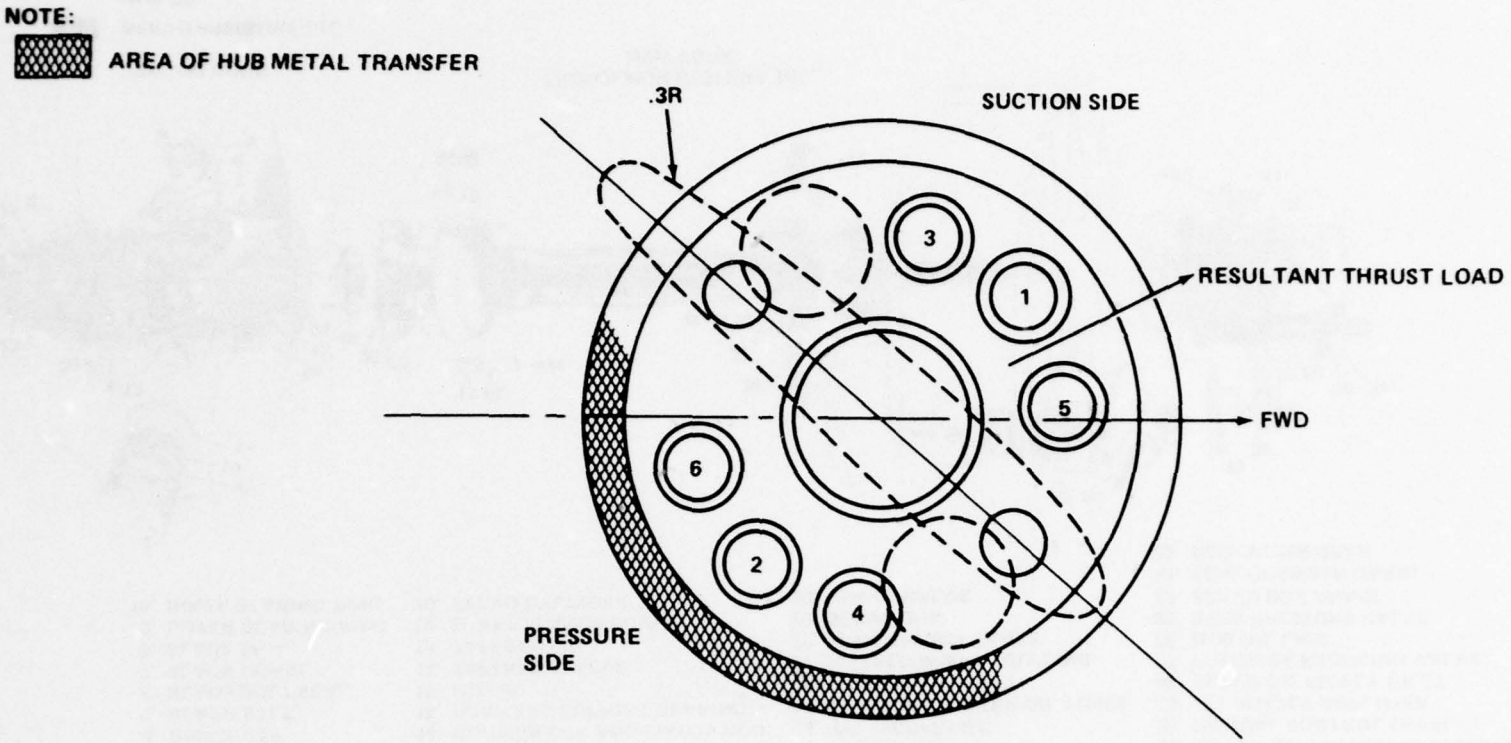

Figure 70 - BARBEY Crank Disk after CPP Evaluation Period
(Note approximate area of metal transfer)

1. PROPELLER HUB
2. PROPELLER BLADE
3. FAIRING CAP
4. DUNCE CAP
5. BLADE BOLT
6. BLADE BOLT SEAL
7. BLADE DOWEL
8. BLADE SEAL
9. OUTER BEARING RING
10. INNER BEARING RING
11. CRANK DISK
12. SLIPPER
13. ACTUATOR
14. GUIDE BLOCK AND PISTON ROD
15. FORWARD SUPPORT BEARING
16. HUB BOLT
17. TAPERED SLEEVE
18. TAPERED PIN
19. SHAFT FLANGE COVER
20. SERVO CYLINDER
21. SERVO PISTON
22. AFT SUPPORT BEARING
23. PURGE ROD
24. TELESCOPE PIPE
25. INNER AND OUTER OIL TUBES
26. PROPELLER SHAFT
27. SPLINED SHAFT COUPLING
28. SPLIT THRUST PLATE
29. SERVO BOX
30. SERVO VALVE
31. FOLLOW-UP SPOOL
32. SERVO FOLLOW-UP LINKAGE
33. AMPLIFIER FOLLOW-UP LINKAGE
34. MANUAL CONTROL LEVEL
35. JET NOZZLE AMPLIFIER
36. SERVO OIL SUPPLY INLET
37. PRESSURE REDUCING VALVE
38. HUB OIL LINE
39. BACK PRESSURE VALVE
40. SERVO BOX DRAIN
41. SEAL CHAMBER DRAIN
42. REDUCTION GEAR

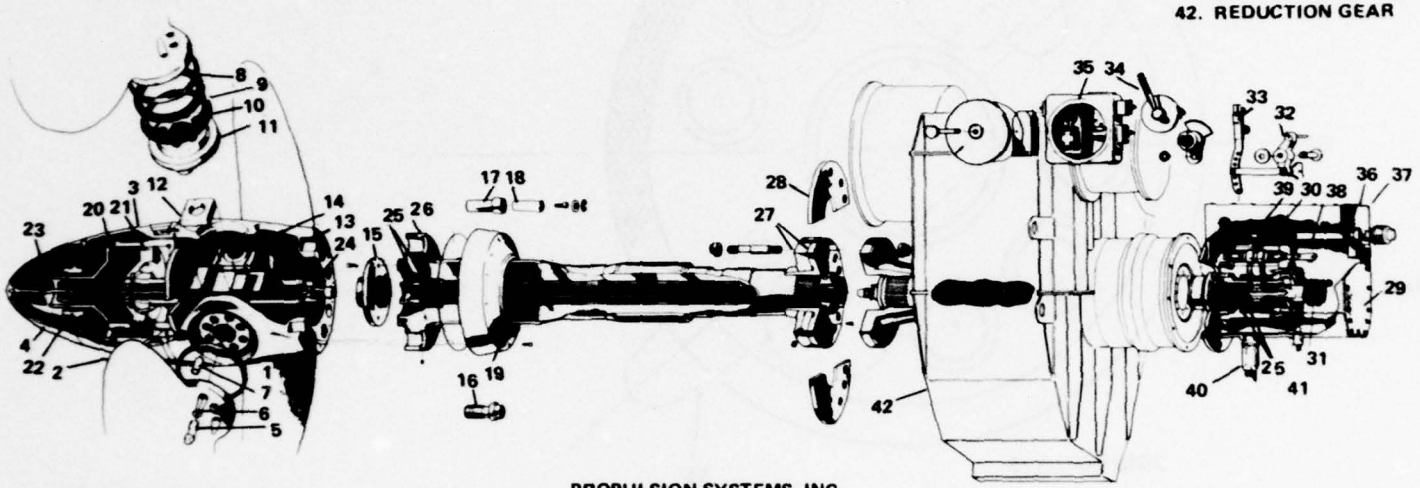

PROPULSION SYSTEMS, INC.
NEW YORK

COLOR CODE

SERVO PRESSURE OIL
HUB OIL
EXHAUST OIL

Figure 71 - Controllable Pitch Propeller on PG-84 Class

the assumed and actual load paths occur in the distribution of the blade loads carried by the propeller palm and in the joint interface (palm/disk) Although they are interrelated, for purposes of discussion these will be considered as two separate and distinct structural characteristics of the palm, bolt, and crank disk assembly. One involves an axial stiffness, the other flexural stiffness. It will be seen that both can, and in the case of BARBEY do, adversely affect the bolt loading characteristics.

The first of these, the load transfer across the bolted palm/disk interface (joint), deviates considerably from design assumptions. Bolt load is related to joint deflection via the interfacing spring characteristics. In most design applications, the interface is modeled as two series springs (axial compressive stiffnesses of the joined surfaces) in parallel with the clamping spring (bolt); see Figure 72. The relationships between the external load F_E, the bolt load F_B, and the preload F_P for an idealized bolted joint are shown in Figure 73. It can be seen that as long as the joined surfaces remain in contact, the amount of the external load as seen by the bolt can be controlled by the ratio of the bolt to joint stiffness (K_B/K_J). This idealized model neglects certain realities such as geometric irregularities (which induce bending loads into the bolt) and system nonlinearities. Laboratory tests by DTNSRDC Code 2814, on a full scale mockup of the BARBEY palm/disk assembly (Appendix C) show that, in reality, the jointed surface exhibits certain nonlinear characteristics which complicate the analysis (Figure 74). Analysis of this test set-up gives some insight into the interpretation of the full-scale test results. Characterisically for each bolt preload value, the bolt load/strain curves (Figure 74) exhibit a quasi-linear range; then, after passing through a nonlinear "knuckle," they eventually align with the linear bolt response (stiffness) curve. Since the assembled materials were Hookian and the applied load was linear, it is conjectured that the nonlinearity was generated as the plates separated.

Consider, for example, the system shown in Figure 75. Here, two plates are clamped together with a bolt which has been prestressed with

NOTE:

COMPONENT	MODULUS
BOLT	E_B
PLATE 1	E_1
PLATE 2	E_2

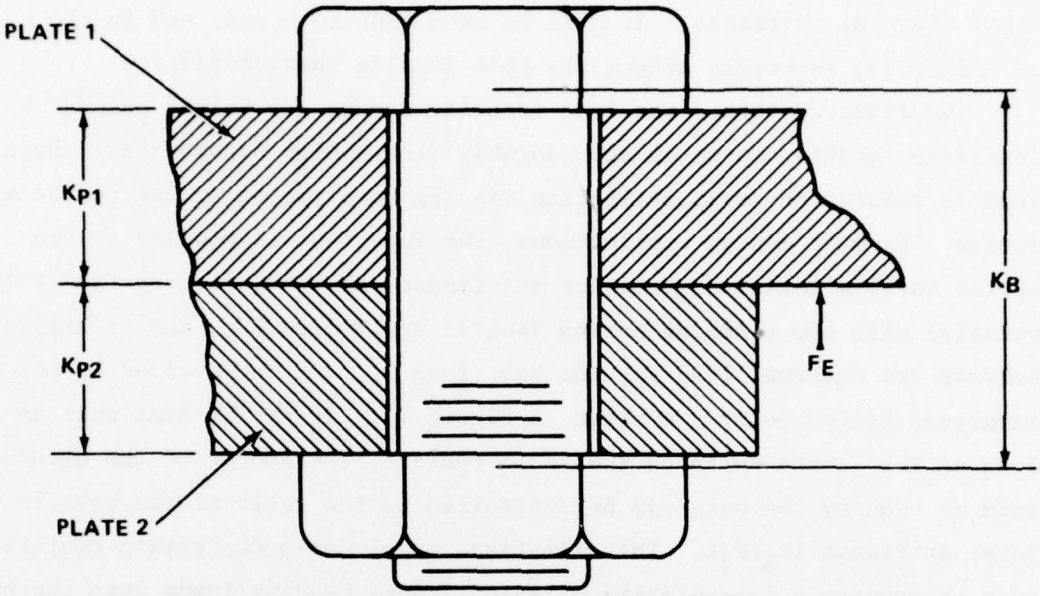

Figure 72a - Typical Bolted Joint

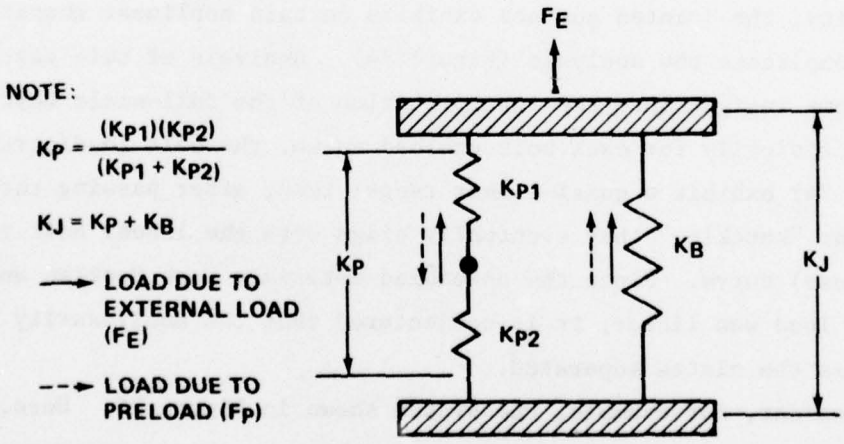

Figure 72b - Analog Model

Figure 72 - Bolted Joint Characteristics

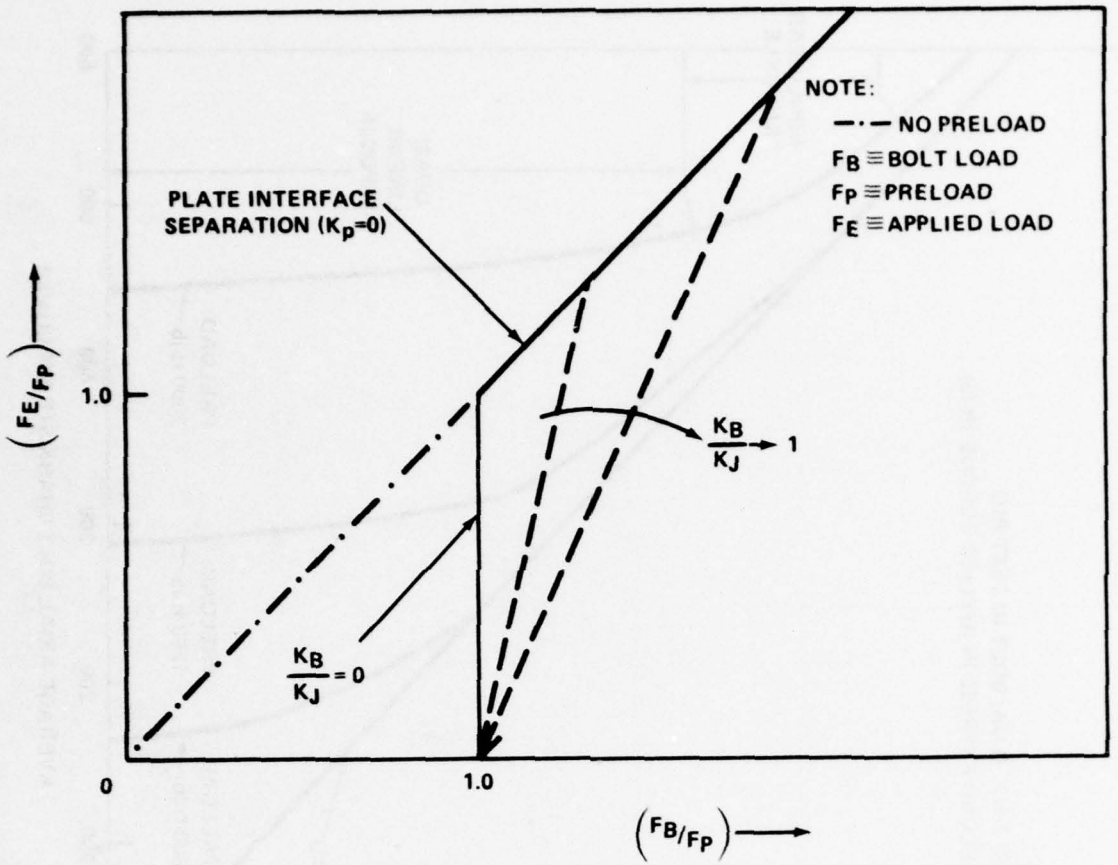

Figure 73 - Idealized Load Relationship for a Bolted Joint

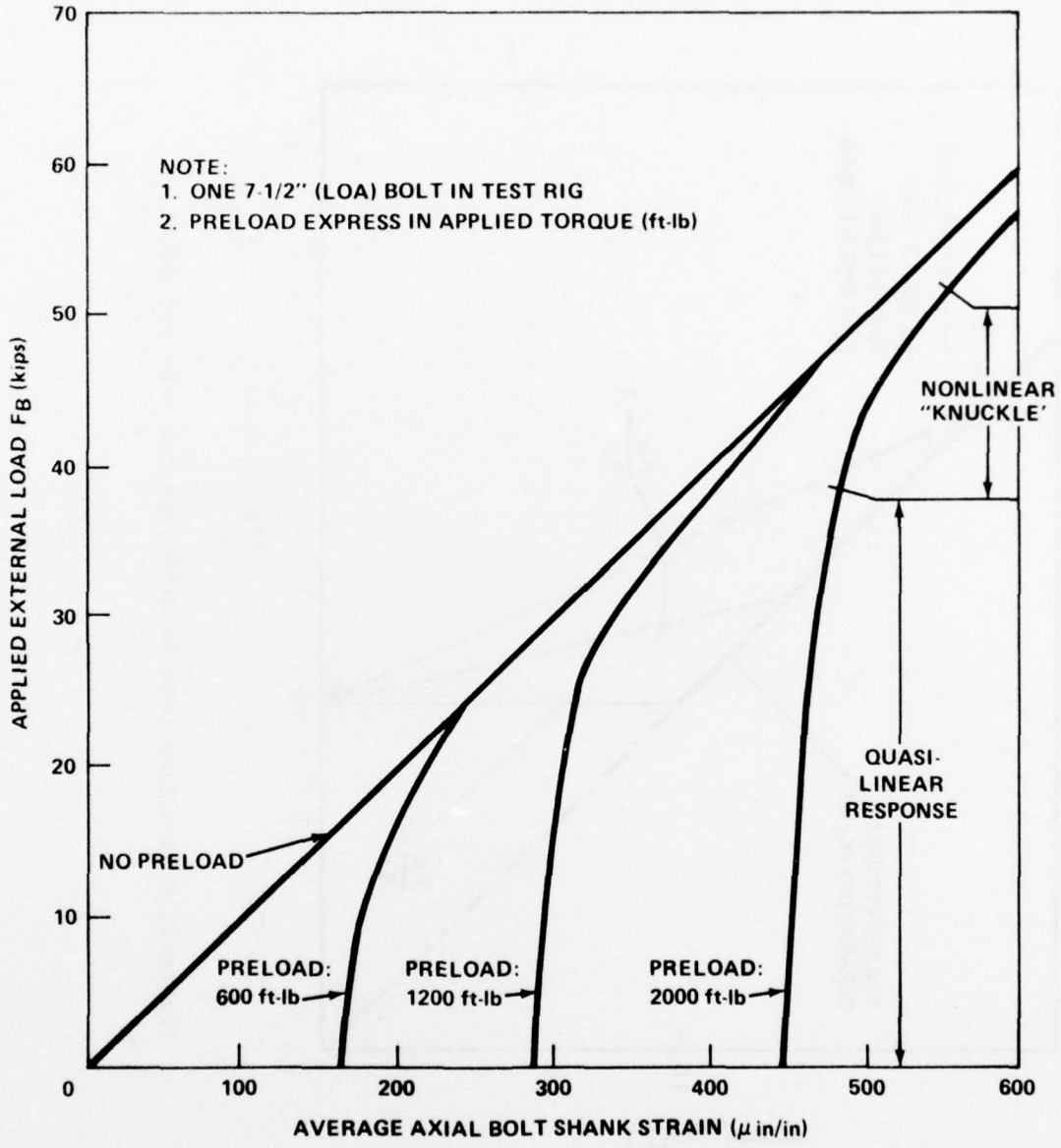

Figure 74 - Bolt Response versus External Load for Various Preloads on Laboratory Mockup of BARBEY Palm/Crank Disk

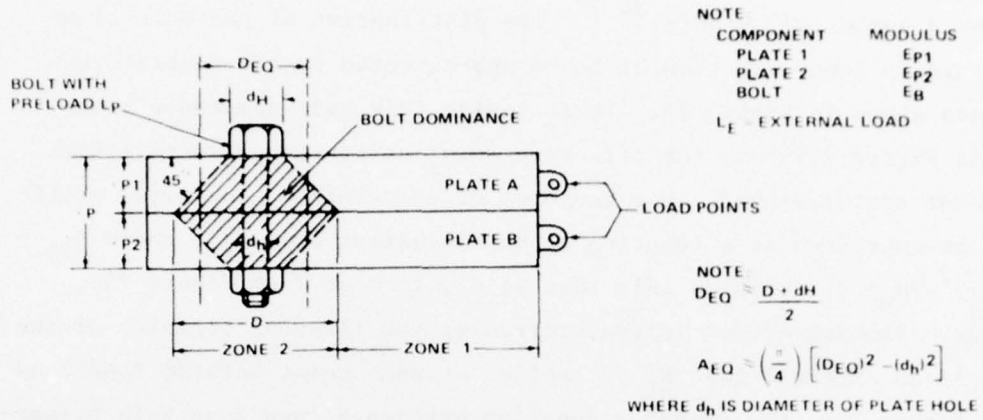

Figure 75a - Clamped Plates with No External Load

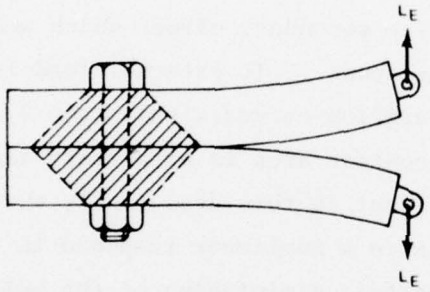

Figure 75b - External Load Causing Plate Separation in Zone 1
(Quasi-linear bolt response)

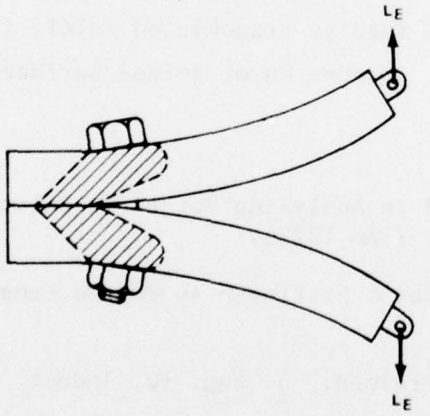

Figure 75c - External Load Causing Plate Separation in Zones 1 and 2
(Nonlinear bolt response)

Figure 75 - Joint Unloading Mechanisms

preload F_P. The determination of an effective joint stiffness K_J has been studied by a number of authors.[34-39] The distribution of the bolt clamping pressure is generally thought to be approximated by the double truncated cones shown in Figure 75. It is inside this bolt dominance zone (Zone 2 in Figure 75) that the effective axial stiffness characteristics of the joint are developed. For purposes of calculation, the axial stiffness can be expressed as a function of an equivalent area A_{EQ}, where $A_{EQ} = (\pi/4[(D_{EQ})^2-(d_h)^2]$. Outside this zone (i.e., in Zone 1 of Figure 75), the primary clamping effect is transferred by the flexural rigidity of the plates. If an external load F_E is applied at some point outside Zone 2 as shown in Figure 75b, the transfer function between F_E and Zone 2 is primarily the flexural rigidity of the plates. Plate separation (changing contact surface area in Zone 1) has only a secondary effect which would tend to quasi-linearize the overall bolt response. If external load is increased to the point where plate separation occurs within Zone 2, Figure 75c, then the change (reduction) in contact area is of primary significance. Since the axial stiffness is proportional to this area (A_{EQ}), the change in the equivalent area with load results in a nonlinear response in the bolt ("knuckle" in Figure 74). After a certain diminishing of the bolt dominance zone, a relatively small increase in external load causes complete plate separation. At this point all load is transmitted solely through the bolt (whose response is linear). Operation of joined surfaces in the

---

[34] Meyer, G., "Simple Diagrams Aid in Analyzing Forces in Bolted Joints," Assembly Engineering, Vol. 15, No. 1 (Jan 1972).

[35] Motosh, N., "Determination of Joint Stiffness in Bolted Connections," J. Eng. for Indust. (Aug 1976).

[36] Fazekas, G., "On Optimal Bolt Preload," J. Eng. for Indust. (Aug 1976).

[37] Thompson, J. et al., "The Interface Boundary Conditions for Bolted Flanged Connections," J. Pressure Vessel Technol. (Nov 1976).

[38] Landt, R., "Criteria for Evaluating Bolt Head Design," J. Eng. for Indust. (Nov 1976).

[39] Faires, V., "Design of Machine Elements," Collier-MacMillan Canada, Ltd (1965).

nonlinear or liftoff portions of the response curve is counterproductive to any goals which are aimed at minimizing fatigue since there is a gross change in the joint transmission characteristics and a much higher percentage of the external load is transmitted through the bolt. Therefore, in an actual installation, bolt loads should be constrained to the quasi-linear region in order to minimize the effects of fatigue. It can be seen, Figure 74, that increasing bolt preload extends this region.

Another, more subtle mechanism which degenerates the force transmission characteristics of the joint involves discontinuties in the palm/crank disk joint interface. As previously mentioned, the joint transmission characteristics (stiffnesses) are developed over a preferential stress distribution pattern (bolt dominance zone); Figures 75 and 76. If the physical geometry of the joint interrupts this pattern with a boundary discontinuity, then the joint will not have the same stiffness ratios as that of a fully developed joint. Since the plate stiffnesses are assumed to be proportional to the equivalent area (A_{EQ}), any reduction in A_{EQ} by the boundary constraints will proportionally reduce these stiffnesses (K_p). This will have the effect of increasing* the external load transmitted through the bolts. Another design consideration related to this aspect of the problem is the fact that the preload stress distribution patterns result in overlapping bearing areas (Figure 76). This creates a double loaded interface between the bolt holes and a resulting tendency for the bolt to bend toward these areas. Since bending affects fatigue life of the assembly, it should be avoided. The considerable bending noted during bolt installation induced a maximum bolt stress of approximately 65 ksi; see Table 13. The bending axis strongly suggests a preference to bend toward the double bearing holes; see Figure 45. As mentioned earlier (see Pretrial Drydock Test) a certain relationship between induced bending and assembly geometry has been determined. However, despite geometric modifications, bolt bending still exists.[40]

---

*That is, more external force would be transmitted through the bolts than would be calculated if this mechanism is neglected.

[40]Antonides, G. et al., "Full-Scale Underway CPP Propeller Stress Trials on the USS SPRUANCE (DD-963)," DTNSRDC Evaluation Report SAD-164E-1962 (Jan 1977).

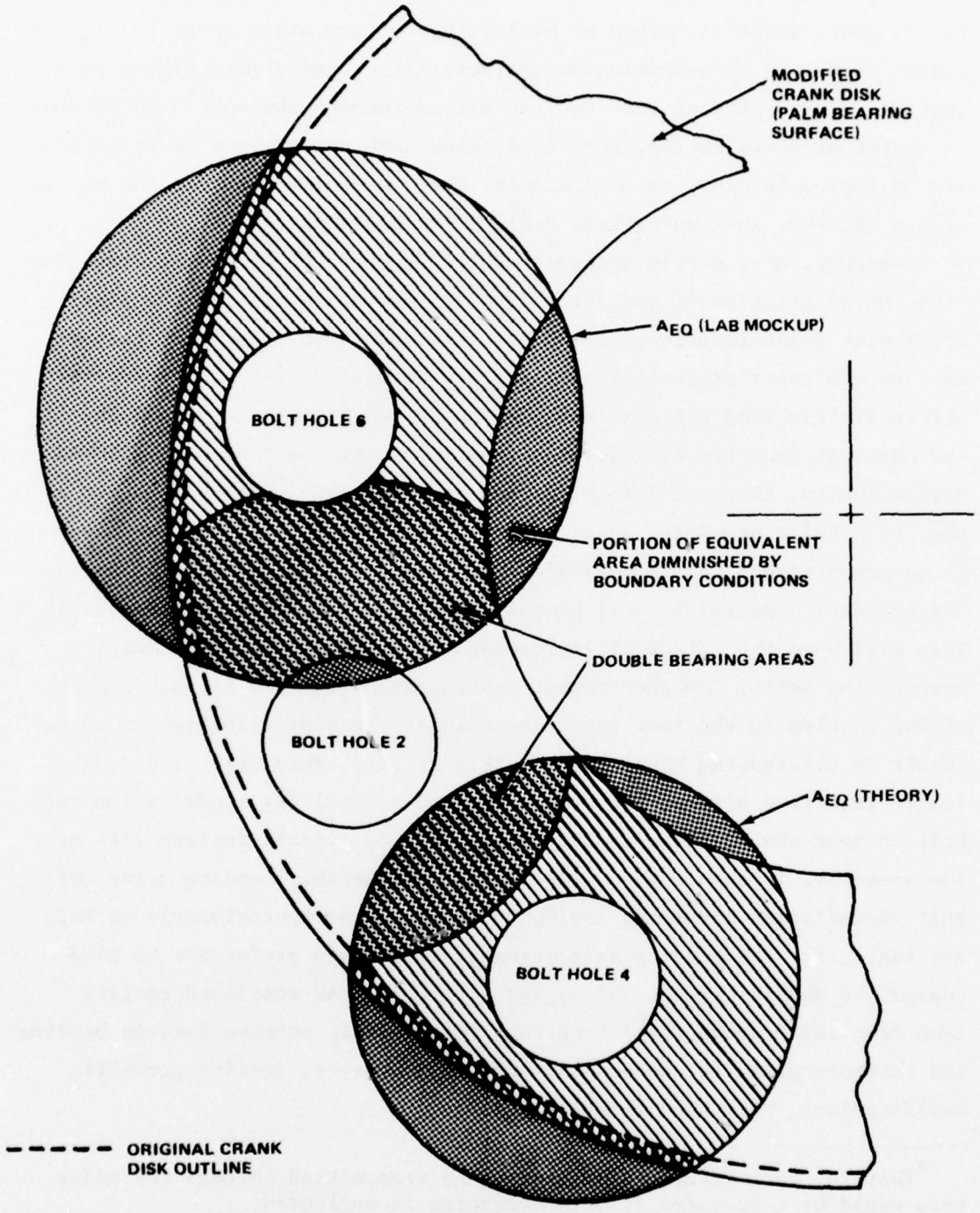

Figure 76 - Calculated and Actual Equivalent Areas on BARBEY CPP Palm/Crank Disk Interface

The laboratory mockup of the palm/crank disk was geometrically generous, allowing unconstrained stress distribution patterns. Load/stress data from the laboratory test were used to determine values of the equivalent joint areas and the joint interface stiffness. In addition, a similar set of joint area and stiffness values was developed by using joint theory.[41] These values are compared in Table 40. It can be seen that the ratio of theory to experiment is approximately 0.5. The reason for this discrepancy is not obvious; however, it must be pointed out that the theory is only approximate. Since the actual values of joint areas and stiffnesses for the BARBEY CPP installation are not known, it will be assumed that the values shown in Table 40 represent an upper and lower boundary on the actural values. The effect of CPP system component geometry on joint area and stiffness is shown graphically in Figure 76.

The differences between calculated and actual A_{EQ}'s are tabulated in Table 41. Again, it is impossible to quantify the exact effect on joint stiffnesses of limiting A_{EQ} by boundary constraints. It is felt that a reasonable lower limit* would be that established by the radius from the bolt hole centerline to the nearest constraint (R_{min}) minus the thread radius (r_{min}); see Figure 77. The upper limit is the calculated area less the area diminished by the boundaries (Figure 76). The importance of neglecting this effect is appreciated when a typical example is considered. For instance, if the bolt loads were calculated by using the characteristics developed in the laboratory mockup and applied to the original crank disk installation, the error would be between approximately 50 and 600 percent. That is, instead of the bolt experiencing 8.7 percent of the external load, the value would be between 13 and 63 percent. It is also estimated that the loads in the bolts of the original crank disk design were approximately 10 to 85 percent higher than those of the modified (measured) crank disk

---

*Justification of the choice of lower limit is based on the observation that the crank disk fatigue damage occurred in the thin wall, Figures 12 and 77. This suggests that the bolt/interface load transmission ratio could be controlled by an equivalent area which was dominated by this dimension.

[41]Stephenson, J. and R. Callander, "Engineering Design," J. Wiley & Sons, New York (1974).

TABLE 40 - SUMMARY OF BARBEY PALM/BOLT/CRANK DISK INTERFACE CHARACTERISTICS

Parameter	Value[1]	
	Mockup[2]	Calculated[3]
Bolt Stiffness K_B		
7-1/2 in. (LOA)	22	–
8-1/2 in. (LOA)	21[4]	–
Joint Stiffness K_J	250	163
Plate Stiffness K_p	228	142
Palm Stiffness K_{p1}	360	241
Crank Disk Stiffness K_{p2}	641	343
Equivalent Lengths:		
Bolt 1_B 7-1/2 in. (LOA)	4.6	–
8-1/2 in. (LOA)	4.8[4]	–
Palm 1_{p1}	2-5/16	–
Crank Disk 1_{p2}		
7-1/2 in. (LOA)	2.0[5]	–
8-1/2 in. (LOA)	2.4[4]	–
Equivalent Area A_{EQ}	45	30
Equivalent Diameter D_{EQ}	8.0	6.7

Notes: (1) Stiffness values in lb/in x 10^{-6}; length in inches; area in (inches)^2
(2) All values determined from palm/crank disk mockup unless otherwise noted.
(3) Calculated areas assume no boundary constraints.
(4) Determined from full-scale installation data.
(5) This value was physically limited by the laboratory test rig to approximately 2.0 in.

TABLE 41 - EFFECT OF BOUNDARY CONSTRAINTS ON CALCULATED EQUIVALENT AREA A_{EQ} OF THE BARBEY CPP PALM/CRANK DISK INTERFACE
(L and U Respectively Designate Lower and Upper Bounds on A_{EQ})

Equivalent Area	Area (in^2)					Percent Act/Cal			
	Calc.	Actual							
		Orig		Mod		Orig		Mod	
		L	U	L	U	L	U	L	U
(A_{EQ}) Mockup	45	2.5	28	8.6	30	6	62	19	66
(A_{EQ}) Theory	30	2.5	20	8.6	21	8	65	29	70

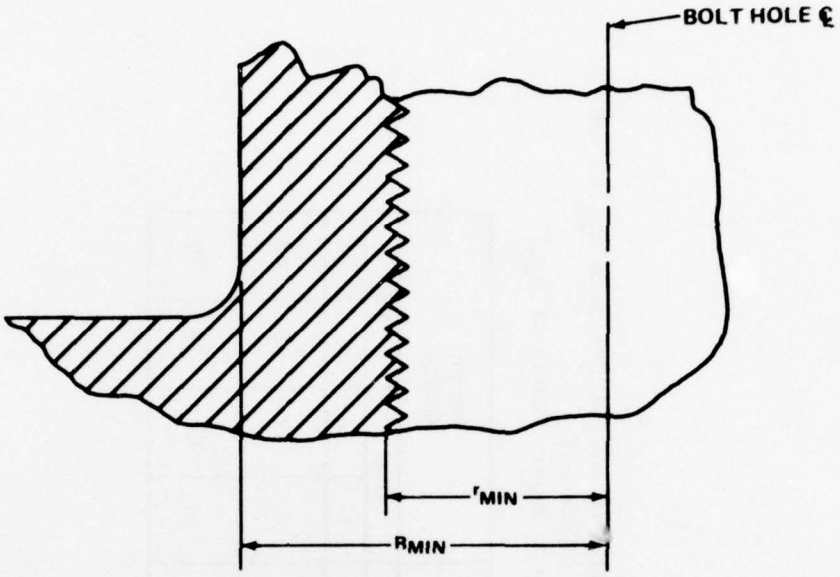

Figure 77b - Modified Crank Disk

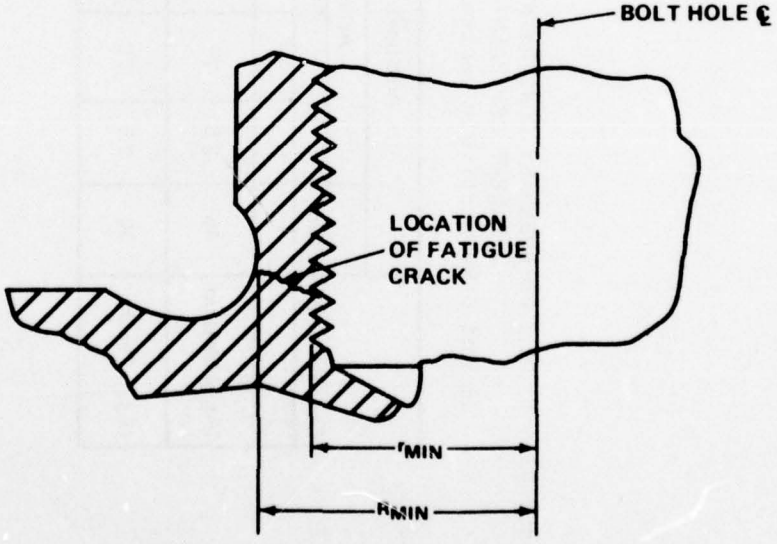

Figure 77a - Original Crank Disk

Figure 77 - Dimensions for Establishing Lower Limits on the Equivalent Area (A_{EQ}) of Crank Disk Interfaces

just considering the effect of A_{EQ} above. The significance of this latter observation will be discussed later.

It is apparent, then, that the interface does not lend itself to simplistic analysis. It has been shown that its characteristics can be grossly affected by load and geometry. The interdependence of the various parts was or can be demonstrated in a study involving a change in bolt length. A cursory analysis might lead one to believe that bolt loads could be reduced by increasing bolt length l_b, thereby producing a lower bolt stiffness. This can be done either by increasing the palm thickness l_{p1}, by increasing the bolt thread reach into the crank disk l_{p2}, or by increasing both l_{p1} and l_{p2} simultaneously.

A more detailed analysis which includes the interfacing characteristics K_p shows (Figure 78) that by increasing l_B, the results at best would be marginal* and then only if the correct parameter variation was made. The same result could be achieved by reducing l_B by one inch at the head (Figure 9a). Obviously, any reduction in l_{p1} would have to be accompanied by a strength analysis. It can be seen that increasing l_B by increasing l_{p1} and l_{p2} has almost no effect (Figure 78). In light of the fact that increasing l_B to reduce $F_{B(EXT)}$ is marginal and that decreasing it for the same reason is probably impractical, one could logically conclude from this study that some other method of reducing $F_{B(EXT)}$ should be considered. It should be noted that this study included only one of the important structural characteristics of the palm (the bolt/interface stiffness) and therefore would not be adequate for a detailed design analysis.

The second structural characteristic which deviates considerably from design assumptions is the nonuniform bolt load distribution of the propeller loads caused by the blade palm geometry (Figures 60 and 61). The mechanism controlling this distribution appears to be the variable flexural rigidity of the blade palm. That is, the palm cannot be considered to be uniformly, much less infinitely, rigid in bending. Conceptually, this can be demonstrated if the palm is modeled as shown in Figure 79. In this figure the

---

*Approximately 5-percent reduction in $F_{B(EXT)}$ for l_b of 2 in., which is approximately an 80-percent increase in l_{p2} (Figure 77b).

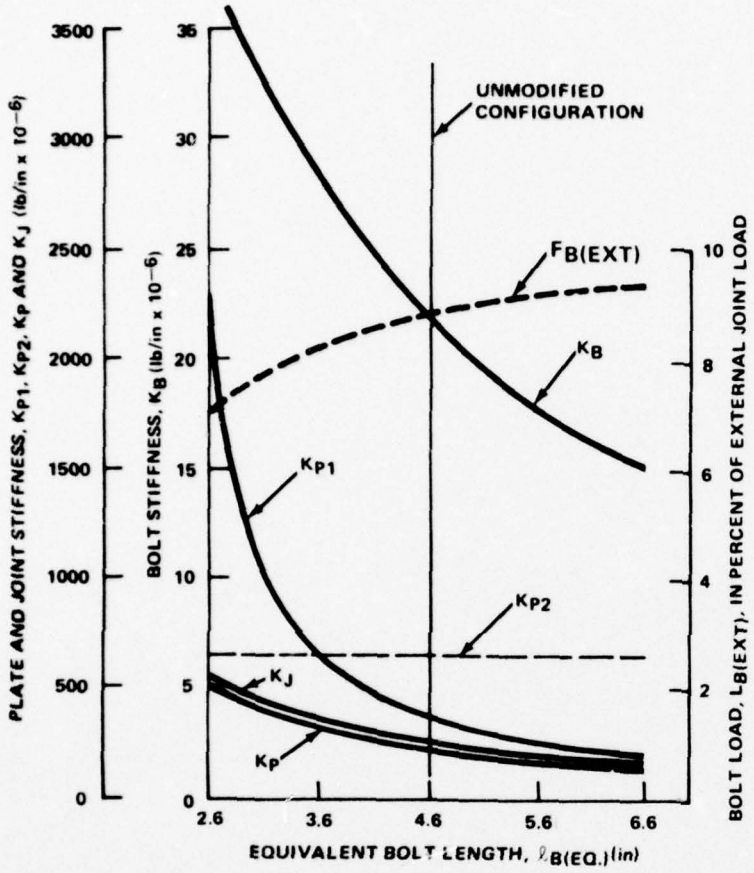

Figure 78a - Varing $\ell_{B(EQ)}$ by Changing ℓ_{P1}

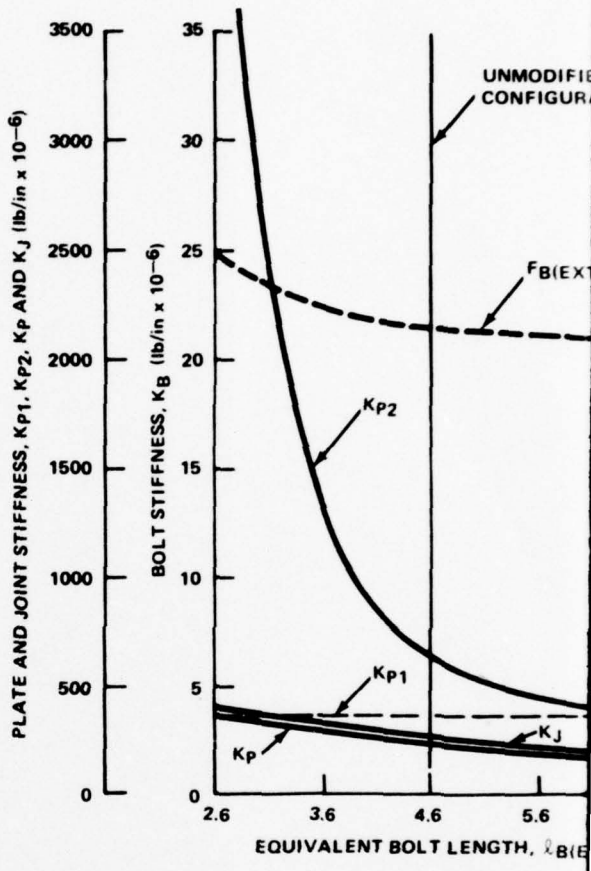

Figure 78b - Varing $\ell_{B(EQ)}$ by Chang

Figure 78 - Effects of Changing Bolt Length (ℓ_B)
Disk Interface Transmission Character

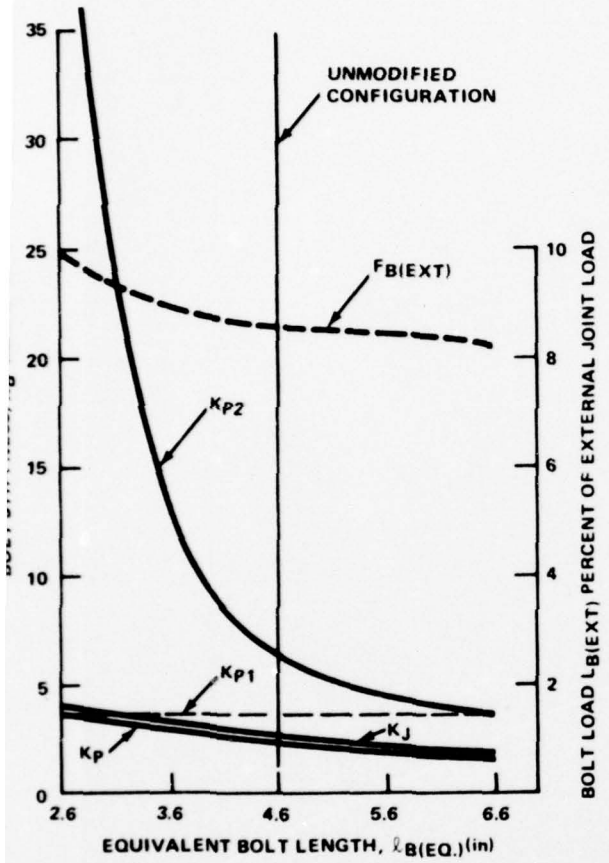

e 78b - Varing $\ell_{B(EQ)}$ by Changing ℓ_{P2}

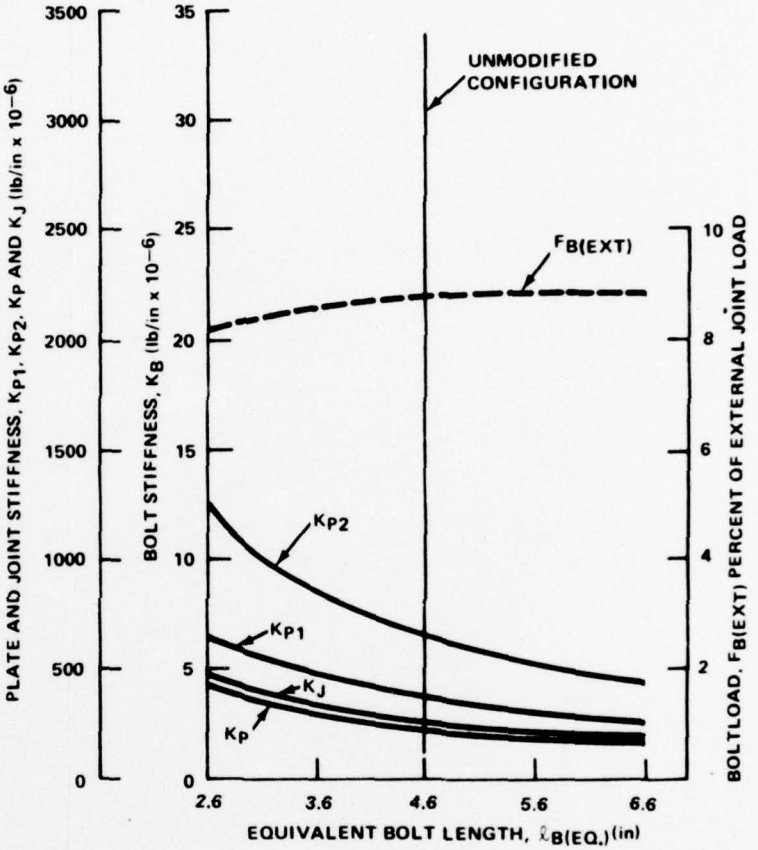

Figure 78c - Varing $\ell_{B(EQ)}$ by Changing ℓ_{P1} and ℓ_{P2} Equally

of Changing Bolt Length (ℓ_B) on BARBEY Palm/Crank
erface Transmission Characteristics

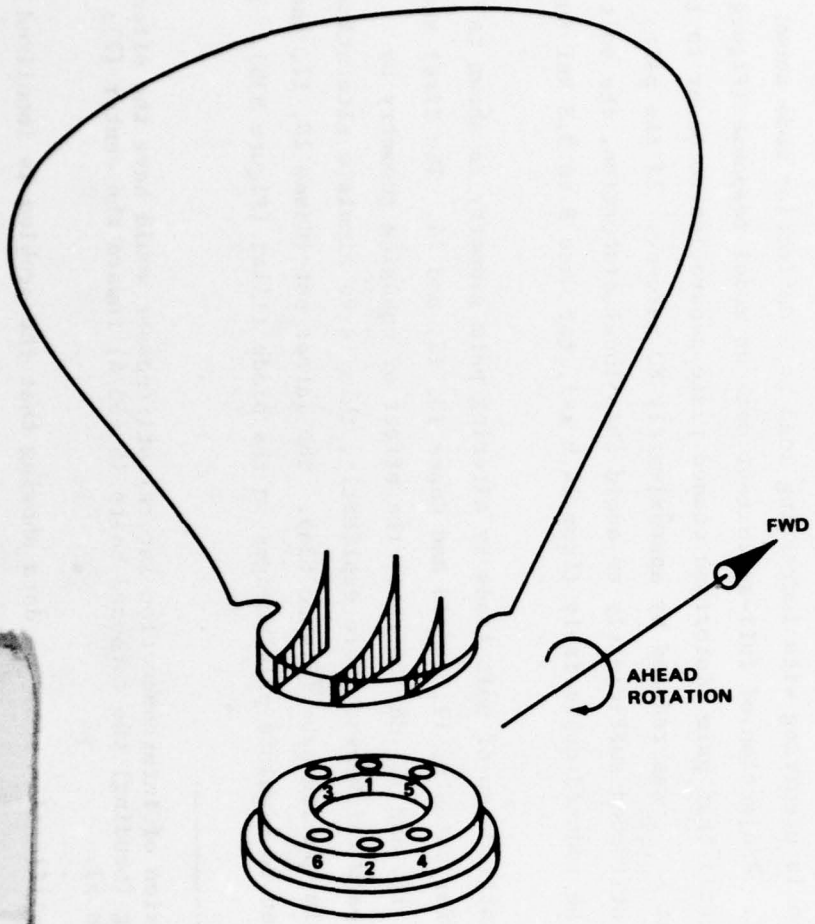

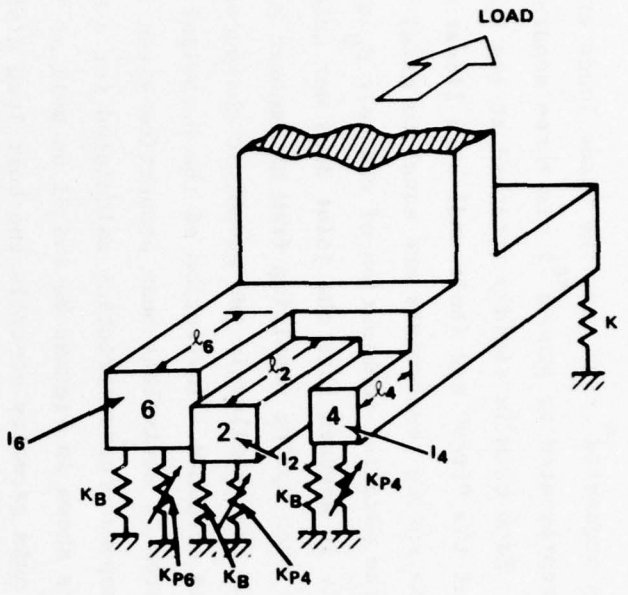

Figure 79 - Relative Palm Thickness at Bolt Hole Locations and Simplified Structural Model

palm has been segmented* such that the blade loads are transferred to the crank disk (represented as ground**) via three separate rectangular cantilever beams. Each beam is rigidly attached at its base (blade end) and constrained at the "free" end (bolt end) by a linear spring. Stiffness values for the spring constraints are equal to axial joint stiffness K_J, where K_J is the parallel combination of the bolt K_B and plate K_p stiffnesses. If it is assumed that the joint does not unload ($K_p > 0$), the deflection δ of each spring resulting from an imposed blade load is a function of K_J and the metallurgic and geometric characteristics of the beam to which it is attached. Inspection of the propeller blade geometry leads to the estimates of equivalent beam properties given in Table 42.

Model response characteristics calculated for a number of parametric variations are shown in Figures 80 and 81 as well as in Table 42. It can be seen that palm geometry controls the bolt load distribution. Interface separation in the vicinity of Bolt 6 ($K_p = 0$) grossly affected the transmission of loads through the interface. Here it is assumed that plate separation is occurring with increasing load in a deflection mode shown in Figure 82. Projection of full-scale test data on model response (Figure 80) indicates that palm distortion caused plate separation to occur to the point that $K_{p(6)}$ was reduced by approximately 80 percent. If the palm could be stiffened sufficiently to avoid this local distortion, the bolt load can be reduced appreciably (from 14.9 ksi, for Case 8 to 3.8 ksi for Case 3).

Redistribution of bolt loads by altering palm geometry is shown in Table 42 for Cases 9, 11, and 13 and Cases 10, 12, and 14. The first set (Cases 9, 11, and 13) demonstrates the effect of changing geometry by altering palm thickness. More explicitly, this is to simulate alterations of the palm via its base (Figure 83a). The latter set (Cases 10, 12, and 14) is used to simulate palm changes in the blade fillet (Figure 83b). It

---

*Inclusion of interconnection lateral stiffnesses would have the effect of rolling (bending) the outboard bolts (6 and 4) toward the center (2); see Figure 53.

**A simplification based on data showing that the problem is localized to the interface.

TABLE 42 - BARBEY PALM PARAMETER VARIATION

Case No.	k_p lb/in x 10^{-6}			ℓEI in			Modulus psi x 10^{-6}	I in^4			Bolt Stress ksi		
	6	2	4	6	2	4	E	6	2	4	6	2	4
1	250	250	250	2.5	3.5	2.2	18.0	49.0	30.9	19.4	3.1	1.3	2.4
2	–	–	–	–	–	–	30.0	–	–	–	3.0	1.4	2.4
3	200	200	200	–	–	–	–	–	–	–	3.8	1.6	2.9
4	100	100	100	–	–	–	–	–	–	–	6.6	3.3	5.4
5	0	0	0	–	–	–	–	–	–	–	33.8	26.4	30.9
6	200	–	–	–	–	–	–	–	–	–	3.7	1.3	2.5
7	100	–	–	–	–	–	–	–	–	–	5.9	1.5	2.7
8	0	–	–	–	–	–	–	–	–	–	14.9	2.0	3.7
9	200	–	–	–	–	–	–	–	49.0	49.0	2.9	1.4	3.0
10	–	–	–	2.5	2.5	2.5	–	–	49.0	49.0	2.3	2.2	2.3
11	200	–	–	–	–	–	–	30.9	–	30.9	2.9	1.3	3.1
12	–	–	–	2.5	2.5	2.5	–	30.9	–	30.9	2.3	2.3	2.3
13	200	–	–	–	–	–	–	19.4	19.4	–	3.0	1.2	3.2
14	–	–	–	2.5	2.5	2.5	–	19.4	19.4	–	2.3	2.3	2.3
15	–	–	–	2.5	2.5	2.5	30.0	–	49.0	49.0	2.3	2.2	2.3

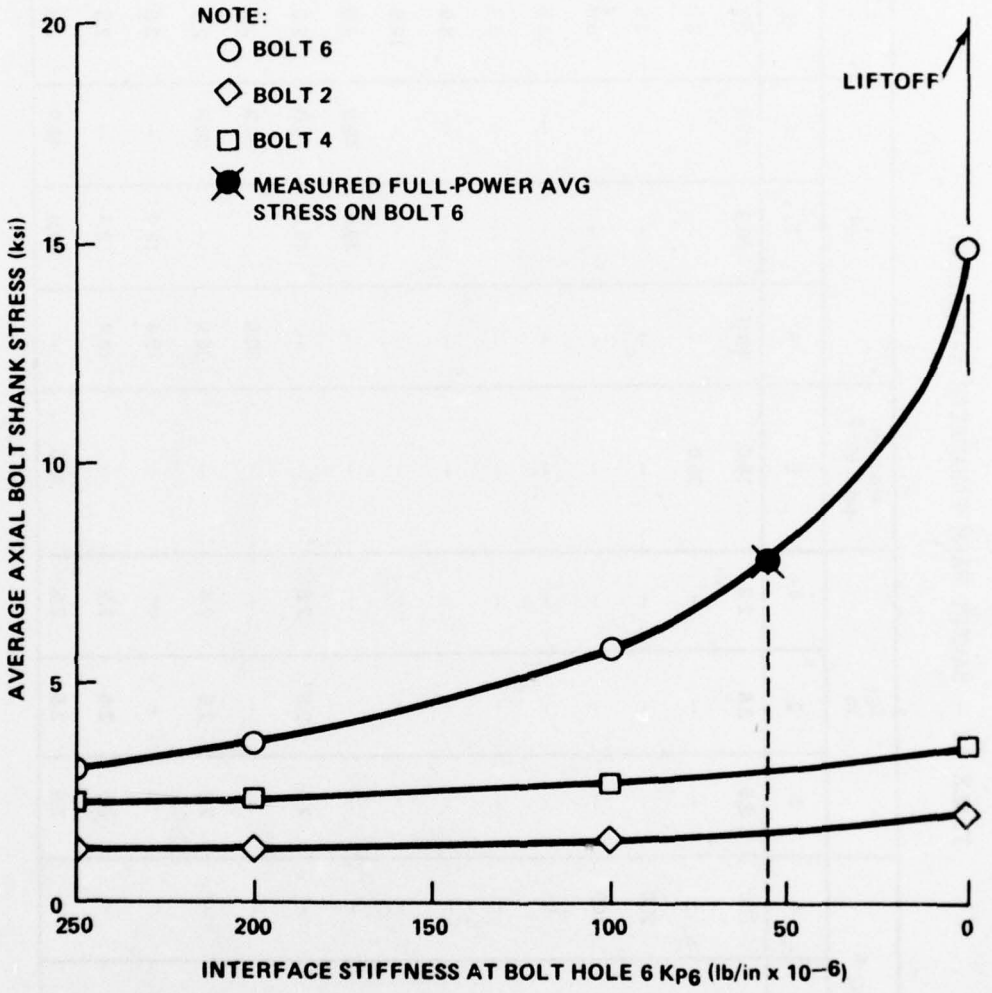

Figure 80 - Effect of Interface Plate Separation at Bolt Hole 6 on Bolt Stress for BARBEY Blade Palm Model

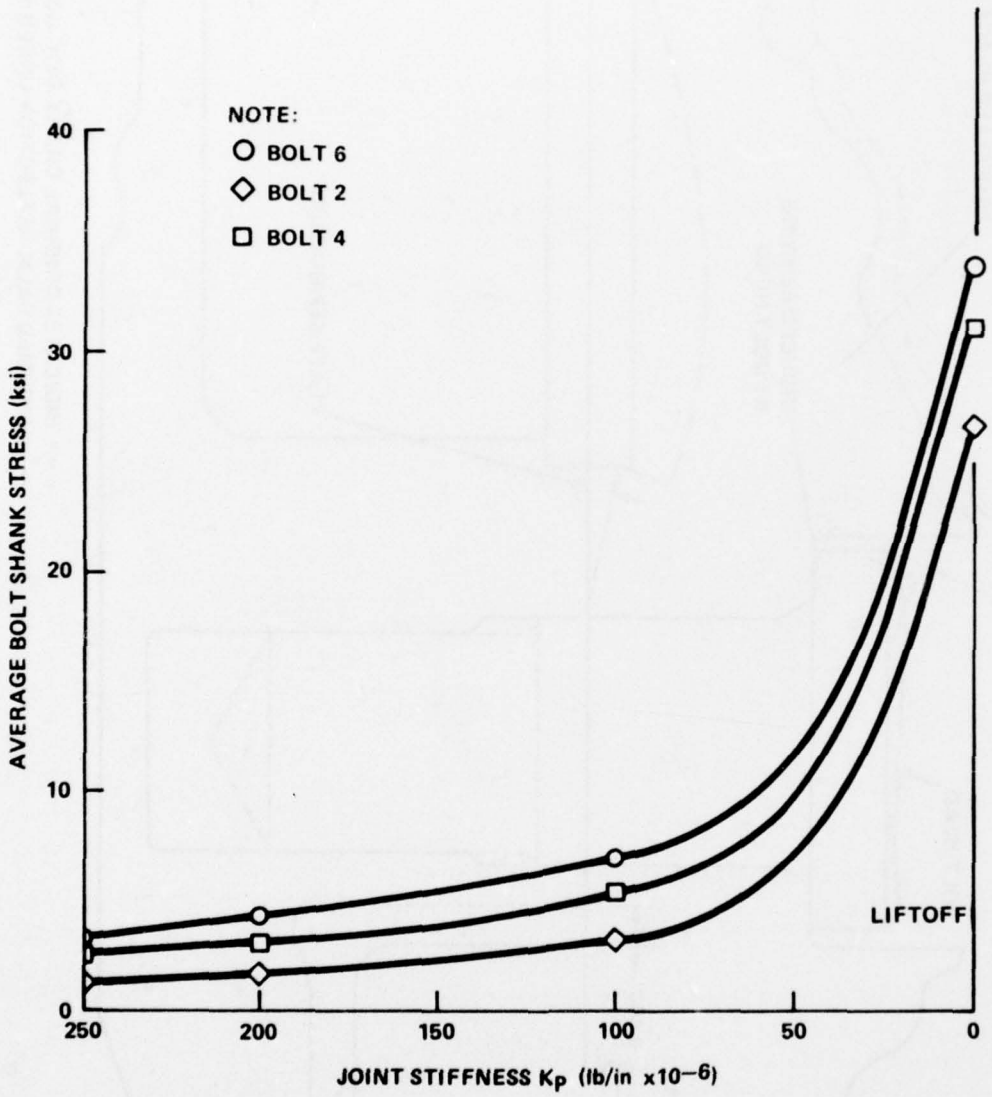

Figure 81 - Variation of Total Joint Stiffness K_p on BARBEY Blade Palm Model

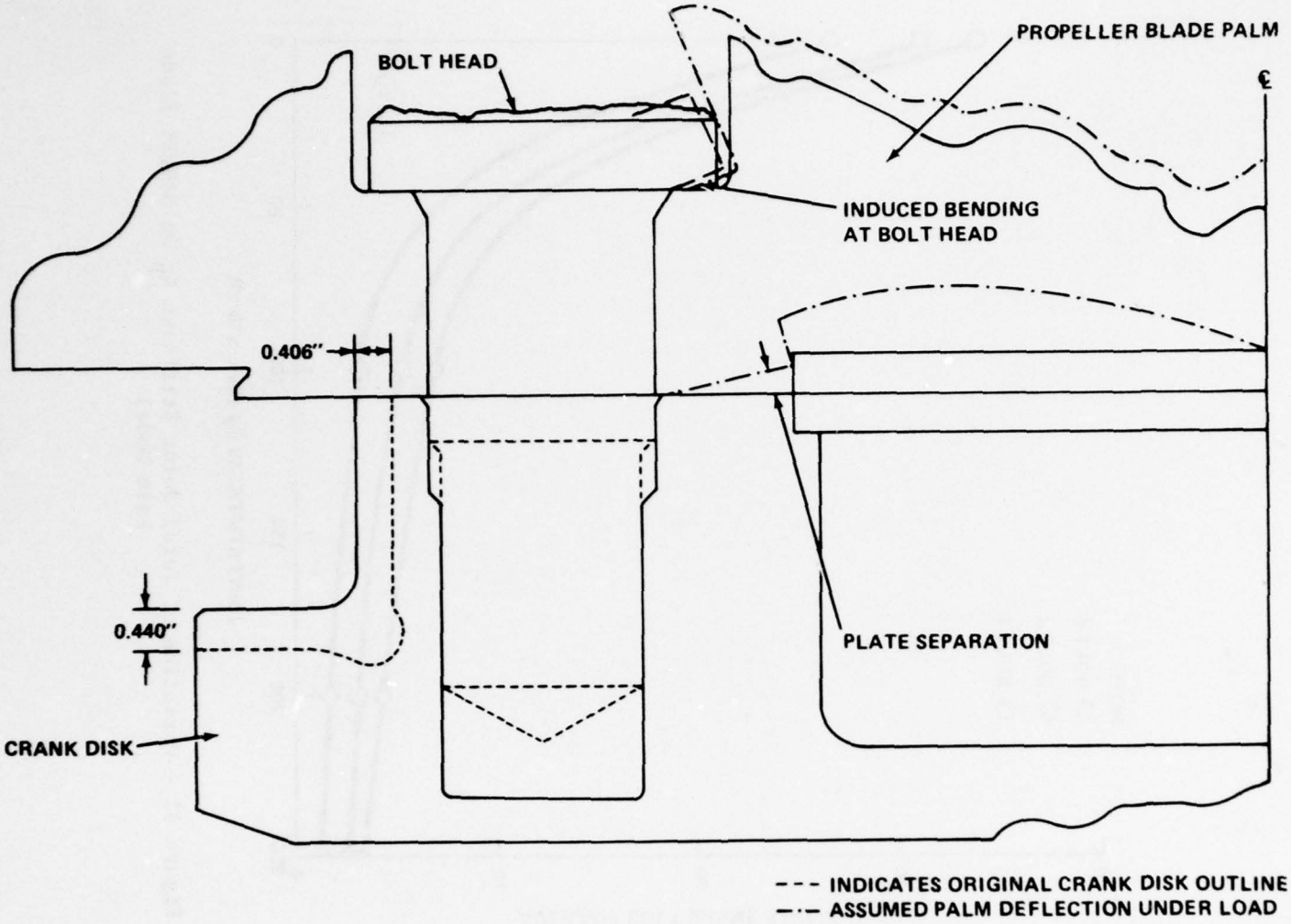

Figure 82 - Assumed Palm Deflection Profile (Exaggerated) for Propeller Palm/Bolt/Crank Disk Assembly

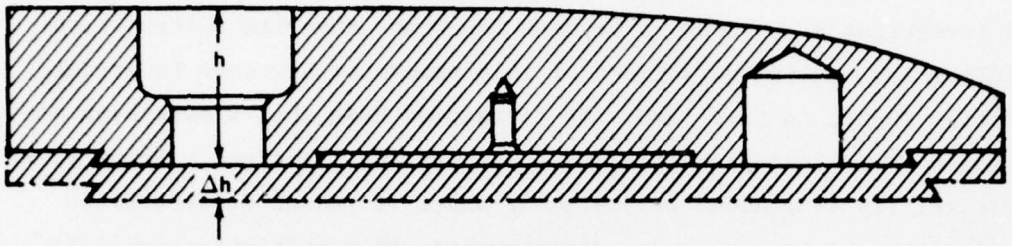

Figure 83a - Changes in Palm Thickness (Cases 9, 11, and 13)

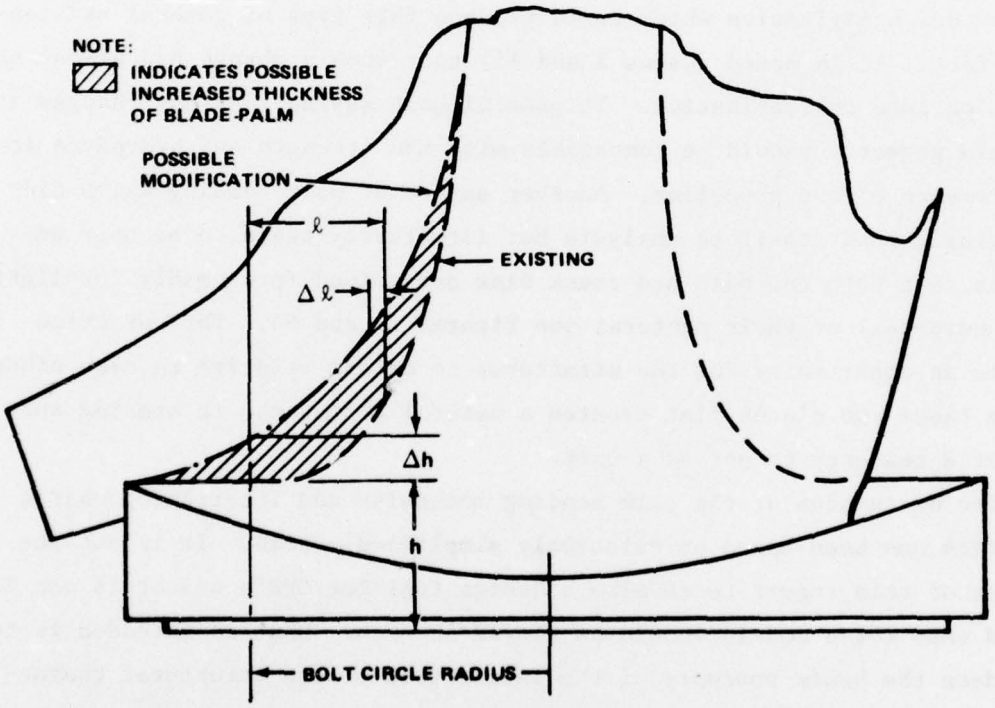

Figure 83b - Changes in Blade Fillet (Cases 10, 12, and 14)

Figure 83 - Proposed Methods for Altering Palm Geometry to Redistribute Bolt Loads

can be seen that base changes improve the bolt load distribution but that properly shaped fillet changes produce the lowest stresses as well as the most uniform bolt load distribution. The values of stiffness (within the limits investigated) is seen to be less important than its distribution. The minimum and maximum variations of this parameter are seen to produce very little change in bolt load. It is assumed here that a more even distribution of bolt loads results in a nonseparating interface. However, if palm flexibility is reduced to the point where it cannot prevent plate separation even with bolt load redistribution, then bolt stress will be higher (see Cases 6, 7, and 8 in Figure 81). Obviously this condition should be avoided.

Redesign of the palms should therefore involve not only bolt load redistribution but also provide sufficient rigidity to avoid total (nonlocalized) palm distortion. A change in the blade material properties is one obvious modification which could produce this type of general stiffening effect. It is noted (Cases 2 and 15) that such a change had almost no effect on load redistribution. It goes without saying that any changes in the palm geometry should be compatible with the strength and hydrodynamic requirements of the propeller. Another aspect of palm bending which did not readily lend itself to analysis but intuitively seems to be poor design is that both the palm and crank disk are voided (presumably for lightening purposes) at their centers; see Figures 16 and 64. This practice creates an opportunity for the structures to deform relative to each other. Having these two plates flat creates a natural resistance to bending and more of a tendency to act as a unit.

The discussion of the palm bending mechanism and interfacing characteristics has been based on relatively simplified models. It is not the purpose of this report to develop a design tool for CPP's and it is not intended that these models should be viewed as such. What is intended is to introduce the basic concepts of the interaction of the structural characteristics of the blade palm with the bolted interface as interpreted through full-scale, underway test results. The differences between the calculated and measured results which were noted earlier in the discussion

appear to be due at least partially to inappropriate modeling. In particular, all previous analytical investigations paid little or no attention to the palm and interface characteristics. Analytics discussed in this report were presented to conceptually emphasize the importance of these characteristics. A more rigorous model is obviously necessary for design purposes. However, any model — no matter how rigorous — which neglects these characteristics is felt to be inadequate.

Results of a more recent investigation[42] which included palm geometry and used a finite element model showed some of the same general trends as discussed here. Chu and McLaughlin concluded that the blade palm was a principal cause of the concentrated (nonuniform) loading in the bolts. Results also suggested that bolt loads can be redistributed more favorably to lessen bolt stresses. It seems appropriate to continue this type of analysis and if warranted by the analytical results, to follow it by model, full-scale model, and full-scale underway tests.

Although the development of an approximate model is an indispensable beginning, it is not the total solution to this problem which appears to be common to a number of high horsepower, bolted blade CPP's.[40] The solution, like many designs, involves compromise of incompatible criteria. For example, minimization of hub diameter in order to reduce hydrodynamic drag places geometric constraints on the CPP design which must simultaneously satisfy blade hydrodynamic criteria, acoustic design, and strength. The first two of these favor a faired (thinner) palm in order to minimize turbulence, thereby reducing cavitation erosion and noise. Conversely, strength considerations dictate a thick palm section in order to achieve adequate palm rigidity. Developing a design rationale is a long and ardous task, one well outside the scope of this report. However, certain aspects of such a rationale would have to reflect the problems addressed herein.

---

[42] Chu, T. and D. McLaughlin, "Contributions to the Development of Design Criteria for Controllable Pitch Propellers," MTI Contract Report MTI 76TR4S (30 Jun 1976).

THE FAILURES

An understanding of the failures on BARBEY will enable the designer to avoid such problems in the future CPP design. Several failure analyses were made following the second (crank disk) failure.[43] * Conclusions were based on interpretation of the visual inspection of the failed parts and/or calculated stresses which were related to some failure criteria (fatigue damage or crack growth). All were performed prior to full-scale underway trials and therefore the stress profile in the CPP system under actual loading conditions was not known. A later analysis** was made which used the measured underway stresses (increased by 10 percent) on Bolt 6. Results generally indicated that the probability of failure of the first bolt in the estimated time frame will increase with increased preload. This is in agreement with Fazekas,[27] who concluded that once preload is beyond the mere suppression of joint separation, its effect on fatigue strength is adverse.

On the other hand, data from Snow and Langer[44] indicate that bolt failure can be relatively insensitive to preload. The actual preload which existed in the original system is not known. It is possible that it could have been anywhere from zero (or very low) to approximately 65 ksi. The upper limit is about where preload would cause yielding of the palm material under the bolt head. There is only a remote probability that the lower valve of preload was present since drydock tests indicated that the

---

[43] Kerwin, J.E. et al., "Failure and Safety Analysis of Controllable Pitch Propellers for the USS BARBEY (FF-1088) and USS SPRUANCE (DD-963)," Office of Naval Research Contract Report N00014-67-A-0204-0082, MITOSP 81496 (15 Apr 1975).

[44] Snow, A.L. and B.F. Langer, "Low Cycle Fatigue of Large Diameter Bolts," Paper presented at the Petroleum Mechanical Engineering Conf. of ASME at New Orleans, La., Sep 18-21, 1966.

* Reported to NAVSEC(6148) in letter from Mechanical Technology, Inc., dated 12 November 1974 and by R.D. Rockwell as Enclosure 1 (Preliminary Failure Analysis of USS BARBEY (FF-1088) Controllable Pitch Propeller Hub Attachments) to DTNSRDC letter Serial 74-172-185 of 15 November 1974.

** Internal DTNSRDC Memo (Code 1730 to Code 1720), 173:NVM:wjm, 76-173-M-183, dated 20 December 1976.

original bolt installation technique (see Introduction) would result in approximately 35-ksi preload.* This is the most likely preload valve for the original installation. It is known from the measured results on the modified system that increasing preload to 55 ksi did not constrain the most highly loaded bolt (No. 6) to a linear response.

It appears, then, that the blade palm distortion at this location negated the normal benefits of preload, regardless of its value. This, together with degenerate interface transmission characteristics, allowed higher axial and bending stresses in Bolt 6. These mechanisms were a direct contribution to the systematic failure of all No. 6** bolts in the original BARBEY installation as well as being the source of the fatigue crack in the crank disk. This also was the most likely source of the second (crank disk) BARBEY failure. Since examination of the remaining portions of the crank disk showed that the material had a very low fracture toughness (8-10 ft-lb Charpy at room temperature), making it susceptible to catastrophic "brittle" fracture at less than yield strength when accompanied by a crack of critical size in the structure. Visual examination and electron microscopy revealed a fatigue crack (3-in. long, 1-in. deep) in Crank Disk 1 emanating from Bolt Hole 6 (Figure 12b). It is likely that other fatigue cracks existed on all crank disks. Given this predisposition to failure, it is conjectured that the original speculation of a domino action (see Introduction) is the most feasible*** explanation of the "simultaneous" failure. It appears that failure was imminent on all crank disks and that there was no particular relation to the crashback mode other than this maneuver, because of loading and flow conditions

---

*An instrumented bolt was "slugged-up" simulating the original technique. Strain measurements indicated about 35-ksi axial preload.

**As the No. 6 bolts cracked or broke, load was transferred to the No. 2 bolts which, in turn, also cracked.

***There was considerable speculation that an inordinate (at least 1.5 x full power ahead) hydrodynamically induced loading mechanism occurred as the blades passed through zero and that this transient high load caused the simultaneous failure of the CPP system. The measured test results do not support this speculation.

creates a very convulsive vibration environment and possibly might tend to keep a detached (broken) blade in the propeller plane.

It is apparent from the preceding qualitative failure scenario that long-term, unimpeded deployment of this type of CPP is unlikely unless the nonuniform, nonlinear propeller blade bolt loading problem is resolved.

CONCLUSIONS

The conclusions are grouped under headings which indicate their contribution to the goals of this work.

FULL-SCALE UNDERWAY TRIAL RESULTS

1. Bolt preloading is accompanied by a certain amount of bending which can be detrimental to the overall stress condition of the bolts.

2. The magnitude and distribution of mean propeller blade stresses for steady, full-power ahead operation compared reasonably well with calculations.

3. The magnitude of fluctuating propeller blade stresses for steady, full-power ahead operation was approximately 45 percent of the mean. This was approximately 100 percent higher than predicted.

4. The mean or fluctuating propeller stresses during maneuvers (turns, crashbacks, etc.) bear no resemblance to predictions.

5. Measured stresses on the propeller blade bolts and crank disk exceeded the failure criteria adopted for the trial and the operational evaluation period that followed.

6. Maximum measured stresses occurred during full-power turns. Contrary to calculation, crashback maneuvers did not produce the highest stresses.

7. Comparison of measured crank disk fillet stresses with predictions submitted prior to measurements show discrepancies of over 100 percent on the nonconservative side.

INTERPRETATION OF RESULTS

1. Unrestricted operation at full power could result in fatigue failure of the modified CPP assembly. However, the ship could (and did) operate without damage to these units on restricted operation.

2. The basic design assumptions concerning the load transfer from the propeller blade palm to the crank disk are invalid.

3. Propeller blade palm distortion under load acts as a nonuniform, nonlinear loading mechanism on the blade bolts.

4. "Normal" jointed interface linear response theory does not apply to the palm/bolt/crank disk interface in juxtaposition to the most heavily loaded bolt (No. 6).

5. Geometric discontinuities adversely affect the interfacing characteristics of the palm and crank disk. Voids in the palm and crank disk encourage relative deflection (palm bending) which also degrades these characteristics.

6. It is possible to construct a mathematical model which reasonably accounts for the various mechanisms that affect the various CPP components.

7. Any model which ignores the flexural rigidity of the palm and the interfacing characteristics of the assembly would be inadequate.

8. Studies on preliminary models indicate that arbitrary changes in the CPP system should be avoided. For example, changes in bolt length to effect lower bolt loads on BARBEY would be, at best, marginal and could possibly increase bolt loads.

9. It appears possible to redistribute bolt loads by altering the flexural characteristics of the blade palm. Changes in the blade fillet produce the most effective changes.

10. Any CPP changes should be compatible with hydrodynamic and strength requirements.

11. A design criterion has to be developed to ensure adequate CPP operation.

12. The problems identified in the BARBEY CPP design seem to be common to a number of high-horsepower CPP designs which are or will be used in ships of the U.S. Navy.

FAILURE

1. The most heavily loaded bolt (No. 6) was subjected to higher loads than the other bolts because of the various mechanisms described above.

2. The mechanism by which the palm loads the most heavily loaded bolt could be independent of preload.

3. The combination of Items 1 and 2 above resulted in the fatigue damage suffered in the first BARBEY failure.

4. The nonuniform bolt load distribution was reflected in the crank disk stress distribution and resulted in fatigue cracks in the crank disks.

5. The material properties of the crank disk were found to be susceptible to catastrophic "brittle" fracture at less than yield strength when accompanied by a crack of critical size in the structure.

6. Crank disk failure was imminent on all ports and had no particular relation to the crashback maneuver.

MISCELLANEOUS

1. The use of vulcanized rubber patches for waterproofing protection of propeller instrumentation provides excellent long-term results.

2. Spray urethane can be used for waterproofing for short-term applications.

3. Propeller blade pressure measurements are feasible but the experimental technique needs further development.

4. The cost of measuring propeller parameters could be considerably reduced by the use of a hydrotelemetry system. Such a system is feasible but still highly developmental at this point.

RECOMMENDATIONS

The following recommendations are a logical extension of this work:

1. An experimental technique necessary to adequately measure both mean and alternating propeller blade loads (pressures) should be developed.

2. A reliable design tool should be developed for the strength analysis of CPP's which includes the interfacing characteristics of the blade palm/bolts and crank disks.

3. Design criteria should be developed to provide realistic guidelines for long-term, unimpeded deployment of future CPP's.

4. The flexibility of alternate options should be retained by keeping abreast of or developing technical information on the threaded blade attachment type CPP used on PATTERSON.

5. The maximum amount of information on candidate materials should be accumulated for CPP application to permit flexibility of choice in the design stage.

ACKNOWLEDGMENTS

The authors express their appreciation to the many people at DTNSRDC who participated in this project. Particular thanks are due Mr. S. Crump who acted as trial director; Messrs. W. Klemens and J. Bohlander for work on blade waterproofing techniques; Messrs. E. Czyryca and M. Vassilaros for laboratory tests and metalurgical contributions; Mr. R. Guillmette for many innovative ideas on the gaging and installation of the instrumentation; Messrs. R. Boswell and T. Brockett for many enlightening discussions and guidance on propeller theory; Messrs. K. Todack, E. Howerton, and W. Mosedale for installation and operation of the trial instrumentation; Messrs. R. Hunt, L. Hundley, W. Koehler, and W. Kellerberg for standardization results; Mr. R. Rockwell and Mr. A. Dinsenbacher for many discussions on model test results; and Mr. B. Zimmerman for telemetry instrumentation. Special thanks are extended to Mr. M. Dean for details of instrumenting the CPP components. It was through his expert technical background and perseverance that the vulcanized waterproofing technique was so successfully developed and implemented on this project.

This work could not have been done without the cooperation and help of the personnel of the Long Beach Naval Shipyard in particular Messrs.

V. Pena, C. Neilson, and S. Sypulski. The overall coordination of the project was handled by A. Witcher of NAVSEA and J. Angelo of NAVSEC.

No one participated in this project more enthusiastically or with more patience over its long duration than the officers and crew of BARBEY. Their cooperation during installation and trials contributed significantly to the success of the project. Particular thanks are extended to the Commanding Officer, Cdr. Timothy R. O'Keefe, and his executive and engineering officers, LCdr. G. Dunne and Lt. J. Boland.

APPENDIX A

CONVERSION FACTORS FOR U.S. CUSTOMARY AND THE INTERNATIONAL (SI) UNITS OF MEASUREMENT

Length

1 kilometer (km)	= 1000 meters	1 inch (in.)	= 2.540 cm
1 meter (m)	= 100 centimeters	1 foot (ft)	= 30.48 cm
1 centimeter (cm)	= 10^{-2} m	1 mile (mi)	= 1.609 km
1 millimeter (mm)	= 10^{-3} m	1 mil	= 10^{-3} in.
1 micron (μ)	= 10^{-6} m	1 centimeter	= 0.3937 in.
1 millimicron (mμ)	= 10^{-9} m	1 meter	= 39.37 in.
1 angstrom (A)	= 10^{-10} m	1 kilometer	= 0.6214 mile

Area

1 square meter (m^2) = 10.76 ft^2

1 square foot (ft^2) = 929 cm^2

Volume

1 liter (ℓ) = 1000 cm^3 = 1.057 quart (qt) = 61.02 $in.^3$ = 0.03532 ft^3

1 cubic meter (m^3) = 1000 ℓ = 35.32 ft^3

1 cubic foot (ft^3) = 7.481 U.S. gal = 0.02832 m^3 = 28.32 ℓ

1 U.S. gallon (gal) = 231 $in.^3$ = 3.785 ℓ; 1 British gallon = 1.201 U.S. gallon = 277.4 $in.^3$

Mass

1 kilogram (kg) = 2.2046 lb_m = 0.06852 slug; 1 lb_m = 453.6 gm = 0.03108 slug

1 slug = 32.174 lb_m = 14.59 kg

Speed

1 km/hr = 0.2778 m/sec = 0.6214 mi/hr = 0.9113 ft/sec

1 mi/hr = 1.467 ft/sec = 1.609 km/hr = 0.4470 m/sec

Density

1 gm/cm^3 = 10^3 kg/m^3 = 62.43 lb_m/ft^3 = 1.940 $slug/ft^3$

1 lb_m/ft^3 = 0.01602 gm/cm^3; 1 $slug/ft^3$ = 0.5154 gm/cm^3

Force

1 newton (nt) = 10^5 dynes = 0.1020 kg_f = 0.2248 lb_f

1 pound force (lb_f) = 4.448 nt = 0.4536 kg_f = 32.17 poundals

1 kilogram force (kg_f) = 2.205 lb_f = 9.807 nt

1 U.S. short ton = 2000 lb_f; 1 long ton = 2240 lb_f; 1 metric ton = 2205 lb_f

Energy

1 joule = 1 nt m = 10^7 ergs = 0.7376 ft lb_f = 0.2389 cal = 9.481 x 10^{-4} Btu

1 ft lb_f = 1.356 joules = 0.3239 cal = 1.285 x 10^{-3} Btu

1 calorie (cal) = 4.186 joules = 3.087 ft lb_f = 3.968 x 10^{-3} Btu

1 Btu = 778 ft lb_f = 1055 joules = 0.293 watt hr

1 kilowatt hour (kw hr) = 3.60 x 10^6 joules = 860.0 kcal = 3413 Btu

1 electron volt (ev) = 1.602 x 10^{-19} joule

Power

1 watt = 1 joule/sec = 10^7 ergs/sec = 0.2389 cal/sec

1 horsepower (hp) = 550 ft lb_f/sec = 33,000 ft lb_f/min = 745.7 watts

1 kilowatt (kw) = 1.341 hp = 737.6 ft lb_f/sec = 0.9483 Btu/sec

Pressure

1 nt/m^2 = 10 $dynes/cm^2$ = 9.869 x 10^{-6} atmosphere = 2.089 x 10^{-2} lb_f/ft^2

1 lb_f/in^2 = 6895 nt/m^2 = 5.171 cm mercury = 27.68 in. water

1 atmosphere (atm) = 1.013 x 10^5 nt/m^2 = 1.013 x 10^6 $dynes/cm^2$ = 14.70 lb_f/in^2
= 76 cm mercury = 406.8 in. water

Angle

1 radian (rad) = 57.296°; 1° = 0.017453 rad

APPENDIX B

PROPELLER STRESS AND HULL/SUPERSTRUCTURE VIBRATION
MEASURED ON THE USS DOUGLAS (PG-100)

BACKGROUND

The PG-84 Class are aluminum-hull patrol gunboats designed for high-speed operation. The first boats of this class were fitted out with titanium propeller blades. The failures experienced by these blades in service were attributed to poor fatigue and stress-corrosion properties in seawater.* The titanium blades were replaced by a stainless steel design and manufactured by using a hand grinding process. This design was found to have intolerable deviations from the propeller blade specifications and experienced excessive, shaft-frequency hull and superstructure vibration.[45] DTNSRDC recommended an improved manufacturing process (digital machine profiling) which eliminated this problem.

Subsequently, DTNSRDC was requested to measure the full-scale propeller blade stresses on DOUGLAS.** The starboard blades of one ship set of the hand-ground stainless-steel type were selected to be instrumented and were returned to the manufacturer for reworking. Two ship sets (fourth and fifth) were also returned and final acceptance of these sets was to be based on satisfactory vibration performance as installed on a PG.***

The DOUGLAS propeller stresses are included as an appendix to the BARBEY report for convenience of documenting additional information on stresses of controllable pitch propellers. Preliminary test results on

---

*As reported by the Annapolis Laboratory of the Center in letter NP/10310 (M871 JLC) Assigt 86113 Report 319/67 of 9 August 1967.

**By NAVSHIPS letter PMS 382:NAM:jr, PG-84 CL/9440, Serial 1538 of 30 October 1968.

***NAVSHIPS letter PMS-382:RTF:alb, PG-84 CL/9440, Serial 382.12/561 dated 27 February 1970.

[45]Noonan, C. and W. Fontaine, "A Study of Vibration Problems Experienced by Aluminum Hull Patrol Gunboats (PG-84 Class)," DTNSRDC Report 3857 (Apr 1972).

DOUGLAS have already been reported informally.* This appendix represents an expanded version of that work. Sections on Materials Investigation, Instrumentation and Blade Vibration were extracted from Reference 21 by Valentine.

MATERIALS INVESTIGATION

The protective system used to cover the gages on the propeller blades was essentially the same as employed on the USS ROOSEVELT (CVA-42).[20] Since the ROOSEVELT blades were of cast bronze and those of DOUGLAS were of cast stainless steel, dynamic and static peel tests were conducted to verify compatibility of the ROOSEVELT protective system (modified to include a primer coat) applied to the DOUGLAS blade material. Such details of the materials investigation as preparation of specimens, dynamics peel tests, and static peel tests are given by Valentine.[21] It was concluded that the protective system with developed modification would be suitable for use on DOUGLAS.

VIBRATION TESTING OF DOUGLAS GUNBOAT BLADE

In order to verify a then recently developed marine propeller dynamics program, it was necessary to obtain some test data on natural frequencies and mode shapes for an actual marine propeller. The 6-foot-diameter gunboat blade, then at Hamilton Standard for strain gaging, was ideal for the purpose. Therefore, appropriate authorization was obtained and a vibration test was conducted.

The test setup is shown in Figure 84. The blade was bolted to a large piece of plate stock which, in turn, was bolted to a hugh block of steel and concrete imbedded in the floor. The vibratory excitation was provided magnetically and, since the stainless steel blade itself was nonmagnetic, a small piece of magnetic material was glued to the surface of the blade. In order to ensure that the placement of the excitation did not affect the

*DTNSRDC letter 962:CJN:9870.1 dated 10 March 1971.

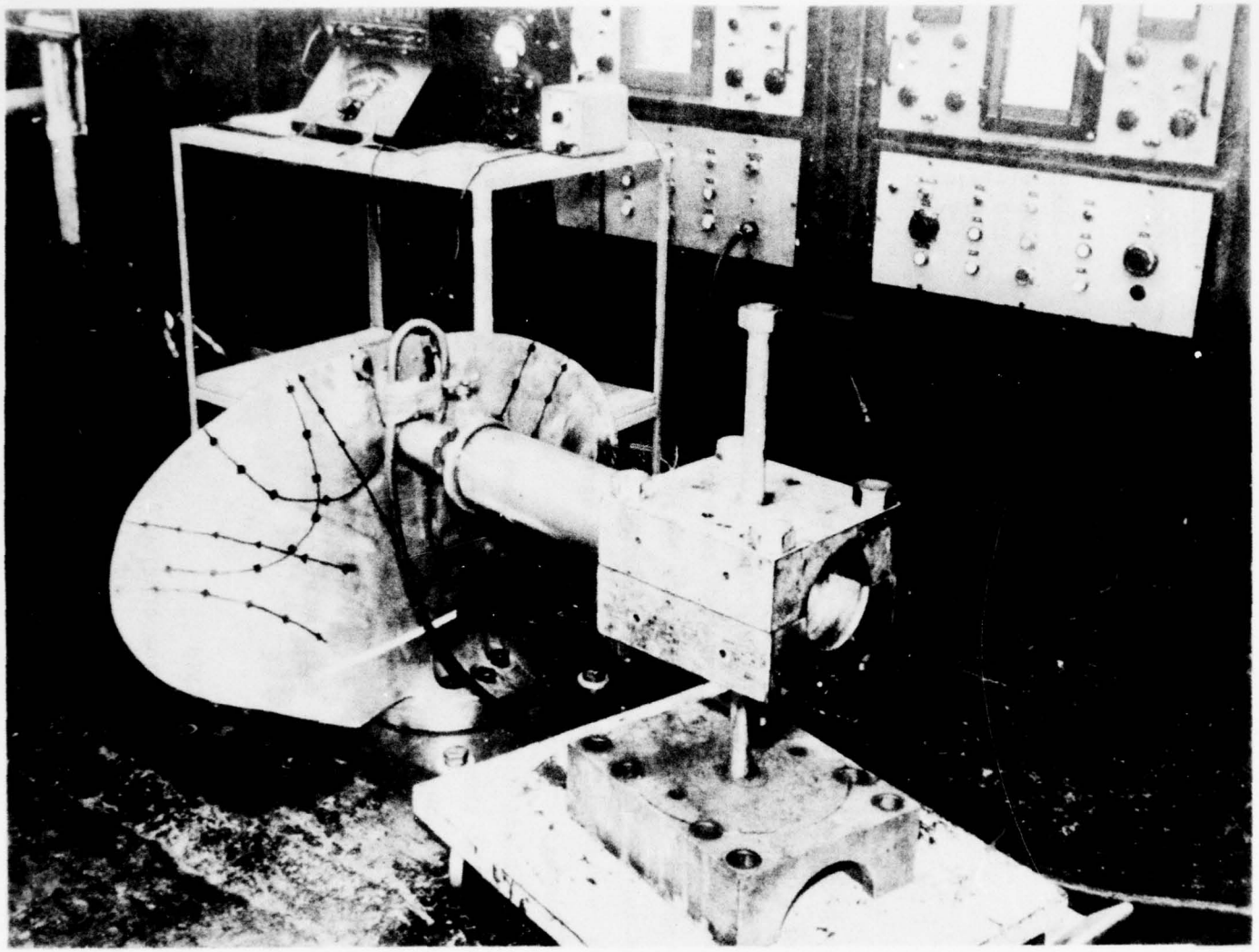

Figure 84 - Test Setup for Determining In-Air Blade Modes and Natural Frequencies on DOUGLAS

results, two runs were made, one with the exciting force at the tip of the blade and the other with the force applied to the leading edge. Both runs agreed to within experimental accuracy.

Experimental and theoretical values of natural frequencies (in hertz) are tabulated below; the theoretical values have convergence tolerances as noted.

Mode	Experiment	Theory
1	112	133 $\pm$ 10
2	202	190 $\pm$ 19
3	262	300 $\pm$ 10
4	346	375 $\pm$ 10
5	477	482 $\pm$ 48

The first mode is the first bending mode with the nodal line at the clamped edge; the higher order mode shapes are shown in Figure 85. The first natural frequency was quite sensitive to the retention stiffness, which was assumed to be rigid in the theoretical calculation. Despite the huge mass of steel and concrete to which the blade was attached, the floor did shake, indicating a flexible retention and thus having the effect of lowering the first natural frequency. The higher modes were not as sensitive to retention stiffness and the agreement between test and theory was much better.

The blade used in the test had been reworked and, since there was insufficient time to perform comprehensive thickness measurements, the thickness values on the drawing were used in the theoretical calculations. The thickness was measured at several locations on the blade centerline and the values were in reasonable agreement with those on the drawing. However, this did not eliminate the possibility of larger discrepancies elsewhere on the blade.

UNDERWAY TEST ARRANGEMENTS

Underway trial instrumentation details are shown in Figure 86. Tests were conducted in Puget Sound (Tacoma-Seattle area) on 20 and 25 January 1971.

Figure 85 - Modal Pattern of 36-Inch-Radius Gunboat Blade

Figure 85a - Second Mode

Figure 85 (Continued)

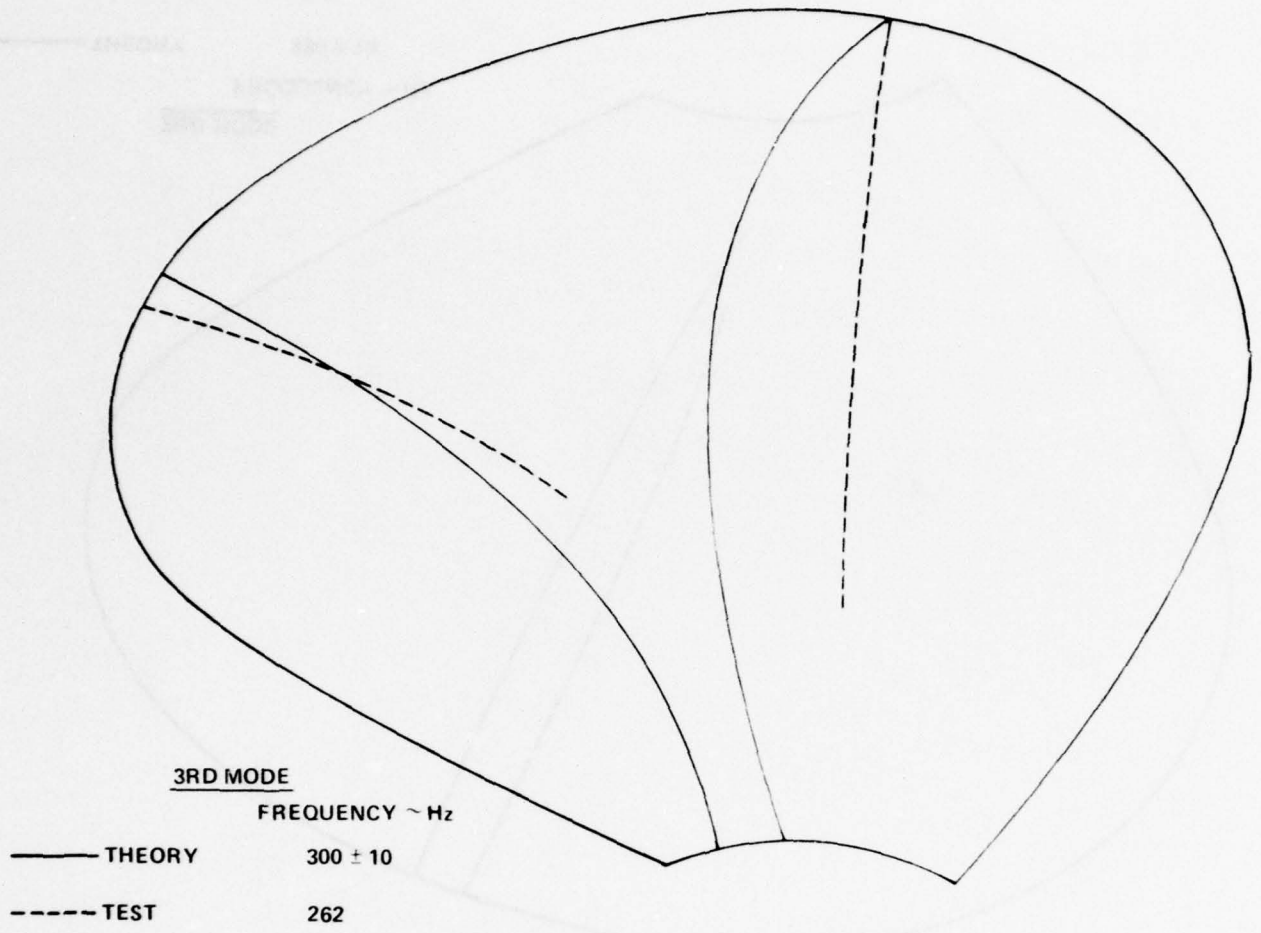

Figure 85b - Third Mode

Figure 85 (Continued)

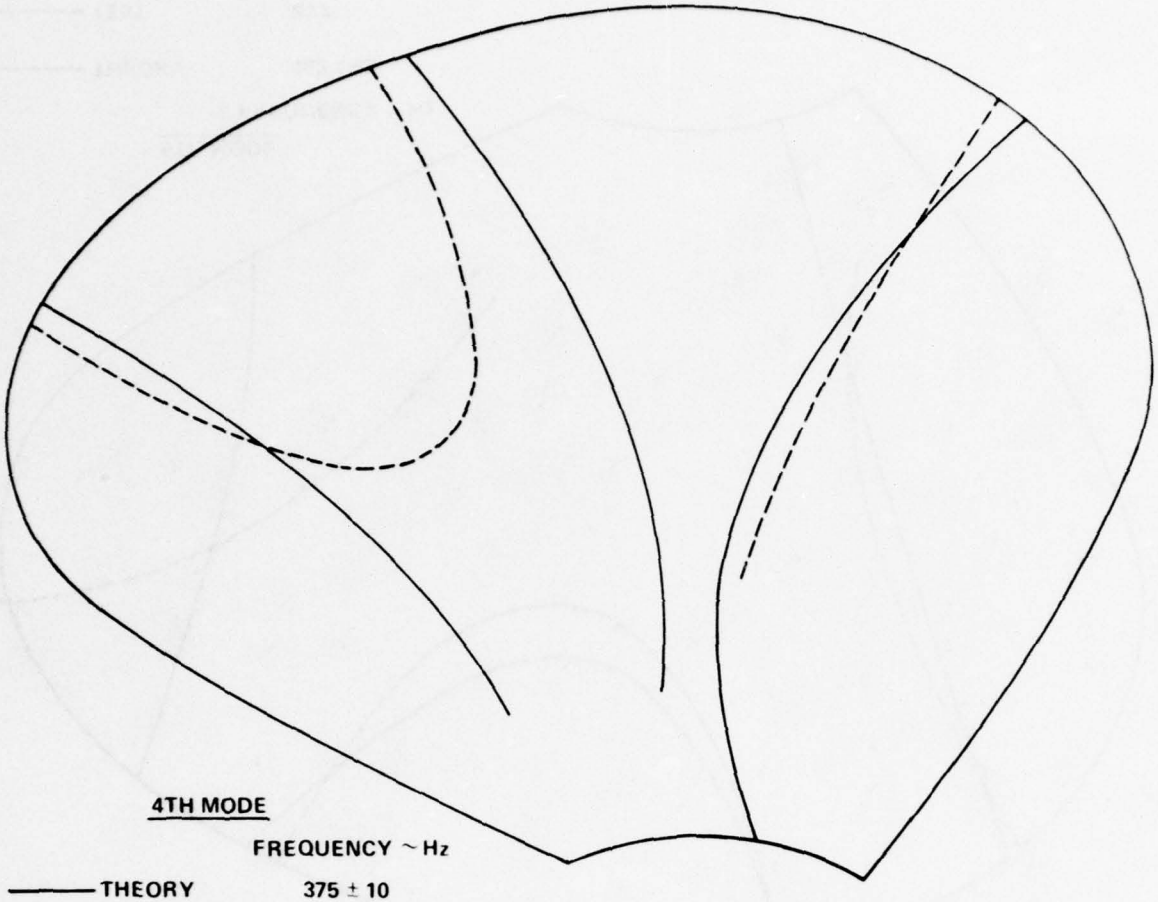

Figure 85c - Fourth Mode

Figure 85 (Continued)

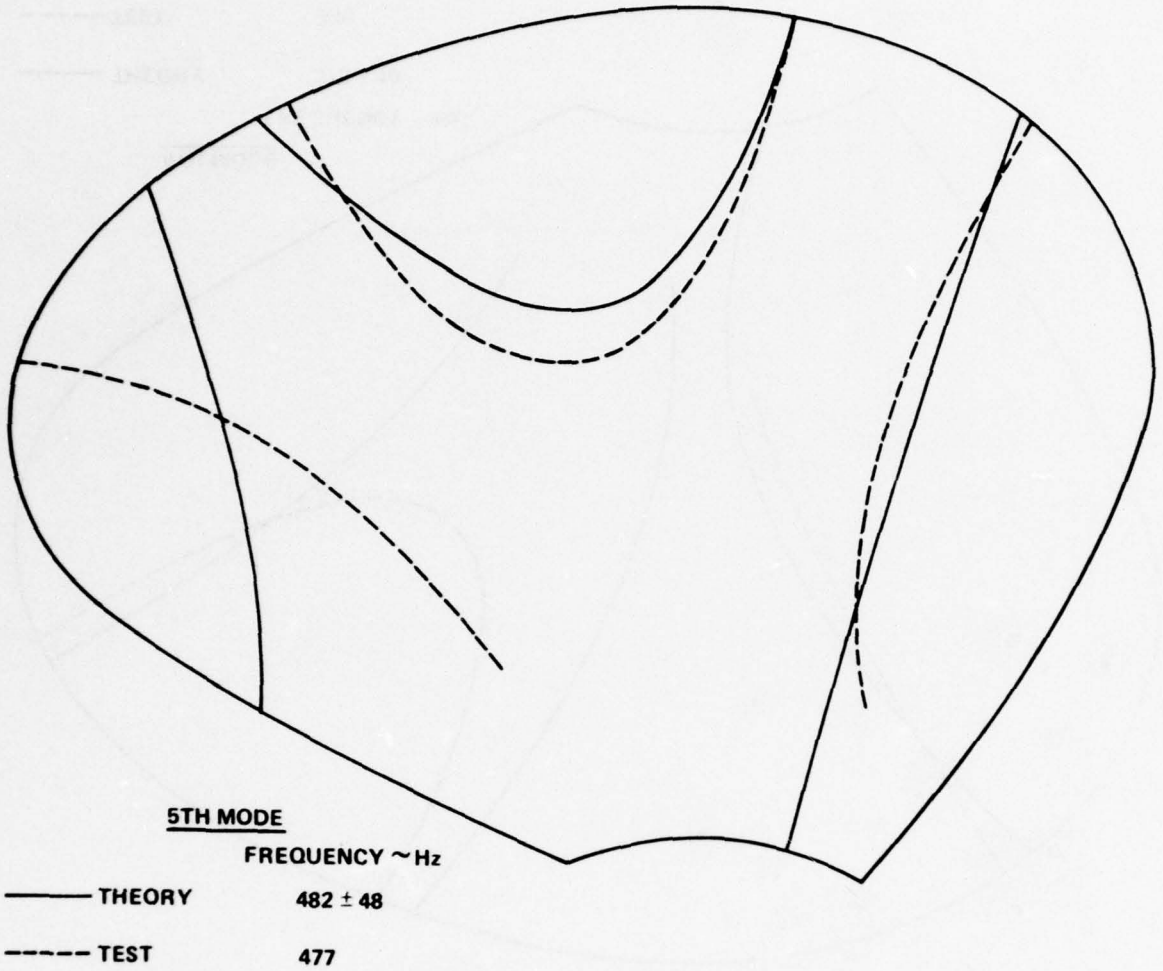

Figure 85d - Fifth Mode

Figure 86 - Details of DOUGLAS Underway Trial Instrumentation

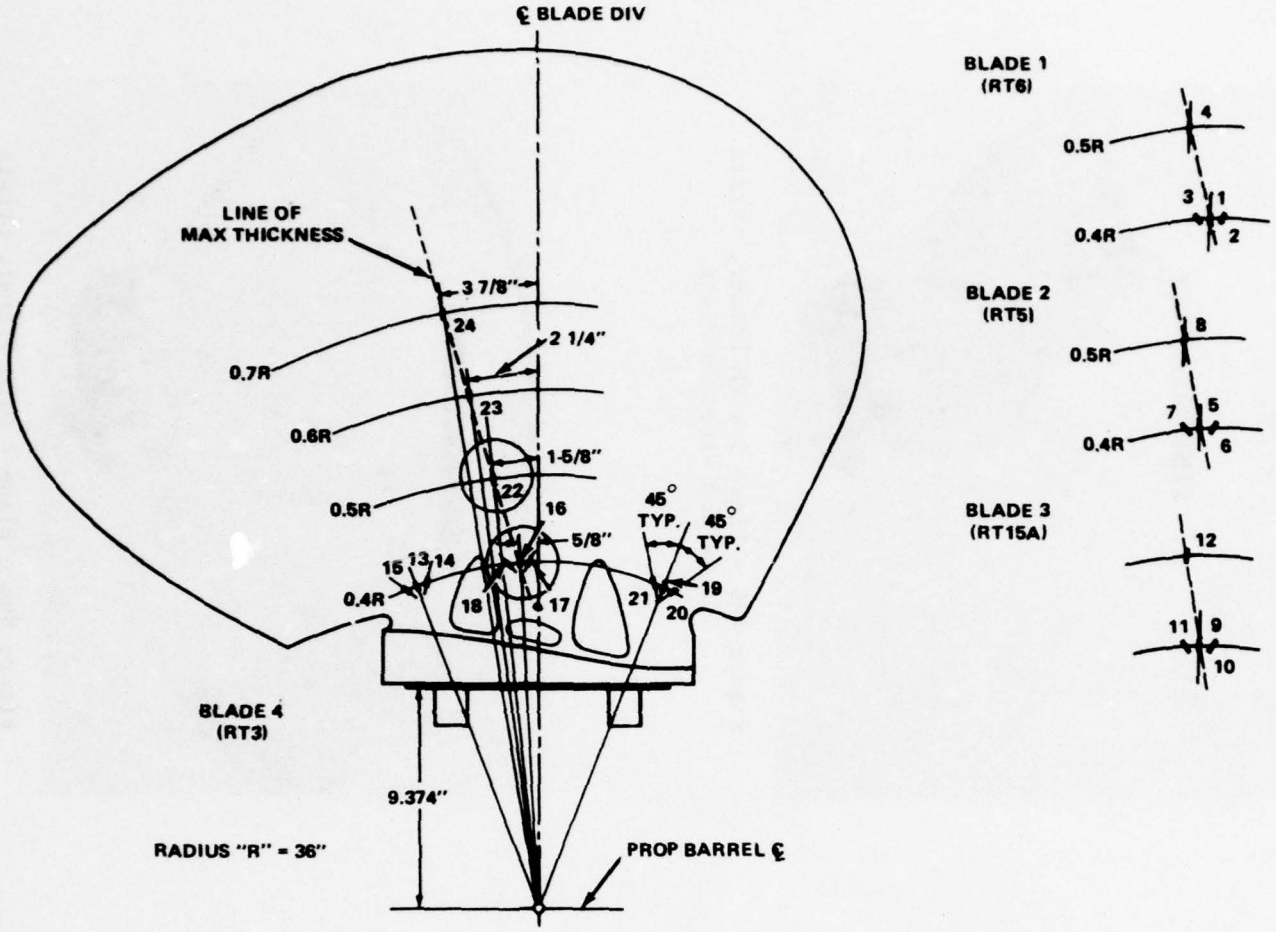

Figure 86a - Strain Gage Layout and Numbering

Figure 86 (Continued)

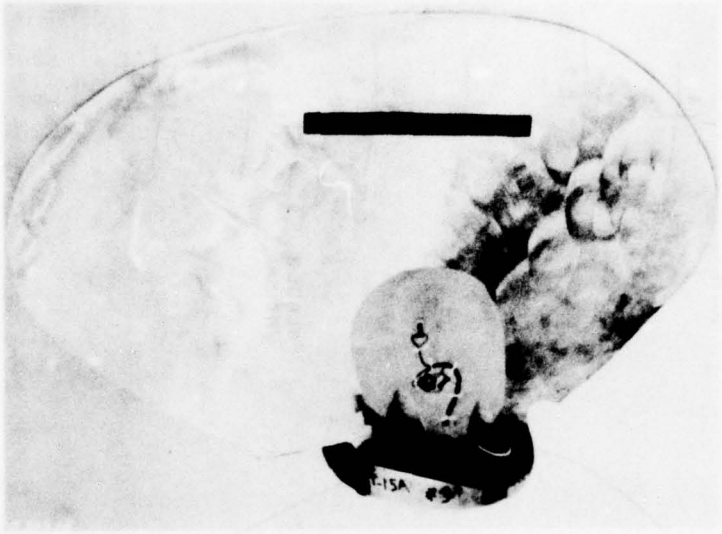

Figure 86b - Blade 3 with Primer, Strain Gages and Wires in Place

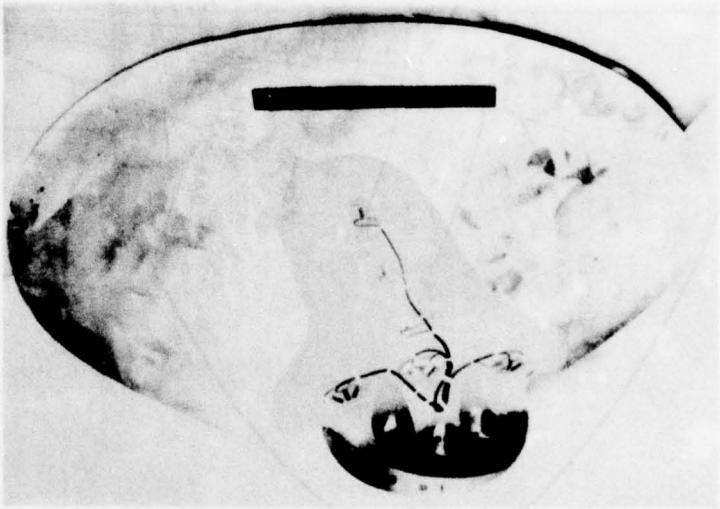

Figure 86c - Blade 4 with Primer, Strain Gages and Wires in Place

Figure 86 (Continued)

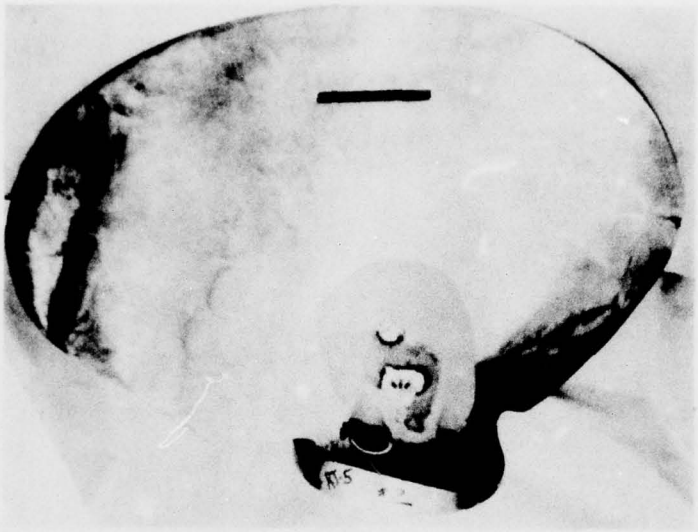

Figure 86d - Blade 2 with Devcon ST
Fairing over Wires

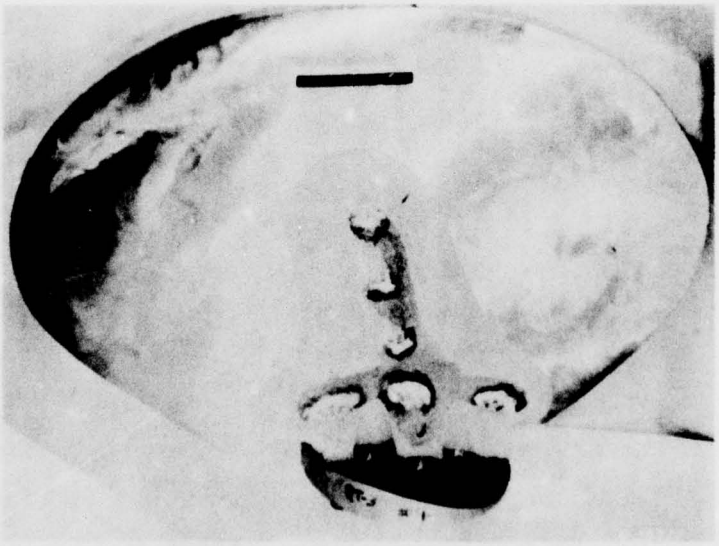

Figure 86e - Blade 4 with Devcon ST
Fairing over Wires

Figure 86 (Continued)

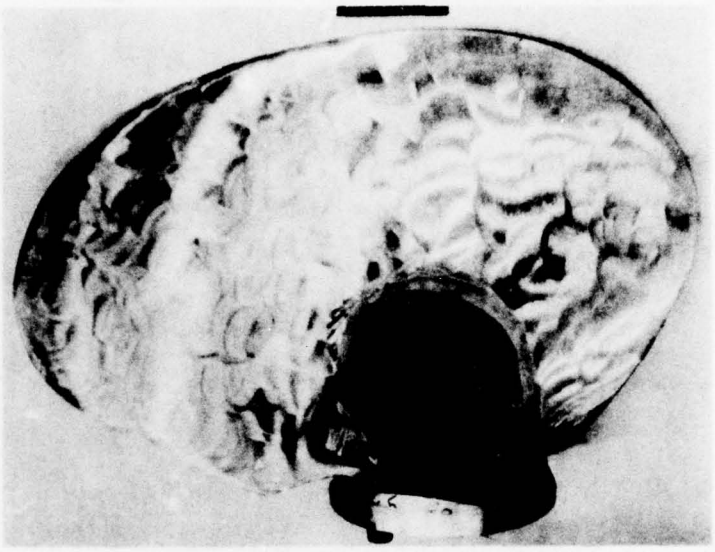

Figure 86f - Blade 2 with Completed Installation

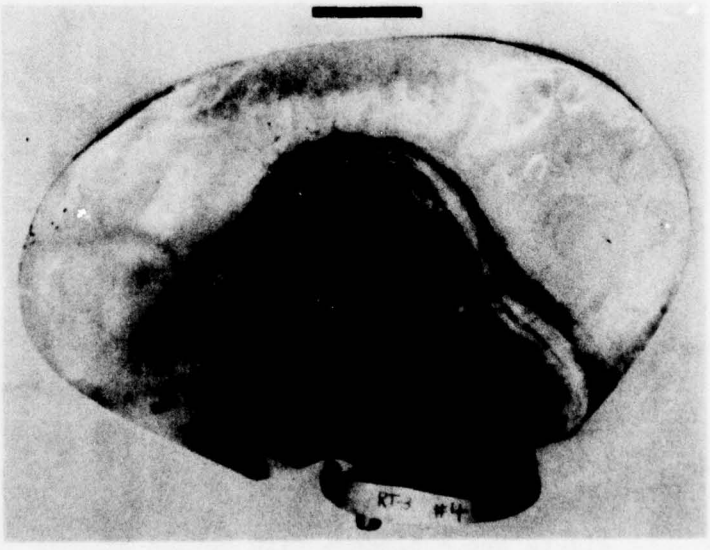

Figure 86g - Blade 4 with Completed Installation

Figure 86 (Continued)

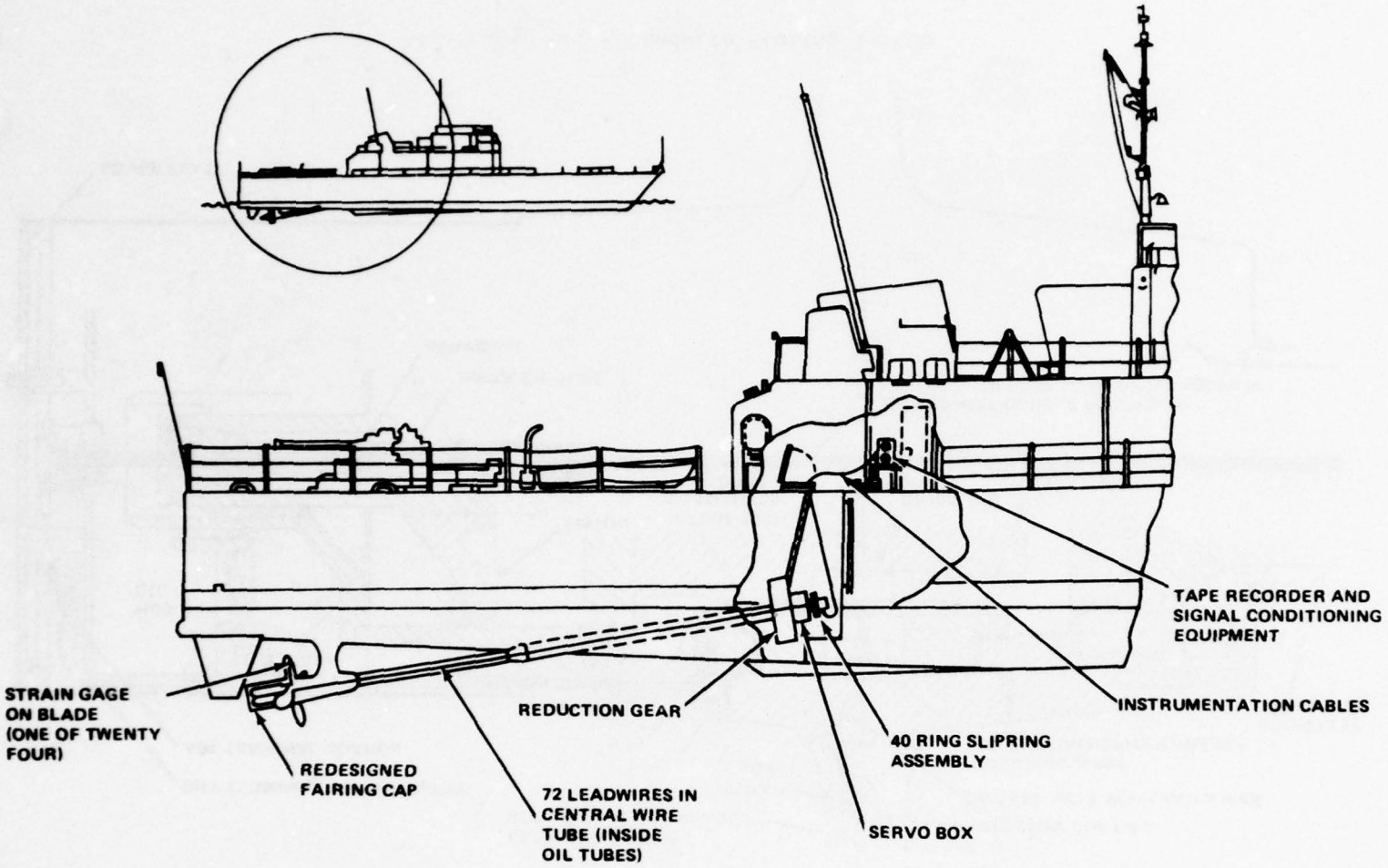

Figure 86h - Leadwire and Cable Routing for Blade Strain Measurement System

Figure 86 (Continued)

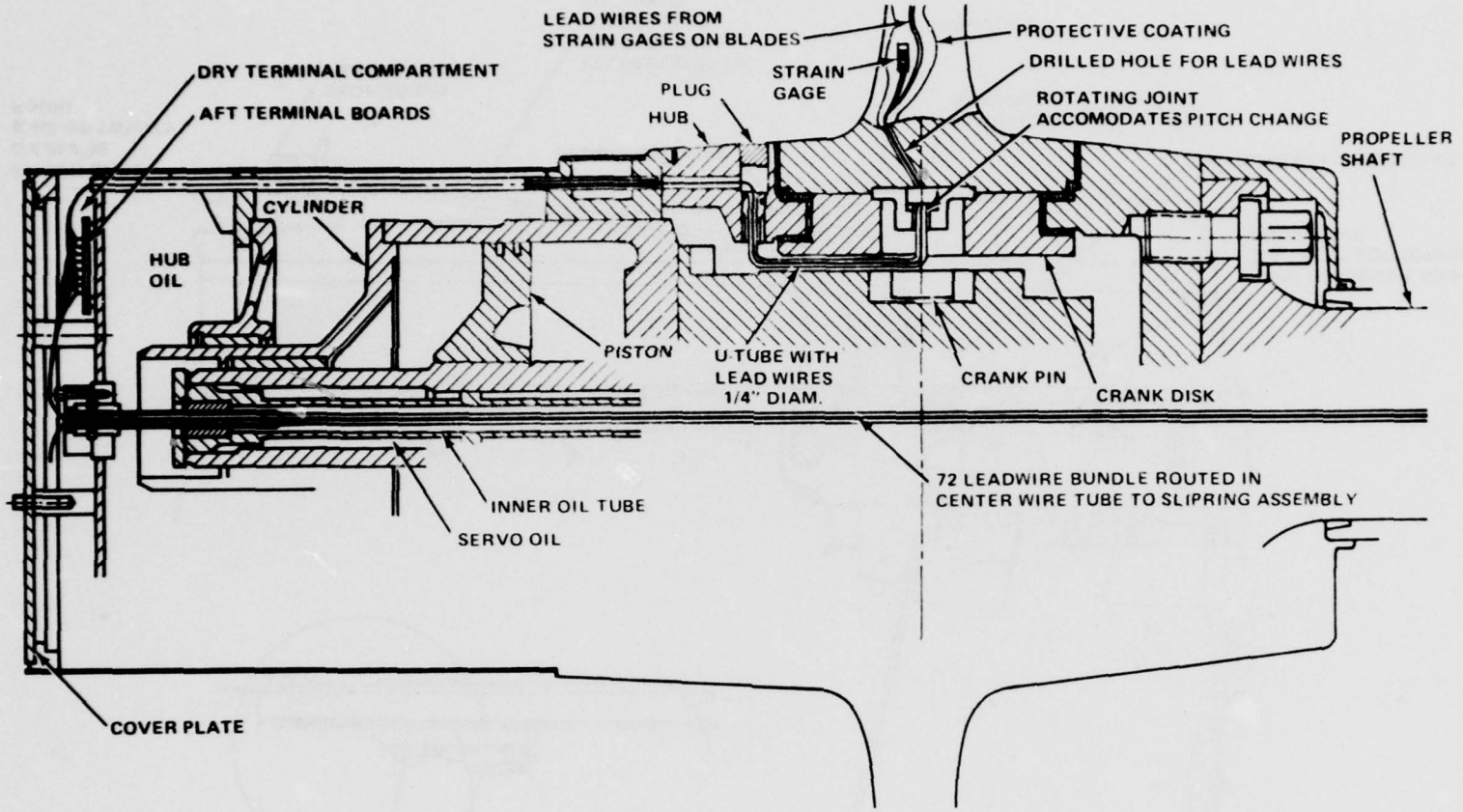

Figure 86i - Leadwire Routing in Hub .

Figure 86 (Continued)

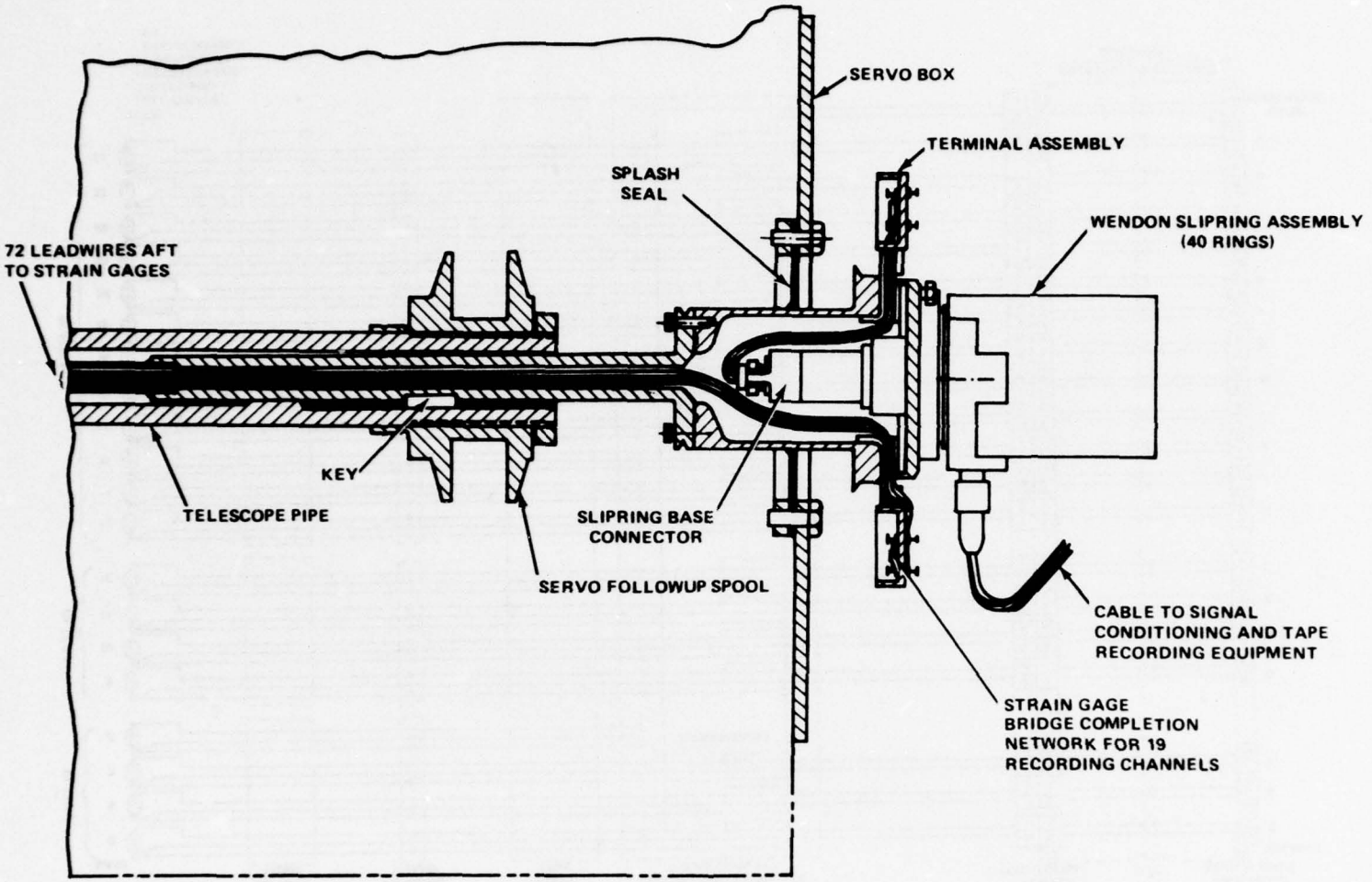

Figure 86j - Leadwire Routing Forward at Servo Box

Figure 86 (Continued)

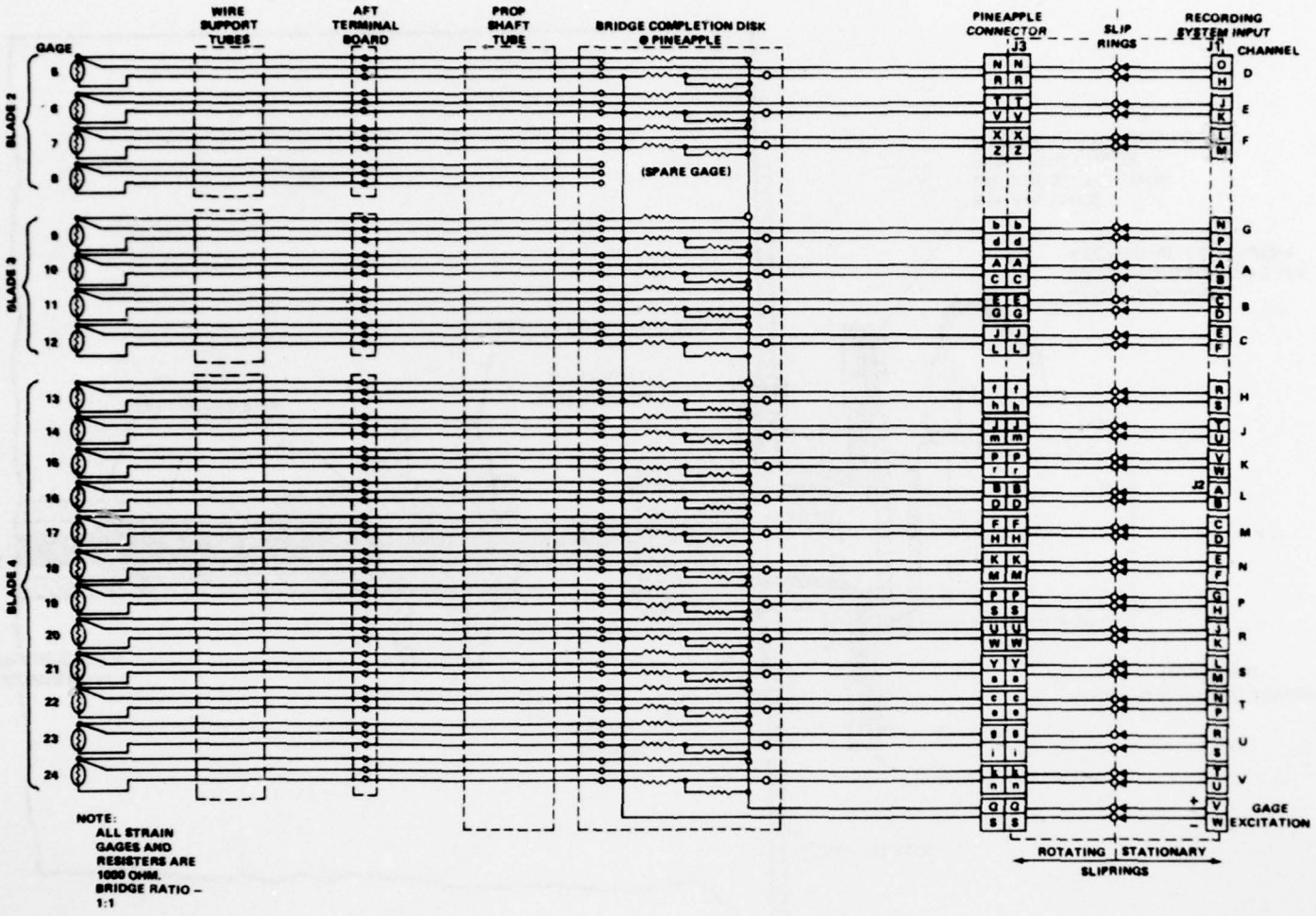

Figure 86k - Details of Strain Gage Wiring

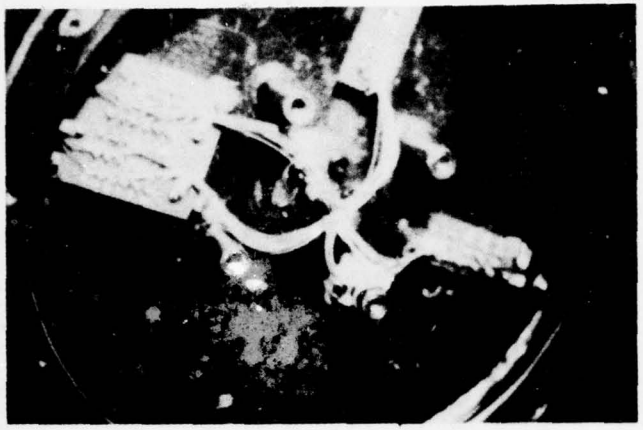

Figure 86ℓ - Strain Cage Terminal Boards in Hub Cavity

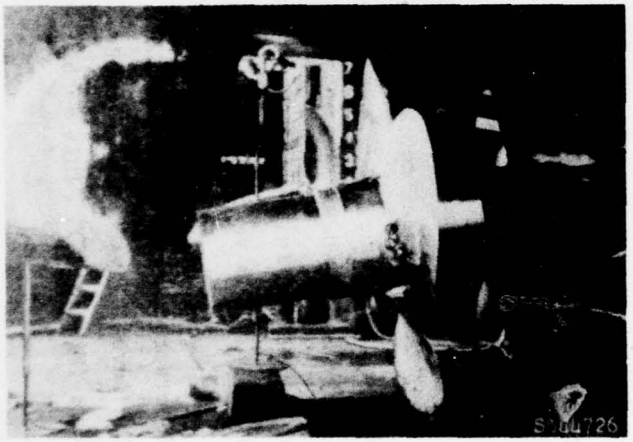

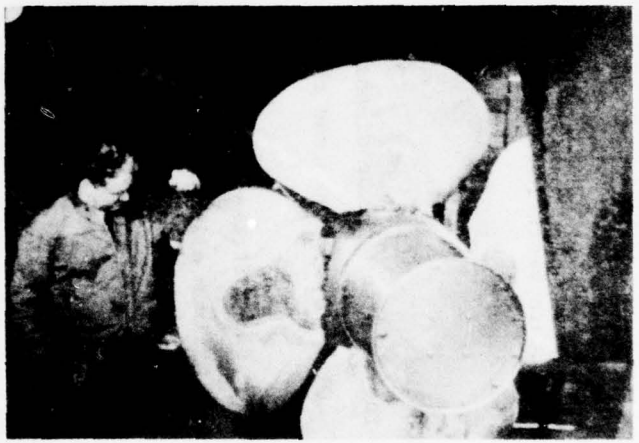

Figure 86m - Instrumented Propeller Installed on Starboard Shaft of DOUGLAS

UNDERWAY TEST RESULTS

Figure 87 indicates the stress response of Blade 4 at the 0.4 radius along the maximum thickness line in the radial orientation. Full power data are plotted on a working stress diagram in Figure 88. Athwartship superstructure vibration (02 level, Frame 66) at shaft frequency is indicated in Figure 89.

DISCUSSION

The results will be discussed in two sections. The first will be on propeller blade stresses and the second on hull/superstrucuture vibration.

Propeller Blade Stress

The maximum allowable propeller blade stress to which these blades were designed is 12,500 psi. It can be seen in Figure 87 that the measured stress for steady ahead operation exceeded this value, however, it should be noted that the design value is not necessarily associated with the metallurgical properties of this propeller material but is a figure which is generally applied to most U.S. Navy propeller designs,[46] which allows a factor of safety (relative to the yield stress) of approximately 3. This design stress together with the full power measured stress is plotted on a working stress diagram in Figure 88.

A limited data analysis indicated that the full-ahead condition produced the highest combined (mean plus single amplitude alternating) stress conditions tested (see Figure 22 in the main body of this report). It can be seen that this was below the 100 million cycles fatigue (in saltwater) line. If the bolt were underway on a 50-percent lifetime basis, of which 1 percent were at full-power, then 100×10^6 cycles would be accumulated in approximately 6 years.

Hull/Superstructure Vibration

The level of vibration measure on the hull and superstructure was excessive (Figure 89). This is based not only on the recommended vibration

---

[46]Morgan, W.B., "Lectures on Propeller Design Theory," NSRDC Lecture Series, Winter 1970.

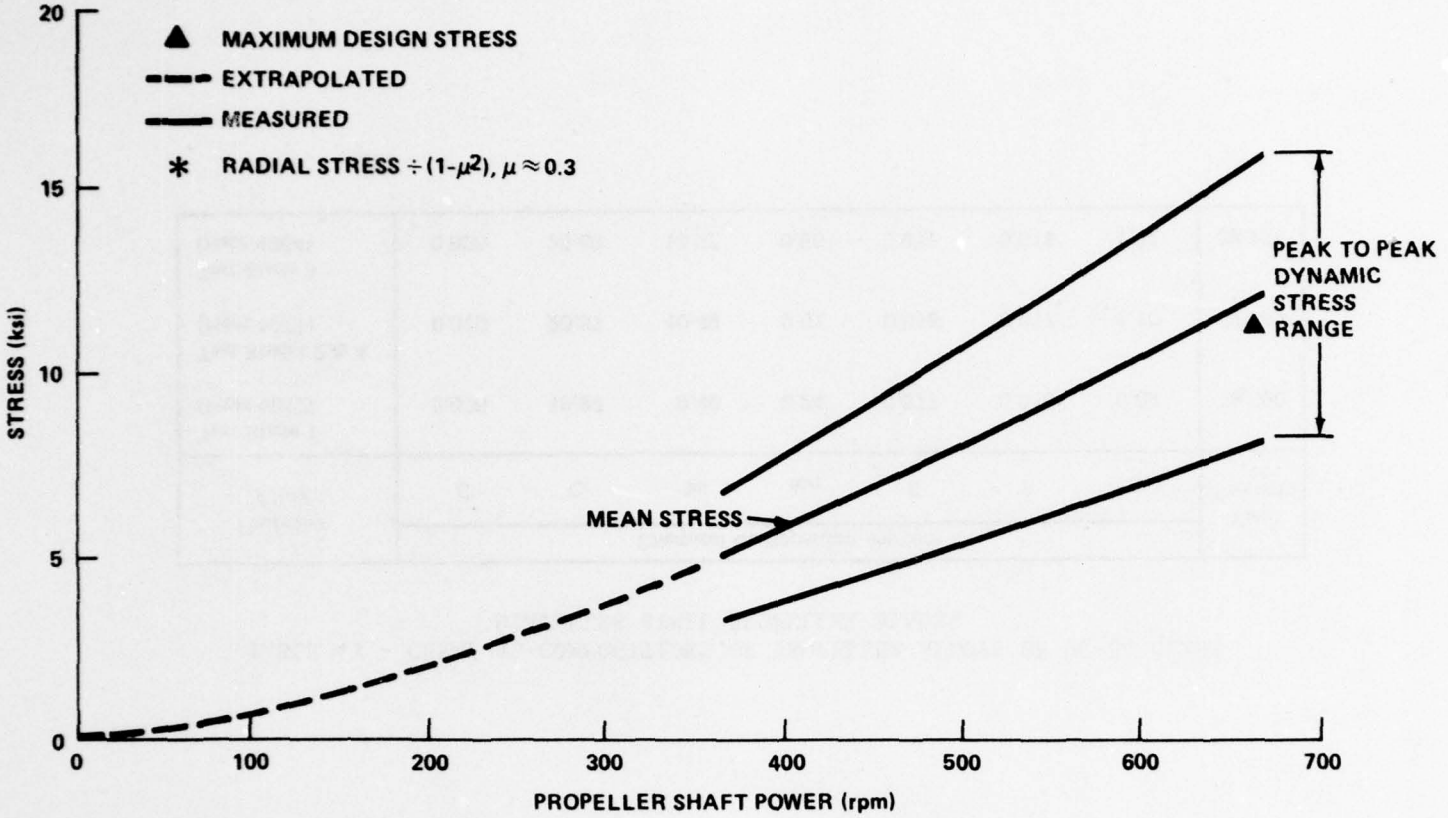

Figure 87 - Measured Stress* on Propeller Blade at 40-Percent Radius (Midchord) for Steady-Ahead Operation on DOUGLAS

TABLE 43 - CHEMICAL COMPOSITIONS OF PROPELLER ALLOYS OF PG-84 CLASS STAINLESS STEEL PROPELLER BLADES

Propeller Alloy	Chemical Composition, Percent							Yield Strength
	C	Cr	Ni	Mn	S	P	Si	
Test Blade 1 (Heat 4812)	0.035	19.97	9.40	0.24	0.077	0.016	0.69	38,500
Test Blades 2 & 4 (Heat 4977)	0.010	20.57	10.49	0.61	0.016	0.017	1.10	38,750
Test Blade 3 (Heat 4964)	0.026	20.60	10.52	0.56	0.017	0.016	1.74	38,125

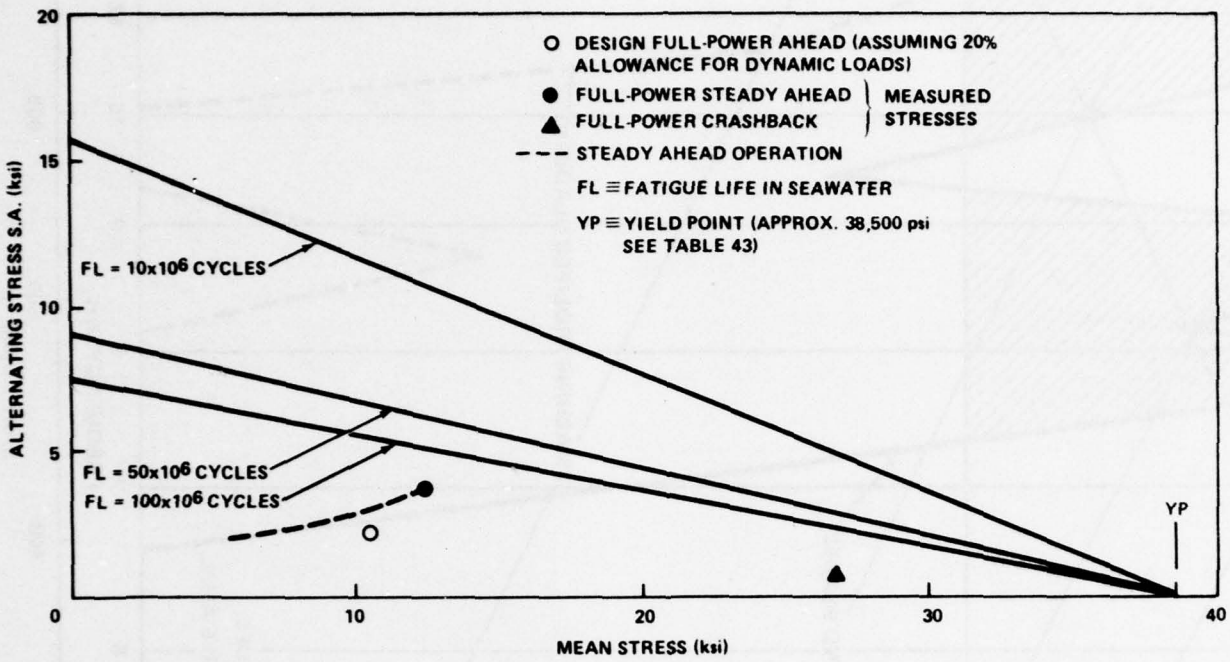

Figure 88 - Working Stress Diagram for CPP Blade Stresses (40-Percent Radius, Midchord) Measured on DOUGLAS

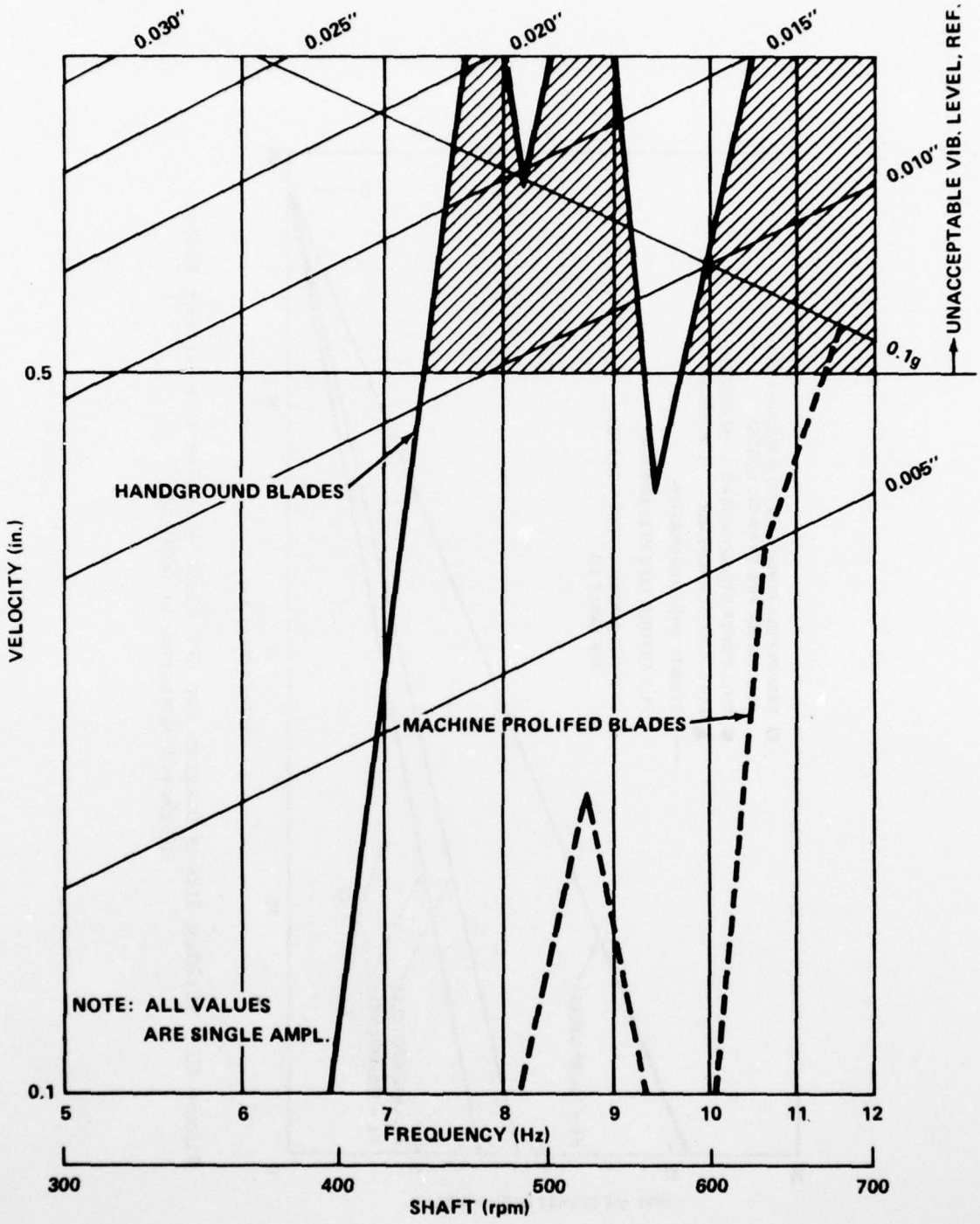

Figure 89 - Athwartship, Shaft-Frequency Vibration Measured on DOUGLAS at 02 Level, Frame 66

criteria for this class,[45] but also on data taken on the same boat five days after the propeller stress trials. This second set of vibration data was taken after the hand-ground stainless steel blades were removed and replaced with machine profiled blades.

CONCLUSIONS

The following conclusions are drawn from a limited analysis of the data:

1. The total stress (static and dynamic) at the 0.4R exceeded the maximum allowable design stress for steady state ahead operation.

2. The dynamic component of the stress had a shaft-frequency single-amplitude of $\pm$ 33 percent of the static stress ($\pm$ 3.7 ksi).

3. The vibration level measured on the hull and superstructure with reworked hand-ground propeller blades was excessive.

4. The vibration level measured on the hull and superstructure with machine profiled propeller blades was acceptable.

APPENDIX C

JOINT STIFFNESS CHARACTERISTICS OF BARBEY

BARBEY JOINT STIFFNESS CHARACTERISTICS WERE DETERMINED FROM AN EXPERIMENTAL LABORATORY MOCKUP OF THE PROPELLER BLADE PALM AND CRANK DISK

TEST SETUP

The laboratory mockup is shown in Figure 90 and typical test results are shown in Figure 91. Tests were done at DTNSRDC (Annapolis) by Code 2814.

BOLT STIFFNESS K_B

Test bolts were installed in the test rig with no preload. External loads were applied and bolt shank strain and elongation were recorded. Test results were used to determine K_B and equivalent bolt length $l_{B(EQ)}$. Values are given below:

Test Sample	K_B(lb/in. x 10^{-6})	$l_{B(EQ)}$(in.)
7 1/2 in.(LOA)	22	4.6
8 1/2 in.(LOA)*	21	4.8

INTERFACE STIFFNESS VALUES

On the assumption that the test rig acts (approximately) as an ideal joint under preload (no plate separation), the quasi-linear portion of the bolt response curve can be used to determine values of joint stiffness K_J. Values of plate stiffness K_p, K_{p1}, and K_{p2} can be found by using the following simple relationships which were derived from the mockup analog:

$$K_J = K_p + K_B \quad (1)$$

$$K_p = (K_{p1})(K_{p2})/(K_{p1} + K_{p2}) \quad (2)$$

*Values for 8 1/2 in.(LOA) bolt determined from drydock measurements.

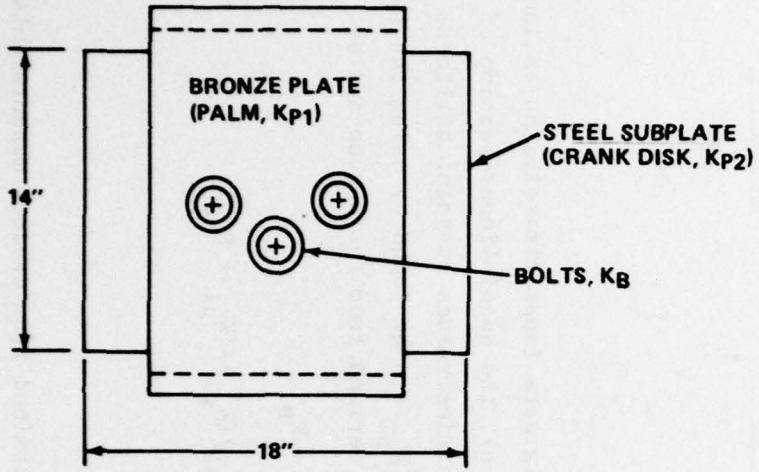

Figure 90a - Top View

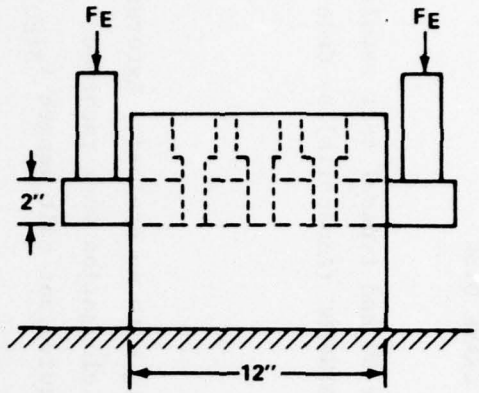

Figure 90b - Front View

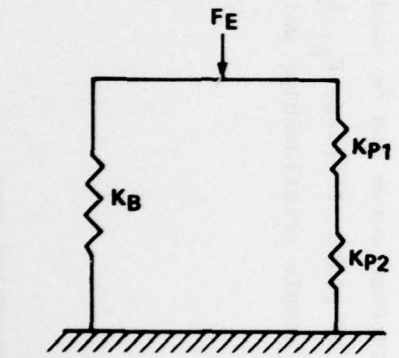

Figure 90d - Test Stand Analog

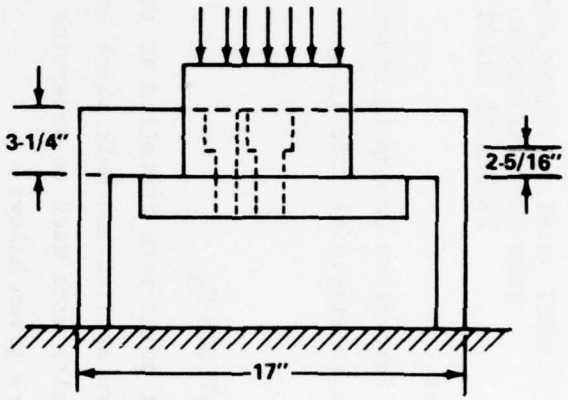

Figure 90c - Side View

Figure 90 - Laboratory Mockup of BARBEY Palm/Crank Disk

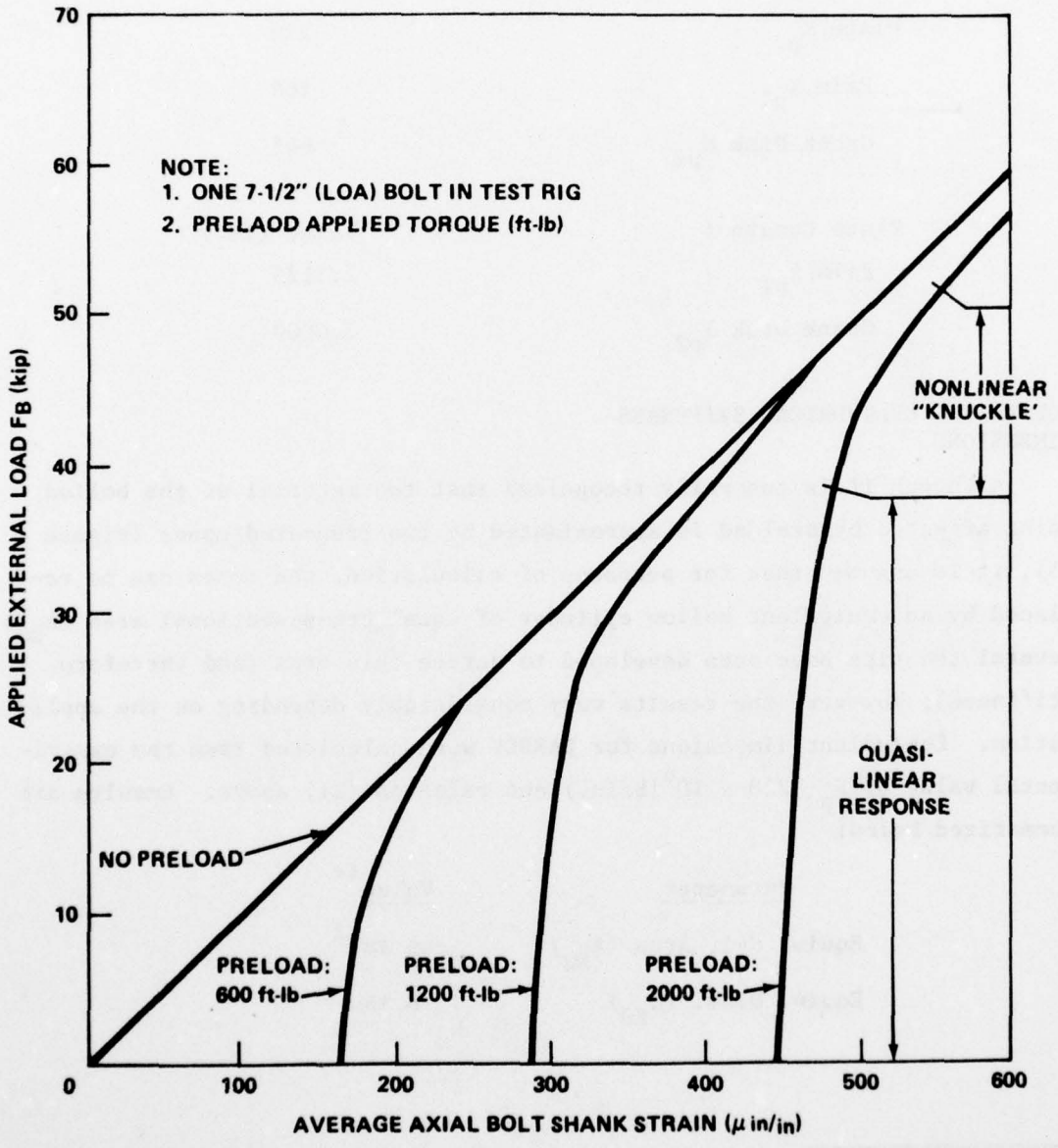

Figure 91 - Bolt Response versus External Load for Various Preloads on Laboratory Mockup of BARBEY Palm/Crank Disk

Values using the 7 1/2 in. bolt in the test rig are given below:

Stiffness Parameter	Value (lb/in. x 10^{-6})
Joint K_J*	250
Plate K_p	228
Palm K_{p1}	360
Crank Disk K_{p2}	641

Plate Lengths:	Value (in.)
Palm l_{p1}	2.3125
Crank Disk l_{p2}	2.0000

EQUIVALENT CYLINDRICAL STIFFNESS DIMENSIONS

Although it is generally recognized that the material of the bolted joint affected by preload is approximated by two truncated cones (Figure 75), it is assumed that for purposes of calculation, the cones can be replaced by an equivalent hollow cylinder of equal cross-sectional area (A_{EQ}). Several theories have been developed to define this area (and therefore stiffness); however, the results vary considerably depending on the application. Equivalent dimensions for BARBEY were calculated from the experimental value of K_p ($\approx 228 \times 10^6$ lb/in.) and relation (2), above. Results are summarized below:

Parameter	Value**
Equiv. Cyl. Area (A_{EQ})	45 $in.^2$
Equiv. Diam. (D_{EQ})	8 in.

*Measured in test rig.

**It should be noted that these values apply only to this test rig where interface clamping stress was not constrained or interrupted by geometric discontinuities.

FORCE TRANSMISSION CHARACTERISTICS

It can be seen that as long as external load is restricted to the quasi-linear curve portion, very little external load is carried by the bolt. Transmission characteristics of the interface for this test setup, 7 1/2 in.(LOA) bolt, are given below:

	Percent of Fe Transmitted	
External Load at Joint	Thru Plates (K_p)	Thru Bolt (K_B)
F_E	91.3	8.7

REFERENCES

1. Boatwright, G.M. and J.H. Strandell, "Controllable Pitch Propellers," Naval Engineers Journal (Aug 1967).

2. Angelo, J. et al., "U.S. Navy Controllable Pitch Propeller Programs," presented at a Joint Meeting of Flagship and Chesapeake Sections of ASNE (19 Apr 1977).

3. Laque, F.L., "Marine Corrosion Causes and Prevention," Chapter 9 of the Corrosion Monograph Series, Wiley-Interscience Publication, John Wiley & Sons, New York (1975).

4. "Controllable Pitch Propellers," NAVSHIPS Technical Manual 0944-005-5010 (Dec 1961).

5. "Liaaen Model D 132/5 Controllable Pitch Propeller System for U.S. Navy Destroyer Escort (DE-1088)," Training Text, Long Beach Naval Shipyard (Feb 1972).

6. "Interim Data on the USS BARBEY (FF-1088) CPP Trials," Presentation 2 to NAVSEA representatives at DTNSRDC/Carderock (May 1975).

7. "Interim Data on the USS BARBEY (FF-1088) CPP Trials," Presentation 3 to NAVSEA representatives at DTNSRDC/Carderock (27 Jun 1975).

8. McCarthy, J.H. and J.S. Brock, "Static Stresses on Wide-Bladed Propellers," NSRDC Report 3182 (Feb 1970).

9. "BARBEY Power Loader," DTNSRDC Drawings E-3280-1, -2, and -3 (20 Jan 1975).

10. "Project BARBEY Antenna Sensor," DTNSRDC Drawings E-3272-1 through -6 (16 Jan 1975).

11. Buchmann, E. and E. Tuckerman, "Model Basin Procedure for the Analysis and Presentation of Vibration Data," Part II, Bulletin 33, Shock, Vibration and Associated Environments, Office of the Director of Defense Engineering (Feb 1964).

12. Taylor, D.W., "The Speed and Power of Ships," Ransdell, Inc., Washington, D.C. (1933) pp. 216–241.

13. Atkinson, P., "On the Choice of Method for the Calculation of Stress in Marine Propellers," Royal Institute of Naval Architects, Vol. 110 (1968).

14. Tatnall, F.G., "Tatnall on Testing," American Society for Metals Publication, Metals Park, Ohio (1966).

15. Conolly, J., "Strength of Propellers," Royal Institute of Naval Architects (1960).

16. Antonides, G., "Propeller-Stress Trials on USS FRANKLIN D. ROOSEVELT (CVA-42)," NSRDC Report 2562 (1968).

17. Wereldsma, I.E., "Stress Measurements on a Propeller Blade of a 42,000-Ton Tanker on Full Scale," Netherlands Research Center T.N.O. for Shipbuilding and Navigation (1963).

18. Dashnaw, F.J. and F.E. Reed, "Propeller Strain Measurements and Vibration Measurements on the USS MICHIGAN," presented to Chesapeake Section of SNAME (1970).

19. Keil, H.G. et al., "Stresses in Blades of a Cargo Ship Propeller," Schifibautechnische Gesellschaft (1970).

20. Hanson, D.B., "Development of Strain Gage Protection Systems for Marine Propellers and Application to USS F.D. ROOSEVELT (CVA-42)," Hamilton-Standard Division of United Aircraft Corporation Report HSER 4704 (25 Aug 1967).

21. Valentine, R.C., "Marine Propeller Strain Gage and Signal Transmission System for the USS DOUGLAS (PG-100)," Hamilton-Standard Division of United Aircraft Corporation Report HSER 5829 (16 Mar 1971).

22. Dean, Mills, "Strain Gage Installation and Waterproofing on Propeller Blades and Associated Components on the USS BARBEY (FF-1088)," DTNSRDC Report (in preparation).

AD-A047 851 DAVID W TAYLOR NAVAL SHIP RESEARCH AND DEVELOPMENT CE--ETC F/G 13/10
THE BARBEY REPORT. AN INVESTIGATION INTO CONTROLLABLE PITCH PRO--ETC(U)
AUG 77 C NOONAN, G ANTONIDES, A ZALOUMIS

UNCLASSIFIED DTNSRDC-77-0080 NL

4 OF 4
AD
A047851

END
DATE
FILMED
1 -78
DDC

23. Dean, Mills, "Vulcanized Rubber Protection for Strain Gages in a Seawater Environment," Experimental Mechanics, Vol. 17, No. 8, pp. 303-307 (Aug 1977).

24. Faires, V.M., "Design of Machine Elements," MacMillan Company, Third Edition, New York (1955), Chapter 5.

25. Horger, O.J., "Metals Engineering Design," ASME Handbook (1965).

26. Snow, A.L. and B.F. Langer, "Low Cycle Fatigue of Large Diameter Bolts," ASME Paper 66-Pet-8 (Sep 1966).

27. Fazekas, G.A., "On Optimal Bolt Preload," Journal of Engineering for Industry, Trans. SNAME (Aug 1976).

28. Motosh, N., "Determination of Joint Stiffness in Bolted Connections," Journal of Engineering for Industry, Trans. ASME (Aug 1976).

29. Stephenson, J. and R. Callander, "Engineering Design," John Wiley & Sons, New York (1974), Chapter 13.

30. Meyer, G. and D. Strelow, "Simple Diagrams Aid in Analyzing Forces in Bolted Joints," Assembly Engineering, Vol. 15, No. 1 (Jan 1972).

31. "Propeller Blade Section Design Coefficients for Type II Sections," NAVSEA Drawing 23-1737515 (21 July 1958).

32. Dean, Mills, "Miniature Pressure Gage (for use in Aerodynamic and Hydrodynamic Research Investigations). Presented at 8th Transducer Workshop, St. Louis, Missouri (22–24 Apr 1975).

33. Beek, G. and J. Heidemans, "Strength Considerations in Controllable Pitch Propeller Design," International Shipbuilding Progress, Vol. 23, No. 266 (23 Oct 1976).

34. Meyer, G., "Simple Diagrams Aid in Analyzing Forces in Bolted Joints," Assembly Engineering, Vol. 15, No. 1 (Jan 1972).

35. Motosh, N., "Determination of Joint Stiffness in Bolted Connections," J. Eng. for Indust. (Aug 1976).

36. Fazekas, G., "On Optimal Bolt Preload," J. Eng. for Indust. (Aug 1976).

37. Thompson, J. et al., "The Interface Boundary Conditions for Bolted Flanged Connections," J. Pressure Vessel Technol. (Nov 1976).

38. Landt, R., "Criteria for Evaluating Bolt Head Design," J. Eng. for Indust. (Nov 1976).

39. Faires, V., "Design of Machine Elements," Collier-MacMillan Canada, Ltd (1965).

40. Antonides, G. et al., "Full-Scale Underway CPP Propeller Stress Trials on the USS SPRUANCE (DD-963)," DTNSRDC Evaluation Report SAD-164E-1962 (Jan 1977).

41. Stephenson, J. and R. Callander, "Engineering Design," J. Wiley & Sons, New York (1974).

42. Chu, T. and D. McLaughlin, "Contributions to the Development of Design Criteria for Controllable Pitch Propellers," MTI Contract Report MTI 76TR4S (30 Jun 1976).

43. Kerwin, J.E. et al., "Failure and Safety Analysis of Controllable Pitch Propellers for the USS BARBEY (FF-1088) and USS SPRUANCE (DD-963)," Office of Naval Research Contract Report N00014-67-A-0204-0082, MIT OSP 81496 (15 Apr 1975).

44. Snow, A.L. and B.F. Langer, "Low Cycle Fatigue of Large Diameter Bolts," Paper presented at the Petroleum Mechanical Engineering Conf. of ASME at New Orleans, La., Sept 18–21, 1966.

45. Noonan, C. and W. Fontaine, "A Study of Vibration Problems Experienced by Aluminum Hull Patrol Gunboats (PG-84 Class)," DTNSRDC Report 3857 (Apr 1972).

46. Morgan, W.B., "Lectures on Propeller Design Theory," NSRDC Lecture Series (Winter 1970).

INITIAL DISTRIBUTION

Copies		Copies	
1	NRL/Dr. Perrone	12	DDC
1	ONR LONDON, ENGLAND	2	HQS COGARD 1 G-ENE 4/64 (CMDR Wagner) 1 G-ENE 5/64 (Morris)
1	NOSC/Fabula		
14	NAVSEA 2 SEA 09G32 4 SEA 032 1 SEA 033 1 SEA 034 1 SEA 03412 1 PMS 378 1 PMS 389 1 PMS 397 1 PMS 399 1 SEA TECH. REP. Bath, England (CMDR Dykeman)	1	MIT, Ocean Engr/Kerwin
		1	American Bureau of Shipping/ Foley
		2	Bath Iron Works Corp. 1 Hausen 1 FFG Prog. Off.
		2	Bird-Johnson 1 Case 1 Ridley
1	NAVSHIPYD/NORVA	2	Gibbs & Cox 1 Tech Lib 1 Olson
2	NAVSHIPYD/PEARL 1 Damon	1	Hamilton-Standard/Valentine
4	NAVSHIPYD/LBEACH 2 LOVAAS	1	J. Hill
21	NAVSEC 2 SEC 6034B 1 SEC 6100 1 SEC 6101A 1 SEC 6101D 1 SEC 6110 1 SEC 6114H 1 SEC 6120 1 SEC 6136 1 SEC 6140 1 SEC 6140B 2 SEC 6144 1 SEC 6144G 1 SEC 6145B 5 SEC 6148 1 SEC 6600 NORVA	1	Hydronautics/Duanne
		1	Ingalls Shipbuilding
		1	Lips Propellers/Lane
		1	Litton Industries
		1	Lockheed M&S/Waid
		1	Propulsion Dynamics, Inc.
		2	Propulsion Systems, Inc. 2 Wennberg
		1	Sulzer Bros./Jung
2	SUPSHIPS 1 BATH 1 Pascagoula		

CENTER DISTRIBUTION

Copies	Code	
1	11	Ellsworth
1	1102.1	Nakonechny
1	15	Cummins
1	1505	Crump
1	1524	Roddy
1	1536	Hunt
1	154	Morgan
1	1544	Cumming
1	1544	Boswell
1	1552	Brockett
1	1556	Santore
1	1556	Nelka
1	156	Hagen
1	17	Murray
1	172	Krenzke
1	1720.6	Rockwell
1	1730.4	Dinsenbacher
1	19	Sevik
1	196	Feit
1	1962	Zaloumis
1	1962	Noonan
1	1962	Antonides
1	1962	Corbin
1	1962	Schauer
1	281	Niederberger
1	2814	Czyryca
1	2814	Vassilaros
1	2841	Klemens
1	2950	Dean
30	5214.1	Reports D[illegible]bution
1	522.1	Lib (C)
1	522.2	Lib (A)